

# Argonne National Laboratory

## TERMINAL REPORT ON THE MIGHTY MOUSE HIGH-FLUX RESEARCH REACTOR PROJECT

by

L. E. Link, Project Engineer

R. H. Armstrong, T. C. Cameron,

R. F. Dickson, J. B. Heineman,

C. N. Kelber, P. H. Kier, H. F. Reed,

R. R. Rohde, J. P. Simon, W. R. Ware

ANL-5928  
Reactors - General  
(TID-4500, 15th Ed.)  
AEC Research and  
Development Report

ARGONNE NATIONAL LABORATORY  
P. O. Box 299  
Lemont, Illinois

TERMINAL REPORT ON THE MIGHTY MOUSE  
HIGH-FLUX RESEARCH REACTOR PROJECT

by

L. E. Link, Project Engineer

and

R. H. Armstrong	P. H. Kier
T. C. Cameron	H. F. Reed
R. F. Dickson	R. R. Rohde
J. B. Heineman	J. P. Simon
C. N. Kelber	W. R. Ware

Reactor Engineering Division

September, 1959

Operated by The University of Chicago  
under  
Contract W-31-109-eng-38



## TABLE OF CONTENTS

	<u>Page</u>
I. INTRODUCTION. . . . .	7
II. SUMMARY . . . . .	12
III. DESIGN DESCRIPTION . . . . .	17
A. Reactor . . . . .	17
1. Core . . . . .	17
a. Fuel Subassemblies . . . . .	17
b. Shroud and Supporting Structure . . . . .	19
2. Control Systems . . . . .	21
a. Mechanical Control . . . . .	21
b. Fluid Control System . . . . .	24
3. Pressure Vessel . . . . .	25
4. Shielding . . . . .	27
a. Thermal Shield . . . . .	27
b. Biological Shield . . . . .	29
5. Experimental Facilities . . . . .	32
a. Vertical Facilities . . . . .	33
Central Thimble (VT-1) . . . . .	38
1-in. ID Thimbles (VT-2 to VT-7) . . . . .	39
2-in. ID Thimbles (VT-8 to VT-14) . . . . .	41
3-in. ID Thimbles (VT-15 to VT-30) . . . . .	42
8-in. ID Vertical Through Holes (VTH-1) . . . . .	42
8-in. ID Cryogenic Through Hole (VTH-2) . . . . .	43
General Purpose Holes (GP-1 and GP-2) . . . . .	44
Cryogenic Access Thimble (VT-31) . . . . .	44
Vertical Access Holes - Thermal Column (TCV-1 to TCV-5) . . . . .	44
Rabbit Systems (RP-1 and RH-1 to RH-6) . . . . .	45
b. Horizontal Facilities . . . . .	46
Expansion Joints . . . . .	46
Shield Gates . . . . .	48
Port Boxes . . . . .	49
Coffins . . . . .	50
Horizontal Beam Holes (HB-1 to HB-14) . . . . .	50
Horizontal Through-holes (HTH-1 to HTH-4) . . . . .	53
Down-beam Holes (DB-1 to DB-7) . . . . .	54



TABLE OF CONTENTS

	<u>Page</u>
c. Graphite Thermal Column . . . . .	57
d. Spent Fuel Irradiation Facilities (SFI-1 and SFI-2) . . . . .	58
6. Coolant System . . . . .	59
a. Primary System . . . . .	59
Moderator-Reflector Coolant . . . . .	61
Experimental Facilities . . . . .	61
Control Blades . . . . .	62
Heat Exchangers . . . . .	62
Pumps . . . . .	63
Emergency Condenser . . . . .	63
D <sub>2</sub> O Quality Control System . . . . .	63
Retention Tanks . . . . .	63
Surge Tanks . . . . .	63
System Pressure Drop . . . . .	63
b. Secondary System . . . . .	64
7. Fuel-handling System . . . . .	64
a. Subassembly Transfer - Canal to Core . . . . .	67
b. D <sub>2</sub> O Fuel Storage Tank . . . . .	71
B. Site and Buildings . . . . .	73
1. Site . . . . .	73
2. Buildings . . . . .	74
a. Reactor Containment Building and H <sub>2</sub> O Canal Annex . . . . .	74
Sub-basement . . . . .	77
Basement . . . . .	77
Main Floor . . . . .	82
Top Floor . . . . .	82
Control Room . . . . .	84
H <sub>2</sub> O Canal Annex . . . . .	84
Utilities . . . . .	85
Heating, Ventilating, and Air Conditioning . . . . .	85
b. Mock-up Wing . . . . .	87
Mechanical Mock-up Facility . . . . .	87
Zero-power Critical Assembly . . . . .	89
Heating, Ventilating, and Air Conditioning . . . . .	89
c. Laboratory and Laboratory Office Wing . . . . .	90
Heating, Ventilating, and Air Conditioning . . . . .	91

TABLE OF CONTENTS

	<u>Page</u>
d. Administration Wing . . . . .	92
Heating, Ventilating, and Air Conditioning . . . . .	92
e. Utility Building . . . . .	93
f. Stack Building . . . . .	93
g. Shield Storage Building . . . . .	94
h. Cooling Tower . . . . .	94
i. Retention Lagoons . . . . .	95
IV. PHYSICS . . . . .	96
A. Parameters Surveyed . . . . .	96
1. Core Size and Moderator . . . . .	96
2. Core Structural Materials . . . . .	97
3. Outer Reflector . . . . .	98
4. Fuel Cycle . . . . .	98
5. Control Elements and Burnable Poisons . . . . .	98
B. Critical Properties . . . . .	99
1. Two-group Age . . . . .	99
2. Cross Sections . . . . .	99
3. Methods of Calculation . . . . .	100
4. Critical Properties of Reference Core . . . . .	100
5. Two-dimensional Flux Plot . . . . .	101
6. Critical Properties of Fresh Core and Partly Used-up Core . . . . .	102
C. Control . . . . .	103
1. Burnable Poisons . . . . .	103
2. Solid Absorbers . . . . .	108
D. Future Supporting Studies . . . . .	110
V. CORE HEAT TRANSFER AND FLUID FLOW . . . . .	112
A. Steady-state Conditions . . . . .	112
1. Selection of Fuel Elements . . . . .	112
2. Selection of Heat Transfer Values . . . . .	112

TABLE OF CONTENTS

	<u>Page</u>
3. Distribution of Energy Input and Temperatures . . . . .	112
4. Burnout . . . . .	114
B. Unsteady-state Conditions . . . . .	114
1. Reactor Shutdown . . . . .	114
2. Loss of Primary or Secondary Coolant Flow . . . . .	114
3. Rupture in Primary Coolant System . . . . .	115
C. Associated Heat Removal Problems . . . . .	116
1. Thermal Shield . . . . .	116
2. Pressure Vessel . . . . .	116
3. Spent Fuel Heat Generation . . . . .	117
4. Curium-245 Samples in the Center Thimble . . . . .	117
VI. RESEARCH AND DEVELOPMENT . . . . .	119
A. Fuel . . . . .	119
1. Cladding . . . . .	119
2. Fabrication . . . . .	122
3. Assembly . . . . .	123
4. Heat Transfer and Flow Tests . . . . .	123
5. Full-scale Flow and Vibration Tests . . . . .	126
B. Zircaloy-2 Pressure Vessel . . . . .	126
C. Control and Instrumentation . . . . .	126
D. Experimental Facilities . . . . .	127
E. Fuel-handling System . . . . .	127
VII. ESTIMATED COSTS . . . . .	128
A. Capital Costs . . . . .	128
B. Annual Operating Costs . . . . .	129

TABLE OF CONTENTS

	<u>Page</u>
APPENDICES	
APPENDIX A: Proposed Research Programs for an Advanced High-flux Reactor . . . . .	133
APPENDIX B: Survey of D <sub>2</sub> O-moderated Annular Cores with H <sub>2</sub> O Inner Reflectors . . . . .	151
APPENDIX C: Shielding and Irradiation Heating Calculations . . . . .	152
APPENDIX D: Heat Transfer and Fluid Flow Studies . . . . .	181
APPENDIX E: Stress Analyses of Pressure Vessel and Experimental Thimbles . . . . .	206
APPENDIX F: Alternate Fuel Element Designs . . . . .	211
APPENDIX G: Alternate Rotatable Vessel Closure and Fuel-handling System . . . . .	213

LIST OF FIGURES

<u>No.</u>	<u>Title</u>	<u>Page</u>
1.	Mighty Mouse - Advanced High-flux Research Reactor . . . . .	12
2.	Site Plan of Mighty Mouse Reactor Complex . . . . .	16
3.	Fuel Element and Core Subassembly Installation . . . . .	18
4.	Core Shroud and Central Thimble Support Structure . . . . .	20
5.	Control Blade - Drive Installation . . . . .	22
6.	Rack-and-pinion Drive Thimble . . . . .	23
7.	Reactor Pressure Vessel . . . . .	26
8.	Pressure Vessel Supports . . . . .	28
9.	Shielding Arrangement (Elevation through Thermal Column). . .	30
10.	Shielding Arrangement (Elevation through Cryogenic Facility). .	31
11.	Orientation of Experimental Facilities . . . . .	36
12.	Relative Positions of Vertical Experimental Facilities . . . . .	37
13.	Typical Vertical Thimble Installation - VT-2 to VT-7 . . . . .	40
14.	Horizontal Through-hole Installation . . . . .	47
15.	Orientation of Horizontal Beam Holes . . . . .	51
16.	Two-dimensional Flux Plot with Experimental Overlay . . . . .	52
17.	Arrangement of Horizontal Through-holes . . . . .	54
18.	Two-dimensional Flux Plot with Experimental Overlay . . . . .	55
19.	Arrangement of Down-beam Holes (30° to Horizontal) . . . . .	56
20.	System Flow Diagram . . . . .	60
21.	Fuel-transfer Mechanism . . . . .	65
22.	Fuel-transfer System . . . . .	66
23.	Loader Body Drive Compartment . . . . .	68
24.	Fuel Loader Extended over Core Subassembly . . . . .	69
25.	Fuel-subassembly Grappler . . . . .	70
26.	D <sub>2</sub> O Fuel Storage Tank . . . . .	72
27.	Reactor Containment Building and H <sub>2</sub> O Canal Annex . . . . .	75
28.	Plan View of Mighty Mouse Buildings and Space Allocations . . .	76
29.	Plan View of Sub-basement Level . . . . .	78

## LIST OF FIGURES

<u>No.</u>	<u>Title</u>	<u>Page</u>
30.	Plan View of Basement Level . . . . .	79
31.	Rabbit Cave for Inspection and Transfer of Samples from Reactor. . . . .	81
32.	Plan View of Main Floor . . . . .	83
33.	Mechanical Mock-up Facility . . . . .	88
34.	Effect of Annular Thickness of Fuel on Peak Flux per Unit of Power . . . . .	97
35.	Disposition of Metal and D <sub>2</sub> O for Two-dimensional Flux Plot . .	102
36.	Neutron Flux vs Radial Distance from Core Centerline . . . . .	105
37.	Comparison of Flux Distributions for Stainless Steel Control Rod Calculated by P <sub>1</sub> and P <sub>5</sub> Approximations . . . . .	110
38.	Axial Temperature Profiles in Active Core Region . . . . .	113
39.	Heat Generated in Core by Fission Product Decay after Operation at 250 Mw for 5 Days . . . . .	115
40.	Primary System Flow vs Time after Loss of Pump Power . . .	116
41.	Schematic of Central Thimble. . . . .	117
42.	Length and Flow Requirements for Three Curium Sample Geometries for Center Thimble . . . . .	118
43.	Alternate Methods of Fuel Tube and Sheet Assembly . . . . .	124
44.	Neutron Fluxes Used in Shielding Calculations . . . . .	154
45.	Estimated Total Core Gamma Flux . . . . .	157
46.	Total Gamma Flux at Core Midplane from Core Surface to Outer Surface of Pressure Vessel . . . . .	159
47.	Total Gamma Flux at Core Midplane . . . . .	160
48.	Fast Neutron Flux at Core Midplane . . . . .	162
49.	Sources of Heating Thimbles in D <sub>2</sub> O Region. . . . .	169
50.	Isotopic Concentration of the Zirconium Series in a Thermal Neutron Flux of $5 \times 10^{15} \text{n}/(\text{cm}^2)(\text{sec})$ (Sample Pure Zirconium) . .	173
51.	Isotopic Concentration for the Iron Series in a Thermal Flux of $5 \times 10^{15} \text{n}/(\text{cm}^2)(\text{sec})$ (Zr Sample Contains 0.05% Iron Initially). . . . .	174

LIST OF FIGURES

<u>No.</u>	<u>Title</u>	<u>Page</u>
52.	Isotopic Concentration for the Tin Series in a Thermal Neutron Flux of $5 \times 10^{15} \text{ n}/(\text{cm}^2)(\text{sec})$ (Zr Sample Contains 0.002% Tin Initially). . . . .	175
53.	Concentration vs Flux for a Portion of the Zr Series at an Irradiation Time of 10 years (Sample Is 100% Zr). . . . .	176
54.	Gamma Flux from Radioactive Core Shroud vs Thickness of Core Shroud ( $E_\gamma = 0.75 \text{ Mev}$ ) . . . . .	180
55.	Schematic of Magnesium Scale Coefficient Test Loop . . . . .	181
56.	Electric-heated Tube Test Section . . . . .	182
57.	Typical Plots of Scale Coefficient as a Function of Test Conditions for Electrically Heated Magnesium Alloy AZ31B Tubes . . . . .	184
58.	Mathematical Model and Constants . . . . .	187
59.	Pressure Drop vs Flow of Primary Coolant . . . . .	198
60.	Total Primary Coolant Flow Following Loss of Primary Pump Power . . . . .	200
61.	Natural Convection Cooling of Spent Fuel Subassemblies at Time t after Shutdown . . . . .	205
62.	Contribution to the Gamma Flux in the Zirconium Pressure Vessel . . . . .	207
63.	Tensile Stress vs Wall Thickness for the Zirconium Pressure Vessel . . . . .	208
64.	Spiral-wound Seam-welded Fuel Tube . . . . .	211
65.	Integral Rotable Closure and Fuel-Control Blade. . . . . Handling Mechanism . . . . .	214

## LIST OF TABLES

<u>No.</u>	<u>Title</u>	<u>Page</u>
I.	Operating Characteristics . . . . .	13-14
II.	Summary of Pressure Vessel Characteristics and Internals . . . . .	27
III.	Summary of Experimental Facilities . . . . .	34-35
IV.	Calculated Primary Coolant Flow Rates through Experimental Facilities . . . . .	61
V.	Calculated Cold Clean Critical Mass for Core Structural Materials . . . . .	98
VI.	Thermal Group Cross Sections . . . . .	100
VII.	Reference Core Characteristics . . . . .	101
VIII.	Critical Properties of Reference Core . . . . .	101
IX.	Summary of Burnup Calculations . . . . .	104
X.	Burnable Poisons Required to Balance $k_{ex}$ over the Fuel Cycle . . . . .	106
XI.	Adjusted Least-squares Fit to $\ln(\bar{Z}_p/\Sigma_{p0}) = At^2 + Bt$ . . . . .	107
XII.	Relative Life Times of Gadolinium Rods in Mighty Mouse. . . . .	108
XIII.	Comparison of Calculated Control Rod Disadvantage Factors . . . . .	109
XIV.	Hot Channel Factors . . . . .	114
XV.	Static Corrosion of Magnesium Alloys in Distilled H <sub>2</sub> O at pH 7 . . . . .	120-121
XVI.	Summary of Scale Coefficient Tests on ANL Special No. 1 and AZ31 Magnesium Tubing . . . . .	125
XVII.	Mighty Mouse Research Reactor Cost Estimate . . . . .	128
XVIII.	Annual Operating Costs . . . . .	130
XIX.	Annual Quantities of Fuel . . . . .	131
XX.	Relative Resolution vs Energy for a Time-of-flight Spectrometer Having a Resolution of 1.5 m $\mu$ sec/meter . . . . .	140
XXI.	Estimates of the Minimum Detectable Capture Cross Section ( $\bar{\sigma}_\gamma$ ) for U <sup>238</sup> . . . . .	142
XXII.	Operating Characteristics of H <sub>2</sub> O-D <sub>2</sub> O-reflected and D <sub>2</sub> O-cooled and moderated Annular Cores . . . . .	151



LIST OF TABLES

<u>No.</u>	<u>Title</u>	<u>Page</u>
XXIII.	Permissible Gamma-ray Energy Flux at Inside of Concrete Biological Shield to Satisfy Design Criteria . . . . .	153
XXIV.	Effective Fast Neutron Removal Cross Sections. . . . .	155
XXV.	Gamma-ray Constants. . . . .	156
XXVI.	Constants for Thermal Flux and Capture Gamma Calculations . . . . .	164
XXVII.	Energy Absorption Coefficients ( $\mu_e$ ) . . . . .	165
XXVIII.	Summary of Gamma-flux Calculations . . . . .	166
XXIX.	Decay Gamma Energy Distribution of Spent Fuel Elements. .	167
XXX.	Central Thimble Heating Inside and Outside the Core . . . . .	170
XXXI.	Activity in Core Shroud . . . . .	176
XXXII.	Activity in Vessel Neck . . . . .	177
XXXIII.	Summary of System Flow Characteristics. . . . .	199

# TERMINAL REPORT ON THE MIGHTY MOUSE HIGH-FLUX RESEARCH REACTOR PROJECT

by

L. E. Link, R. H. Armstrong, T. C. Cameron, R. F. Dickson,  
J. B. Heineman, C. N. Kelber, P. H. Kier, H. F. Reed,  
R. R. Rohde, J. P. Simon, W. R. Ware

## I. INTRODUCTION

This report is a documentation, from inception in 1955 to termination in 1958, of the research and development program pertinent to the conceptual design and ultimate construction at Argonne of an advanced research reactor with a peak thermal flux of  $5 \times 10^{15}$  n/(cm<sup>2</sup>)(sec). More specifically, it describes the basic reactor complex, the problems involved, the various approaches pursued, the present status and estimated cost of the project, along with recommendations for future research and development essential to the successful culmination of the project.

A preliminary design study of this reactor concept, identified as the Mighty Mouse Research Reactor, was published as ANL-5688.<sup>1</sup>

The advanced research programs in the fields of chemistry, physics, and metallurgy, that would be facilitated in the environment provided by the Mighty Mouse Reactor are outlined in Appendix A.

---

<sup>1</sup>L. E. Link, et al., "The Mighty Mouse Research Reactor - Preliminary Design Study," ANL-5688 (March, 1957).

II. SUMMARY

The Mighty Mouse (Fig. 1) is a pressurized, heavy water-cooled, moderated and reflected, heterogeneous thermal-type reactor designed to facilitate a broad basic research program in the neutron flux range from  $1$  to  $5 \times 10^{15}$   $n/(cm^2)(sec)$  consistent with an operating power level of 250 Mw.

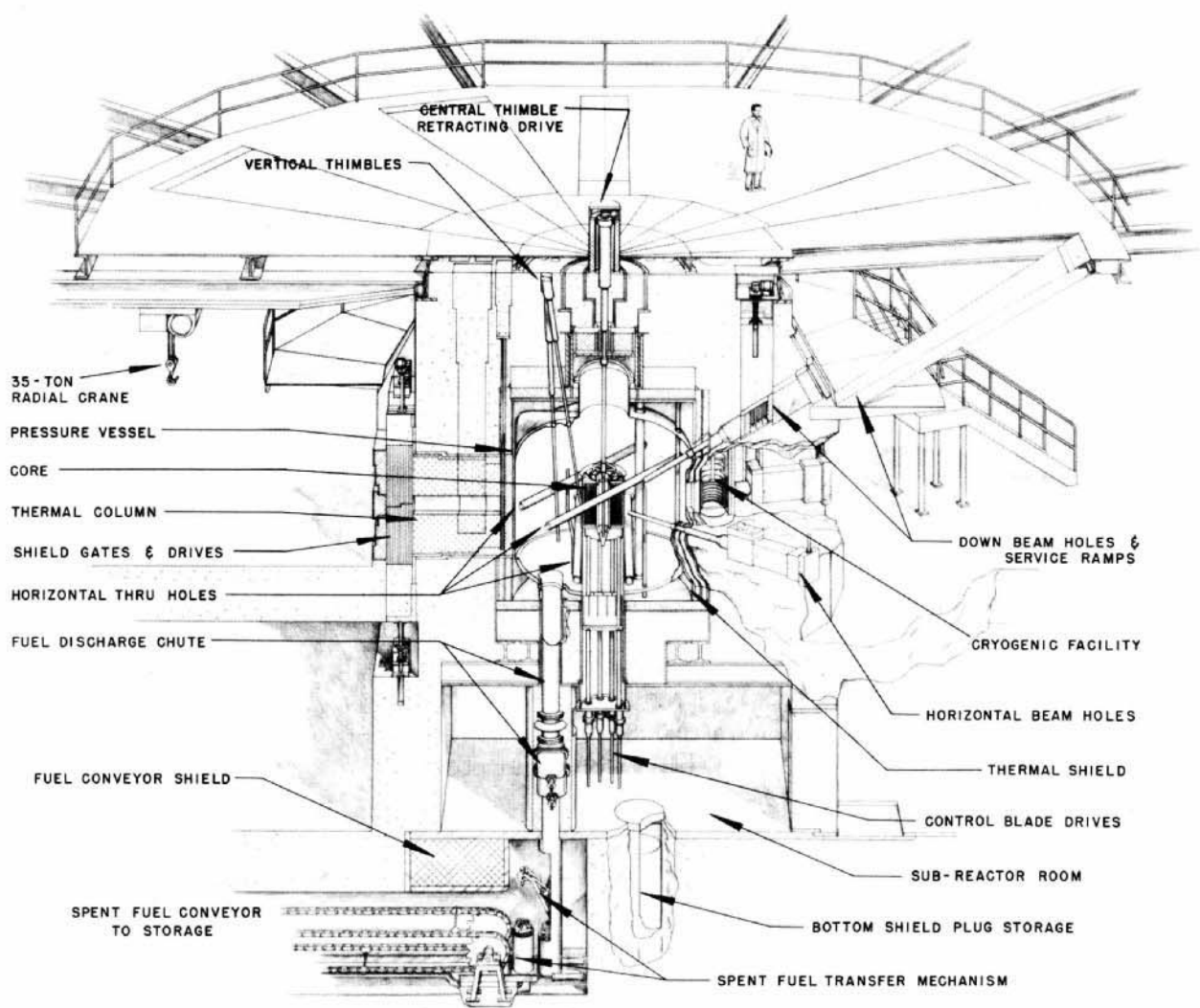


FIG. 1  
MIGHTY MOUSE - ADVANCED HIGH-FLUX RESEARCH REACTOR

The reactor is comprised of eight subassemblies that form an annular cylindrical core, the active portion of which is 36 in. OD, 12 in. ID, and 36 in. high. Each subassembly contains 455 magnesium-clad (0.010-in.) tubular fuel elements (0.375-in. OD, 0.030-in. wall thickness) arranged in a 0.450-in. square lattice, and a control blade.

The control blades (2 regulating; 6 safety) are augmented by burnable poisons incorporated in the fuel. Shim control is accomplished with gaseous  $\text{BF}_3$  contained in fixed-dimension chambers installed in the core shroud. The poison concentration is adjusted by changing the pressure of the gas. The control blades are actuated by rack-and-pinion-driven shaft extensions which operate through labyrinth-type, collected-leakage-sealed thimbles at the vessel bottom.

The core is centrally located in a pressure vessel (13 ft OD x 13 ft high) fabricated from zirconium (1-in. wall thickness) with a bolted flanged closure at the top. The bulk primary coolant flow is upward through the core, with parallel flows at lower velocity through the outer reflector. The flow streams merge and exit through the top of the vessel.

In addition to the perforations for eight control blade drive shafts and coolant inlet and exit flow, there are 62 openings in the vessel designed to accommodate various horizontal and vertical experimental facilities which extend to, or parallel, the core region. The experimental facility liners and the experiments contained therein are cooled by auxiliary heavy water systems that exit into the bulk coolant-reflector.

The operating characteristics of the Mighty Mouse are summarized in Table I.

Table I

OPERATING CHARACTERISTICS

Power Level	250 Mw
Power density (avg.)	495 kw/liter core volume
Core life at full power	120 hr
Initial loading - total (90% enriched)	3141 gm $\text{U}^{235}$
Initial mass (cold clean critical)	1591 gm $\text{U}^{235}$
End cycle	
Burnup	1550 gm $\text{U}^{235}$
Fission products	1500 gm
Thermal neutron flux in core	
Average	$3 \times 10^{15} \text{ n}/(\text{cm}^2)(\text{sec})$
Peak	$5 - 7 \times 10^{15} \text{ n}/(\text{cm}^2)(\text{sec})$
Metal: $\text{D}_2\text{O}$ ratio in core	1:4
Total heat transfer surface in core	1972 $\text{ft}^2$

Table I (Cont'd.)

Total flow area in core	4.465 ft <sup>2</sup>
Average heat flux	433,000 Btu/(hr)(ft <sup>2</sup> )
Maximum heat flux	
Inside fuel tube	734,000 Btu/(hr)(ft <sup>2</sup> )
Outside fuel tube	578,000 Btu/(hr)(ft <sup>2</sup> )
Maximum/average flux	
Radial	1.2
Axial	1.5
Convection coefficient	
Inside tube	7,300 Btu/(hr)(ft <sup>2</sup> )(°F)
Outside tube	5,740 Btu/(hr)(ft <sup>2</sup> )(°F)
Maximum fuel surface temperature	283°F
Burnout/maximum heat flux	5.5
Hot channel factors	
Bulk temperature rise	1.19
Film temperature rise	1.40
Fuel temperature rise	1.00
Primary coolant flow	
Total	54,000 gpm
Fuel	43,000 gpm
Control rods and inner reflector	1,100 gpm
Experimental facilities and miscellaneous	4,700 gpm
Coolant velocity in core	
Inside fuel tubes	25.0 fps
Outside fuel tubes	18.6 fps
Inlet temperature of D <sub>2</sub> O to core	110°F
Outlet temperature of D <sub>2</sub> O from core	146°F
Inlet pressure to core	85.0 psig
Outlet pressure from core	62.0 psig

The thermal shield (16 in. thick) is external to the pressure vessel wall, and is composed of steel plates cooled with borated water. The biological shield is magnetite concrete. The average thickness is  $9\frac{1}{2}$  ft. The thermal and the biological shields contain seven experimental facilities which abut the pressure vessel wall. Some of these facilities located in the graphite thermal column, and the cryogenic facilities, feature horizontal and/or vertical access ports.

The reactor shield structure ( $\sim 35$  ft across flat sides) is encircled by a balcony that leads to a steel deck above the reactor for access to thimble ports in that region. The deck can support relatively light experimental apparatus that must be located close to the test facility. The deck structure also contains ramps that depress at angles coincident with down beam holes to facilitate loading and unloading operations from the balcony level. The main horizontal beam holes are located  $4\frac{1}{2}$  ft above the main floor level.

The reactor is centrally located in a containment building (160 ft dia.) shown in the site plan, Fig. 2. The ground floor and basement are used largely for experiments and related apparatus. The sub-basement contains the primary coolant system and some of the fuel-handling equipment.

The Utility Building houses most of the operating equipment and utilities, i.e., secondary coolant system and refrigeration equipment for the experimental facilities, and the heating and ventilation system components.

The Mockup Wing houses the critical assembly and other equipment required to evaluate the mechanical and nuclear characteristics of all experiments prior to installation in the reactor.

The Canal Annex is connected to the Reactor Building to facilitate transfer and storage of active materials.

The Laboratory Building contains 18 large laboratories, as well as offices and service facilities for a minimum of 50 staff experimenters.

The Administration Building contains offices for the administrative and the operating staff, as well as minor appurtenances such as conference rooms, library, and auditorium.

The cost of the proposed Mighty Mouse Reactor complex is estimated at \$70,467,000 (see Table XVII, page 128). This includes escalation and contingency factors reflecting the state of the research and development program at the termination of the project (see Section VI). The annual operating cost is estimated at \$2,900,000 (see Table XVIII, page 130).

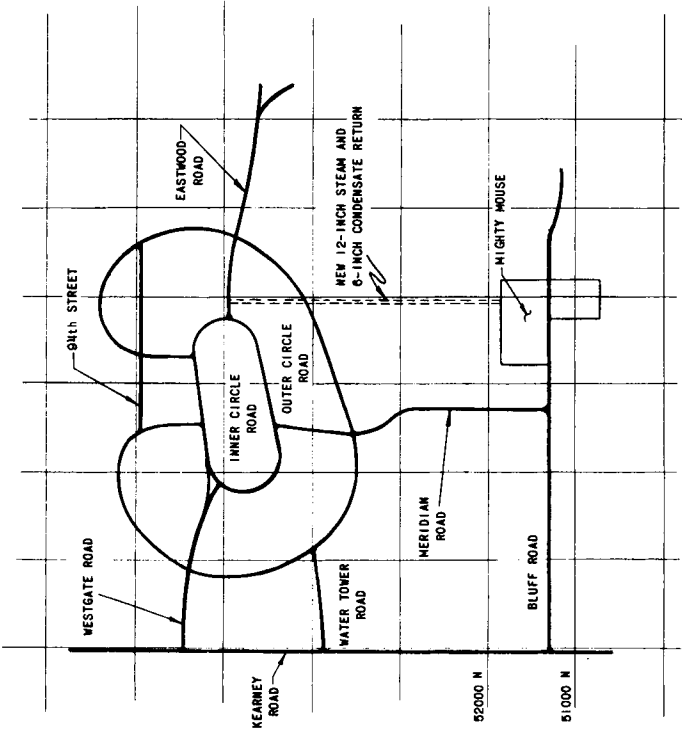
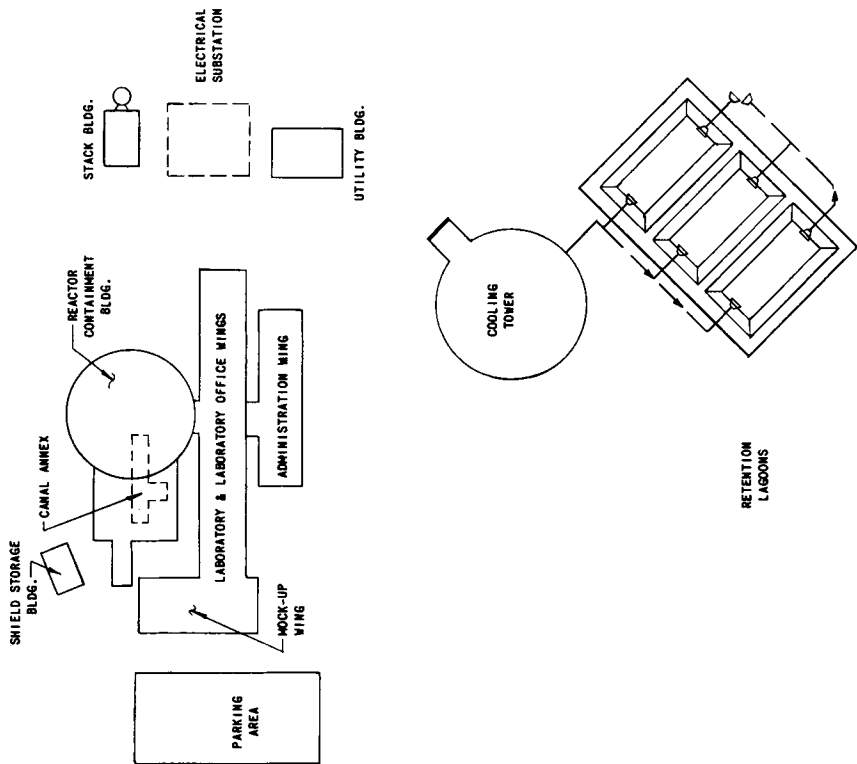


FIG. 2  
PROPOSED SITE PLAN OF MIGHTY MOUSE REACTOR COMPLEX  
(REF DWG. PE-X-244)



### III. DESIGN DESCRIPTION

#### A. Reactor

##### 1. Core

##### a. Fuel Subassemblies

The high power density and short fuel cycle warrant subdivision of the fuel elements into large subassemblies to expedite fuel loading and unloading operations.

The total core loading consists of eight subassemblies. Each subassembly (Fig. 3) contains 455 magnesium-clad tubular fuel elements, arranged on a 0.450-in. square lattice, and a control blade. The active length (36 in.) of each fuel tube contains approximately one gram of highly enriched uranium dispersed in a magnesium matrix (0.010-in. wall thickness). The inner and outer surfaces of the fuel zone are clad with magnesium (0.010 in. min). Since uranium and magnesium do not alloy, a probable method of fabrication is to disperse the uranium (in metal, oxide, carbide, or silicide form) and burnable poisons in the magnesium by powder metallurgy techniques, and clad the matrix with suitable magnesium.

The upper and lower 2-inch inactive lengths are formed into a crowned configuration to define the outer flow channels and to space the tubes in the subassembly lattice properly. The individual elements are joined at the tube corners by a fusion or braze technique. While the reference design does not indicate spacers along the active length of the tubes, it is recognized that hydraulics tests may demonstrate the need for at least a center spacer. The tube bundle is bonded at the top and bottom to a magnesium strap to complete the subassembly.

Each subassembly contains a mechanically driven control blade as an integral part of its structure. The primary function of this design feature is to facilitate control blade removal. In addition, it will prevent criticality problems in the storage of spent fuel in heavy water.

The fuel subassemblies are vertically aligned in the core shroud by spring clips at the top and bottom of each subassembly. In addition, each subassembly features five groups of four tubes which extend above the tube bundle and connect to a hold-down bridge serving to equalize the hydraulic thrust on the subassembly created by the upward flow of coolant. The bridge also contains the linkage that locks the fuel assembly to the core shroud.





## b. Core Shroud and Supporting Structure

The zirconium core shroud (Fig. 4) consists of an outer shell (36 in. OD;  $\frac{5}{32}$ -in. wall, 8 ft 6 in. long) and an octagonal inner shell (11 in. across flats;  $\frac{3}{16}$ -in. wall). The inner and outer sections are connected by eight strut members to form rigid cavities to accommodate the fuel subassemblies. Each strut member also supports the control elements.

The portion next to the inner reflector hole contains the envelope of the  $\text{BF}_3$  gas control system, and the outer section provides a track for the mechanical drive control blade. The portion of the shroud below the core contains control connecting rod guides. Struts in the center of the inner octagonal shell provide support for the center thimble. The shroud is supported near the bottom of the reactor vessel, where it is bolted to the 36-inch  $\text{D}_2\text{O}$  inlet nozzle. In addition, the shroud is braced in the vessel by zirconium structural members that are bolted to the shroud and to plates welded to the inner surface of the reactor vessel (see Fig. 7).

The core shroud is subjected to a thermal flux of  $5 \times 10^{15} \text{ n}/(\text{cm}^2)(\text{sec})$ , which results in an integrated flux of  $1.6 \times 10^{24} \text{ n}/(\text{cm}^2)(\text{sec})$  after 14 years of reactor operation. Although the effect of radiation on the mechanical properties of zirconium has appeared to reach saturation at exposure levels up to  $2.4 \times 10^{20} \text{ nvt}$ , it is suspected that the structural soundness of the shroud will be threatened by prolonged irradiation in the Mighty Mouse. The unknown extent of irradiation damage to the shroud structure, and the possibility of improved fuels requiring different support schemes, make it essential that the design provide for ultimate removal and replacement of the shroud and internal structure.

The procedure for extracting the core shroud from the pressure vessel will be to drain the  $\text{D}_2\text{O}$  from the vessel and fill it with  $\text{H}_2\text{O}$ . A permanent flexible diaphragm, connecting the pressure vessel neck to the biological shield, will enable the cavity which is normally occupied by the top shielding plug to be filled with water. This column of water will serve as a shield for personnel while they remove the vessel cover and during the time they are loosening the shroud supports. The shroud will be removed into a reinforced lead coffin positioned above the vertical opening in the biological shield, and a new shroud installed.

The method of calculating the activation of the shroud structure, transfer coffin shielding, and the activity level at the surface of the water shield is described in Appendix C.

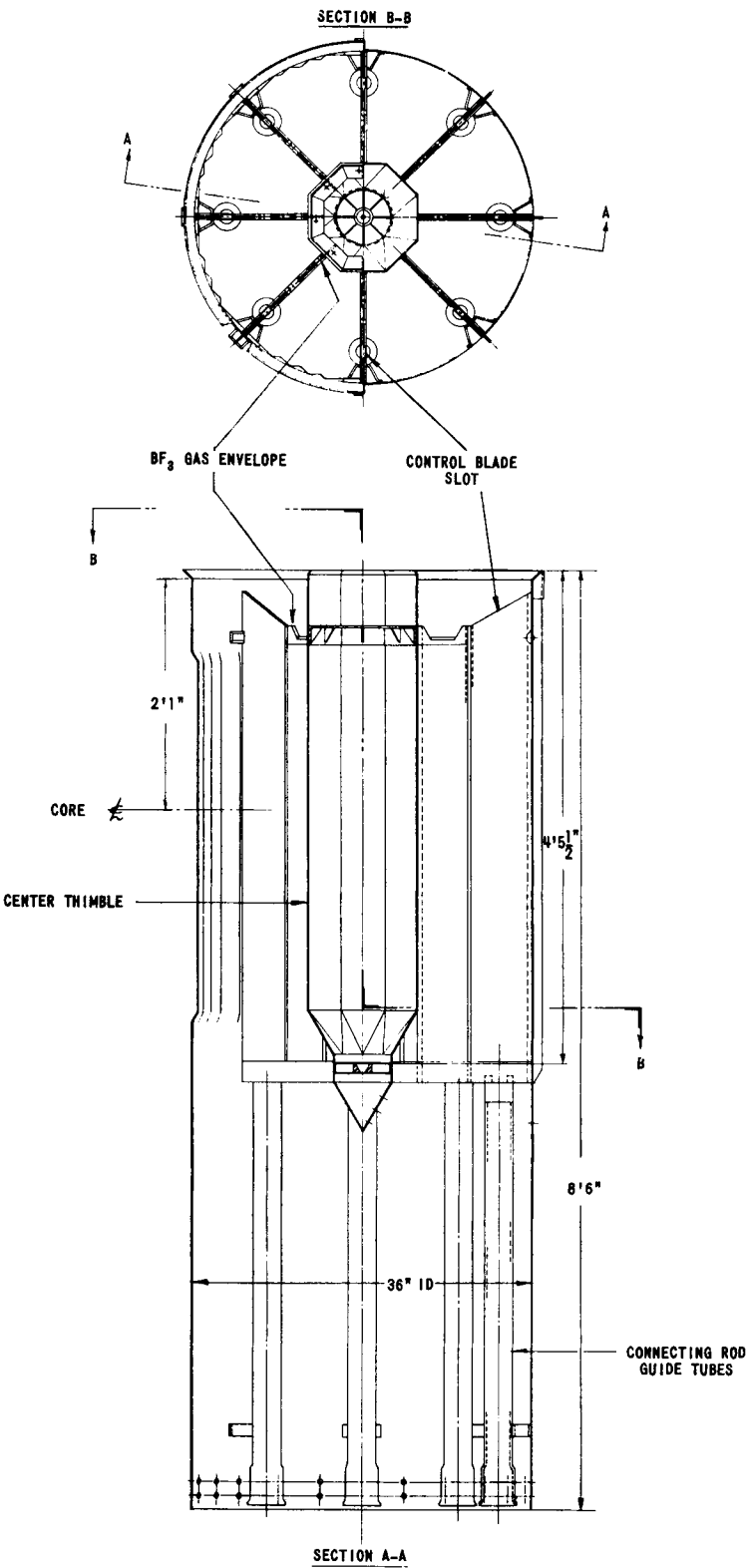


FIG. 4  
CORE SHROUD AND CENTER THIMBLE SUPPORT STRUCTURE  
(Ref. Dwg. RE-1-21960-F)

## 2. Control Systems

Reactor control is achieved through the combination of a mechanical and a fluid control system. The control elements of the two systems are located in the eight radial slots in the core between the fuel subassemblies. The portion of the slots nearest the inner reflector is assigned to the fluid system for shim control. The outer portion of the slots is allotted to the mechanically operated blades for regulating and safety purposes.

### a. Mechanical Control

Mechanical control is effected with eight control blades ( $\frac{1}{4}$  in. x 5 in. x 12 in.) fabricated of relatively low-cross-section material; any of the 18-8 series stainless steels are acceptable. Two of the blades function as regulating rods. All blades are vertically centered in the core in the scram or full-in position.

During reactor operation the blades are actuated upward out of the core by rack-and-pinion-type drive mechanisms located in the subreactor room (Fig. 5). Maximim blade withdrawal is 26 in. The blades are attached to the drives through connecting rods centered in guide bushings in the tubular support columns. The support columns also shield the rods against the dynamic force of the incoming coolant.

The connecting rods and support columns are fabricated in sections to facilitate removal and replacement in the subreactor room. Zirconium is used throughout to minimize parasitic neutron absorption.

Each blade is provided with a remotely operated latch to disengage the blade from the rod. The blades are replaced whenever the fuel assembly is replaced and are disconnected by a compound movement in the latching mechanism. Coolant flow past the blades prevents excessive heating of the latch components.

The vertical thimbles in the subreactor room contain and support the rack-and-pinion assemblies (Fig. 6). The pinion drive shaft enters the thimble through a flanged opening near the top. A mechanical labyrinth-type, collected-leakage seal is used on the drive shaft at the point of entry to the seal housing. Clear, filtered D<sub>2</sub>O is pumped into the drive shaft housing on the reactor side of the shaft seal to prevent settling of sediment into the drive mechanism and bearings. A shut-off valve, integral with the pinion shaft, prevents loss of reactor water should seal removal become necessary. Drain plugs at the bottom of the thimbles provide for removal of foreign matter should any collect at

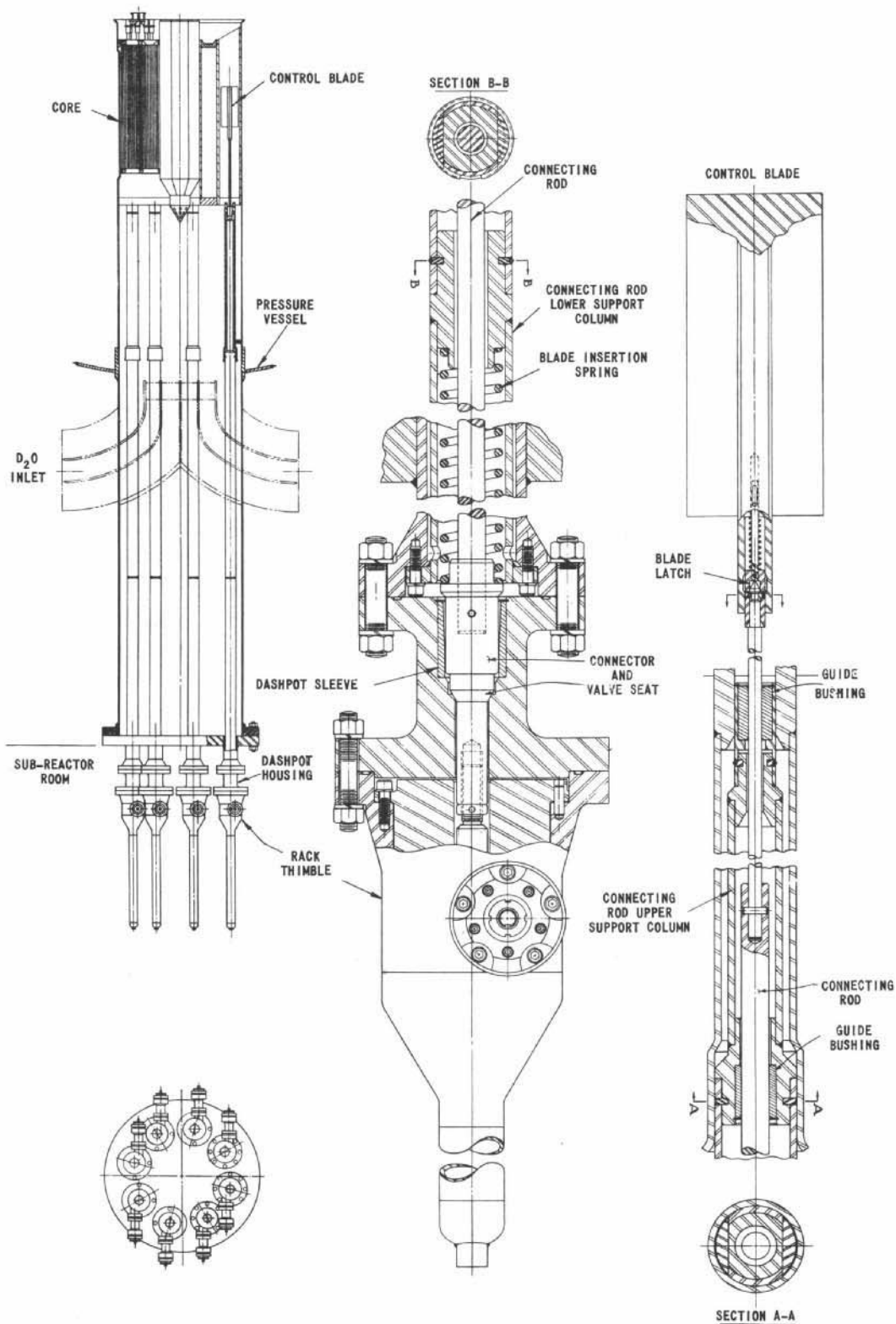


FIG. 5  
CONTROL BLADE - DRIVE INSTALLATION  
(Ref. Dwg. RE-5-23345-F)

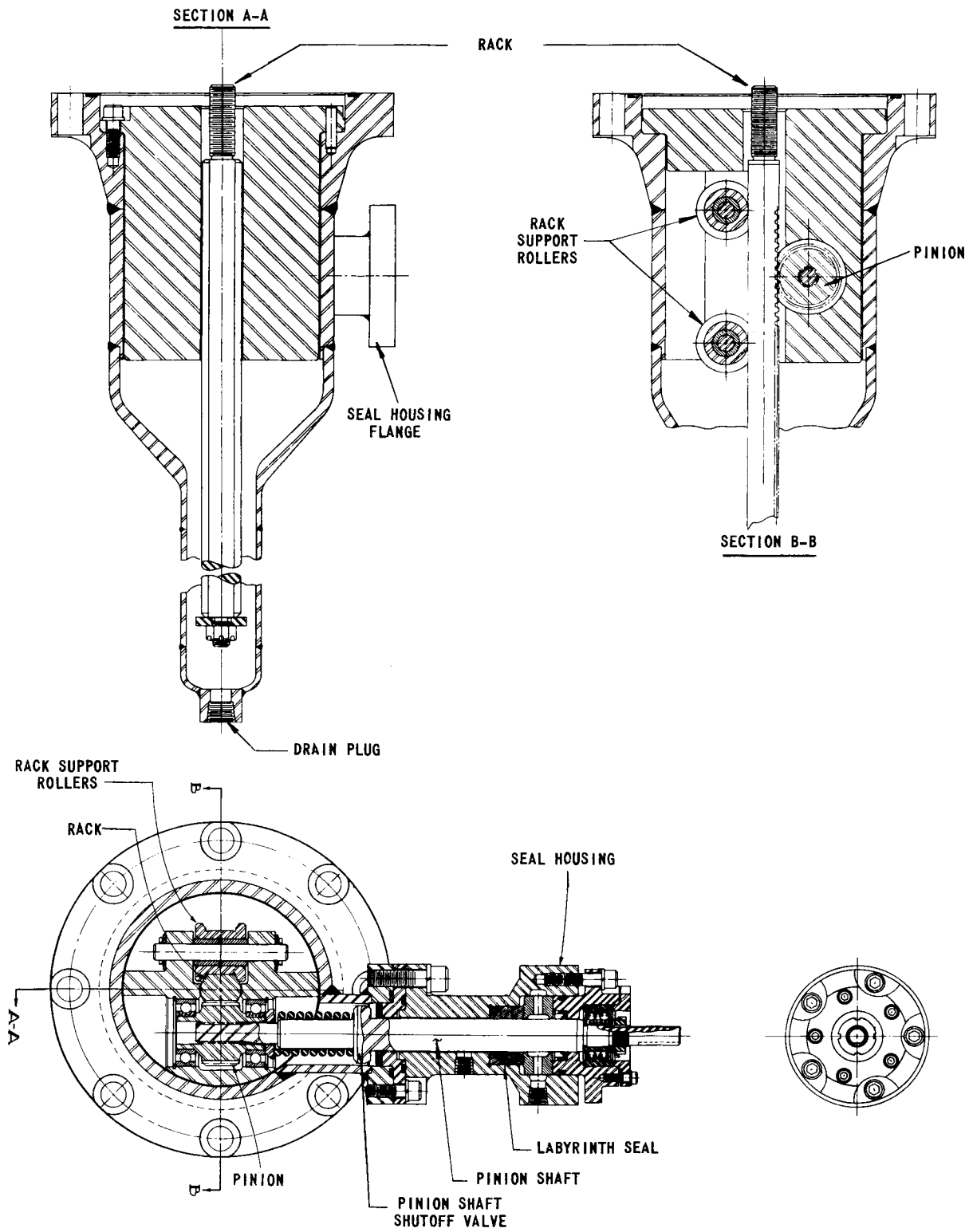


FIG. 6  
RACK-AND-PINION DRIVE THIMBLE  
(Ref. Dwg. RE-5-23344-E)

these points. The pinion drive shafts are coupled to gear head motors through universal-joint extension tubes and magnetic clutches. The reversible motors provide blade motion at the rate of four inches per minute. Release of the control blade is accomplished by de-energizing the magnetic clutch stator. A compression spring (Fig. 5) acting against blade withdrawal adds to the force of gravity to rapidly insert the blade. Full scram can be accomplished in approximately 0.3 sec. The connector between the rack and the connecting rod acts as a piston to decelerate the rod as it enters the dash pot housing. The connector when "full in" functions as a valve plug to permit the removal of the rack-and-pinion thimble without the loss of reactor water.

Indication of the blade position is achieved through a synchrotransmitter and receiver. A lead screw coupled directly to the pinion shaft drives the transmitter through a set of reduction gears. The same lead screw actuates a pair of limit switches to restrict movement of the control rod. The lead screw is positioned on the reactor side of the magnetic clutch to provide continuous indication of blade position. The indicators, clutches and motors are mounted on platforms suspended from the ceiling to maximize the available amount of floor space (see Fig. 10).

#### b. Fluid Control System

The proposed fluid system consists of eight separately controlled, recirculating systems of boron-10-enriched boron trifluoride gas. Each system is self-contained except for an external make-up source of enriched gas to each circuit. Each system contains a reservoir of enriched boron trifluoride gas maintained at a predetermined pressure by circuit compressors. The flow of gas from the reservoir through the reactor is controlled by remotely operated, motorized, pressure-regulating valves installed in both the inlet and the outlet lines of the reactor circuit. The gas flows through the inlet regulating valve to the manifold secured to the water inlet extension tube cover directly below the reactor core. Six zirconium tubes, each in the form of an inverted "U," extend from the manifold into the reactor fluid control slot.

In the core each slot allotted for fluid control contains a completely enclosed zirconium envelope that extends from the top of the core to the lower end of the inlet water extension tube. The lower portion of the envelopes are flange-sealed to the extension tube cover. The control tubes are contained within these envelopes with the closed end of the "U" at the top of the core. Boron trifluoride flows up through the core and back down through the manifold to the outlet regulating valve. The sealed envelopes prevent the escape of gas into the reactor should leakage occur in one of the gas tubes. A self-contained counter-flow circulating system provides cooling within the envelopes. Instruments may be incorporated in the cooling system to detect possible gas leakage.

The gas leaving the manifold is directed to a filter circuit before entering the outlet pressure-regulating valve. The filters remove the solids formed in the reactor by radiation damage or burnup. Duplicate filters connected in parallel allow filter replacement without the interruption of gas flow. The gas from the outlet regulating valve passes through a second filter to a storage tank for recycling through the system.

The removal of the gaseous byproducts formed during the transmutation of the boron trifluoride is performed in a side-stream purification system on the outlet side of the reactor. A portion of the gas leaving the outlet regulating valve is passed through a heated reaction chamber packed with elemental boron-10. The boron-10 reacts with the elemental fluorine in the gas to form enriched boron trifluoride. After the fluorine is removed, the gas is directed to a liquid nitrogen condenser where the boron trifluoride is liquified and the remaining gaseous helium is vented away. The liquid boron trifluoride is drained to a heated chamber for vaporization back to its gaseous state. The purified gaseous boron trifluoride is stored for recirculation through the system.

An auxiliary flushing and evacuation system is available for removing moisture and particles from the gas circuits. Each circuit is thoroughly flushed with a dry inert gas and evacuated before boron trifluoride is admitted to the system. This procedure reduces internal corrosion and contamination. Accumulators, charged to a high pressure with enriched boron trifluoride, are provided in each system for emergency shutdown. The accumulators are connected to the reactor inlet lines through solenoid-operated shutoff valves. Interruption of the solenoid current will open the valves and saturate the reactor control circuit with high-density gas. Pressure and flow transducers installed throughout the system give constant indication of circuit conditions.

### 3. Pressure Vessel

The pressure vessel (Fig. 7) is a cylinder (13 ft ID x 13 ft high) with ellipsoidal heads fabricated from zirconium (1-in. wall). The upper ellipsoidal head contains an envelope-type projection which flares into a flanged service opening (44 in. ID). The upper head also contains two 24-inch coolant outlet nozzles.

The lower head contains a centrally located 36-inch coolant inlet nozzle. The nozzle also houses the guide tubes for the rods interconnecting the control blades and drive mechanisms. Two 24-inch D<sub>2</sub>O inlet lines enter the 36-inch extension beneath the vessel. The 36-inch extension contains additional control blade shaft guide bearings, a flow divider and a bottom shield plug which opens in the ceiling of the subreactor room. The lower head also contains a tube (22 in. ID) for the fuel loading and unloading mechanism.



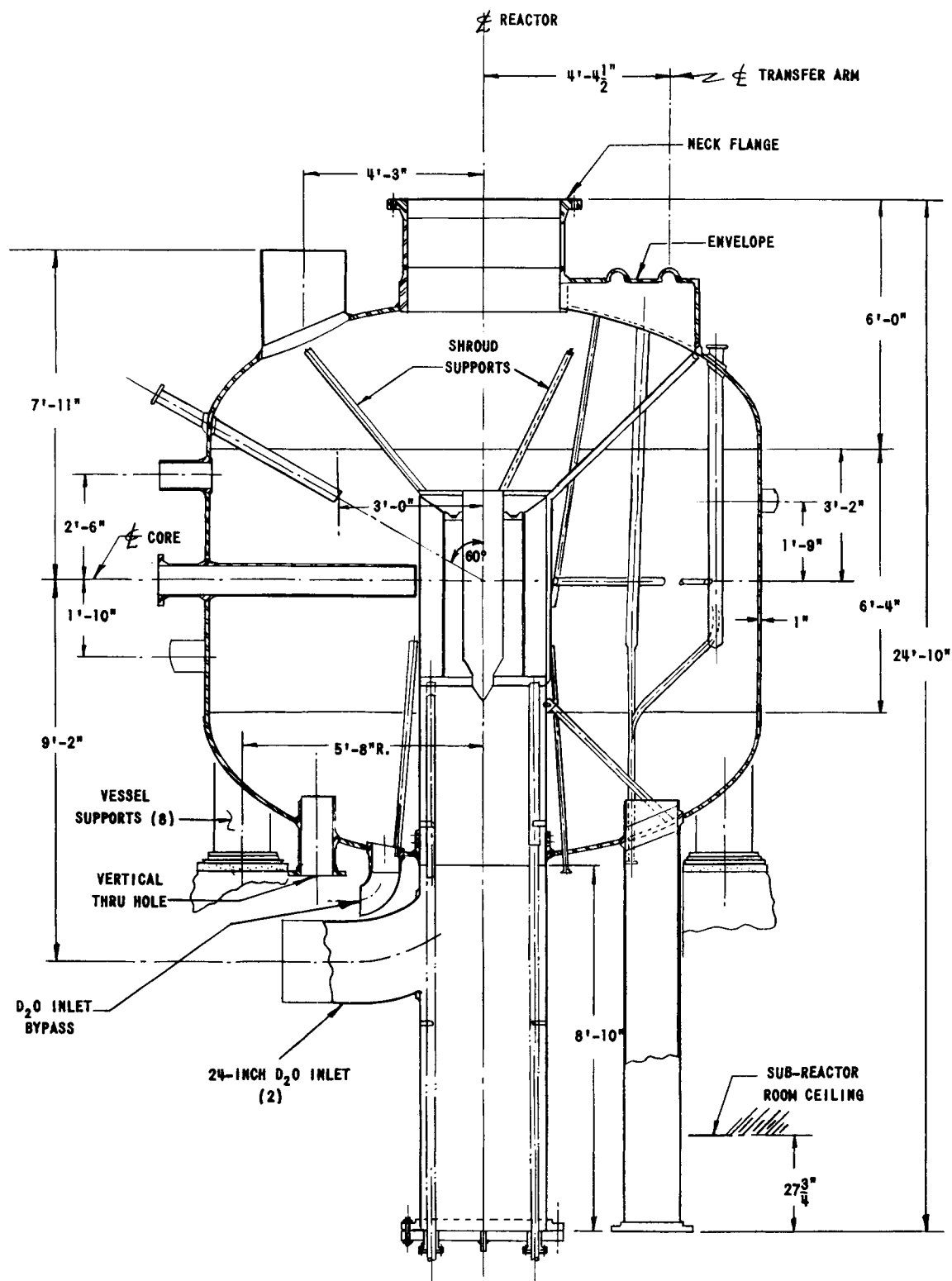


FIG. 7  
REACTOR PRESSURE VESSEL  
(Rev. Dwg. RE-1-21871-F)

The additional vessel openings for experimental facilities are described in Section 5.

Table II lists the respective weights of the pressure vessel and internals. The totals do not include the coolant lines or the extension below the lower head.

Table II

SUMMARY OF PRESSURE VESSEL CHARACTERISTICS  
AND INTERNALS

Design pressure	100 psi
Operating pressure	60 psi
Operating temperature	130°F
Volume	1550 ft <sup>3</sup>
Weights (less D <sub>2</sub> O)	
Vessel	12 tons
Core, internal structure, control rods	1 ton
Closure	$\frac{1}{2}$ ton
Experimental facilities	2 $\frac{1}{2}$ tons

Accordingly, the empty weight of the vessel and internals is 16 tons. When filled with D<sub>2</sub>O (1590 gal), the total weight at operating temperature is about 68 ton.

The vessel is mounted on eight dual-tube supports (Fig. 8) designed to allow circulation of a borated coolant between the inner and outer sections. Lead plugs (6 in. thick) are inserted in the cavities of the support to provide a radiation shield. A lubrite bearing element ( $\frac{1}{2}$  in. thick) in the base of the support compensates for thermal expansion of the pressure vessel. The supports rest on a ring-type bed plate ( $1\frac{1}{4}$  in. thick) that is grouted into the concrete foundation.

4. Shielding

a. Thermal Shield

The core is surrounded by about 5 feet of D<sub>2</sub>O which holds the thermal neutron flux at a high level throughout the reflector. This high thermal flux is convenient for experimental holes, but it creates a major shielding problem because of the capture gamma production that occurs in the reactor vessel wall. The total capture gamma flux at the inside surface of the vessel from 4-, 6-, and 8-Mev gammas in the zirconium is estimated to be about  $1.42 \times 10^{13}$  Mev/(cm<sup>2</sup>)(sec). The core gammas at this surface are lower by a factor of 10. A thermal shield is

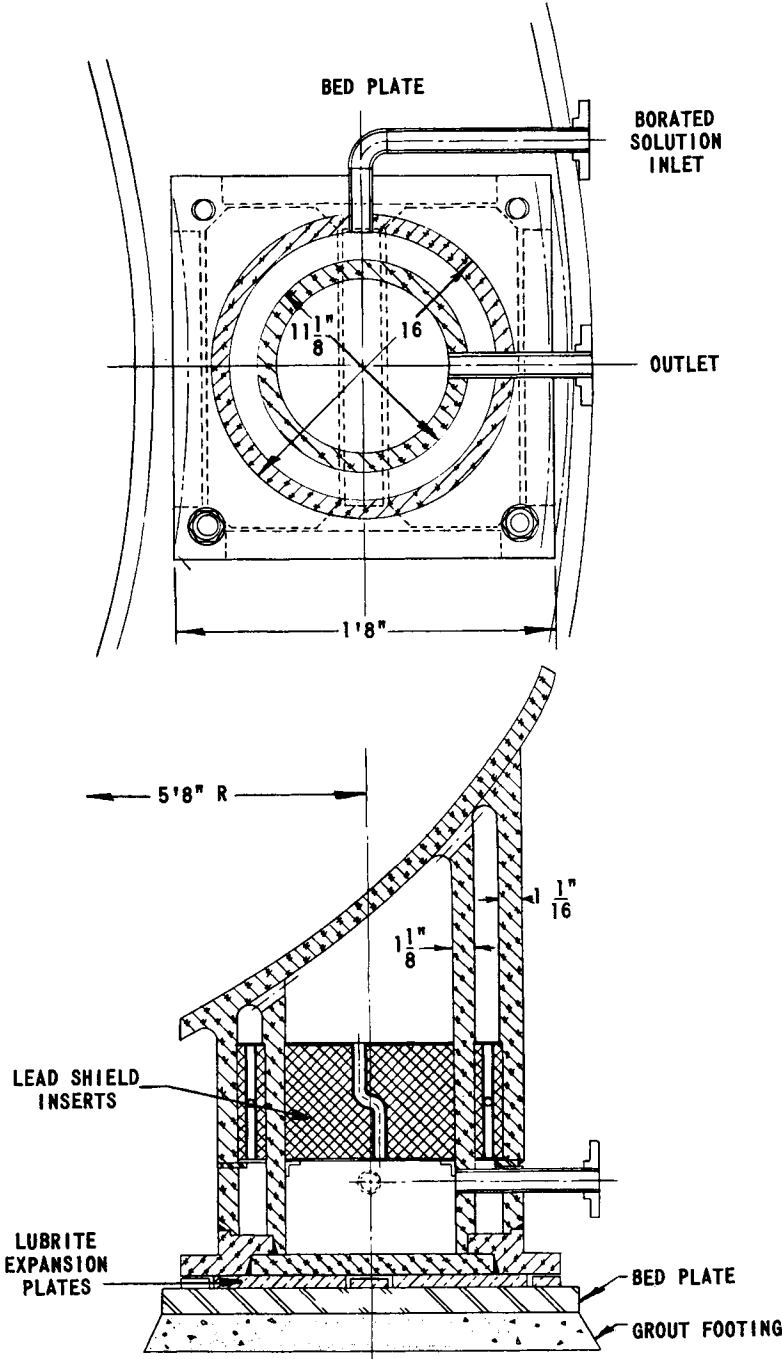


FIG. 8  
PRESSURE VESSEL SUPPORTS  
(Ref. Dwg. RE-1-24394-F)

required to attenuate all forms of radiation to a level such that the final reduction to tolerance levels by the Biological Shield does not create a temperature difference greater than 50°F in the Biological Shield.

The design chosen for the thermal shield provides a  $\frac{1}{4}$ -inch steel plate immediately outside the vessel, followed by a  $1\frac{1}{2}$  in.-wide coolant passage filled with a borated water solution. The borated solution is sufficient to lower the thermal flux below the level created by the thermalization of the fast flux beyond this point.

The capture gamma flux from the reactor vessel and the  $\frac{1}{4}$ -inch steel plate are the major sources of radiation which determine the balance of the shield design. It is shown in Appendix C that, for the case of magnetite concrete, the total incident gamma flux cannot exceed  $2 \times 10^{11}$  Mev/(cm<sup>2</sup>)(sec). It was determined that 12 in. of steel will produce the required attenuation. The vertical thermal shield conforming to this design is shown in Fig. 9. The steel is divided into two 6-inch slabs with a 1-inch space for circulating borated solution between them.

The thermal shield under the core is an 8-in. high boxlike framework made of  $\frac{1}{4}$ -inch steel plate, containing lead balls to a height of 6 in. and a circulating borated coolant. Below the core in the 36-inch inlet duct and at the intersection of the inlet pipes is a removable steel thermal shield that also serves as a flow divider, plus a 12-inch steel cover backed by 10 in. of lead encased in steel (Fig. 10).

The thermal shield above the vessel is similar to the vertical thermal shield. Above this area, a steel container filled with lead and cooling coils provides additional shielding. A 2-inch steel plate inside the reactor vessel neck lowers the neutron flux. A composite steel and lead plug over the closure area completes the shield (Fig. 9).

The thermal shield will absorb about 1.5 Mw during steady-state operation, due to neutron absorption in the borated solution. The gamma heating of the shield presents no problems since the heat generation rate is low and adequate cooling is provided.

#### b. Biological Shield

The design calculations for the biological or bulk shielding were made for magnetite concrete having a density of 3.62 gm/cm<sup>3</sup>. On this basis 7.5 ft is adequate to reduce the radiation to tolerance levels at the outer face. Dense concrete was chosen to reduce the thickness of the shield. However, space requirements for the proposed number and size of experimental facilities sets the biological shield thickness at about 10 ft. Consequently, in final design, the average density of the biological shield need be at some level between magnetite and ordinary

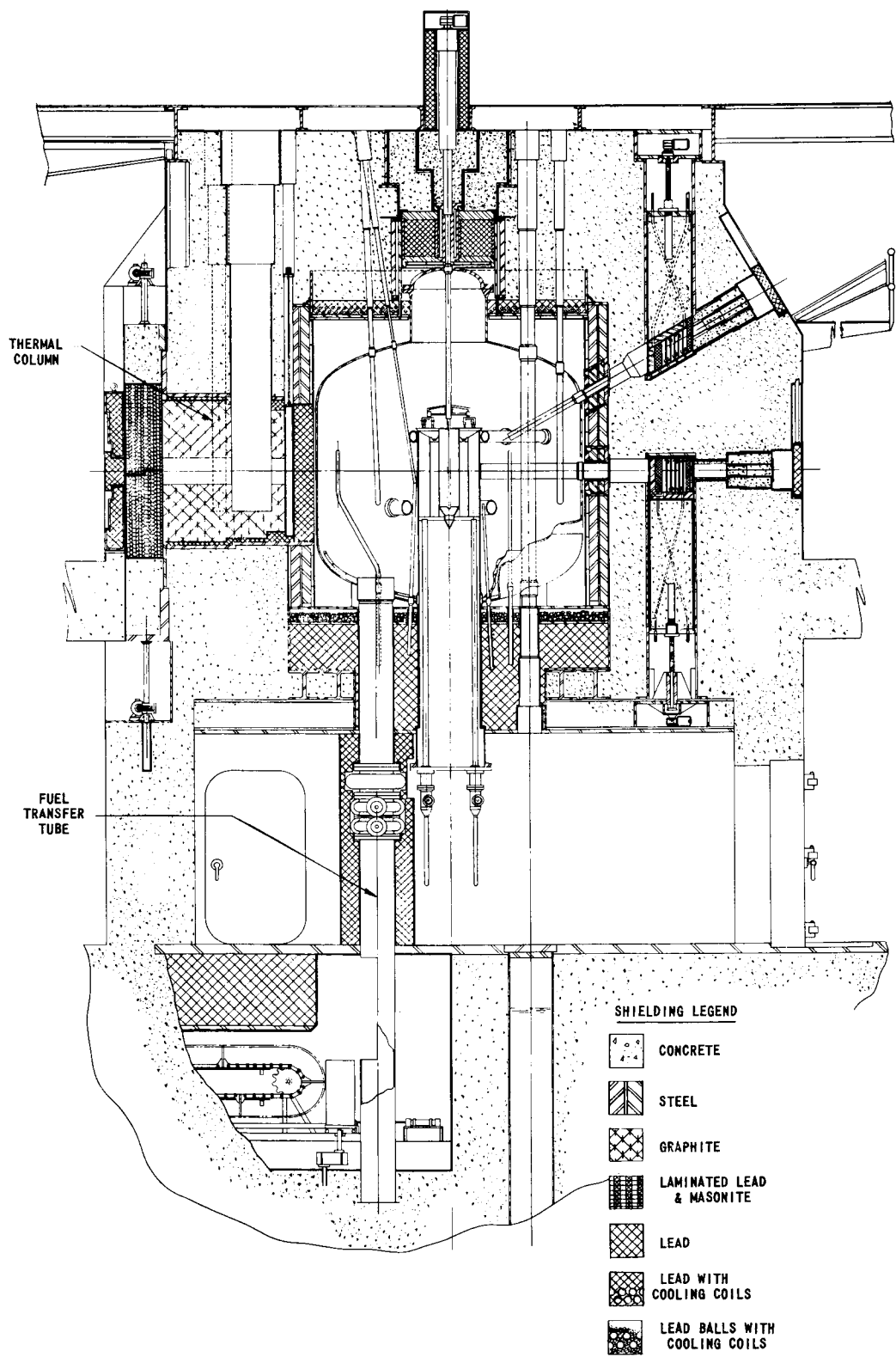


FIG. 9  
SHIELDING ARRANGEMENT (ELEVATION THROUGH THERMAL COLUMN)  
(Ref. Dwg. RE-5-23342-F)

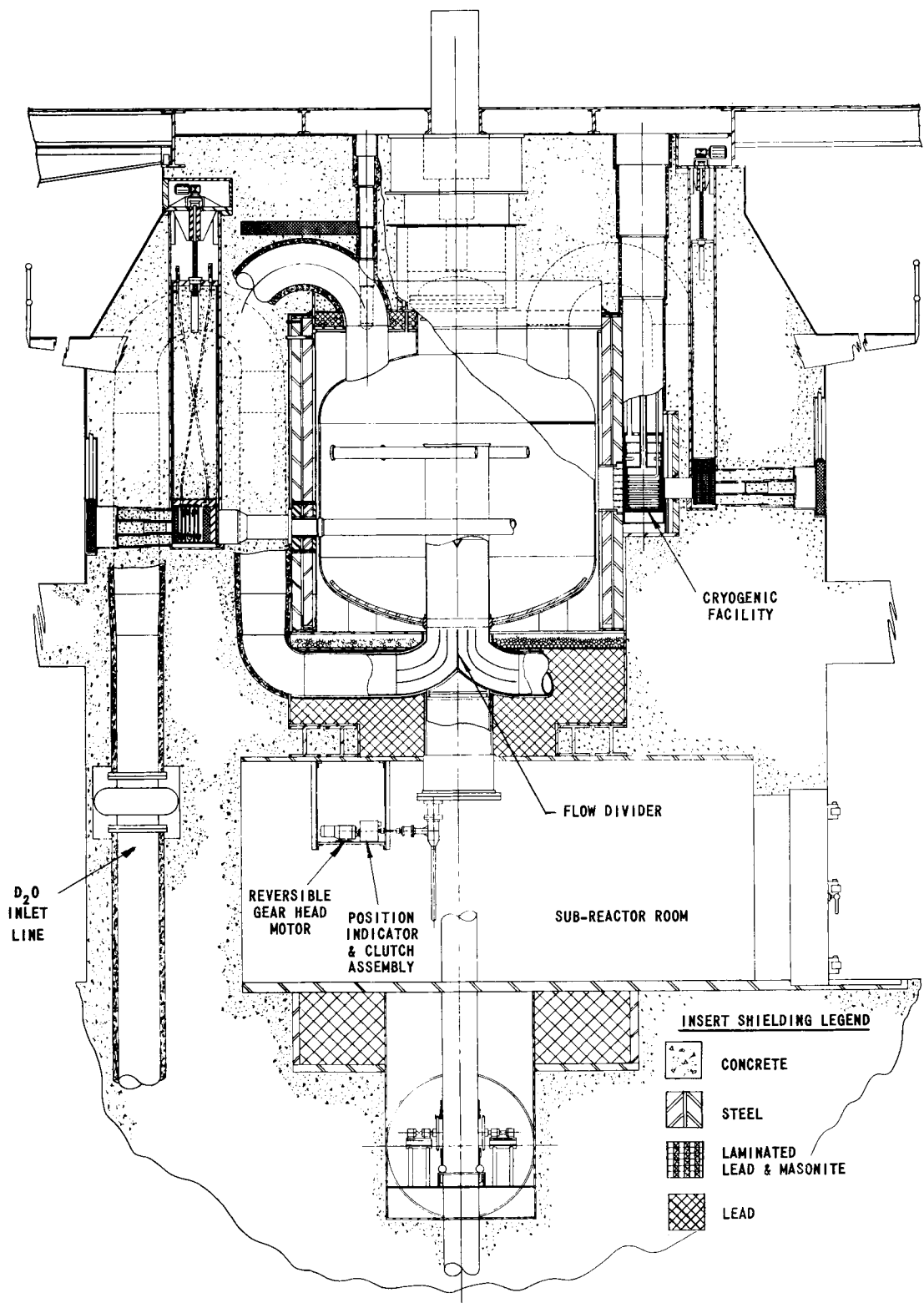


FIG. 10  
SHIELDING ARRANGEMENT (ELEVATION THROUGH CRYOGENIC FACILITY)  
(Ref. Dwg. RE-5-22232-F)

concrete. While calculations show the 10-ft concrete thickness is adequate, analyses have not been made for the areas of the water pipe and experimental facility penetrations where the shield may be weak and require more dense shields.

The shielding pertinent to the experimental facilities is described in the following section.

## 5. Experimental Facilities

The design of the experimental facilities is guided by several primary considerations:

- (1) to install the maximum number of facilities in the space available and in the region of highest neutron flux, consistent with a minimum cost in reactivity;
- (2) to incorporate maximum flexibility in utilization without sacrificing the basic function of each facility in its respective location;
- (3) to adhere to well-established or conventional designs and material, wherever possible; and
- (4) to design for maximum life expectancy, with access for maintenance and repair to components in critical regions where mechanical integrity may be compromised.

Some deviation from the above criteria is necessary due to problems associated with the high heat flux generated in the Mighty Mouse. One of the typical problems confronted is that of removing the heat generated in facilities that closely approach the core. Gamma heat generation in material near the core face is not adequately removed by normal circulation of the primary D<sub>2</sub>O coolant. Therefore, auxiliary, high-velocity coolant systems must be employed to prevent local boiling at the metal surfaces.

Another problem is that of compensating for thermal expansion at facility penetrations in the pressure vessel walls. For example, heating of the vessel walls creates an upward movement of 0.06 in. at the point of entry of the horizontal beam holes. This causes a bending moment in the vessel wall and places the beam hole in shear. These physical stresses, combined with operating pressures and thermal stresses, preclude rigid interconnection, and expansion joints become the most practical means of eliminating the undesired stresses.

Special gates must be designed to resolve the problem of shielding the high levels of fast neutron flux in beam holes that terminate at the core face. These and other associated problems are discussed in subsequent sections.

To a large degree, the basic features of the experimental facilities listed in Table III have been defined and much of the design calculations have been performed. However, the design effort on the more complex facilities (e.g., Cryogenic Facility) has served only to identify the more promising concepts and corresponding avenues of research and development. In the case of experimental facilities external to the reactor proper (e.g., Spent Fuel Irradiation Facility), there is little more than a recognition of the potential of utilizing spent fuel for irradiation studies.

Figure 11 shows the relative position of the experimental facilities installed within the reactor vessel and adjacent shielding.

#### a. Vertical Facilities

There are 49 vertical facilities for irradiation experiments and isotope production. Figure 12 gives the relative position and the nomenclature used to identify each facility. Access to all holes is from the top of the reactor. The through-holes have access ports that open into the subreactor room.

Each of the thimbles and through holes is equipped with stepped shield plugs fabricated of steel, lead, and concrete. The tips of the plugs are cooled by light water circulated through passages cast or drilled through the steel and lead sections. The plugs are pierced by two spiral conduits to accommodate experimental leads and cooling pipes to the samples being irradiated. The tops of the plugs feature a gastight seal to prevent in-leakage of air during operation, thereby reducing the possibility of  $A^{41}$  production. Prior to operation, the thimbles are purged with inert gas to remove any air present. Protection from streaming is accomplished through one step approximately halfway down the plugs, and by offsets in the tip and at the top of the plug at the bolting flange. Cooling water flowing through the annulus between the inside and outside tubes gives protection from streaming through those openings in addition to the stepped design. The lower sections of the plugs will become quite active due to their proximity to the core and must be properly shielded when withdrawn from the thimbles. A universal coffin will be provided for removing and transporting the plugs to storage holes in the main floor during periods of shutdown when experiments are being removed from the thimbles.

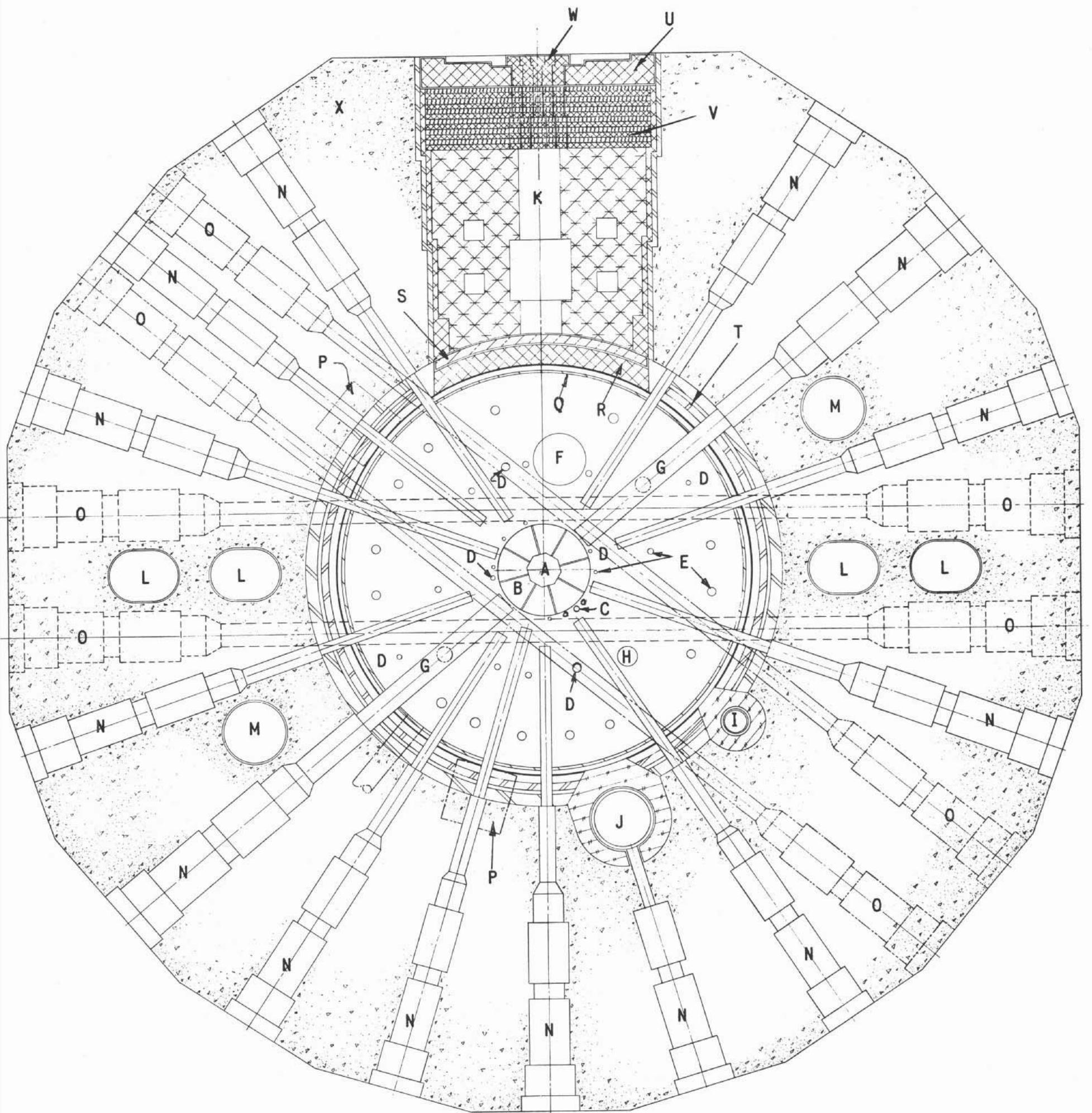


Table III  
SUMMARY OF EXPERIMENTAL FACILITIES

Facility	Size; ID in.	Position, Degrees Clockwise from Thermal Column Centerline	Distance from Vertical Centerline of Core, in.	Neutron Flux Range x 10 <sup>-15</sup> n/ (cm <sup>2</sup> )(sec)		Remarks
				Thermal	Fast	
<u>Vertical Thimbles</u>						
VT- 1	1.5	Center	Center	5 -7	2.6	Retractable.
VT- 2	1.0	92	20	2 -4	2.3	At angle of 8.5 degrees to vertical.
VT- 3	1.0	126				
VT- 4	1.0	157				
VT- 5	1.0	174				
VT- 6	1.0	274				
VT- 7	1.0	306				
VT- 8	2.0	26	43	0.8-1		At angle of 2 degrees to vertical.
VT- 9	2.0	81				
VT-10	2.0	189				
VT-11	2.0	206				
VT-12	2.0	261				
VT-13	2.0	320				
VT-14	2.0	333	66	0.1-2		Any of the 3-inch ID thimbles may be used as "startup" instru- ment holes.
VT-15	3.0	25				
VT-16	3.0	37				
VT-17	3.0	82				
VT-18	3.0	98				
VT-19	3.0	125				
VT-20	3.0	158				
VT-21	3.0	172				
VT-22	3.0	188				
VT-23	3.0	205				
VT-24	3.0	219				
VT-25	3.0	262				
VT-26	3.0	278	113			Cryogenic beam facility. N <sup>16</sup> gamma-irradiation thimble.
VT-27	3.0	304				
VT-28	3.0	318				
VT-29	3.0	340				
VT-30	3.0	356				
VT-31	22	163				
GT- 1	6.0	50	In D <sub>2</sub> O outlet			
GT- 2	6.0	230				
<u>Vertical Through Holes</u>						
VTH-1	8.0	137	48	0.7-0.9		Lower end access in subreactor room.
VTH-2	8.0	130	96			Cryogenic through hole.
<u>Vertical General Purpose Holes</u>						
GP- 1	24 x 24	197	93			
GP- 2	24 x 24	310				
<u>Vertical Access Holes</u>						
TCV-1	24 x 24	Located in thermal column graphite.				Cadmium ratio >10 <sup>4</sup> in. graphite thermal column.
TCV-2	8 x 8					
TCV-3	8 x 8					
TCV-4	8 x 8					
TCV-5	8 x 8					

Table III (Cont'd.)

Facility	Size; ID in.	Position, Degrees Clockwise from Thermal Column Centerline	Distance from Vertical Centerline of Core, in.	Neutron Flux Range x 10 <sup>-15</sup> n/ (cm <sup>2</sup> )(sec)		Remarks
				Thermal	Fast	
Rabbit Systems						
Pneumatic						
RP-1	0.75	148	19	0.9-2	2	Terminates at bottom edge of active core.
Hydraulic						
RH-1	1.5	83	19	2 -4	2	Terminates at horizontal centerline of core.
RH-2	1.5	263				
RH-3	1.5	157	43	0.8-1	}	Terminate at 1.5 ft above horizontal centerline of core.
RH-4	1.5	337	43	0.8-1		
RH-5	1.5	60	66	0.1-0.2		
RH-6	1.5	240	66	0.1-0.2		
Horizontal Beam Facilities						
HB-1	3.0	30	30	0.9-2		
HB-2	8.0	50	19	2 -4	2	
HB-3	3.0	71	30	0.9-2		
HB-4	4.0	110	19	2 -4	2	
HB-5	3.0	147	24	1 -3	0.6	
HB-6	4.0	163	Terminates in the 22-inch cryogenic facility.			
HB-7	4.0	180	30	0.9-2		
HB-8	3.0	196	24	1 -3	0.6	
HB-9	4.0	210	30	0.9-2		
HB-10	8.0	230	19	2 -4	2	
HB-11	3.0	251	30	0.9-2		
HB-12	4.0	290	19	2 -4	2	
HB-13	3.0	310	30	0.9-2		
HB-14	3.0	327	24	1 -3	0.6	
HTH-1	8.0	90	19	0.9-2	2	
HTH-2	6.0	130	19	0.9-2	2	
HTH-3	8.0	270	19	0.9-2	2	
HTH-4	6.0	310	19	0.9-2	2	
Down Beam Hole						
DB-1	2.0	30	45	0.6-0.8		Holes are angled down toward the core at 30 degrees to the horizontal.
DB-2	4.0	71				
DB-3	4.0	147				
DB-4	2.0	180				
DB-5	4.0	210				
DB-6	4.0	251				
DB-7	2.0	327				
Horizontal Thermal Column Access Hole						
TC-1	16 x 16	0	Terminates at neutron shutter.		Access from above through TCV-1.	
Spent Fuel Irradiation Facilities						
SFI-1	Located in cave facility in basement adjacent to D <sub>2</sub> O fuel storage.					Source of photoneutron and gamma flux.
SFI-2	Located in light-water storage canal.					Source of gamma flux.



A CENTER THIMBLE  
 B FUEL SUBASSEMBLIES  
 C PNEUMATIC RABBIT HOLE  
 D HYDRAULIC RABBIT HOLES  
 E VERTICAL THIMBLES  
 F FUEL TRANSFER TUBE  
 G GAMMA IRRADIATION THIMBLES  
 H VERTICAL THROUGH HOLE  
 I CRYOGENIC THROUGH HOLE  
 J CRYOGENIC BEAM FACILITY  
 K THERMAL COLUMN  
 L D<sub>2</sub>O INLET

M D<sub>2</sub>O OUTLET  
 N HORIZONTAL BEAM HOLES  
 O HORIZONTAL THROUGH HOLES  
 P GENERAL PURPOSE FACILITIES  
 Q PRESSURE VESSEL  
 R GAMMA SHIELD  
 S NEUTRON SHUTTER  
 T THERMAL SHIELD  
 U LEAD SHIELD  
 V LEAD AND MASONITE GATE  
 W LEAD PLUGS  
 X CONCRETE BIOLOGICAL SHIELD

--- FACILITIES BELOW CORE CENTERLINE  
 --- FACILITIES ABOVE CORE CENTERLINE

FIG. II  
 ORIENTATION OF EXPERIMENTAL FACILITIES  
 ( Ref. Dwg. RE-5-22260-E )

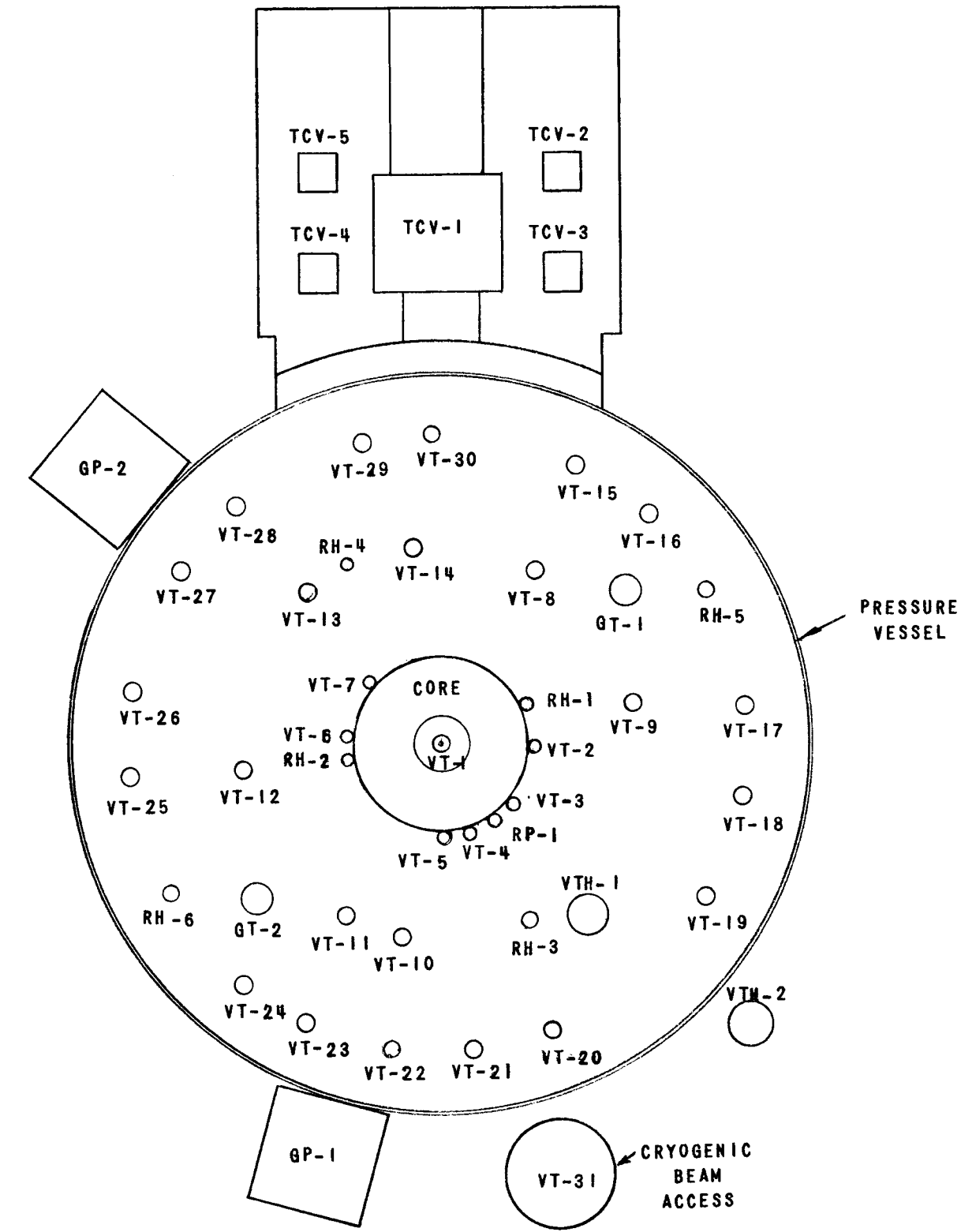


FIG. 12

RELATIVE POSITIONS OF VERTICAL EXPERIMENTAL FACILITIES  
(ELEVATION: 100 ft)

The removal of samples from the thimbles is accomplished through the use of shielded casks with built-in grapple mechanisms.

Each thimble is serviced by utilities that are carried through conduits under the steel deck one foot above the biological shield. The normal requirements will be met by permanent installations of the following utilities:

- Demineralized water ( $H_2O$ ) and drain
- Process water ( $D_2O$ ) and drain
- Compressed air (100 psi) and hot exhaust
- Helium supply and return
- 120 volt ac, 60 cycle, 1-phase
- 240 volt ac, 60 cycle, 3-phase
- 120 volt dc signal circuit
- Intercom jacks
- Telephone jacks
- Two spare conduits (2 in. ID)

Space has been allocated for the installation of special utilities, piping, and wiring, as may be required. When distances between experiments and instrumentation are not critical, leads may be carried in ducts to the basement areas where space is available for experimental apparatus.

#### Central Thimble (VT-1)

The central thimble (1.5 in. ID) provides access to the region of maximum thermal neutron flux [ $7 \times 10^{15} \text{ n}/(\text{cm}^2)(\text{sec})$ ] and may be used for either irradiation experiments or isotope production. It is located in the center of the inner reflector and terminates at the bottom edge of the core.

Preliminary design calculations indicated that up to approximately one gram of highly fissionable material, such as curium-245, may be irradiated in the central thimble. The heat produced in the tube walls and the samples contained therein is removed by  $D_2O$  circulated through the thimble. Due to the possibility of accidental release of active material or fission products from the sample, it is not desirable to discharge the cooling water into the reflector. Therefore, a re-entry-type thimble formed of two concentric tubes is necessary to direct the cooling water down the inside tube to the sample and thence back up the annulus between the inner and outer tubes. Instrumentation leads to the sample are carried in the inside tube. The velocity of the coolant through the thimble for the case of 1 gram of curium-245 will be about 20 fps in the annulus, and about 30 fps over a tubular-type curium sample (see Appendix D).

The volume of metal contained in the lower section of the tube is critical in its effect on the core; therefore every effort has been made to design it with the minimum wall thickness allowed by the ASME Unfired Pressure Vessel Code. The wall thickness chosen is 0.031 in. where the tube is 1.5 in. in diameter, and 0.063 in. where the tube increases to 3 in. in diameter.

A secondary function of the center thimble is to provide positive hold-down of the fuel assemblies during operation. Supplementing the locks integral with the fuel assembly, the center thimble has a hold-down spider permanently attached to the outer tube. When the fuel is to be removed, the center thimble must be retracted out of the core to permit access by the remote-controlled fuel-removal equipment.

The retracting mechanism consists of an electric motor-driven ball-nut screw assembly which provides a 9-ft travel. The outer sleeve of the thimble passes through a dynamic seal in the pressure vessel cover and is connected to the ball-nut that is driven by rotating the hollow lead screw. Guides riding in the outer sleeve prevent the ball-nut and attached thimble from rotating so as to maintain proper positioning of the fuel hold-down arms on the thimble. The hold-down arms must mate with the pins on the fuel assemblies.

Due to the 9-ft travel of the thimble, it is necessary to project the thimble housing, drives and motor 5 ft above the top floor of the reactor. During fueling and sample-removal operation, a special shielding coffin is lowered over the exposed thimble.

It is anticipated that it may be desirable to remove some irradiated samples before the end of the fuel cycle. In such instances a mechanical rabbit could be used in the central thimble to insert and remove material. However, the secondary function of the central thimble as a fuel hold-down device precludes any possibility of utilizing the retractable feature for this purpose. The mechanical rabbit might be an integral part of the special coffin into which the rabbit and the irradiated sample can be drawn and then transferred to the canal or other locations for unloading.

#### 1-in. ID Thimbles (VT-2 to VT-7)

Figure 13 shows one of the six thimbles installed in the reflector at an angle of 8.5 degrees to the vertical axis of the core shroud. The lower ends of the thimbles terminate 6 in. below the horizontal centerline of the core and 1 in. from the core face. The unperturbed thermal neutron flux at this point is  $2-4 \times 10^{15} \text{ n}/(\text{cm}^2)(\text{sec})$ . The fast neutron flux (10 kev - 10 Mev) is approximately  $2.3 \times 10^{15} \text{ n}/(\text{cm}^2)(\text{sec})$ .

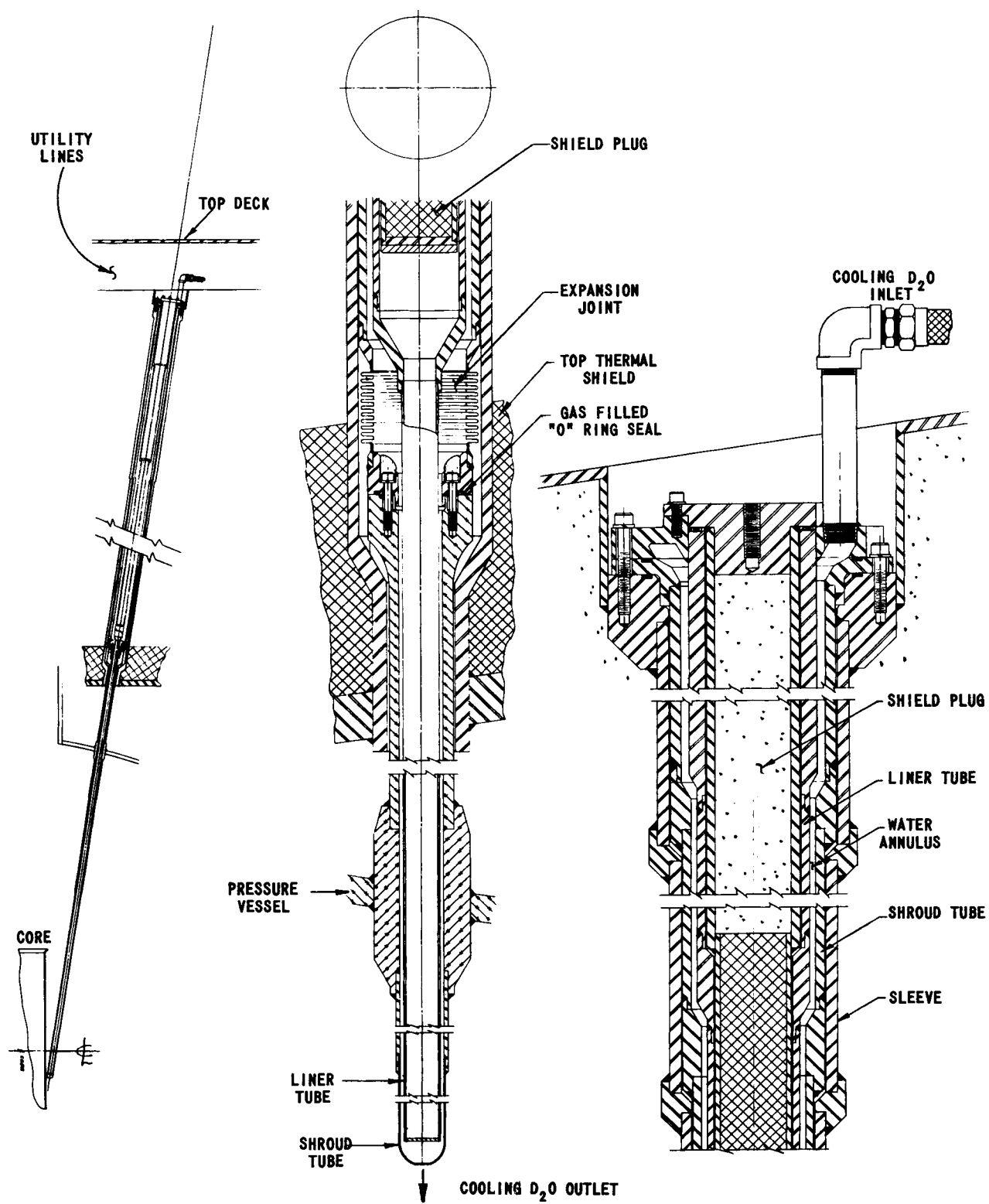


FIG. 13  
TYPICAL VERTICAL THIMBLE INSTALLATION - VT-2 TO VT-7  
(Ref. Dwg. RE-5-24226-E)

The thimbles are designed for "dry" irradiations. However, auxiliary cooling must be provided to remove the heat generated in the zirconium tubes (18 watt/gram). By using the minimum wall thickness allowed (0.03125 in.), the volume of metal in such a small thimble has little influence on the core and generates but a nominal amount of additional heat. Calculations indicated that the additional flow of D<sub>2</sub>O at 25 fps through the  $\frac{5}{32}$ -in. annulus between the tubes and into the bulk reflector will be sufficient to remove the 19,000 watts of heat generated in the tube wall.

The inner tube is flanged and bolted at the top of the access hole and may be removed for inspection and repairs. The section of the outer tube located inside the vessel is welded to the wall and cannot be removed. The section outside the vessel can be removed by unbolting the expansion joint with extension tools and withdrawing the entire unit.

#### 2-in. ID Thimbles (VT-8 to VT-14)

Seven 2-in. ID thimbles are located in the D<sub>2</sub>O reflector at an angle of 2 degrees to the vertical axis of the core. The lower ends of the thimbles terminate 1.5 ft below the horizontal centerline of the core and 24 in. from the core face. The unperturbed thermal neutron flux in this region ranges from 0.8 to  $1 \times 10^{15}$  n/(cm<sup>2</sup>)(sec).

Calculations of the heat generation in the tube walls indicated that supplementary cooling is not required within the pressure vessel, as the flow of D<sub>2</sub>O reflector water is sufficient to keep the wall temperature at about 200°F in the lower section of the tube. The thickness of the single-wall tube was calculated to be 0.0625 in. The volume of zirconium in the tube wall is 560 cm<sup>3</sup>. Approximately 6700 watts are generated in the bottom 4 ft of the tube, and 1300 watts in the remaining 4 ft within the reflector. The total of 8000 watts (27,000 Btu/hr) is removed by the D<sub>2</sub>O reflector water flowing at 0.1 fps.

The portion of the thimble between the pressure vessel wall and the thermal shield requires supplementary cooling due to the low velocity of the helium atmosphere in this zone. Calculations showed that temperatures of about 700°F will exist if some means of water cooling is not employed. This section of the tube is, therefore, of double-walled construction; D<sub>2</sub>O cooling water flows down the annulus between the tubes and into the reflector at the vessel wall.

The construction details are similar to those of the 1-in. ID thimble with the exception that the shroud tube terminates at the vessel wall. Structural bracing in the reflector should be designed to allow complete withdrawal of the thimble when necessary. When the thimble is withdrawn, a 2.250-in. opening into the pressure vessel is available for entry of periscopes or other apparatus.



### 3-in. ID Thimbles (VT-15 to VT-30)

There are 16 vertical thimbles located near the periphery of the pressure vessel, 4 ft from the core, that terminate  $1\frac{1}{2}$  ft below the horizontal center line. The neutron and gamma-flux levels at these positions are sufficiently low so that forced coolant is not required along the thimble liners. The wall thickness is a maximum of 0.0937 in., which gives a metal volume of  $12,600 \text{ cm}^3$  for each tube. The heat generated in this volume is 6140 watts (20,900 Btu/hr). This results in a wall temperature of  $170^\circ\text{F}$  with a reflector velocity of 0.1 fps. The section of the tube in the void between the vessel and the thermal shield is jacketed for water cooling in the same manner as the 2-in. ID thimbles.

All other construction details are identical, except for size, with those of the 1-in. and 2-in. ID thimbles.

In addition to irradiations and other experiments, the 3-in. vertical thimbles may be used as instrument holes and, if necessary, as entry ports into the pressure vessel for periscopes during fueling operations. In the latter case, the inner thimble is easily removed at the top flange to provide a 3.50-in. entry hole into the  $\text{D}_2\text{O}$  reflector zone.

It is foreseen that for some experiments it may be desirable to insert a lead-type stringer directly into the  $\text{D}_2\text{O}$  reflector. This could be accomplished by using a modified thimble that extends only a short distance into the reflector with an adequate seal through which the stringer is passed. In such cases the apparatus would be fabricated of zirconium and designed to meet the pressure requirements.

### 8-in. ID Vertical Through Hole (VTH-1)

Two vertical through holes (8 in. ID) are provided for those experiments desiring access from both ends. The holes extend through the  $\text{D}_2\text{O}$  outer reflector, 30 in. from the core face, in an unperturbed thermal neutron flux of  $10^{15} \text{ n}/(\text{cm}^2)(\text{sec})$ .

A double-walled tube with forced cooling water circulating between the walls is necessary for adequate heat removal. A working pressure of 100 psi in the vessel requires a minimum wall thickness of 0.1718 in. for the inner tube. The outer tube is not critical from a pressure standpoint, but for structural rigidity the wall thickness is 0.0625 in. The  $\text{D}_2\text{O}$  coolant flows through the annulus (0.35 in.) at 5 fps and exits through slots in the outer tube into the bulk reflector.

The liner tube features a bellows-type expansion joint near the upper end of the tube. Similar expansion joints are provided at the top and bottom of the shroud tube external to the pressure vessel. Transition from shrouds to steel liners are made with mechanical joints that are accessible for maintenance.

When access to the through hole is desired from the bottom (in the subreactor room) the bottom shield plug is lowered into a storage pit in the floor directly below the opening. The pit is filled with light water for shielding purposes. It is large enough to accept other items of equipment in addition to the plug.

Removal of the bottom shield plug can be accomplished in either of two ways. The plug can be lowered from atop the reactor with the aid of a special handling tool and the overhead crane. A second method would involve a special coffin with a built-in device for lifting or lowering the plug. The coffin would extend from the floor to the ceiling of the sub-reactor room to prevent exposure of personnel to the active end of the plug.

The liner tube may also be removed for inspection and maintenance by unbolting flanges at the top and bottom of the facility. The liner must be withdrawn from the top of the reactor into a coffin designed for that purpose.

#### 8-in. ID Cryogenic Through Hole (VTH-2)

The cryogenic through hole is designed to facilitate irradiation of cold materials outside the pressure vessel in a thermal flux zone of about  $10^{13}$  n/(cm<sup>2</sup>)(sec). Access to the facility is from either the top of the reactor or from the subreactor room.

The design is similar to that of the 8-in. ID vertical through hole (VTH-1) except that aluminum is substituted for zirconium in the irradiation section, and light water coolant is used instead of D<sub>2</sub>O. A bismuth shield (8 in. thick) is located at the horizontal centerline of the reactor to reduce the gamma heating load on the refrigeration system components installed in the hole, and thus to reduce the capacity of refrigeration service equipment that must be located convenient to the facility. The concept of this facility is further complicated by requirements for very high vacuum. The operating temperature is contingent upon the successful resolution of the foregoing problems. However, it is expected that it will be practical to achieve temperatures at least as low as 20°K.

The facility may also be used for normal temperature irradiations involving bulky apparatus such as in-pile engineering test loops.

### General Purpose Holes (GP-1 and GP-2)

There are two 24-in. square vertical holes that extend down to 2 ft above the core centerline immediately outside the pressure vessel in a zone of thermal flux of approximately  $10^{13} \text{ n}/(\text{cm}^2)(\text{sec})$ .

Both holes have access ports at the top of the reactor and are designed to accommodate large experiments that require special shielding, moderation or converters. The lower sections are fabricated of expanded aluminum tube sheets to provide water passages for cooling the walls. Conduits for instrumentation and piping are recessed in the thimble walls. The shield plugs are of conventional stepped design and fabricated of the same material surrounding the holes.

A special coffin is used to remove and transport samples or equipment installed in these facilities.

### Cryogenic Access Thimble (VT-31)

The purposes of this vertical hole are to provide access to the inner end of the cold neutron beam hole (HB-6) and to accommodate piping and instrumentation leaks, etc., to the 100-liter low-temperature tank. The 22-in. diameter of the hole will facilitate removal of the tank, if necessary. The thimble may also be used for solid-state, low-temperature studies.

The thimble walls are of expanded aluminum tube sheets through which  $\text{D}_2\text{O}$  coolant is circulated. The walls are vacuum-insulated from the cold tank.

A bismuth shield surrounds the thimble in the tank zone. The bismuth shield contains  $\text{D}_2\text{O}$  cooling coils.

### Vertical Access Holes - Thermal Column (TCV-1 to TCV-5)

Five vertical holes provide access to regions in the graphite thermal column having a thermal flux of about  $10^{12} \text{ n}/(\text{cm}^2)(\text{sec})$  and a cadmium ratio in excess of  $10^4$ . One of the thimbles is 24 in. square and intersects the horizontal thermal column hole (16 in. square) at a distance 12 in. from the inner face of the graphite. Large-size apparatus may be installed in the hole or it may be used for experiments where access from both ends is desirable, using the Horizontal Thermal Column (TC-1) as the lower access. The four remaining holes are 8 in. square and terminate in the graphite on either side of TC-1.

The holes are lined with stainless steel down to the thermal shield over the thermal column. The holes in the graphite are not normally lined; they are defined by removing vertical graphite stringers as needed.

The junctions of the vertical access holes with the shield around the thermal column are gastight, and the lower end of the shield plugs seat on a gasketed joint to seal the graphite zone from the outside atmosphere. All instrument leads, piping, etc., pass through a sealed junction in order to isolate the irradiation zone. The lead conduits are set into the thimble walls. This makes it possible to fabricate the plugs in sections for ease of handling.

Utilities are furnished in the same manner as for all other vertical facilities.

#### Rabbit Systems (RP-1 and RH-1 through 6)

Both hydraulic and pneumatic rabbit systems are provided for irradiations where the exposure time does not conform to scheduled reactor shutdown, or for experiments that require rapid transport of the specimen from point of radiation to point of measurements.

There are six hydraulic rabbit tubes (1.5 in. ID), two each located 1 in., 24 in., and 48 in. from the face of the core to give a wide range of both neutron flux spectrum and intensity for various types of experiments. There is one pneumatic rabbit tube (0.75 in. ID) that terminates at the bottom edge of, and 1 in. from, the active section of the core in a thermal neutron flux ranging from  $0.9 - 2 \times 10^{15} \text{ n}/(\text{cm}^2)(\text{sec})$ .

All rabbit tubes enter at the bottom of the pressure vessel, extend upward through the reflector, and terminate near the horizontal centerline of the reactor. From the bottom of the pressure vessel the tubes are carried through the biological shield to terminals in the basement. The hydraulic rabbit terminals are located in a  $\text{D}_2\text{O}$  canal equipped with remote-handling facilities to de-can the samples. If desired, the samples can be sent to a light water storage canal for shipment in casks to other areas.

The pneumatic rabbit terminal allows the shuttle to be sent directly to laboratories in the area for rapid sample processing to facilitate experiments involving isotopes of short half-life. As the name implies, the pneumatic rabbit shuttle is propelled and cooled by gas, helium being the most likely choice.

The hydraulic rabbit shuttles are cooled and propelled by  $D_2O$  pumped through the single-wall tube and into the reflector at the ends of the tubes. The shuttles are returned by reducing the coolant flow until the pressure in the tube is exceeded by the pressure in the vessel to effect a reverse flow that propels the shuttle back to the transfer station in the rabbit canal. There is a critical period in which the flow is zero or too low for effective heat removal; therefore, system valving must be designed to reverse the flow as rapidly as possible.

Design of the tube should incorporate means of removing or dislodging shuttles at any point along the length. For example, special grapples on flexible shafts could be employed to grasp the shuttle in such cases.

#### b. Horizontal Facilities

There are 26 horizontal facilities designed principally for physics experiments. The distance between the respective facilities and the core face varies from a minimum of 1 in. to a maximum of 24 in. to give a wide range of flux spectrum to meet the needs of the individual experimenter.

The beam holes and through holes are circular in section to allow the thinnest walls consistent with the working pressure (100 psi) and to hold the volume of metal near the core to an absolute minimum.

Calculations of the heat generation indicated the need for supplementary cooling, and cooling water flow rates for the various sized tubes have been established accordingly.

Figure 14 shows one side of the most complex of the horizontal installations: the horizontal through-hole. However, the various shroud and liner tubes, expansion joints, shield gates, plugs, and cooling provisions are typical of all beam holes into the reactor vessel.

#### Expansion Joints

The expansion joints are installed in the shroud tubes to compensate for axial and radial movement of the pressure vessel to which the shroud tubes are welded. The outer flanges of the expansion joints for the liner and the shroud tube are bolted to a steel housing embedded in the concrete biological shield. The flanges are located inside the shield gate opening so that with special extension tools the liner and the expansion joint in the shroud tube may be removed for inspection and/or repair.

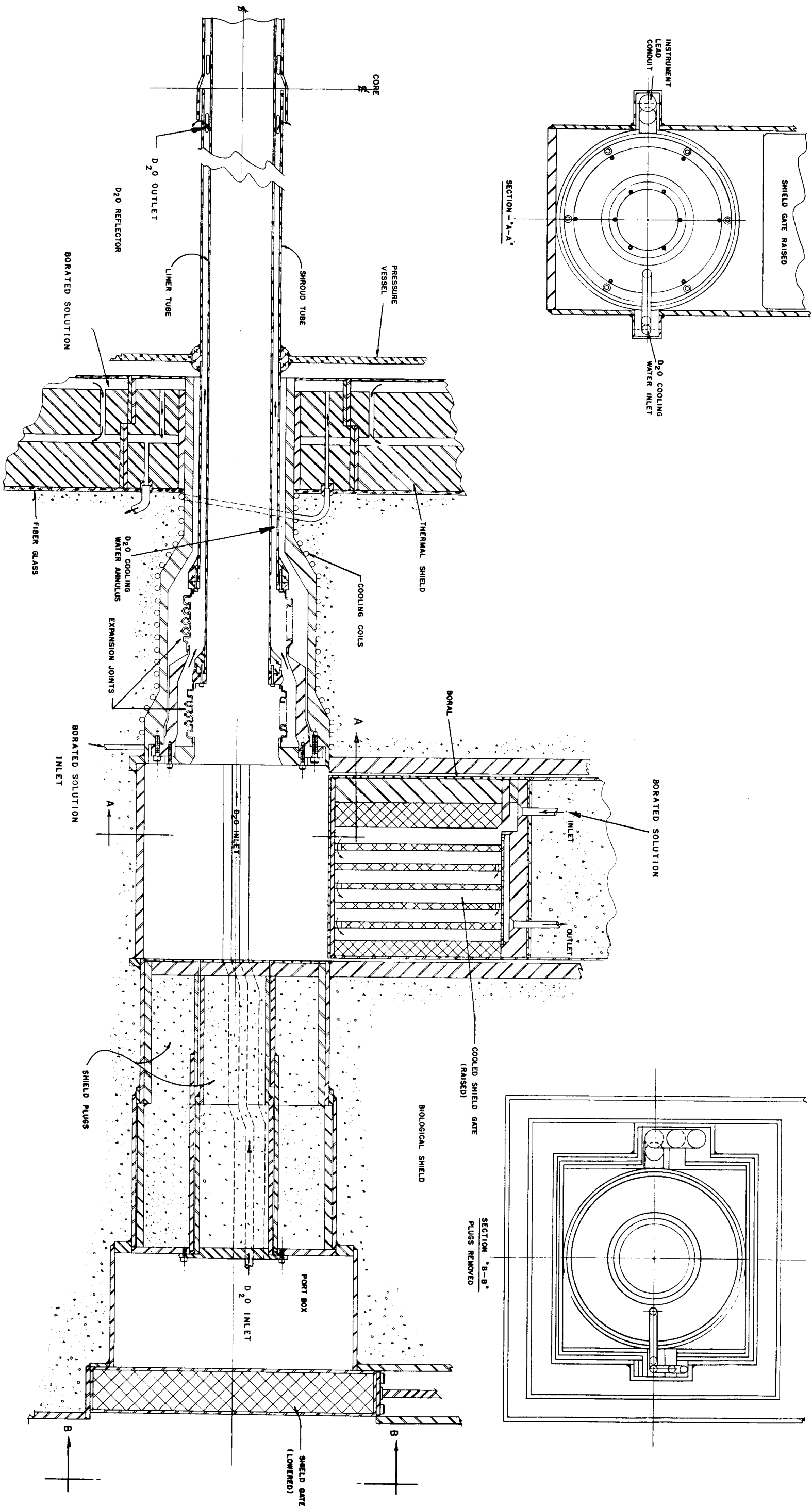


FIG. 14  
HORIZONTAL THROUGH-HOLE INSTALLATION  
(Ref. Dwg. RE-5-23406-F)

The annulus between the liner tube and the shroud tube provides a channel for coolant flow.

### Shield Gates

The nature of instrumentation, collimation equipment, etc., necessitates a shield gate to shut off the neutron beam when desired by the experimenter. The location and design of a gate to give maximum neutron and gamma attenuation is guided by several factors. The first, affecting the location, is the desire to have the neutron beam impinge upon the surface of the gate at a point deep within the biological shield, giving the best conditions for absorbing the scattered neutrons and capture gammas. However, the neutron flux at a point further from the core would be distance attenuated and, hence, would permit a thinner shield gate.

The compromise is a reasonable degree of accessibility to the mechanical seals and expansion joints of the double-walled tube, with maximum attenuation and nominal scattering achieved by placing the gate midway between the outer face of the biological shield and the thermal shield. Space allocations are also improved by this arrangement.

A second factor that affects the gate design is the preference of experimenters for a vertical-type rather than a rotating-type gate. This preference is justified in view of the difficulties of inter-connecting leads or piping between installed experiments and instrumentation external to the biological shield. A vertical gate can be designed with a trench around the gate so that the experimental apparatus, such as collimators, and necessary piping, leads, etc., can be assembled in one rigid unit that can be inserted into the beam hole and removed when necessary without disturbing the alignment or connections.

The third major factor that influences the gate design is the high degree of attenuation necessary because of the dense flux in the beam holes. A fast neutron flux (200 kev) of  $1.2 \times 10^{11}$  n/(cm<sup>2</sup>)(sec) impinges on the gate of the 8-in. ID beam holes and must be moderated sufficiently to be removed by an absorber such as boron. This moderation is achieved by having the neutrons pass through steel and/or water of the proper thickness to thermalize at least a major percentage of the total flux. The thermal neutrons pose no problem. The gamma flux from the core and that produced in the material ahead of the gate through capture is removed by lead of proper thickness.

The gate design evolved is a box, 24 in. long, containing a 3.5-in. steel plate followed by 9.75 in. of lead slabs separated by channels through which borated water is circulated. The borated water serves to moderate the fast and the thermal neutrons, absorbs thermalized neutrons in the boron, and cools the lead and steel shield material. Calculations showed that this arrangement will give the following dose rates at the face of the reactor operating at 250 Mw:

With Gate Open

2-Mev gammas =  $3.8 \times 10^8$  mr/hr  
 7-Mev gammas =  $8.45 \times 10^7$  mr/hr  
 200-kev neutrons =  $4.4 \times 10^{10}$  n/(cm<sup>2</sup>)(sec)

With Gate Closed

2-Mev gammas = 100 mr/hr = 13 x tolerance level  
 7-Mev gammas = 70 mr/hr = 9 x tolerance level  
 200-kev neutrons =  $6.63 \times 10^3$  = 13 x tolerance level  
 Total 35 x tolerance level

Concrete-filled shield plugs are provided for the beam holes to reduce further the dose rate in event work must be performed in the port box. Additional shielding is furnished by the vertical operating port gate that may be closed when desired.

The water-cooled gate is electric motor-driven and may be opened or closed in 60 sec. Operation is controlled from buttons located on the face of the reactor, but interlocks in the circuit allow opening or closing only when safety switches are closed in the control room.

Each of the seven down-beam holes is located directly above a horizontal beam hole; that eliminates the possibility of using a top-operated shield gate. Therefore these beam holes are equipped with bottom-operated gates that are driven from below by motors located in the ceiling of the subreactor room. All other horizontal, through, and down beam holes have top-operated gates with drive motors located in recesses in the top floor of the reactor. Concrete-filled extensions are employed on each gate to eliminate voids at critical areas in the biological shield.

The gates may be removed from the biological shield for repair or replacement with the aid of special coffins. The gate drive motors are readily accessible for maintenance and repair in areas not subject to radiation.

Port Boxes

The port boxes provide space for interconnections between installed experiments and external instrumentation, and nominal space for equipment that must be installed inside the biological shield. Utilities and instrumentation leads are carried in conduits from the port boxes to terminals on each face of the biological shield.



The D<sub>2</sub>O cooling water line for the beam hole is brought out to the port box in a trench similar to that furnished for the leads and can be regulated at that point according to the type of experiment or equipment in the hole. Connections for cooling the dummy plugs or collimators are also made in the port box so that the activated water can be properly shielded from personnel and equipment in the reactor room.

### Coffins

A heavily shielded coffin (~35 ton), similar to the Universal coffin at MTR, services the down-beam holes and the through-holes. The coffin is suspended from the 50-ton overhead rotating crane and is guided on ramps that depress from the top deck in alignment with the down-beam hole. Adjusting screws on the coffin afford precise alignment with the hole.

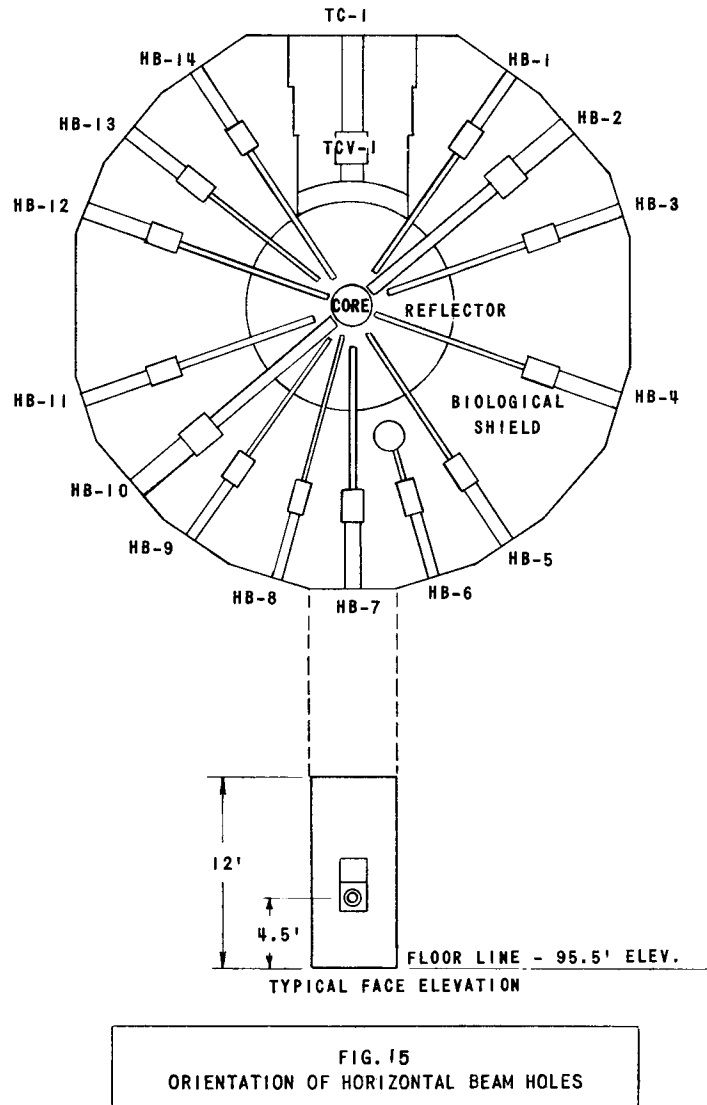
The down-beam balcony is 8 ft wide and will support a nominal amount of equipment; however, the permissible loading is considerably less than the 1500 lb/ft<sup>2</sup> concentrated load allowed on the main floor.

### Horizontal Beam Holes (HB-1 to HB-14)

The 14 horizontal beam holes lie in a plane corresponding to the horizontal centerline of the core (Elevation = 100 ft) and 4.5 ft above the main floor of the reactor room (see Fig. 15). The number of holes was influenced by the desire to have not less than 5 ft of the face of the biological shield available for each experiment. Further limitations were imposed by space requirements for the through-holes and the thermal column.

The sizes and number of beam holes that closely approach the core were restricted by the effects of structural metals, voids, and contained experiments on reactivity, as well as space available around the core. Every effort was made to have each hole directly in front of a fuel assembly rather than a control blade slot, to reduce shadowing from the neutron-absorbing material. Exceptions were necessitated by space requirements for the vertical facilities.

Another factor which influenced the arrangement of beam holes was the necessity of maintaining a balanced flux pattern around the core. This was accomplished by pairing holes of equal diameter on opposite sides of the fuel assembly. The holes that terminate farther out in the reflector are not as critical in this respect and could be located as desired.



The minimum size of the beam holes preferred by experimenters was determined to be 3 in. ID. The maximum size (8 in. ID) was determined by the effect on reactivity of large metal volume and voids near the core. Calculations which included the effects of other holes and facilities showed that beam holes in excess of 8 in. ID would be critical in their depressing effect and that only two holes of this diameter could be tolerated.

As shown in Fig. 16, the two 8-in. ID beam holes (HB-2 and 10) and the two 4-in. ID holes (HB-4 and 12) terminate 1 in. from the core in a thermal flux ranging from  $2$  to  $4 \times 10^{15}$  n/(cm<sup>2</sup>)(sec), and a fast flux of  $2 \times 10^{15}$  n/(cm<sup>2</sup>)(sec). The heat generation in these tubes is of such magnitude that auxiliary cooling is required. Approximately 500,000 Btu/hr is generated in the 8-in. ID beam hole; of this amount, 300,000 Btu/hr is generated in the ends of the liner and the shroud. Considering the area of the tube ends, a heat flux of 380,000 Btu/(hr)(ft<sup>2</sup>) must be effectively removed to prevent excessive metal temperatures and local boiling.

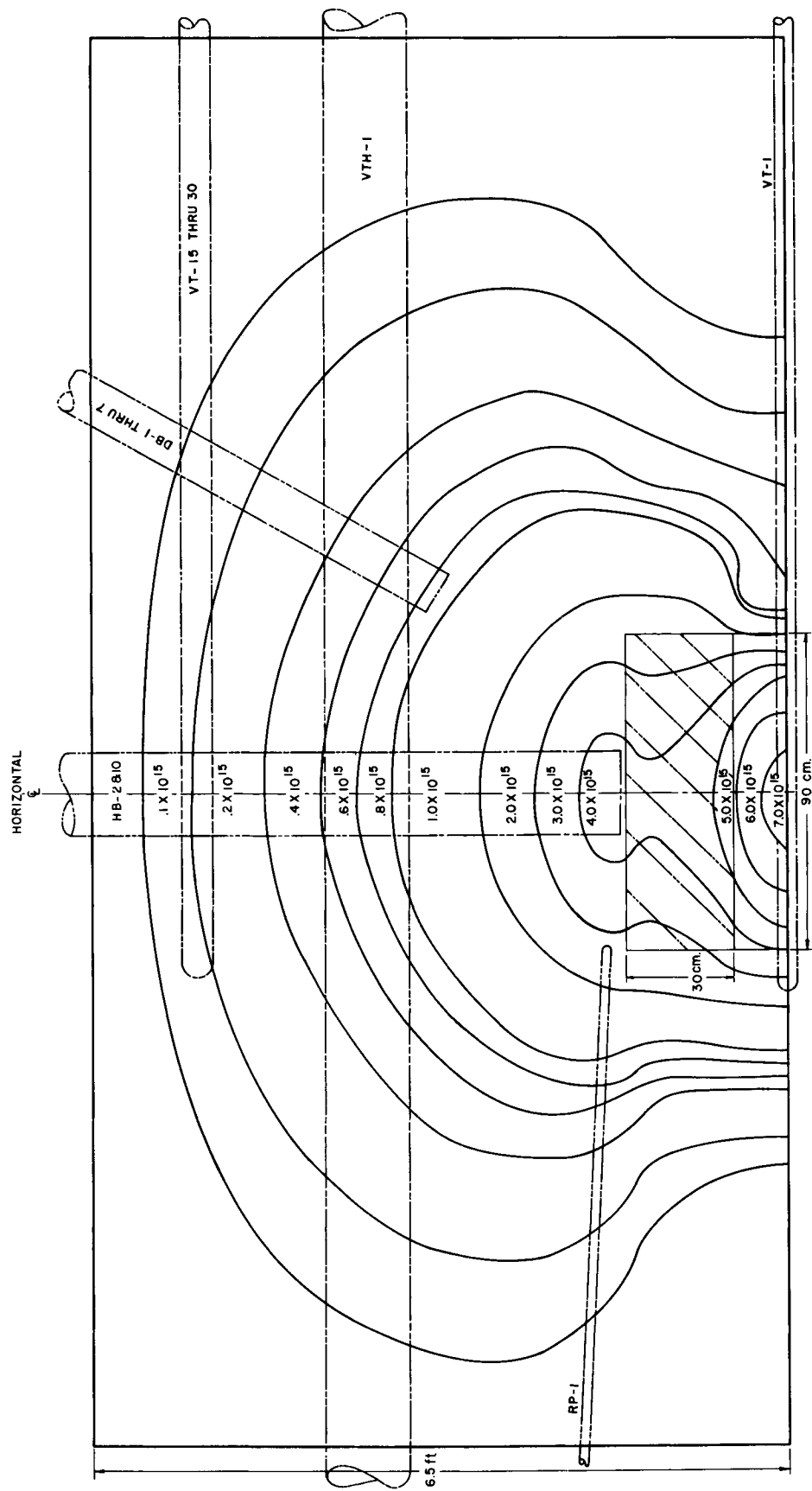


FIG. 16  
TWO-DIMENSIONAL FLUX PLOT WITH EXPERIMENTAL FACILITY OVERLAY  
(Ref. Dwg. RE-6-24364-D)

The heat generation in the 4-in. ID beam holes is not as critical, but sufficiently high (180,000 Btu/hr) to warrant additional coolant flow. The heat flux in the ends of these tubes is approximately 290,000 Btu/(hr)(ft<sup>2</sup>).

Calculations showed that a flow of D<sub>2</sub>O coolant through the annulus in the thimble and into the bulk reflector would have to be of the order of 150 gpm at 10 fps to effect adequate heat removal. The tubes of smaller diameter and those further from the core will require proportionately less coolant. The plugs and/or instruments within the tubes are cooled independently.

In the event of pump failure or other malfunction of the primary cooling system, the beam holes will be cooled by natural convection. Small bleed holes along the top of the shroud tubes will permit steam to escape from the annulus, while similar holes along the bottom of the shroud will allow entry of the reflector-coolant. Leakage of supplementary coolant water through the annulus will not reduce the flow appreciably.

One of the 4-in. ID horizontal beam holes (HB-6) does not penetrate the pressure vessel, but terminates at the outer edge of the cryogenic access thimble (VT-31). The purpose of this beam hole is to provide a source of very low-energy neutrons cooled and moderated by the 100-liter tank in VT-31.

The special function and location of HB-6 permits design features that differ from other beam holes. No supplementary cooling other than in the bismuth shield around the cold moderator tank is required. No expansion joints are required and the tube walls can be aluminum. The vertical shield gate is made of borated lead and steel, since the fast flux has been well moderated and the low-energy neutrons are easily removed by the boron.

#### Horizontal Through-holes (HTH-1 to HTH-4)

Four horizontal through-holes are provided for beam experiments requiring access from either or both ends (Fig. 17). Two of the holes (8 in. ID) are located 1 ft 10 in. below the horizontal centerline of, and tangent to, the core. The other two holes (6 in. ID) are tangent to, and 1 ft 9 in. above the centerline of the core. All four holes are 1 in. from the core face and in a thermal flux zone (Fig. 18) ranging from 1 to  $2 \times 10^{15}$  n/(cm<sup>2</sup>)(sec).

The extreme heat generated in the sections adjacent to the core requires supplementary cooling (300 gpm) for each of the holes. The coolant enters from both ends of each hole, flows through the liner-shroud annulus, and discharges into the bulk reflector.

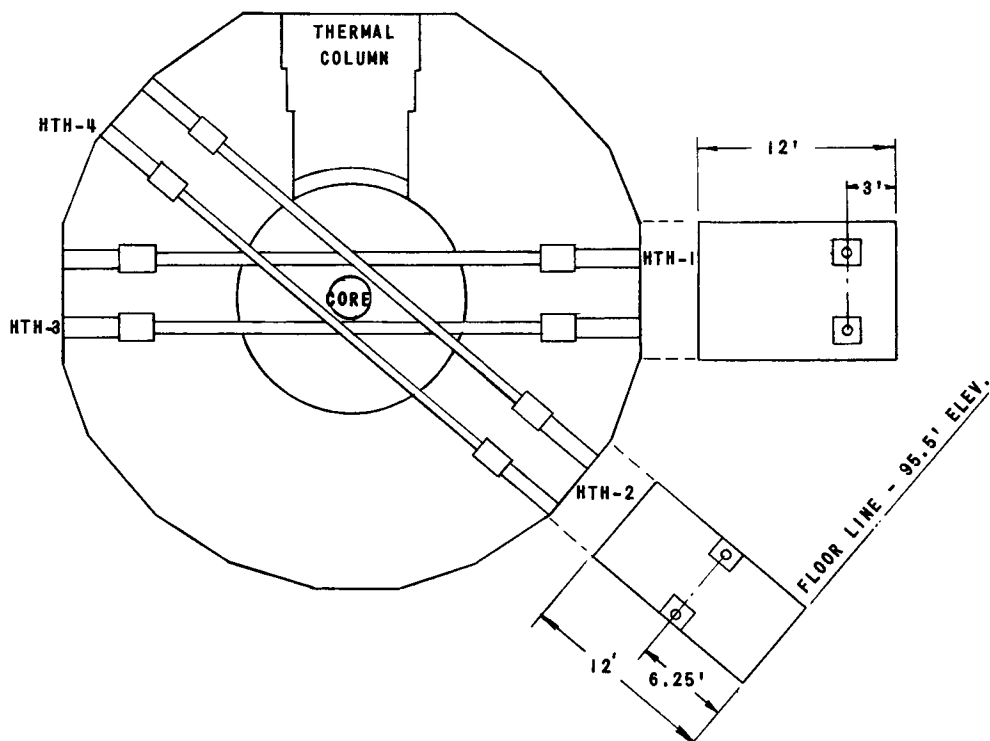


FIG. 17  
ARRANGEMENT OF HORIZONTAL THROUGH HOLES

The construction of the tubes inside of the pressure vessel is identical with that of the vertical through-hole (VTH-1). Outside of the pressure vessel the through-holes are similar in construction to the horizontal beam holes, except that a thermal expansion joint is installed at one end of the liner tube.

#### Down-beam Holes (DB-1 to DB-7)

Seven down-beam holes - three 2-in. ID and four 4-in. ID - penetrate the  $D_2O$  reflector to within 24 in. of the core at an angle 30 degrees to the horizontal (see Fig. 19). The angled installation poses certain disadvantages with respect to operating procedures; however, they are offset by the thermal neutron flux range  $[0.6 \text{ to } 0.8 \times 10^{15} \text{ n}/(\text{cm}^2)(\text{sec})]$  afforded in this region (see Fig. 16).

The insertion and removal of plugs, collimators and other experimental equipment requires special handling procedures for the coffins. The use of the 50-ton crane and the top deck ramps has been described previously.

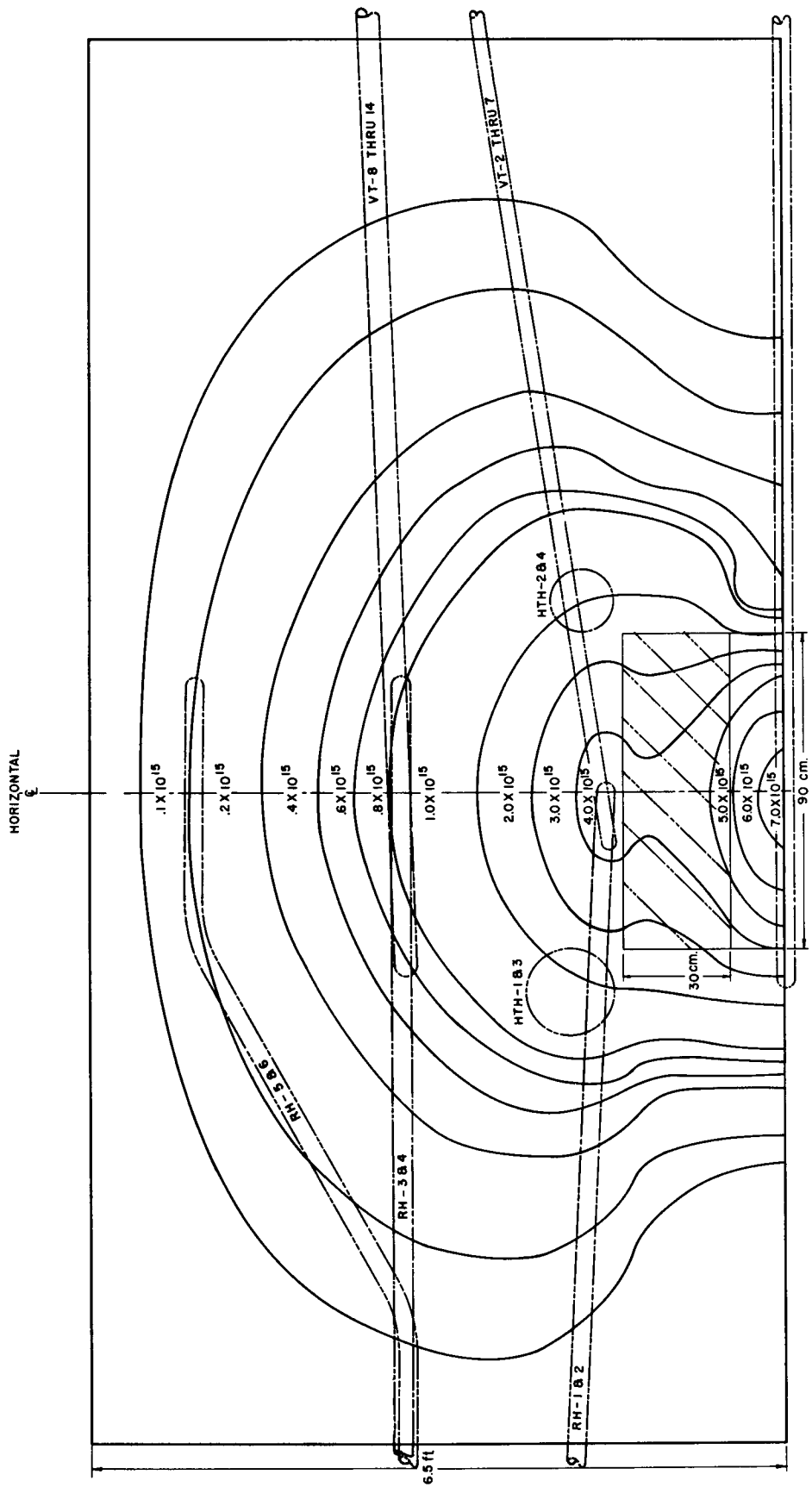
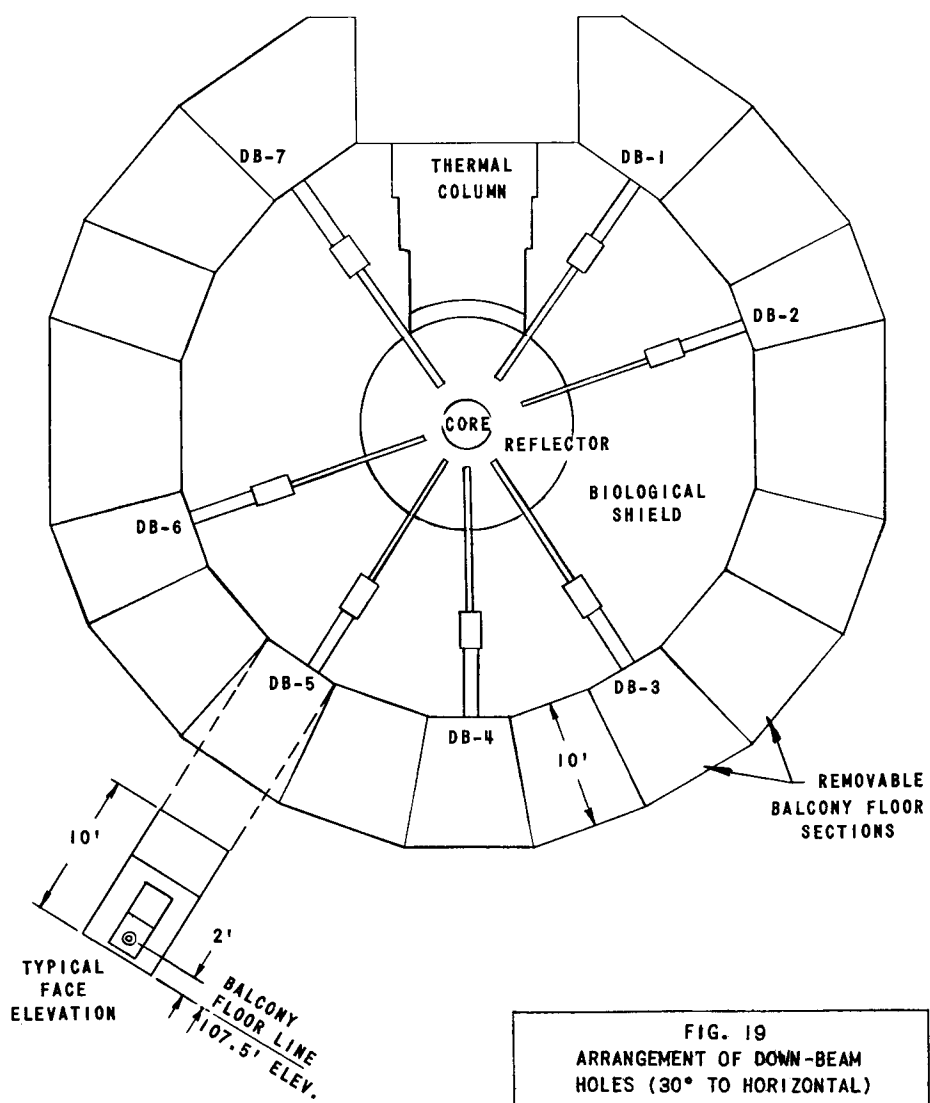


FIG. 18  
TWO-DIMENSIONAL FLUX PLOT WITH EXPERIMENTAL FACILITY OVERLAY  
(Ref. Dwg. RE-6-24364-D)



Another disadvantage is the necessity of moving experimental equipment on the down-beam balcony when the overhead crane is used to service the horizontal beam holes directly below the balcony. The floor of the balcony is made in sections that can be removed to facilitate crane operations at the main floor level.

The design and construction of the down-beam holes is similar to those of the horizontal beam holes, with cooling shrouds, expansion joints, borated water-cooled shield gates, and utilities furnished for each hole.

Based on a working pressure in the vessel of 100 psig and metal temperatures of about 250°F, the wall thickness of the liner tubes for all beam holes is calculated from the Unfired Pressure Vessel Code as follows:

Inside Diameter, in.	Wall Thickness, in.
8	0.1675
6	0.125
4	0.0837
3	0.0781
2	0.0625

The wall thickness of the shroud tubes for all beam holes is 0.0625 in. in a zone 3 ft around the core, and increases to 0.125 in. from that point to the pressure vessel wall.

### c. Graphite Thermal Column

A graphite thermal column (6 ft x 7 ft) is provided for experiments that require a relatively pure thermal flux of the order  $10^{12}$  n/(cm<sup>2</sup>)(sec) and a cadmium ratio of  $\sim 10^4$ .

As shown in Fig. 9, the thermal shield in front of the thermal column is replaced with a gamma screen (12 in. thick) comprised of an aluminum frame filled with lead and containing water-cooling coils. Between the lead screen and the graphite is a 4-in. wide channel that contains a neutron shutter. The shutter is a stainless steel box with vertical passages through which borated water is circulated. The borated solution serves as a coolant and a thermal neutron attenuator. The shutter is raised or lowered by ball-nut lead screws that are geared to an electric motor recessed in the top of the reactor. The entire gate and drives are supported by a steel frame that can be removed for inspection and/or repair.

The graphite is composed of 16-in. square stringers, 2.5 in. and 3.5 ft long, laid horizontally across the 6-ft width of the column. This arrangement permits the flow of heat toward the cool walls. The graphite stringers are staggered to reduce streaming.

Should supplementary cooling prove necessary to reduce the graphite temperature, the edges of the stringers can be beveled to accommodate cooling coils without effecting neutron streaming toward the face of the reactor.

The graphite is enclosed on four sides with a thermal shield of conventional design and materials. A highly neutron-absorbing shield (Boral) is placed next to the graphite to reduce the neutron flux as rapidly as possible. Next to the Boral is a thick lead shield for gamma attenuation. The lead contains cooling coils and thus serves also as a



heat sink. The lead is attached to a steel shell (2 in. thick) that provides further attenuation and structural support for the lead and Boral shields. The steel shell, in turn, is supported by a steel I-beam structure that is embedded in the concrete biological shield.

The vertical thimble holes (TCV-1 to TCV-5) penetrate the top shield and into notches milled in the graphite blocks.

The horizontal access hole (TC-1) is 16 in. square and accommodates a graphite stringer that can be bored out to a smaller size hole or several smaller holes consistent with the nature of the experiment. The biological shield gate at the outer surface of the graphite is composed of laminated lead and masonite. In addition to the upper and lower sections, each section contains five removable segments of the same material to facilitate access to the column without opening the parent gate sections. Each gate section is operated independently by a ball-nut screw driven by an electric motor with controls located at the reactor face. Indicators register the gate position at all times.

Additional shielding is supplied by an outer lead-filled door with an 18-in. square opening. The outer surface is stepped so that portable shielding slabs can be installed to reduce streaming. Lifting lugs are provided on the door to facilitate removal for inspection of the thermal column.

#### d. Spent Fuel Irradiation Facilities (SFI-1 and SFI-2)

The spent fuel subassemblies removed at the end of each fuel cycle will provide an intense source of photoneutrons and gamma flux for irradiation studies. SFI-1 will utilize the spent fuel immediately upon removal to the D<sub>2</sub>O fuel storage canal. SFI-2 will use the spent fuel after a decay period of 2 to 3 weeks and subsequent transfer to the H<sub>2</sub>O storage canal.

SFI-1 is the more complex of the two facilities. It will require special remote-controlled fuel-handling equipment and manipulators in a heavily shielded cave near the D<sub>2</sub>O fuel storage canal. The spent fuel from the reactor is transported on a narrow gauge rail cart from the D<sub>2</sub>O canal to a gamma facility cave in the basement. The gamma cave is separated from the fuel assembly by the steel wall of the storage canal. All remote-controlled operations are monitored through the cave window.

The SFI-2 facility located in the H<sub>2</sub>O storage canal is simply a group of four 12-in. square stainless steel thimbles, open at the top, that extend down from the surface of the water to the floor of the canal where spent fuel subassemblies are stored. Items to be irradiated may be

lowered through the thimbles and suspended near the fuel. If desired, the thimbles may be filled with water for shielding purposes.

6. Coolant System

a. Primary System

The core generates 250 Mw of fission heat that must be removed by the D<sub>2</sub>O primary coolant and rejected through heat exchangers to the H<sub>2</sub>O secondary coolant. The total primary flow is 54,000 gpm, of which 43,000 gpm enters the bottom of the core at a temperature of 100°F and spills into the moderator-reflector from the top of the core at 146°F and 100 psia. The remaining 11,000 gpm are used to displace the flow through the reflector zones and to cool the control rods and experimental facilities.

The primary flow is distributed in the following manner:

Core flow	43,000 gpm
Moderator-reflector circulation	5,200 gpm
Experimental facilities	3,700 gpm
Control rod slots	400 gpm
Inner reflector	700 gpm
Bypass flow control	1,000 gpm
Total D <sub>2</sub> O flow	54,000 gpm

As shown in the system flow diagram (Fig. 20), the effluent from the top of the pressure vessel flows down through two 24-in. pipes in the biological shield to the sub-basement and into the degasser tank. The radiolytic gases are helium-entrained from the tank and re-circulated, through the recombiner and cooler condenser, back to the D<sub>2</sub>O storage tank.

The bulk primary flow from the degasser is divided into four parallel circuits, each comprising three heat exchangers and a pump. Part of the bulk primary coolant is bypassed through D<sub>2</sub>O quality control system. The flow from the pumps and the quality control system is returned to the reactor up through two 24-in. inlet pipes that pass through the concrete shield in the form of an inverted "U" and down to the inlet header at the bottom of the pressure vessel. The inverted "U" return bend, along with a small vent line at the top of the bend, is designed to prevent loss of D<sub>2</sub>O from the pressure vessel in the event of a rupture in the system upstream of the return bend.

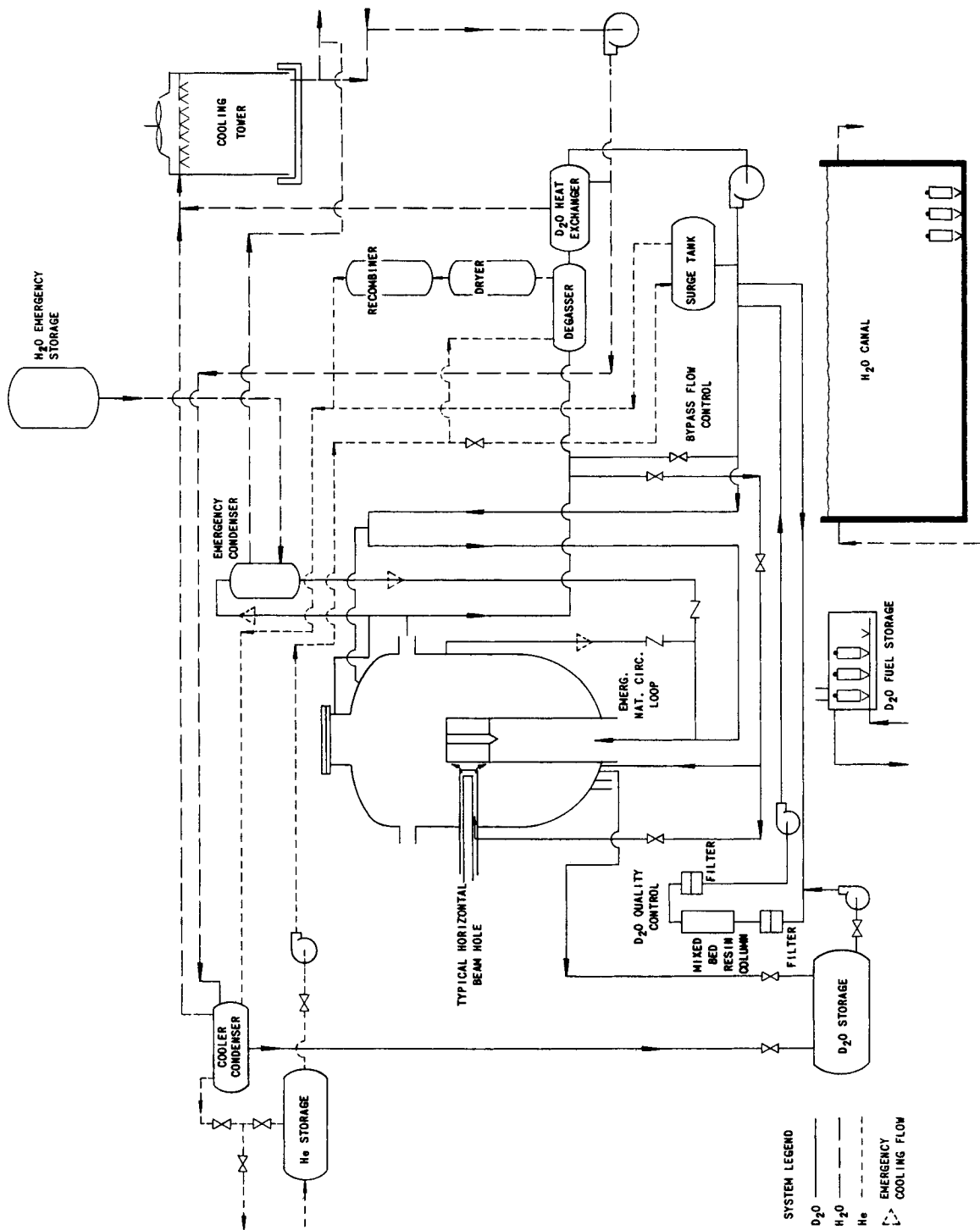


FIG. 20  
SYSTEM FLOW DIAGRAM

Moderator-Reflector Coolant

The moderator-reflector coolant is circulated through four 10-in. pipes that branch from the top of the two 24-in. return bends. The lines are valved near the top of the concrete shield and lead down through the shield to respective headers equally spaced around the main 36-in. inlet header in the vessel bottom. The moderator-reflector flow (5200 gpm) exceeds that required to match the core temperature rise to ensure that local flow restrictions will not prevent adequate cooling of the core shroud and structural components of the beam holes.

Experimental Facilities

The coolant for the experimental facilities is circulated from the main inlet lines to two shielded rooms in the basement. Independently valved lines lead from these rooms to the coolant annulus of the respective test facilities. The D<sub>2</sub>O circulates through the annulus and discharges into the bulk reflector coolant.

The coolant flow through the respective annuli is governed by the metal volume and the location of the facility relative to the core. The flows required for adequate cooling are summarized in Table IV.

Table IV

<u>CALCULATED PRIMARY COOLANT FLOW RATES</u> <u>THROUGH EXPERIMENTAL FACILITIES</u>				
<u>Facility</u>	<u>ID, in.</u>	<u>Flow, gpm</u>	<u>Total No.</u>	<u>Total Flow, gpm</u>
Beam holes	8	150	2	300
Through-holes	8	300	2	600
Through-holes	6	200	2	400
Beam holes	4	80	4	320
Beam holes	3	80	7	560
Beam holes	4	50	4	200
Beam holes	2	40	3	120
Vertical thimbles	8	170	1	170
Vertical thimbles	3	10	16	160
Vertical thimbles	2	30	7	210
Central thimble	1.5	60	1	60
Vertical thimbles	1	50	6	300
Hydraulic Rabbits	1.5	50	6	300
Total Flow				3700 gpm

There is also an external bypass flow control line that is operated in conjunction with the vessel circulation lines and the test facility coolant lines. Each can be operated independently while the main core flow is held constant.

Control Blades

The total mass flow for the eight control blades is 400 gpm. The coolant flows upward through a  $\frac{1}{32}$ -in. gap between each blade and guide slot that extends the length of the core. Analysis shows the resultant velocity of 23.7 fps in each gap will produce a large enough convection coefficient for adequate cooling.

Heat Exchangers

The twelve heat exchangers are of the floating head, double tube-sheet-type and are designed for a total duty of 317 Mw in anticipation of future operation at higher power. Each unit is 4 ft dia, 22.5 ft long, and fabricated with stainless steel tubes and tube-sheet and a carbon steel shell.

The operating characteristics of each exchanger are as follows:

	<u>Tube Side</u>
Effective heat transfer area	9,000 ft <sup>2</sup>
No. of tubes ( $\frac{3}{8}$ in. OD, No. 18 BWG)	4,750
Pressure	100 psig
Temperature	
Inlet	150°F
Outlet	110°F
D <sub>2</sub> O velocity	6.2 fps
Pressure drop	8 psi
	<u>Shell Side</u>
Pressure	75 psig
Temperature	
Inlet	85°F
Outlet	115°F
H <sub>2</sub> O velocity	6.9 fps
Pressure drop	9 psi

The combined operating characteristics are:

Heat exchanged	1.08 x 10 <sup>9</sup> Btu/hr
Total heat transfer area	108,000 ft <sup>2</sup>
Mean temperature difference	28.8°F
Over-all heat transfer coefficient	347 Btu/(hr)(ft <sup>2</sup> )(°F)

### Pumps

Each of the four flow circuits is serviced by a 450-hp centrifugal pump that discharges 13,500 gpm against an 80-ft head of D<sub>2</sub>O, assuming a pump efficiency of 60%. A throttle valve is installed in each circuit to control the flow until full-power operation is established.

Two 2000-gpm pumps are available in the event of operating pump failure or loss of power. The emergency pumps are powered by diesel motor-generator sets installed in the reactor building.

### Emergency Condenser

An emergency condenser is installed in the concrete shield to condense any steam that might be generated in the pressure vessel during emergency shutdown cooling by natural convection.

### D<sub>2</sub>O Quality Control System

The demineralizing system will process 50 gpm of primary coolant bypass flow during normal operation. Three ion-exchange columns are available, one operating and two for emergencies and/or standby operation during replacement of the strong, mixed-bed resins. Filters are installed upstream and downstream of the ion exchangers to remove coolant-entrained insolubles. If necessary, chemical control of corrosion inhibitors can be installed in this system.

### Retention Tanks

The primary coolant supply is contained in two 50,000-gal retention tanks installed in the sub-basement. Small vertical pumps are used for initial filling of the primary system. The impellers are immersed in the water and the drive motors are mounted above the tanks to minimize leakage.

### Surge Tanks

Two helium-pressurized surge tanks are employed to dampen fluctuations in system pressure. Each tank is installed after the header that interconnects two of the 24-in. lines from the pumps. The size of the tank and the interconnecting piping have not been affirmed.

### System Pressure Drop

The detailed design of the coolant system and components has not been finalized. Therefore pressure drop analysis is based upon proposed components - core, shield lines and return bends, heat

exchangers, degassing tank, valve and fitting losses, and approximate lengths of 24-in. pipe - using the equation

$$\Delta P = (K_1 + K_2 + \dots) V^2 / 2g \quad ,$$

where K represents entrance, exit, and friction loss factors, and V the local velocity. The various factors and the system pressure drop curve are discussed in Appendix D, along with the derivation and calculations to determine the flow "coast-down" time in the event of power failure.

Accordingly, the system pressure drop is 37 psi, of which 23 psi is ascribed to the core.

#### b. Secondary System

The secondary coolant (H<sub>2</sub>O) is cycled from the heat exchangers at 115°F to the cooling tower and returned at 85°F by four 500-hp pumps at a total mass flow rate of 72,000 gpm. All of the secondary system equipment - pumps, valves, etc. - are installed external to the reactor shell.

A 100-hp pump is installed for emergency cooling in the event of power failure. Under similar conditions, the emergency condenser is supplied with H<sub>2</sub>O from a gravity storage tank.

### 7. Fuel-handling System

The high photoneutron flux precludes the use of manual visual manipulators for fuel-handling operations. Further, the top of the reactor must be free of fuel-removal mechanisms to permit this area to be used for thimble installations and access ports. Consequently, the design evolved is a blind, remote-controlled, mechanized system that transfers a fuel assembly (and control blade) from a station beneath the pressure vessel, through the fuel transfer tube, to the core shroud.

The mechanism (Fig. 21) comprises a telescopic column with a retractible pantographic linkage at the upper end. The outboard end of the linkage contains a fuel grapple and the necessary mechanical motions to lock or unlock the fuel subassembly and control plate in the core shroud. The unit can be indexed to any preselected fuel octant in the shroud. The entire mechanism, including the fuel subassembly, is retracted into, and withdrawn out of the reactor, through the 22-in. ID fuel-transfer tube, to the loading and unloading station beneath the vessel.

The fuel-transfer system (Fig. 22) consists of a fuel-loader section (20 in. dia. x 17.5 ft high) mounted above an elevating tube (54 ft high) that operates through a packing gland at the lower end of the

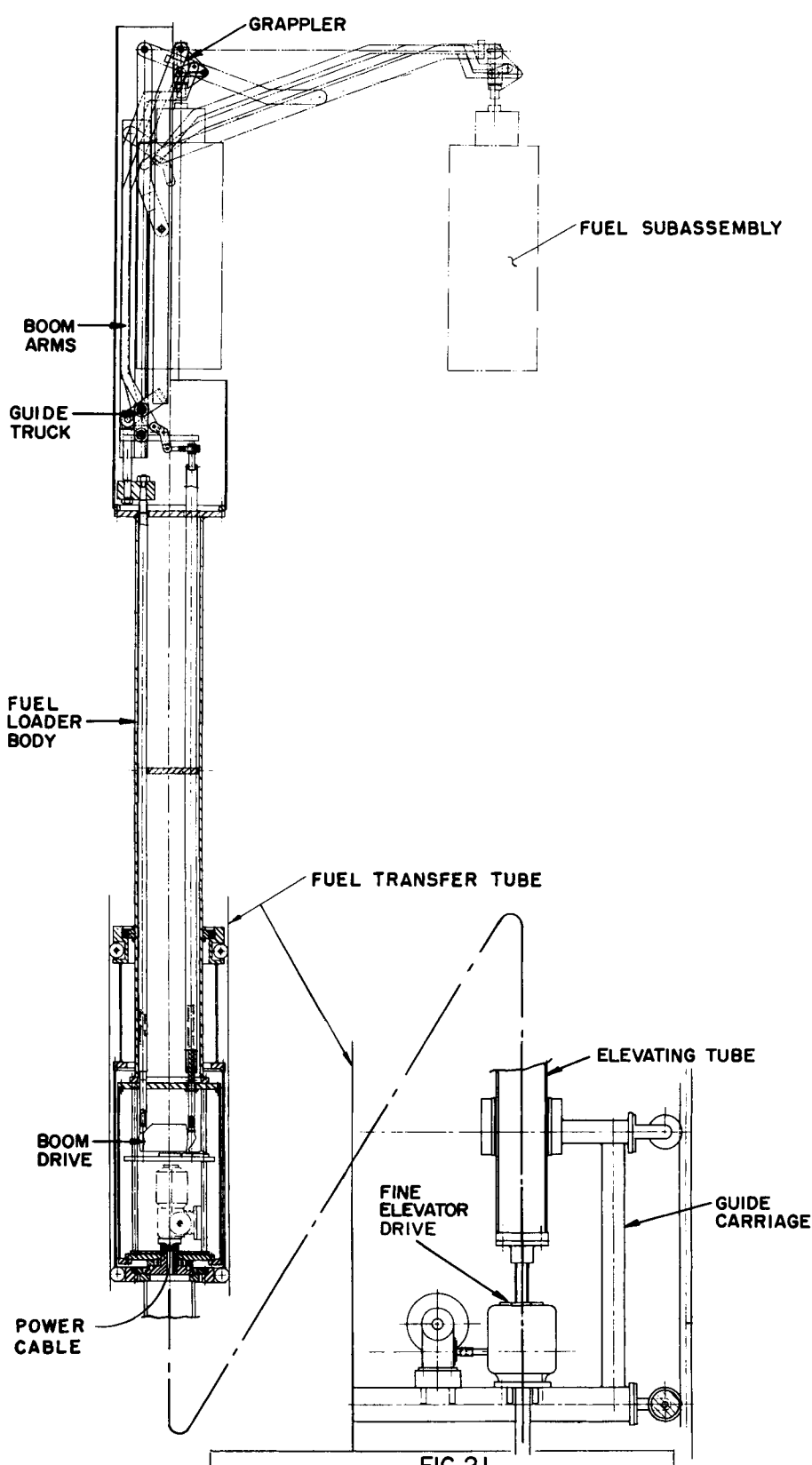


FIG. 21  
FUEL-TRANSFER MECHANISM



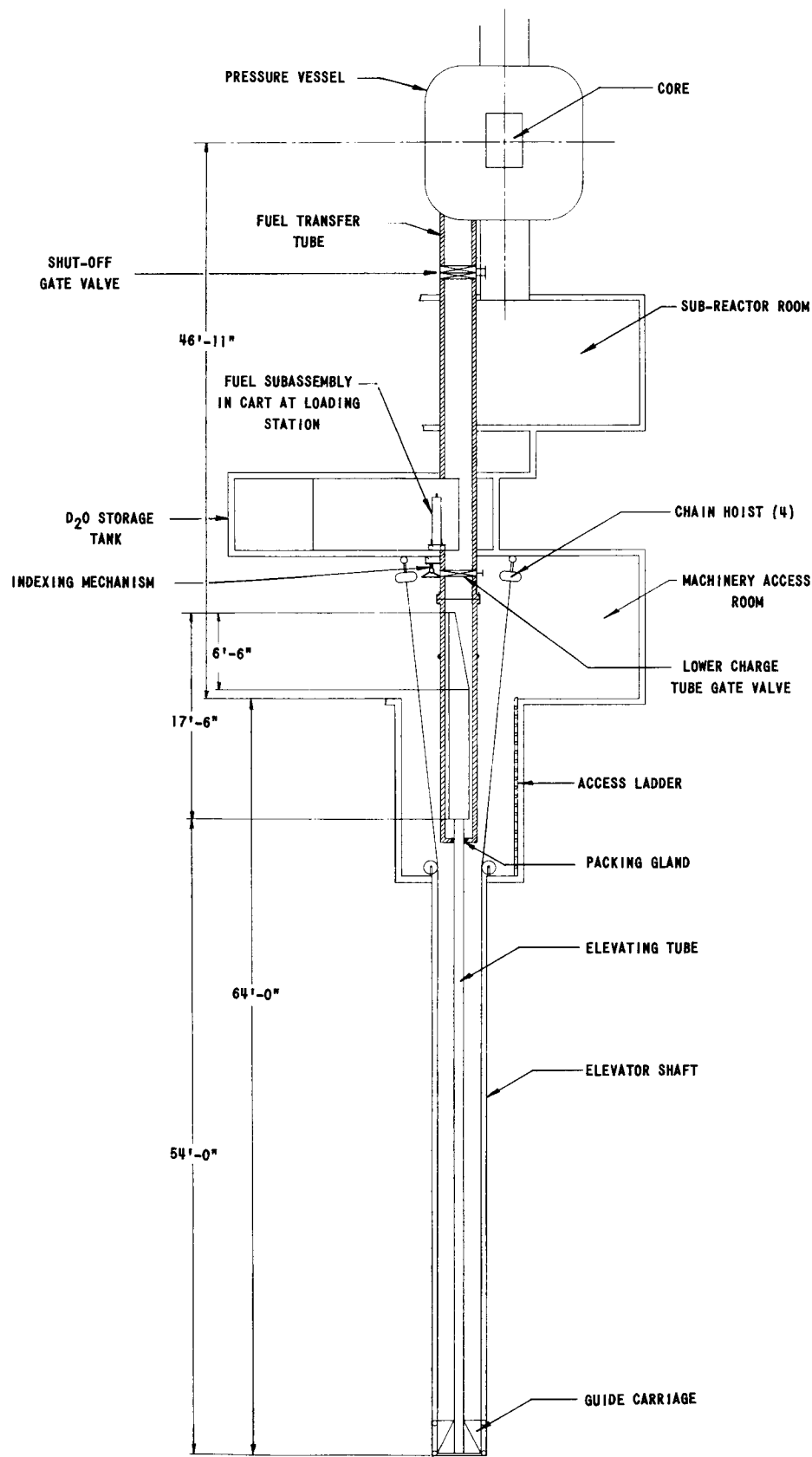


FIG. 22  
FUEL TRANSFER SYSTEM  
(Ref. Dwg. RCD-543-L1)

fuel-transfer tube. The extreme lower end of the elevating tube is assembled to a guide carriage. The upper end is attached to a pad that is guided by rollers in the fuel-transfer tube. The pad (Fig. 23) carries the lower end of the water-tight rotatable loader body that houses the rotation drive, the boom arm actuation drive, and the grappler drive. The boom arms support the grappler that carries the fuel subassembly through the loading and unloading cycle. Figure 24 shows the loader assembly in the extended position above the core shroud.

The power and control circuits are carried in a cable that extends from the loader body, through the center of the elevating tube, and into the machinery access room. A gate valve in the upper end of the fuel-transfer tube is closed during reactor operation. Prior to loading operations, the valve is opened to allow the fuel-loading mechanism to enter the pressure vessel.

#### a. Subassembly Transfer - Canal to Core

The loading cycle begins by transferring the fuel subassembly from the D<sub>2</sub>O storage canal to the loading station. The transfer mechanism also indexes the fuel to the correct angular position. The fuel loader body is elevated, by four electrically driven chain hoists, from its normal position at the bottom of the fuel-transfer tube to a position adjacent to the fuel-loading station. This position is indicated to the operator by counters in the control room; limit switches stop the mechanism at the correct level. Minor errors in elevation indicated by the controls are corrected by the operator by manipulation of the fine elevator drive (Fig. 21) contained in the carriage at the base of the elevating tube.

The boom drive is actuated to extend the grapple head over the fuel-grappler pin (Position A, Fig. 25). The grappler jaws are lowered over the fuel-grappler pin and locked by the down motion of the cam shell (Positions B and C, Fig. 25). The boom is raised to lift the subassembly out of the fuel-transfer cart. The grappler boom arms are retracted, along with the subassembly, into the fuel-transfer tube for elevation up into the reactor vessel.

After the subassembly has been elevated above the core shroud, the loader head is indexed by the rotation drive to the preselected angular position, and the boom arms are extended to lower the subassembly into the shroud cavity. The control blade extension rod is raised and engaged with the locking chuck in the lower end of the control blade.

Continued actuation of the grappler drive raises the grappler sleeve upward, simultaneously locks the control blade in place and extends the fuel-locking bars outward into slots in the core shroud to

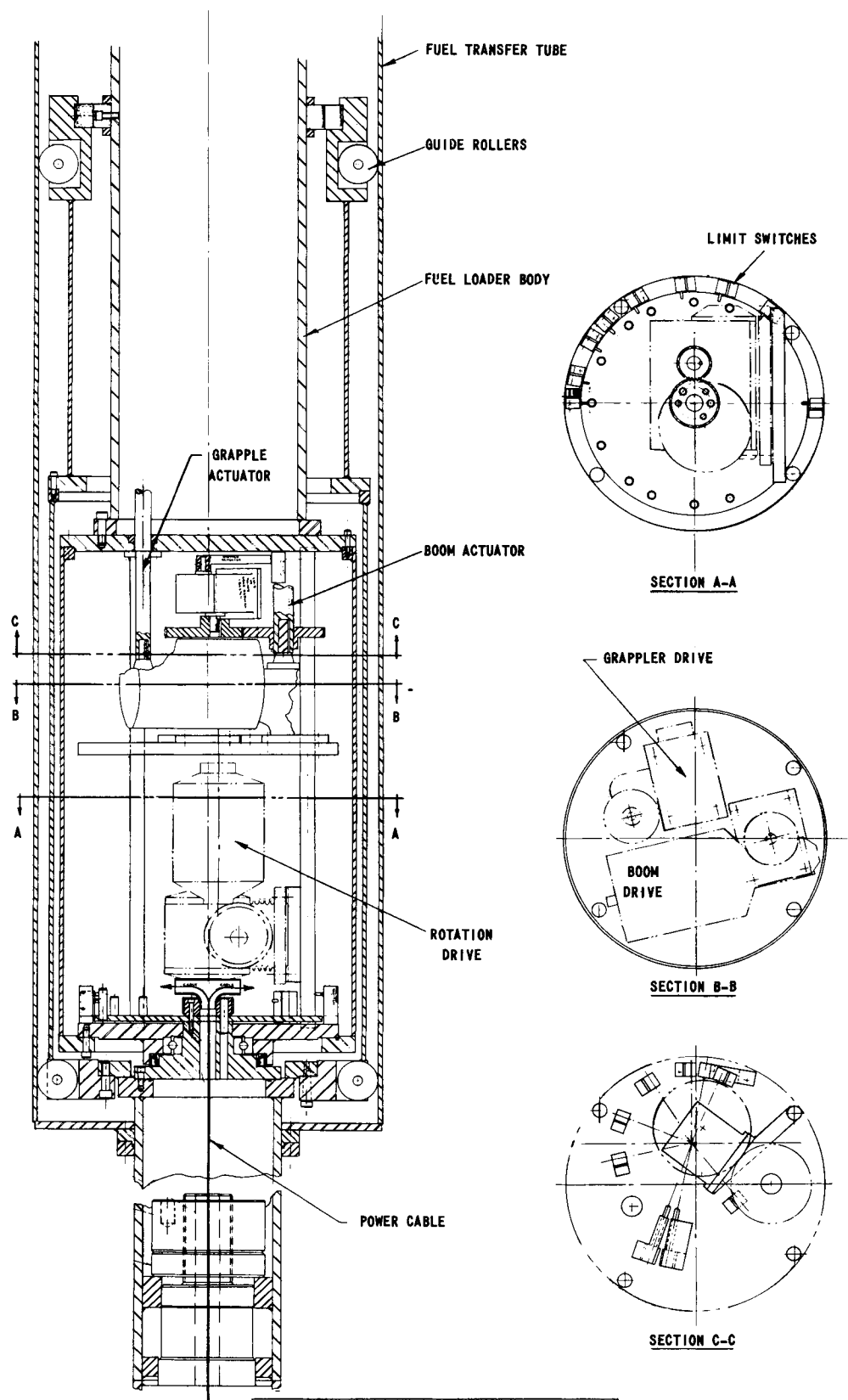


FIG. 23  
LOADER BODY DRIVE COMPARTMENT  
(Ref. Dwg. RCD-543-L-3)

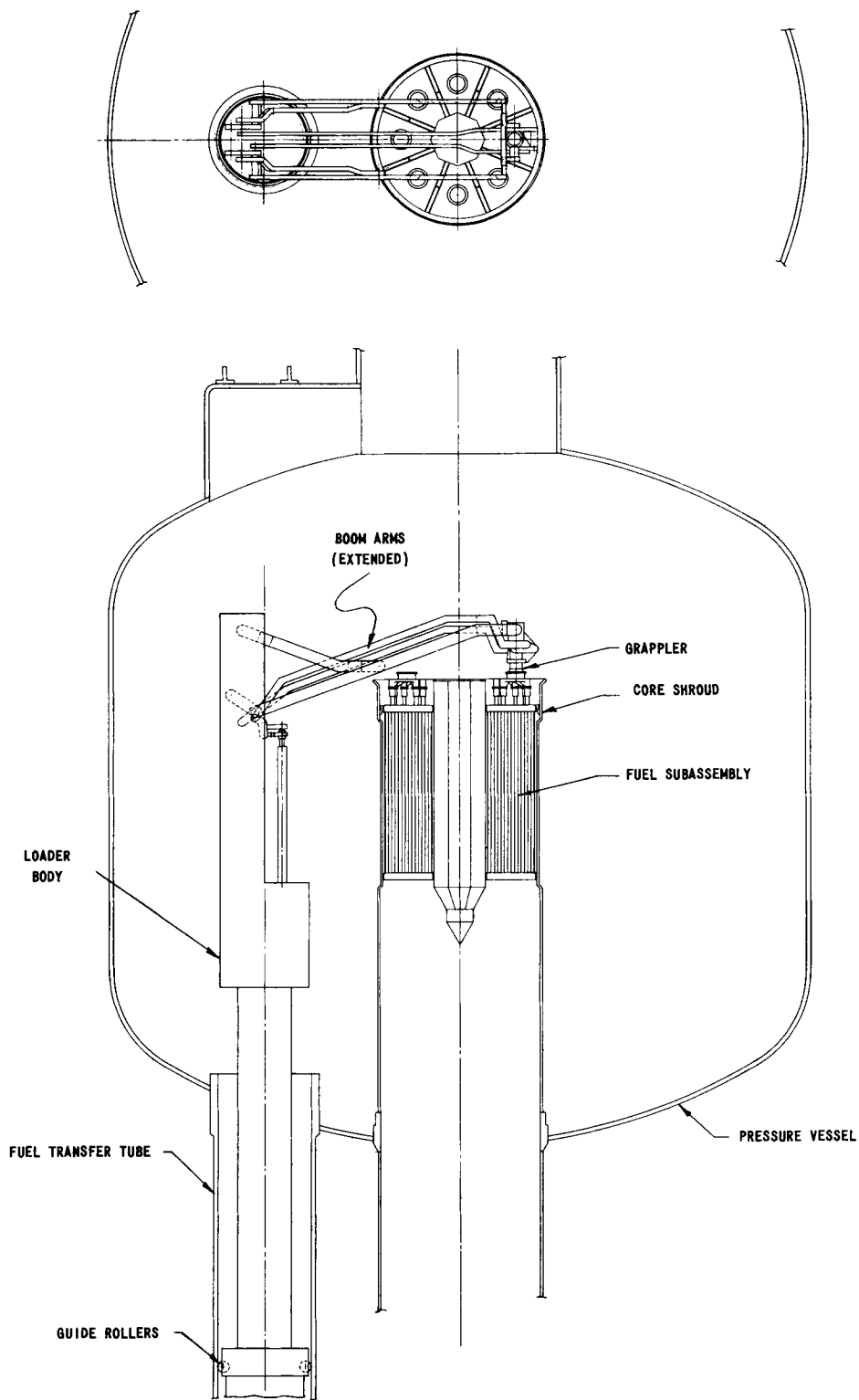
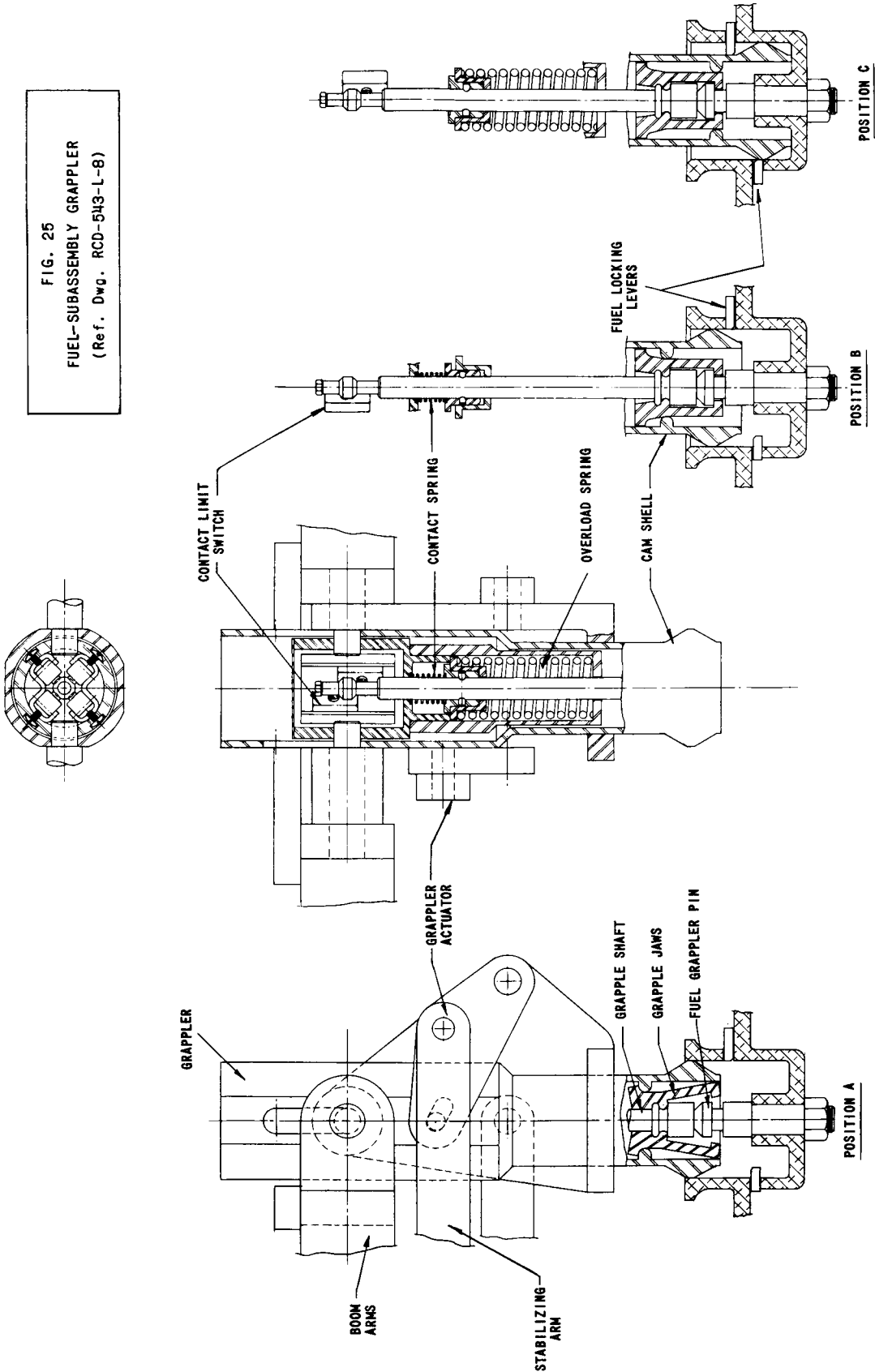


FIG. 24  
FUEL LOADER EXTENDED OVER CORE SUBASSEMBLY  
(Ref. Dwg. RCD-543-L-8)



immobilize the fuel subassembly (see Position C, Fig. 25 and Fig. 3). The grappler is disengaged, the boom retracted and the mechanism lowered out of the reactor. The foregoing cycle is repeated for each of the eight subassemblies. The unloading cycle is the reverse of the loading cycle.

Instrumentation in the control room enables the operator to closely control all phases of the loading and unloading cycles. Limit switches, interlocks, counters and other safety devices are incorporated in the system to ensure positive execution of each operation in the established sequence.

Maintenance and/or repair of the fuel-transfer mechanism is accomplished by lowering the unit into the charging tube and closing the gate valve to isolate the tube from the reactor. The transfer tube is pumped dry, uncoupled, and lowered into the elevator shaft to expose the transfer mechanism.

#### b. D<sub>2</sub>O Fuel Storage Tank

The D<sub>2</sub>O fuel storage tank (Fig. 26) is a stainless steel tank (7 ft dia.) designed for an internal pressure of 100 psia. The tank comprises three sections: one section is used to transfer fuel to and from the reactor; the second section is used to store spent fuel for periods up to three weeks prior to transfer to the H<sub>2</sub>O storage canal; and the third section is a lateral extension of the main tank for placing a fuel subassembly in the vicinity of the Spent Fuel Irradiation Facility (SFIF-1). The primary D<sub>2</sub>O coolant flows through the tank, a filtering system, and back into the main D<sub>2</sub>O system.

The equipment within the tank consists of fuel carts on casters, roller chain conveyors for transporting the carts, turntables with guide plates to route the carts to the desired tank section, an indexing mechanism for positioning the subassembly relative to its ultimate position in the core shroud, and a hydraulic actuating mechanism for positioning the cart.

In the unloading sequence, the vertically mounted roller chain conveyor moves an empty fuel cart onto the indexing mechanism adjacent to the fuel-transfer tube. The spent fuel subassembly is lowered by the fuel-handling mechanism into the properly indexed cavity in the cart. The cart is moved by the hydraulic actuator to the conveyor where the cart is engaged and transported by the pick-up rods to the storage transfer station. The turntable at this station is rotated to position the guide plate to receive the cart and route it to either the storage canal or to the irradiation facility turntable. In the latter case, the spent fuel cart is picked up and conveyed to a position in front of the SFIF-1. The lead shield external to the tank wall can be removed to allow radiation from the fuel assembly into the shielded experimental facility.

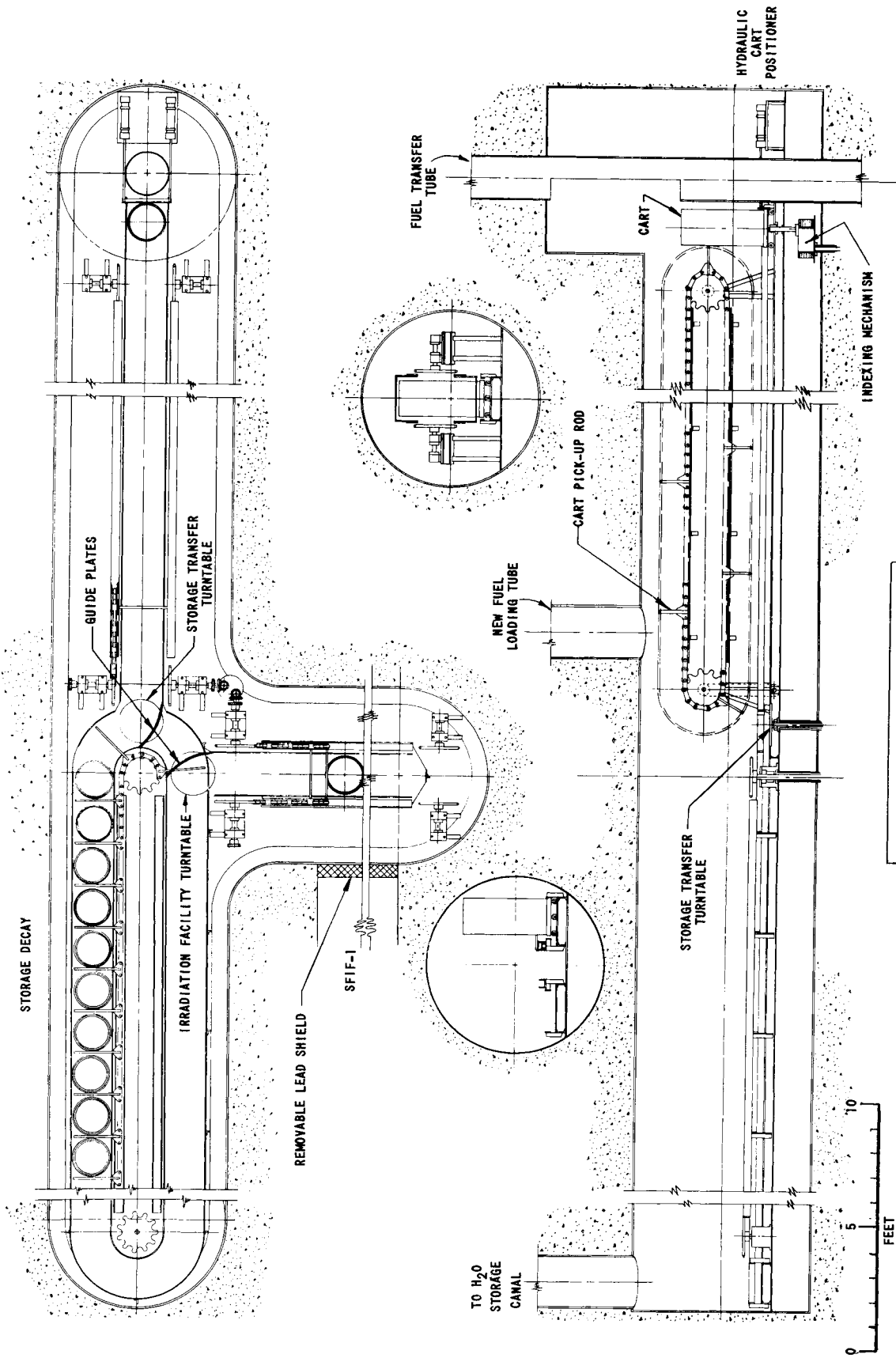


FIG. 26  
D<sub>2</sub>O FUEL STORAGE TANK  
(Ref. Dwg. RE-5-24242-E)

The loading cycle is accomplished by positioning an empty cart (from the decay storage area) beneath the new fuel-loading tube. The cart with the new subassembly is conveyed to the indexing mechanism. The action of this mechanism inserts a keyed shaft into the cart bottom and rotates the cart and, hence, the subassembly to a position corresponding to the ultimate position of the subassembly in the core shroud. The fuel-handling mechanism is operated to remove the subassembly for transfer to the core as described previously.

The drive sprockets of the conveyors and the turntables are operated by shaft extensions to drive mechanisms external to the tank wall and biological shield.

Following a 3-week decay period, the spent fuel subassemblies are transferred from the  $D_2O$  storage tank, through the unloading tube, into a coffin for further transfer to the  $H_2O$  canal and final disposition.

## B. Site and Buildings

### 1. Site

The proposed site of the Mighty Mouse Reactor complex at Argonne National Laboratory is directly south of the Experimental Boiling Water Reactor (Bldg. 331); this location is bordered by Meridian Road to the west and by Bluff Road to the south (see Fig. 2).

One quadrant of the area surrounding the Reactor Containment Building is clear of obstructions so that six horizontal beam holes can be used for long beam time-of-flight neutron studies.

The cooling tower and the stack building are south and east, respectively, of the Containment Building. The vapors and air expelled from both structures are entrained by the prevailing southwesterly winds away from existing buildings on the ANL site.

The following building and process requirements are serviced by the Laboratory Utilities System:

- (1) Domestic water is supplied for dumping water, toilet and shower rooms, janitor closets, and fire protection.
- (2) Laboratory water is supplied to all process areas and laboratories.
- (3) Sanitary sewer services drinking fountains, toilet and shower rooms, janitor closets, etc., except where activity is a factor.



- (4) Laboratory waste sewer services all drains in the process areas, laboratories, hot showers, and special equipment where activity is present. The majority of these drain lines run to the retention tanks and hence to the laboratory waste sewer system.
- (5) Clear water drains involving equipment and process cooling water are connected direct to the laboratory waste sewer system.
- (6) Storm sewer system provides adequate storm water drainage.
- (7) Natural gas is supplied to required areas.
- (8) Steam is supplied for heating and, as required, for processing.

Owing to the large amount of cooling water necessary for the operation of the reactor, it is proposed to use water from the nearby Chicago Sanitary and Ship Canal. A pumping station on the canal will be sized to handle the needs of the Mighty Mouse site and any foreseeable future expansion of the Laboratory cooling water supply.

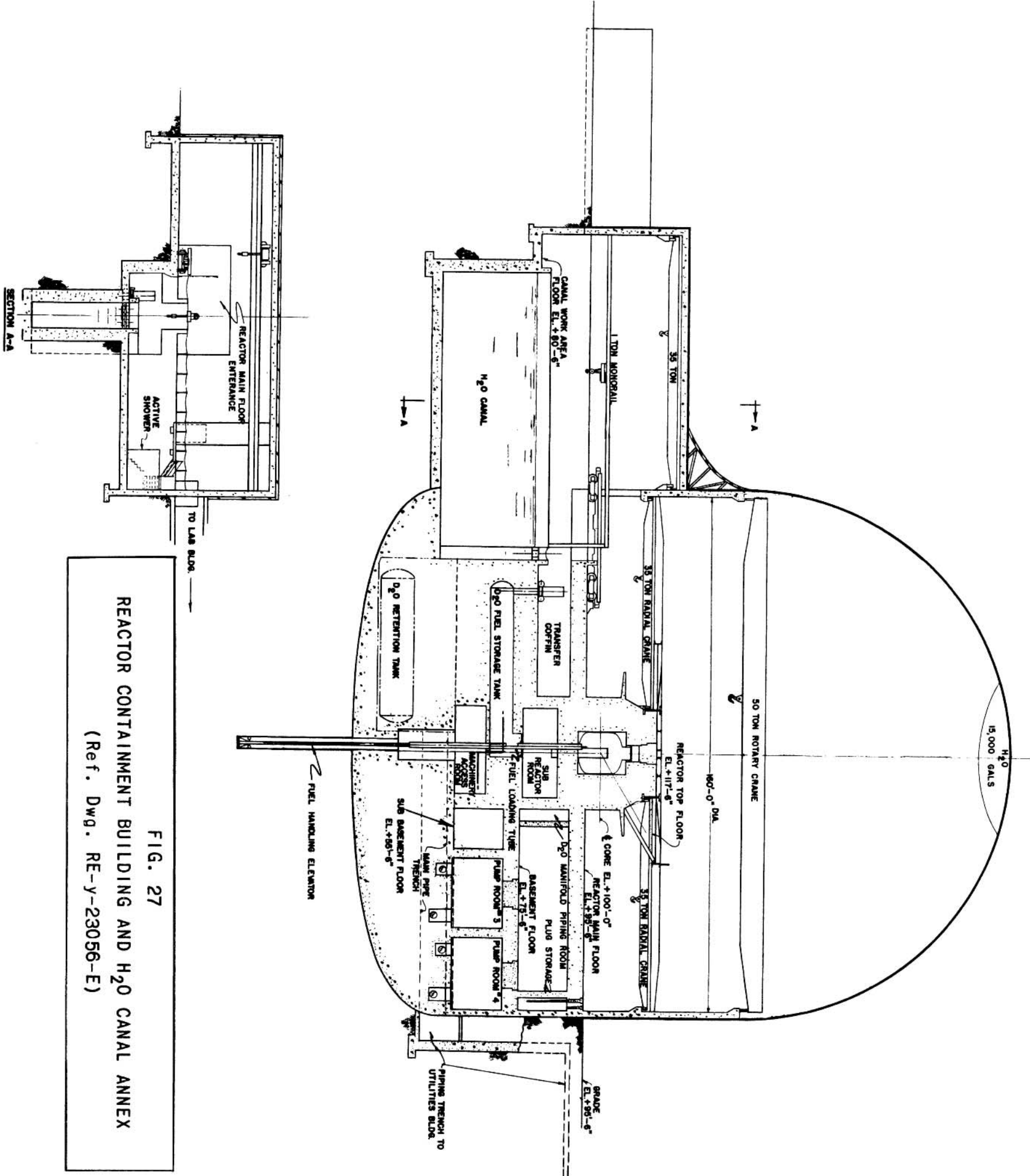
## 2. Buildings

Except where the basic functional requirements dictate the shape and size of the structure, the architecture is similar to existing buildings at ANL.

### a. Reactor Containment Building and H<sub>2</sub>O Canal Annex

The Reactor Containment Building consists of two integral structures: one contains the reactor and operating equipment, and the other a rectangular annex that houses the H<sub>2</sub>O canal, coffin and crate storage, and shipping area (see Figs. 27 and 28).

The reactor is housed in a structurally framed reinforced concrete cylinder, capped at grade level with a cylindrical steel tank with a hemispherical head, as shown in Fig. 27. The building is 164 ft OD, 204 ft high, with 74 ft below grade and 130 ft above grade level. The steel dome is constructed of welded steel plate, 1 in. thick in the cylindrical section, and  $\frac{3}{4}$  in. thick in the hemispherical section. The top dome structure supports a 15,000-gal tank of light water for emergency cooling.



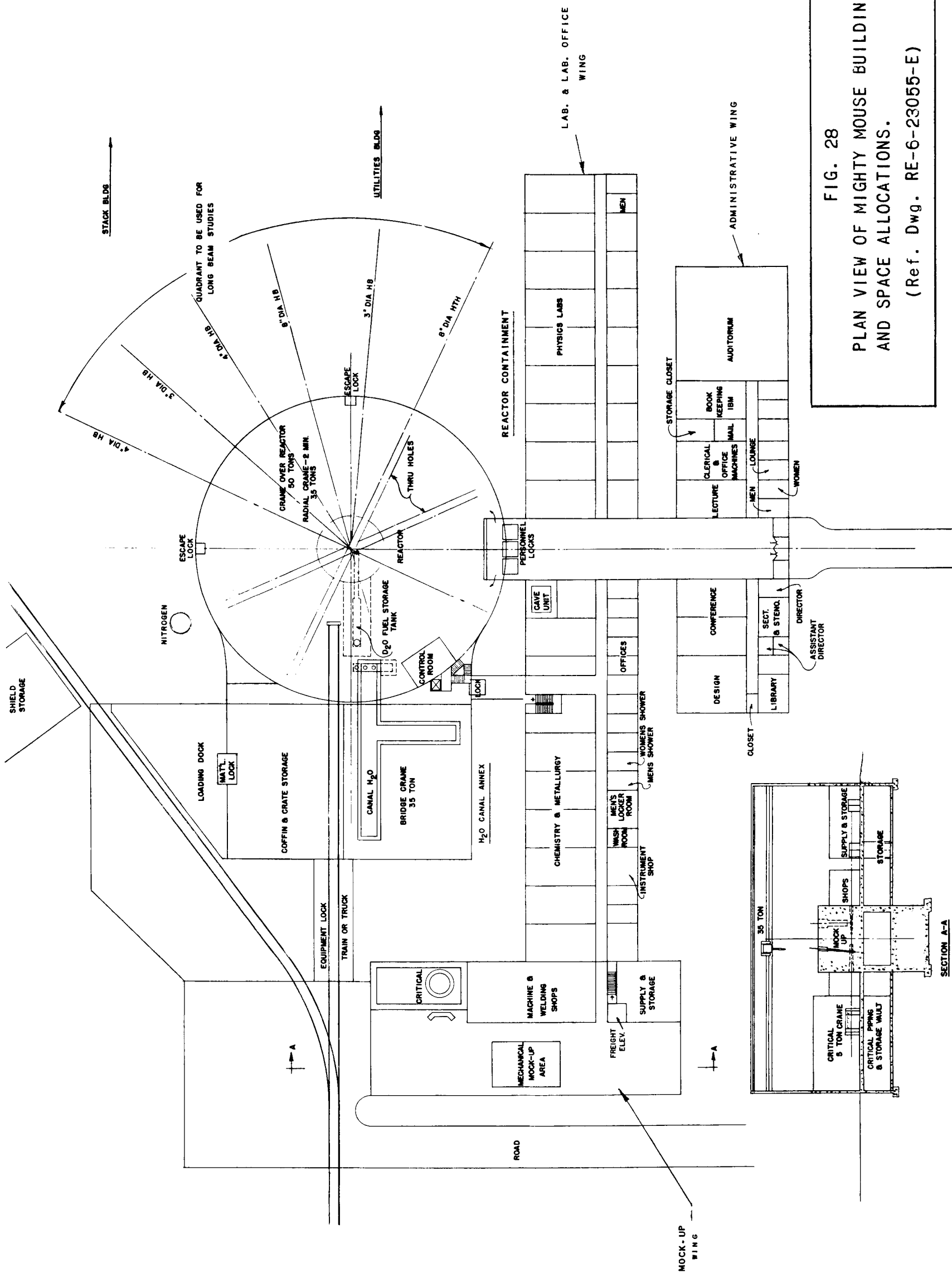


FIG. 28  
PLAN VIEW OF MIGHTY MOUSE BUILDINGS  
AND SPACE ALLOCATIONS.  
(Ref. Dwg. RE-6-23055-E)

### Sub-basement

The sub-basement, or lowest level (Fig. 29), has a ceiling height of 15 ft, a floor loading of 5000 lb/ft<sup>2</sup>, and a net usable area of 19,855 ft<sup>2</sup>. Most of the floor area is allocated to the D<sub>2</sub>O circulation and cooling system. Large-sized equipment, i.e., heat exchangers, pumps, and their control valves, are installed in individually shielded and ventilated cubicles.

Other shielded areas are reserved for the D<sub>2</sub>O clean-up and demineralizer system; the H<sub>2</sub>O clean-up and demineralizer system for processing water from the H<sub>2</sub>O canal; and the helium gas system for processing and circulating helium in and around the pressure vessel.

The shielded D<sub>2</sub>O fuel storage tank is placed on a mezzanine level between the sub-basement and the basement level. A right-angled extension into the sub-basement floor allows the transfer of an expended fuel element into the canal area adjacent the irradiation facility for use as a source for radiation damage studies.

The remaining floor area contains the H<sub>2</sub>O canal footing and walls, stairways (3), elevator shafts, entrance to the machinery access room, and aisles. The aisle ways are large enough for the removal of the large equipment. The equipment can be passed up and, if necessary, out of the building through hatches in the floors of the two upper levels.

All horizontal utility and water-cooling lines are installed below the floor level in shielded trenches that connect to the pipe tunnel from the Utilities Building. Vertical piping to the reactor, with the exception of the primary D<sub>2</sub>O coolant lines, extends through the floor into a shielded manifold room in the basement where the valving for the secondary D<sub>2</sub>O systems is installed. The whole D<sub>2</sub>O system can be retained or returned to two retention tanks below floor level at the lowest point in the system.

### Basement

The basement level (Fig. 30) has a ceiling height of 15 ft, and a gross area of 21,400 ft<sup>2</sup>. The floor loading is 1,500 lb/ft<sup>2</sup> normal, or 6,000 lb concentrated. The floor area is allocated to permanent facilities for operation and maintenance of the reactor and auxiliary equipment, and to temporary test equipment for the reactor experiments.

The permanent facilities include:

- (1) two shielded D<sub>2</sub>O manifold rooms that house the secondary D<sub>2</sub>O system piping and valving;

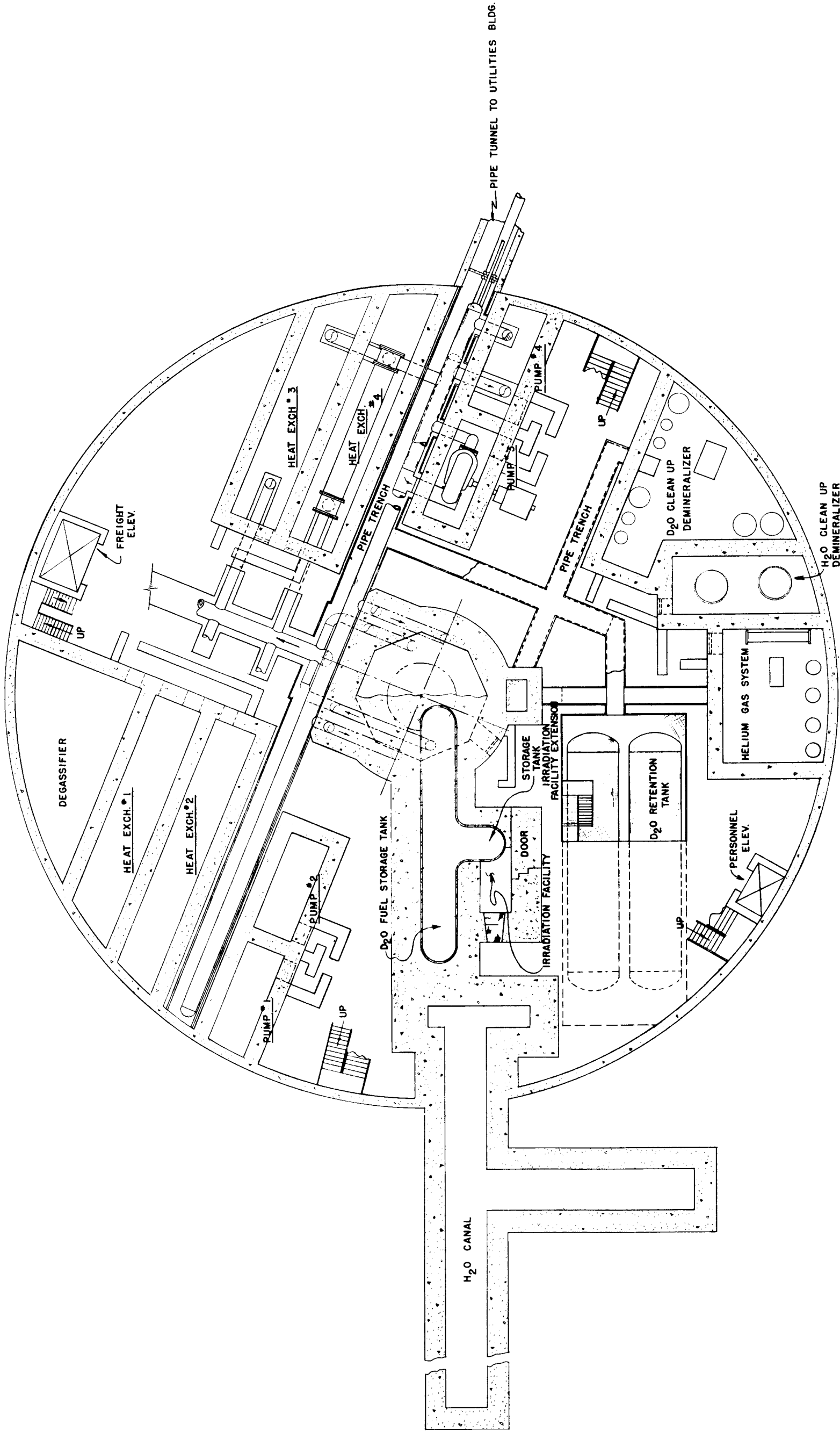


FIG. 29  
PLAN VIEW OF SUB-BASEMENT LEVEL  
(Ref. Dwg. RE-6-23060-E)

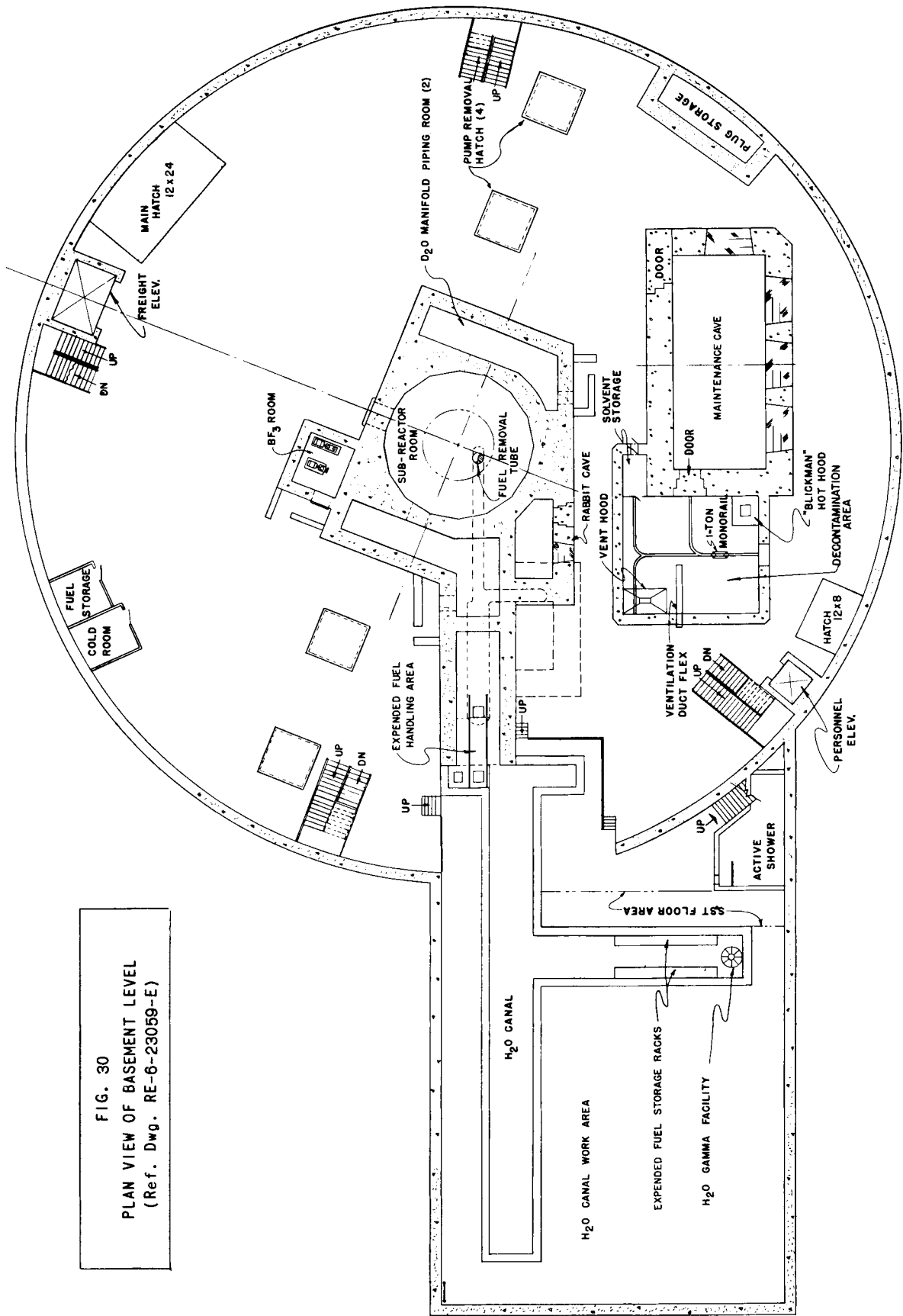


FIG. 30  
PLAN VIEW OF BASEMENT LEVEL  
(Ref. Dwg. RE-6-23059-E)

- (2) a shielded  $\text{BF}_3$  equipment room for the control and processing of the reactor fluid control system;
- (3) a shielded area on the mezzanine level to facilitate coffin transfer of expended fuel from the  $\text{D}_2\text{O}$  fuel storage tank to the  $\text{H}_2\text{O}$  canal (the  $\text{H}_2\text{O}$  canal opening is also on the mezzanine level);
- (4) the sub-reactor room for maintenance of the control blade drives, and for access to the vertical through-holes;
- (5) a cold room for storing liquified gases and other refrigerants for the cryogenic facilities;
- (6) a fuel storage vault;
- (7) a shielded beam plug storage area; and
- (8) a rabbit cave and a maintenance cave.

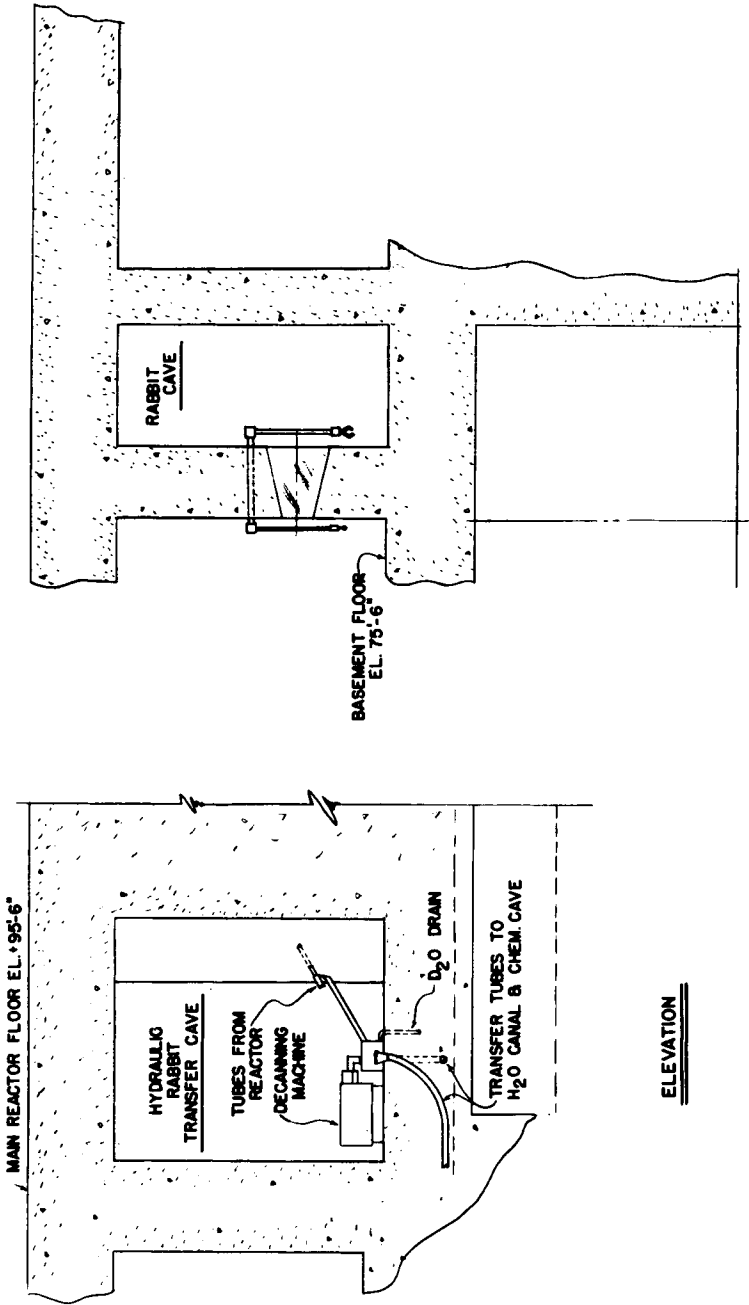
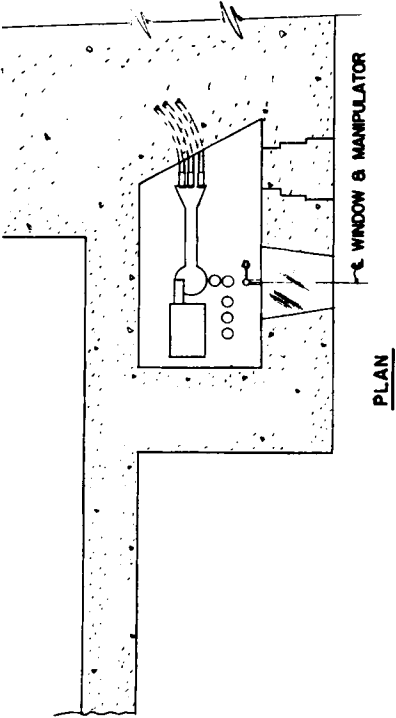
The rabbit cave (Fig. 31) is 11 ft long, 6 ft wide, and 15 ft high. It is designed to facilitate immediate inspection of samples expelled from the hydraulic rabbit test facility in the reactor. The windows, manipulators, and decanning machine are similar to that presently used in the Chemistry Division caves. From the rabbit cave, the samples are transferred (pneumatically or hydraulically) to either the  $\text{H}_2\text{O}$  canal or the Chemistry Wing. The rabbit cave is designed for gamma, beta, and alpha containment.

The maintenance cave is sized to accept a vertical beam tube. It is 40 ft long, 17 ft wide, and 15 ft high. There are four window stations, each to be serviced with Argonne No. 8 manipulators. The permanent equipment installed within the cave is to include a heavy-duty General Mills Manipulator, remote-controlled machining and welding apparatus, and a 2-ton bridge crane that sweeps the entire cave area.

Contaminated operational or experimental equipment is brought into the cave through a shielded door, disassembled, repaired or inspected, re-assembled, and transferred into the adjoining decontamination area for ultimate disposition or return to service.

The vertical support columns in the basement are arranged to define potential cubicles that can be walled with composite shielding brick. Each cubicle is serviced with utilities and an independent exhaust system.

FIG. 31  
RABBIT CAVE FOR INSPECTION AND  
TRANSFER OF SAMPLES FROM REACTOR  
(Ref. Dwg. RE-6-23123-D)





The floor and the ceiling are constructed of high-density concrete (3 ft thick) to shield the upper and lower floor levels.

### Main Floor

The main floor (Fig. 32) has a gross area of 21,400 ft<sup>2</sup>, a gross volume of 2,202,000 ft<sup>3</sup>, and a net usable area of 19,855 ft<sup>2</sup>. The floor loading is 1,500 lb/ft<sup>2</sup> normal or 6,000 lb concentrated.

Most of the floor area will be used for thermal column and horizontal beam experimental equipment. The entire floor area surrounding the reactor is serviced by two 35-ton radial cranes. The beams of the cranes are mounted on trucks that rotate on rails supported at the outer edge by the cylindrical concrete section of the building. The inner rails are supported by the reactor biological shield.

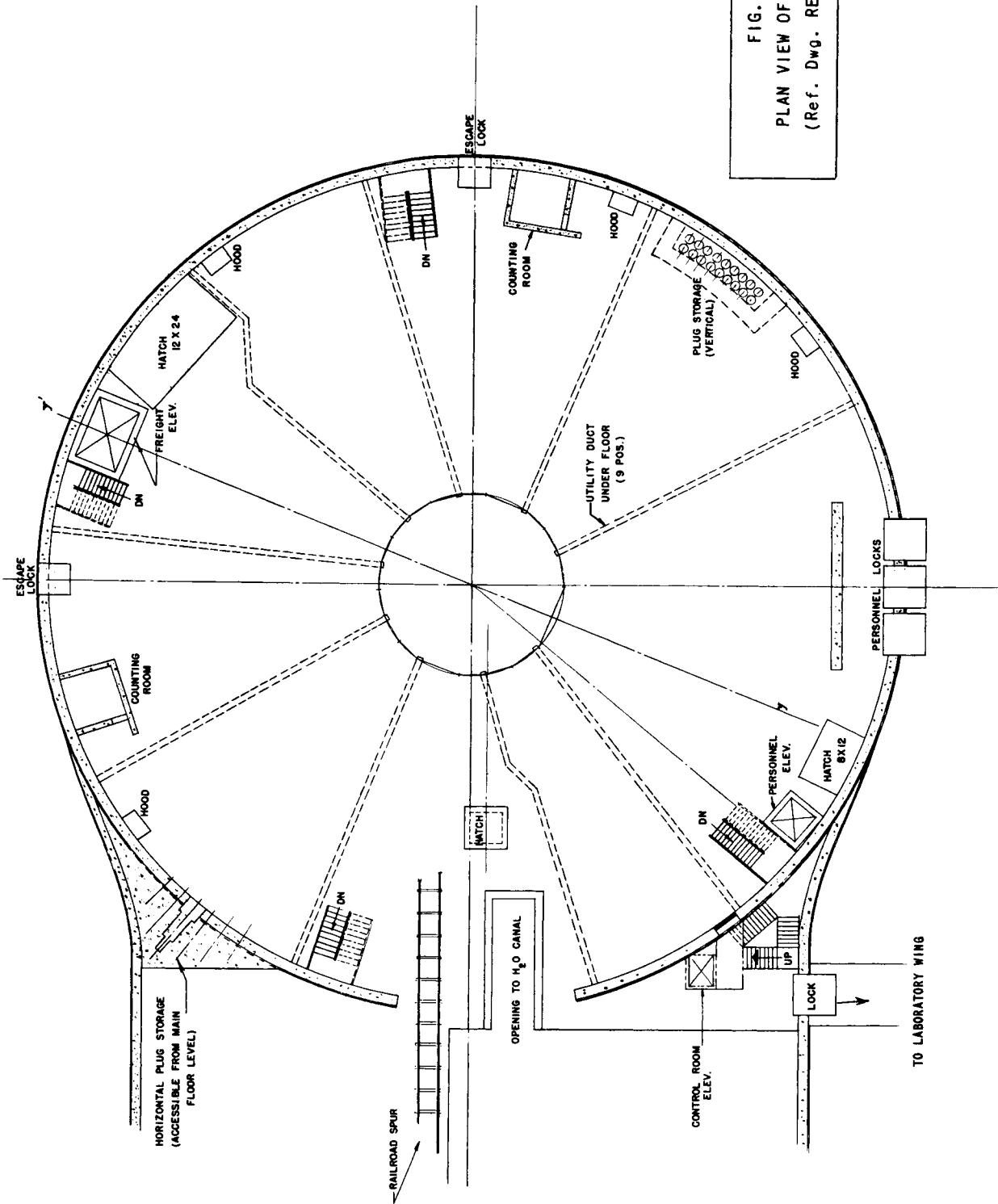
All floor openings (equipment hatches, elevators, stairwells) are located at the periphery of the main floor. Openings in the containment shell at grade level include three personnel locks for normal building access, three emergency escape locks, an access lock from the Laboratory wing to the control room, and the opening for the railroad spur in the region of the H<sub>2</sub>O canal annex.

### Top Floor

The top floor (Fig. 1) is designed to support light equipment and instrumentation at the vertical experimental facility access openings in the top of the biological shield. The floor structure consists of ten radial girders that bear on the concrete shell of the building and on the reactor biological shield. The floor structure contains seven ramp segments that depress in line with the down-beam holes to facilitate transfer of equipment from the holes into a shielded coffin supported by the 50-ton overhead rotary bridge crane. The crane can also be used to service the horizontal beam holes at the main floor level by removing the floor plates in the balcony and the top floor above the designated work area.

The capacity of the overhead crane is based on the calculated weight of the core shroud transfer coffin. The coffin is assumed to be a lead cylinder (41 in. ID, 57 in. OD, 10 ft high), sheathed in 1-in. thick steel, and capped with cylindrical covers 8 $\frac{1}{4}$  in. thick. The resultant weight, including a safety factor of 1.2, is 42 tons, exclusive of any cooling apparatus. Accordingly, the crane capacity was set at 50 tons. The dose rate from the proposed coffin will not exceed 13 mr/hr at any point of the outer surface (see Appendix C).

FIG. 32  
PLAN VIEW OF MAIN FLOOR  
(Ref. Dwg. RE-6-23058-E)



The 50-ton crane can be used directly for transfer operations from the vertical facilities to the H<sub>2</sub>O canal, or to support a high-speed crane to facilitate rapid transfer of light loads.

### Control Room

The reactor control room is located above the top floor, with direct communication to experimenters on top of the reactor. Other areas throughout the containment building are in communication with the control room by telephone and are in visual contact through closed circuit television. The control room can be entered through the rear, by either staircase or elevator, from the H<sub>2</sub>O canal annex.

### H<sub>2</sub>O Canal Annex

The H<sub>2</sub>O Canal Annex (see Figs. 27 and 28) is contained within a 1-in. thick steel structural extension of the reactor containment shell. The annex is 80 ft wide, 108 ft long, and 43 ft high. The permissible floor loading is 1,500 lb/ft<sup>2</sup> normal and 6,000 lb concentrated. The gross area is 11,250 ft<sup>2</sup>, the gross volume 776,080 ft<sup>3</sup>, with a net useable area of 10,806 ft<sup>2</sup>.

The total area is divided into two, approximately equal, sections. One section is for the storage, handling and shipping of transfer casks, coffin and equipment. The other section contains the "T"-shaped H<sub>2</sub>O canal and work area. A stainless steel floor area is assigned for the decontamination of low-level irradiated items. An active shower is also located in this area for personnel in the building.

Shipping casks and other heavy items in the shipping area and the H<sub>2</sub>O canal or work area are transported by the 35-ton crane. Light underwater lifts at the canal are handled by the 1-ton monorail crane.

The storage and shipping section of the annex is on the same level as the reactor main floor and can be entered from either the main floor of the reactor area or from the outside of the building through one of three locks: (1) the personnel lock in the vicinity of the control room; (2) the material lock from the truck loading dock and (3) the equipment lock that will accommodate a large truck or train car to be brought directly on to the main floor.

The "T"-shaped H<sub>2</sub>O canal (see Fig. 30) is 8 ft wide, 28 ft deep, 88 ft long at the top of the "T," 40 ft along the stem, and lined with a stainless steel. The 23.5-ft section perpendicular to the 88-ft length

inside the dome structure affords more working area near the reactor and allows the fuel-transfer coffin to be operated without interfering with routine work around the canal. The water in the canal and the work area floor elevation are at the mezzanine level.

The top of the "T" is allocated to equipment for processing sample holders and specimens expelled from the hydraulic rabbit terminal in this area. The stem is a storage area for the expended fuel elements prior to their shipment to a fuel-processing plant. The stem also contains a permanent gamma irradiation facility with expended fuel elements as the source of radiation.

### Utilities

In addition to the utilities furnished by the Laboratory Utility System, the following utilities are originated within the Reactor Containment Building: (1) process  $D_2O$ ; (2) demineralized water; (3) process exhaust; (4) vacuum; (5) helium; and (6) liquid nitrogen.

Utilities are brought through ducts fastened to the ceiling of the basement level, and up through vertical ducts embedded into the faces of the reactor biological shield to the horizontal beam holes, thermal column, down-beam holes and vertical facilities.

### Heating, Ventilating, and Air Conditioning

The design philosophy for the heating, ventilating, and air conditioning of the proposed buildings is based primarily on the precise control of the filtration, volume, and directional flow of supply and exhaust air, consistent with established safe practices for the protection of Laboratory personnel in areas where radioactive materials are processed or stored. The general philosophy is to always have air flow from clean areas inward toward potentially contaminated areas to prevent the spread of radioactivity. Where adjoining areas both contain radioactive materials, the air flow is toward the area containing materials that represent the highest potential radiation hazard. The various areas of the building in order of increasing radioactive contamination hazard are: (1) Operating area - Main Floor; (2) Sub-basement; (3) Storage and water canal area; (4) Basement; and (5)  $D_2O$  Canal area.

The entire building is heated by the ventilation air. Re-heat coils are provided for the various zones where direct supply air is introduced; low-pressure steam coils are installed in fan-coil circulating units located in other areas. The space temperatures are maintained at  $75^{\circ}F \pm 2^{\circ}F$  with an outside temperature of  $-10^{\circ}F$ .

Steam and condensate lines extend from the Utility Building, through the pipe tunnel, to the Reactor Building. The condensate returns by gravity flow to the Utility Building.

The air supply for the Reactor Building originates in the Utility Building. The inlet filters, pre-heat coils, cooling coils, and fan are located in the latter building. The main supply air duct (68,500 cfm) extends through the pipe tunnel to the Reactor Building. An automatic isolation butterfly valve is installed at the entrance of the duct to the containment shell.

Three main exhaust systems serve the Reactor Building: General Exhaust System; Prefiltered Special Exhaust System; and a high-efficiency absolute prefiltered Beam Hole Exhaust System that discharges into the Prefiltered Special Exhaust System before leaving the Reactor Building.

The General Exhaust System will exhaust a maximum of 15,800 cfm and a minimum of 8,800 cfm from the operating area. The capacity of the Beam Hole Exhaust System will vary from 3,000 to 10,000 cfm, depending on the number of beam holes open at one time.

The ducts from the general and the prefiltered exhaust systems extend overhead to the Stack Building and into a combined walk-in final filter chamber containing 72 high-efficiency absolute-type filters. The prefiltered system features two exhaust fans (one a standby) to provide the required additional static pressure on the inlet side of the final filter chamber. On the effluent side, two stack booster fans (one a standby) equipped with back-draft butterfly valves discharge 68,500 cfm up a 150-foot stack to the atmosphere.

All areas of the Reactor Building are air conditioned with the exception of the D<sub>2</sub>O canal area, which has limited occupancy for short periods of time. The air-conditioned areas are held to 80°F and 50% maximum relative humidity during the air-conditioning season.

Cooling and dehumidification is accomplished by a central system, located in the Utility Building that supplies chilled water to central and individual air-conditioning units. Refrigeration for the water is provided by absorption-type or centrifugal-type refrigeration machines with multicell winterized cooling tower. The estimated cooling load of the building is 350 tons. A cooling tower of appropriate capacity is located at ground level near the Utility Building. Cooling loads are based on indoor summer conditions stated above, and outside temperatures of 95°F dry bulb, and 75°F wet bulb.

A separate air-supply system is provided for cooling the four pump motors located in the sub-basement. An automatic isolation butterfly valve at the containment shell closes in the event of a reactor incident. The duct work in the building is airtight and under positive pressure with respect to the building. The heated air from the motors is exhausted outside the building through another isolation valve in the reactor shell.

b. Mock-up Wing

The Mock-up Wing (see Fig. 32) is 160 ft long, 70 ft wide, and 73 ft high, with 56 ft above grade level. The basement has a 15-ft ceiling, a gross floor area of 10,300 ft<sup>2</sup>, a gross volume of 153,000 ft<sup>3</sup>, and a net usable area of 9,800 ft<sup>2</sup>. The floor loading is 500 lb/ft<sup>2</sup>, normal. The main floor has a gross area of 10,200 ft<sup>2</sup>, a gross volume of 622,200 ft<sup>3</sup>, and a net usable area of 8,630 ft<sup>2</sup>. The floor loading is 1,500 lb/ft<sup>2</sup>, normal, or 6,000 lb, concentrated. The installations in the building include: (1) a Mechanical Mock-up Facility to performance test all mechanical equipment prior to installation in the reactor; (2) a Zero-power Critical Assembly to predetermine the effects on reactivity of the various experiments to be installed in the reactor; (3) a machine shop and supply room; (4) a freight elevator to the basement; and (5) a 35-ton overhead crane that services the entire wing.

Mechanical Mock-up Facility

The Mechanical Mock-up Facility (Fig. 33) is a structure of dense concrete, 35 ft long, 30 ft wide, and 22 ft high. Installed in each of the three walls and top is at least one counterpart of the horizontal, down-beam, and vertical facilities installed in the reactor. The simulation includes all utilities offered at the reactor face, a tilting floor section and balcony at two of the down-beam holes, and a working area between building wall and face of the mock-up structure identical to the distance between the reactor face and the containment shell.

Each facility features an independent heat source controlled to simulate the reactor environment in that region. The respective heating coils are installed in the hollow center region of the mock-up structure to facilitate maintenance. The 8-in. vertical through-hole extends downward through this region into the "subreactor" room.

Dense concrete is used to protect personnel against radiation from equipment that has been used previously in the reactor. The heavy crane and floor loading are required for handling the transfer coffin.

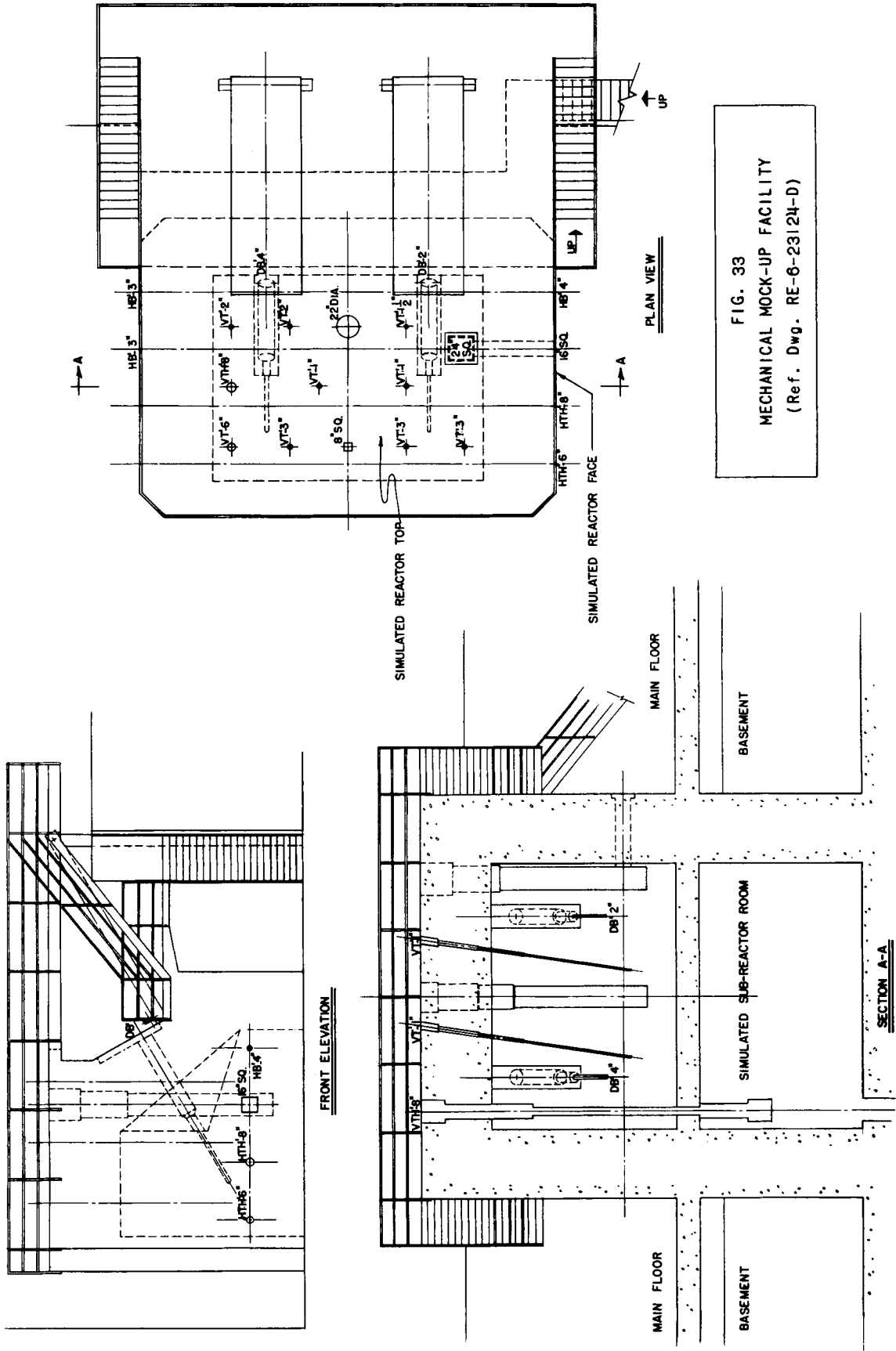


FIG. 33  
MECHANICAL MOCK-UP FACILITY  
(Ref. Dwg. RE-6-23124-D)

### Zero-power Critical Assembly

A zero-power, D<sub>2</sub>O-moderated critical assembly is installed in a shielded room in the corner of the high bay. The core is contained in an aluminum vessel on the main floor level. The retention tanks, pumps, and heat exchanger are installed in a shielded room in the basement.

The shield and the vessel are penetrated by at least one of each vertical thimble and horizontal beam facility installed in the Mighty Mouse reactor. In addition, there are two hydraulic rabbit and one pneumatic rabbit installations.

The area inside the shielded room is serviced by a 5-ton crane. The slab roof of the room can be removed to facilitate operations with the 35-ton overhead crane.

### Heating, Ventilating, and Air Conditioning

A central air-handling unit in the basement supplies filtered and heated outside air to the main floor and basement. The warm air supply also provides 100% of the ventilation air for the building. In addition, there is one recirculation unit located in the basement and on the main floor. Individual re-heat coils are installed in the duct work to the main floor, machine shop, storage, and basement, to compensate for the transmission heat loss in these areas. The heat losses are based on maintaining an inside temperature of 70°F with outside conditions at -10°F and 15-mph winds.

A separate air-handling unit is installed in the critical assembly room on the main floor. The air is drawn from the main floor area and heated consistent with the heating demands of the critical room.

The exhaust fan equipment room is heated by finned-tube radiators mounted on the walls.

The main floor, machine shop, storage, and basement areas are maintained at a slightly higher static pressure relative to the critical and mechanical mock-up areas.

The entire building is air conditioned with the exception of the mock-up area and basement critical area. Cooling and de-humidification is accomplished by a central system, located on the service floor of the administration building, that supplies chilled water to four air-handling units. The estimated cooling load of 150 tons is based on summer conditions of 80°F dry bulb and 50% relative humidity indoors, and 95°F dry bulb, and 75°F wet bulb outdoors.



The main air-handling supply unit supplies cooled air directly to the main floor, machine shop, storage, and basement areas. The cooling coil in this unit will satisfy the ventilating air load.

The recirculation unit on the main floor has a chilled water coil that can be controlled independently to satisfy the transmission and internal heat loads in the basement area by further cooling the recirculation air supplied to the basement.

The first floor of the critical room is serviced by a recirculation unit with a chilled water coil that can be controlled to satisfy the transmission and internal heat loads in the area by further cooling of the air supplied indirectly from the main floor.

The Mock-up Wing is exhausted by two separate systems. One system draws air from the critical and the mechanical mock-up areas through Type H, 25 FG pre-filters installed in the exhaust intakes in each area. The air is discharged through a bank of vertical filters of the walk-in type, to a 60-foot stack. The critical and the mechanical mock-up areas receive 10 air changes per hour.

The second or general exhaust system removes a total of 16,300 cfm of air from the main floor, machine shop, storage, and basement areas. The air is discharged through final filters (similar to those used for the mock-up exhaust system) to the 60-ft stack.

c. Laboratory and Laboratory Office Wing

The Laboratory and Laboratory Office Wing is 412 ft long, 58 ft wide and 27 ft high, with 12.5 ft above grade level. The main floor has a ceiling height of 10 ft, a gross area of 25,504 ft<sup>2</sup>, a gross volume of 193,552 ft<sup>3</sup>, and a net usable area of 13,940 ft<sup>2</sup>. The floor loading is 100 lb/ft<sup>2</sup>. The service floor, or partial basement, has a ceiling height of 15 ft, a gross area of 16,104 ft<sup>2</sup>, a gross volume of 331,552 ft<sup>3</sup>, a net usable area of 11,420 ft<sup>2</sup>, and a floor loading of 200 lb/ft<sup>2</sup>.

The wing is portioned into standard module-size laboratories (a module is 27 ft long and 10 ft wide). Each module has panelled, hollow walls that accommodate utilities from the service floor. The laboratories are equally divided by the entrance hall and equipped for chemistry and metallurgy experiments on one side, and physics experiments on the other side. There are 18 double module-size laboratories, 10 large offices, and 12 small offices for the convenience of experimenters. The balance of the wing is allocated to an instrument shop, wash rooms, showers and locker rooms, in close proximity to the work areas. The chemistry laboratories include a small cave for processing canisters expelled from the hydraulic

rabbit tube interconnecting the Chemistry Wing and the basement of the Reactor Containment Building. The cave is equipped with Argonne No. 8 manipulators, decanning machine, and sample hold-up area, and is designed for alpha and gamma containment.

### Heating, Ventilating and Air Conditioning

Heating is accomplished by a split system. Two-thirds of the heat is supplied by hot water convectors installed along the outer walls of the offices, and by hot water radiant panels embedded in the floors of the laboratories. The remaining one-third is supplied by the ventilation system air. The basement is heated by the ventilation system air. The exhaust fan lofts are heated by fin-tube steam radiators along one wall.

The ventilation system air supply is filtered through roughing and secondary filters. A total of 47,000 cfm of outside air is divided into separate supplies for offices, laboratories, and corridor variable air-supply system. The air flow is from the offices, across the corridor, to the laboratories. In addition, each 20-ft module laboratory is supplied directly with 2,000 cfm of conditioned air. If necessary, the air supply to the laboratories can be augmented by the corridor variable air supply system. Supply fans are located on the service floor. The service floor is ventilated with outside air consistent with the heat generated by the operating equipment in that area.

The main floor is air conditioned with 100% outside air, cooled to maintain laboratory conditions of 80°F and 50% relative humidity. The service floor area is not air conditioned. The cooling and dehumidification is accomplished by a central system that supplies chilled water to air-conditioning units in the ventilation system. The centrifugal-type or absorption-type refrigeration equipment and chilled water unit are located on the service floor of the Administration Building. The cooling load for the Laboratory Building is estimated at 196 tons.

The air supply from the offices and corridors direct to the laboratories is 100% exhausted. The exhaust air from all areas used to process or store radioactive materials is discharged to the atmosphere through roughing pre-filters and AEC final filters installed in the fan lofts above these areas. The exhaust system specifications include polyvinyl chloride or glass-reinforced polyester plastic ducts.

Three fume hoods are installed in each 10-ft module. Each hood has a maximum door opening of 3.7 ft<sup>2</sup>. Pneumatic velocity controllers are installed in each radioactive hood to ensure a minimum face velocity of 135 fpm across the door opening. The hood exhaust requirements are estimated at 28,500 cfm. Roughing-type filters are installed on all hoods and in laboratory bypass ductwork.

The service floor areas are exhausted by four ducts adjusted to maintain a constant positive static pressure relative to the laboratories.

d. Administration Wing

The Administration Wing is 234 ft long, 58 ft wide, and 13 ft above grade level with a partial basement (ceiling height 13 ft). The gross area is 24,954 ft<sup>2</sup>, and the gross volume 311,362 ft<sup>3</sup>. The net usable area (including the auditorium) is 17,269 ft<sup>2</sup>. The Administration Wing is interconnected with the Laboratory Wing and Reactor Containment Building by a common entrance hall. The telephone switchboard and receptionist desk are in the entrance hall.

Heating, Ventilating and Air Conditioning

Two-thirds of the heating load for all outer offices and rooms is supplied by a hot water convector system controlled by an "indoor-outdoor" thermostat. The balance of the heat load is supplied by the ventilation system air. The interior offices are heated by the ventilation system air. The system is zoned and thermostatically controlled consistent with the respective zone requirements. The service floor areas are heated by the ventilation system air.

The Administration Building is ventilated for convenient comfort cooling. The outside air supply is determined by the make-up air requirements. A minimum of 50% of the air requirement is recirculated. The building is maintained at a slightly higher static pressure to ensure that the flow of air through main connecting corridor is toward laboratory facilities.

The Administration Building proper has 27,000 cfm of air flowing with half, or 13,500 cfm, of fresh outside make-up air. This outside air is supplied from a fan unit located on the service floor.

The service floor area is ventilated with 8,600 cfm of outside air supplied by a fan located on the service floor.

The auditorium is supplied with 50% fresh air by a separate system.

The entire Administration Wing is air conditioned to maintain 80°F and 50% relative humidity indoors with outdoor summer conditions of 95°F dry bulb, and 75°F wet bulb. Cooling and dehumidification is accomplished by a 500-ton centrifugal-type or steam absorption-type refrigeration system located on the service floor. The system is

provided with a multicelled, winterized cooling tower to be installed either on the roof, or at a suitable ground elevation. The cooling load for the building, main corridor, and auditorium is estimated at 152 tons.

There are two exhaust systems: one for the auditorium, and the other for the remainder of the building. The exhaust fans are located on the roof. The air exhausted is controlled to ensure positive flow from the building.

The service floor is exhausted by four ducts adjusted to maintain positive static pressure relative to the laboratory area.

e. Utility Building

The Utility Building is a three-level structure (sub-basement, basement, and main floor), 100 ft long, 70 ft wide, 65 ft high, with 25 ft above grade. The gross area is 21,000 ft<sup>2</sup>, gross volume 385,000 ft<sup>3</sup>, with no net usable area. The building contains the secondary cooling system pumps, air conditioning compressors for the containment building, ventilation equipment, and compressor for the cryogenic facility. The building also serves as a junction for site utilities.

The building is heated with outside air distributed to individually controlled reheat coil units installed on each level. The building is maintained at 70°F with outdoor conditions of -10°F and 15-mph winds.

The three levels receive four air changes per hour, with filtered outside air introduced directly into each level. In addition, a total of 34,000 cfm of filtered outside air is cycled through the motors of the six secondary coolant system pumps by two fans and discharged to the atmosphere. The cryogenic compressor motor is cooled independently with a fan that cycles 8,000 cfm of filtered outside air through the motor and out to the atmosphere.

The air from the three levels is exhausted by a central fan and discharged up a stack.

f. Stack Building

The Stack Building is 80 ft long, 60 ft wide, and 20 ft high, all above grade level. The gross area is 4,800 ft<sup>2</sup>, gross volume 76,800 ft<sup>3</sup>, with no net usable area. The building contains a walk-in final absolute-type filter chamber, and a fan loft comprising four large stack exhaust fans that discharge through the 150-ft stack.

During the winter season, the building temperature is maintained at 60°F by steam unit heaters supplied with low-pressure steam from the Utility Building.

Summer ventilation is accomplished by roof-type exhaust fans that remove the heat generated by the stack exhaust fans. Inlet air louvers are installed in the building walls. The roof fans and inlet louvers are operated by thermostats. No provision has been made for winter ventilation. However, during filter exchange operations, the roof exhaust fans discharge through the final filter chamber and up the 150-ft stack.

g. Shield Storage Building

The Shield Storage Building is a steel, Butler-type structure, 50 ft long, 48 ft wide, with a floor loading of 1,000 lb/ft<sup>2</sup>. The gross area is 2,400 ft<sup>2</sup>, gross volume 48,400 ft<sup>3</sup>, with a net usable area of 2,300 ft<sup>2</sup>. The structure will be used to store portable shielding slabs for use in reactor experiments. The slabs will be transported by heavy-duty fork-lift trucks.

Suspended unit heaters provide for the transmission and infiltration heat losses based on maintaining a 50°F indoor temperature, with outdoor conditions of -10°F and 15-mph winds.

Summer ventilation is provided by a manually controlled roof-type exhaust fan.

h. Cooling Tower

Waste heat from the reactor D<sub>2</sub>O heat exchangers is liberated in a natural draft, reinforced concrete cooling tower, 205 ft in diameter at the base and 290 ft high. The effluent from the heat exchangers (at 115°F) is cycled by the four 500-hp pumps in the Utility Building through a 6-ft-diameter pipe to the cooling tower 800 ft from the reactor containment building. The water enters an annular ring approximately 30 ft above the base of the tower. The water flows around the circumference of the tower, through radial piping, and downward on the splash plates and into an integral basin at the bottom of the tower. The cooled water (30°F) returns through a 7-ft-diameter suction line to the Utility Building and back to the reactor vessel.

Two 100-hp horizontal centrifugal pumps are installed in the piping for emergency shut down cooling.

The operation of the cooling tower compares favorably with mechanical draft towers, with the added advantages that it requires no exterior power source; it is virtually free of maintenance problems; and has no ground fog problem. Advantage is taken of the temperature differential between the air at the top and bottom of the tower to produce a "stack effect." This "stack effect" is promoted by the shape and size of the tower structure that confines a column of air lighter than that of the surrounding atmosphere. This feature ensures maximum cooling capacity even with zero wind velocity.

i. Retention Lagoons

Three earthen retention lagoons (capacity 1,752,600 gal) will retain the blow-down water from the cooling tower for about one hour. Water samples will be checked for radioactive contamination. If free of contamination, the water will be allowed to spill drain onto the surrounding area.

#### IV. PHYSICS

##### A. Parameters Surveyed

The fundamental aim of the physics studies was to evaluate the parameters of the system that yielded the maximum thermal neutron flux per unit power, consistent with heat-removal limitations. These limitations are real since a survey of existing reactors e.g. CP-5 showed that a power level of about 250 Mw would be required to create fluxes of the order of  $5 \times 10^{15} \text{n}/(\text{cm}^2)(\text{sec})$ .

Although heat transfer can be improved by pressurization and by boiling both methods were rejected on the grounds that they interfere fundamentally with the use of Mighty Mouse as a research reactor. With pressurization, access to the core is greatly inhibited, and a heavy pressure vessel severely depletes the flux. Boiling creates a large-amplitude, moderately high-frequency noise in the neutron beams that is objectionable in scattering experiments. The upper limit of conventional heat transfer schemes yields a heat-removal rate of about 0.5 Mw/liter which, in turn, yields a core volume of about 500 liter.

##### 1. Core Size and Moderator

The inner reflector (thermal column) should have a radius of about  $2\sqrt{\tau}$ , where  $\tau$  is the Fermi age in order to thermalize the greatest proportion of the neutrons that leak out of the core. If the core is dilute, some thermalization will occur within the core bounds and the optimum inner radius will be slightly less than  $2\sqrt{\tau}$ . If the thickness of the annulus is  $t$ , then the outer radius is  $2\sqrt{\tau} + t$ . To yield a minimum critical mass, the height should be about  $2(2\sqrt{\tau} + t)$ , which results in a core volume of

$$V = 2\pi t(2\sqrt{\tau} + \frac{t}{2}) \approx 5 \times 10^5 \text{ cm}^3 \quad . \quad (1)$$

The two most reasonable media to be employed as moderator and coolant are  $\text{H}_2\text{O}$  ( $\sqrt{\tau} \approx 5.5 \text{ cm}$ ) and  $\text{D}_2\text{O}$  ( $\sqrt{\tau} \approx 11 \text{ cm}$ ). Substitution of these values in Eq. (1) gives, for  $\text{H}_2\text{O}$ ,  $t \approx 33 \text{ cm}$  and, for  $\text{D}_2\text{O}$ ,  $t \approx 25 \text{ cm}$ . Thus, the over-all size of the core will be about the same with either media. Under these conditions  $\text{D}_2\text{O}$  is the obvious choice since, in any event, the core thickness is a few times the square root of the age, and  $\text{D}_2\text{O}$  has far less parasitic capture than  $\text{H}_2\text{O}$ . The ranges of parameters to be studied then are: inner radius, 10 to 20 cm; and core thickness, 20 to 40 cm.

The peak flux per unit power is not strongly dependent on the inner radius (over the indicated range), and the initial choice of 15 cm is optimum. The variation of peak flux per unit power with annular thickness is plotted in Fig. 34. The geometry of the reference core is then: inner radius, 15 cm; outer radius, 45 cm; and height, 90 cm.

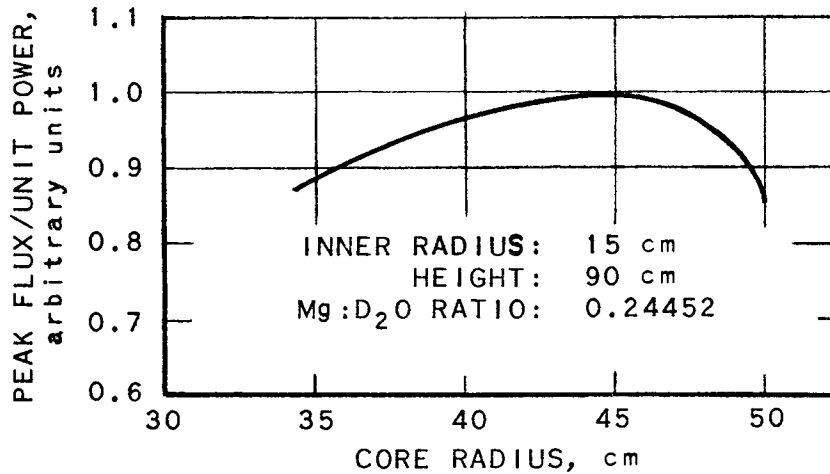


FIG. 34  
EFFECT OF ANNULAR THICKNESS OF FUEL  
ON PEAK FLUX PER UNIT OF POWER

Since the reactor cost is directly related to reactor power, exploratory studies were made to determine the performance characteristics of a core when the power level and, concomitantly, the peak flux requirements were relaxed. Based on the foregoing considerations, it is clear that lowering the power level to the order of 50 to 100 Mw will favor selection of  $\text{H}_2\text{O}$  for the inner reflector, since the critical mass for a very thin annulus will be smaller, and the flux peaking greater with  $\text{H}_2\text{O}$  than with  $\text{D}_2\text{O}$ .

Accordingly, a survey was made of  $\text{D}_2\text{O}$ -moderated cores with  $\text{H}_2\text{O}$  inner reflectors (see Appendix B). The conclusion is that the peak flux per megawatt is higher in reactors with an  $\text{H}_2\text{O}$  inner reflector and a small core, but that heat transfer limitations prevent the attainment of absolute flux levels comparable to those occurring in the reference core design.

## 2. Core Structural Materials

The reference core design includes 100 liters of metal in the form of fuel tubes and supporting structure. Parasitic capture in this material influences the clean cold critical mass and, hence, the peak flux available per unit power. Table V lists the cold clean critical mass pertinent to each of the materials considered.

The selection of magnesium as the structural material was based on the assumption that continued research would evolve methods of retarding the corrosion rate to make it consistent with the short fuel cycle.



Table V

CALCULATED COLD CLEAN CRITICAL MASS  
FOR CORE STRUCTURAL MATERIALS

<u>Material</u>	<u>Metal Volume, liter</u>	<u>U<sup>235</sup> Critical Mass, gm</u>
Mg	100	1,250
Al	150	3,000
	100	2,500
	90	2,250
	75	1,900
Zr	70	1,250

3. Outer Reflector

The reflector savings afforded by D<sub>2</sub>O coupled with the small neutron age in D<sub>2</sub>O suggest making the outer reflector sufficiently large that the fast flux is well attenuated and that the thermal flux is attenuated through at least one power of e. The outer reflector thickness of 150 cm thus yields a large volume in which the flux decreases to values characteristic of MTR.

4. Fuel Cycle

No effort was made to study the effects of varying the fuel cycle since 120 hr of operation at 200 to 300 Mw corresponds to approximately 1,500 gm of stored fission products. This is within an order of magnitude of the products in CP-5 and is considered a reasonable limit for a reactor proposed for a populated site.

5. Control Elements and Burnable Poisons

The control capabilities of the "grey" absorbers (stainless steel blades, and dilute BF<sub>3</sub> tubes) described on page 21 are considered adequate for shim control (other than compensation for burnup) and for startup regulation. The safety rod system has not been studied in detail.

Studies of burnable poisons to control the excess reactivity required to compensate for fuel burnup and for xenon override included investigations of cadmium, boron-10, lithium-6, and gadolinium rods. Of these, small gadolinium rods of varying concentration appear to be the most reasonable answer.

## B. Critical Properties

### 1. Two-group Age

Experimental data on dilute, highly enriched D<sub>2</sub>O-moderated reactors are limited to a series of clean criticals performed by Snell.<sup>2</sup> A theoretical analysis of these experiments was reported by Garabedian.<sup>3</sup>

Supplementary work by Spinrad<sup>4</sup> covered methods for the fitting of two-group constants to be used in critical calculations for D<sub>2</sub>O-moderated reactors. He concludes that a two-group age of ~200 cm<sup>2</sup> in the reflector gives good results; in the core, the two-group age ( $\tau_{2g}$ ) is determined by

$$1 + \tau_{2g}B^2 = [\exp(\tau_G B^2)] (1 + \tau_Y B^2) \quad , \quad (2)$$

where  $\tau_G$  and  $\tau_Y$  are, respectively, the Gaussian and Yukawa ages in the D<sub>2</sub>O mixture, and  $B^2$  is the material buckling. While it is not clear that the age in the inner reflector should also be as large as 200 cm<sup>2</sup>, the larger value is certainly a conservative choice.

### 2. Cross Sections

The cross sections were calculated for a system temperature of 300°K and a D<sub>2</sub>O density of 1.1 gm/cm<sup>3</sup>. The thermal group cross sections (Table VI) were based on a Maxwellian spectrum with a characteristic temperature of 300°K. The D<sub>2</sub>O cross sections are based on a value for the thermal diffusion length,  $L$ , of 115 cm.

The method of equivalence factors was used to derive the fast group cross sections in other than pure D<sub>2</sub>O and H<sub>2</sub>O. The method and the fundamental constants are described in ANL-5800.<sup>5</sup>

<sup>2</sup>A. H. Snell, "Criticality Studies on Enriched Uranium - Heavy Water Systems," Mon P-454 (December 15, 1947; Decl. March 7, 1957).

<sup>3</sup>H. L. Garabedian, "Theoretical Calculations of Critical Masses for Certain P-9 Piles," CNL-36 (March 3, 1948; Decl. December 28, 1955).

<sup>4</sup>B. I. Spinrad, "Fast Constants in the Two-Group Method for Solution of the Critical Problem." Paper No. 9 presented at the General Information Meeting, October 24-26, 1949, Oak Ridge, Tenn., TID-277, p. 45.

<sup>5</sup>"Fast Group Constants for Metal-Water Mixtures by the Method of Equivalence Factors," Reactor Physics Constants, ANL-5800, Sec. 3.6.4, p. 165.

Table VI  
THERMAL GROUP CROSS SECTIONS

Material	<u>Macroscopic Cross Section, cm<sup>-1</sup></u>		
	Capture	Transport	Fission
D <sub>2</sub> O	0.57 x 10 <sup>-4</sup>	0.44203	
Mg (FS-1)	0.00292	0.16704	
Al (2S)	0.01227	0.08584	
Zr (Zr-2)	0.00832	0.3430	
U-235*	579.25		504.86
Xe-135*	2.795 x 10 <sup>6</sup>		
ν	2.47		

\*Microscopic cross section in barns

3. Methods of Calculation

Two-group critical calculations were done by hand, using the method of Spinrad and Kelber.<sup>6</sup>

The vertical buckling, assumed to be the same for all three regions, was determined by first finding the reflector savings for a sphere of equal volume immersed in D<sub>2</sub>O. The resultant value of 22 cm on a side is in excellent agreement with the method of Garabedian.<sup>3</sup> The addition of the total reflector savings of 44 cm to a core height of 90 cm yields an equivalent bare height of 134 cm.

4. Critical Properties of Reference Core

The sensitivity of the cold clean critical core to small changes in parasitic capture led to the establishment of the reference core configuration and characteristics given in Table VII.

The reference reactor corresponds closely to the core condition after 120-hr operation. Actually the Xe:U atomic ratio is slightly less; however, the difference is not significant.

The critical properties of the reference core are listed in Table VIII.

---

<sup>6</sup>B. I. Spinrad and C. N. Kelber, "A Two-Group Iteration Method for Annular Cylinders," ANL-5687 (March, 1957).

Table VII

REFERENCE CORE

Inner Reflector	D <sub>2</sub> O (radius characteristics 15 cm)
Core Annulus	
Thickness	30 cm
U-235 (no U-238 included)	1,591 gm
D <sub>2</sub> O volume fraction	0.803345
Mg (FS-1) volume fraction	0.196488
Xe-135/U atomic ratio	$1.5 \times 10^{-5}$
Nonsaturating fission products:	$\Sigma_a$ (fp) = 0.00033 (1550 gm at 50 barn/fission)
Active height	90 cm
Outer Reflector	D <sub>2</sub> O (150 cm thick)
Top and bottom reflectors	D <sub>2</sub> O (150 cm thick)

Table VIII

CRITICAL PROPERTIES OF REFERENCE CORE

U-235	1,591 gm
Neutron lifetime	$1.5 \times 10^{-3}$ sec
Void coefficient	$\Delta k/k = (-0.37)(\text{void fraction})$
Temperature coefficient	$\Delta k/k = (-3.2 \times 10^{-4})/^{\circ}\text{C}$
Response to thermal poison	
distributed uniformly through core	32 cm <sup>2</sup> poison = 1% in $k_{\text{eff}}$
Peak/avg. thermal flux	1.8

5. Two-dimensional Flux Plot

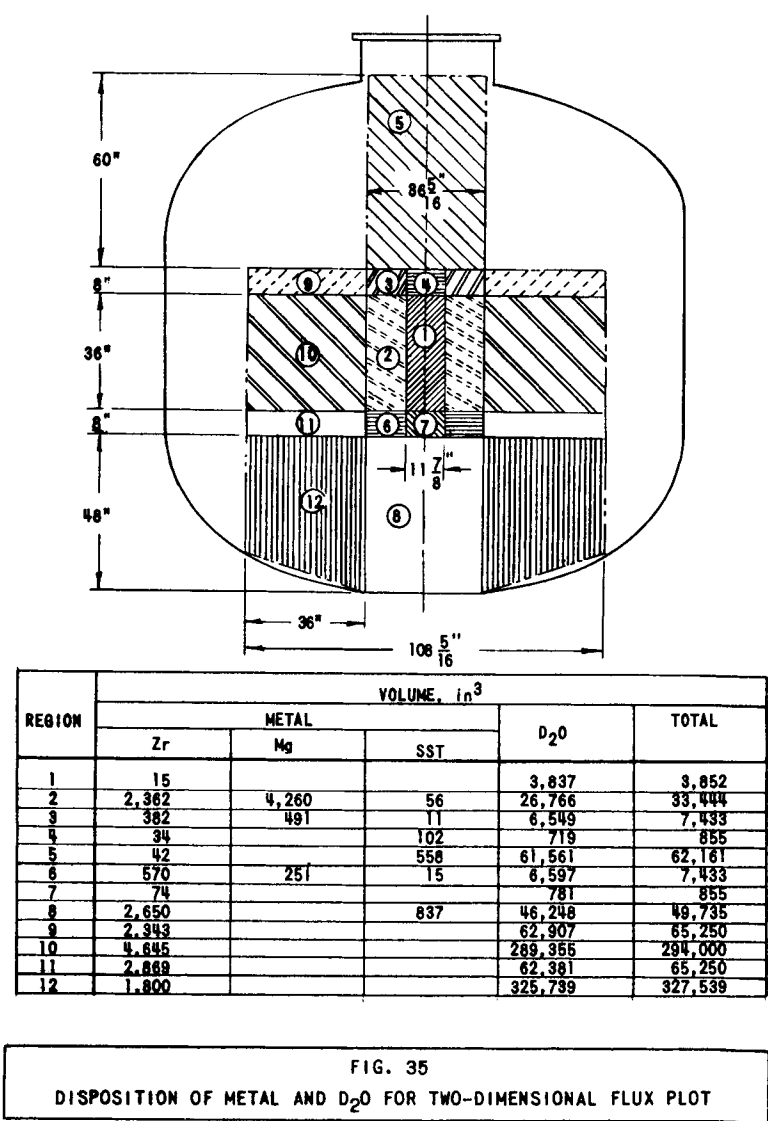
Three-group, two-dimensional flux distributions inside the pressure vessel (see Figs. 16 and 18) were computed on the IBM-704, using the PDQ-2 Code.<sup>7</sup> The volume inside the pressure vessel was divided into 12 regions, each having a different composition (see Fig. 35). The three-group constants, applicable for the end of the fuel cycle, were computed by the method of Deutsch,<sup>8</sup> with equivalence factors for D<sub>2</sub>O moderator.<sup>5,9</sup>

---

<sup>7</sup>G. G. Bilodeau, et al., "PDQ: An IBM-704 Code to Solve the Two-Dimensional Few-Group Neutron Diffusion Equation," WAPD-TM-70 (August, 1957).

<sup>8</sup>R. W. Deutsch, "Computing 3-Group Constants for Neutron Diffusion," Nucleonics, 15 (No. 1), 47-51 (1957).

<sup>9</sup>C. N. Kelber, "Equivalence Factors for D<sub>2</sub>O," Nuc. Sci. Eng., 3 (5), 633-634 (1958).



6. Critical Properties of Fresh Core and Partly Used-up Core

Constant power operation was selected over constant flux operation because: (1) at constant power operation, a sudden drop in power level does not effect as sharp a reduction in reactivity, and the magnitude of the reduction is not as great as in the constant flux mode of operation; and (2) operation at constant flux implies constantly decreasing power and, consequently, an increasingly large backlog of Xe-135, which makes it mandatory to choose the constant power mode of operation. This problem is reviewed in detail in ANL-5688.<sup>1</sup>

Operation at a constant power of 250 Mw corresponds to an average peak flux, over the fuel cycle, of  $5 \times 10^{15}$  n/(cm<sup>2</sup>)(sec) and a burnup of 1550 gm U-235. Since the flux through the core is relatively flat, a large effect from nonuniform burnup is not anticipated. Thus, an initial

loading of 1,591 gm + 1,550 gm = 3,141 gm, should be sufficient to maintain criticality over the fuel cycle. This was confirmed by a series of critical calculations for each 24-hr interval, using the results of the preceding calculation to establish initial conditions.

Starting at time  $t = 0$ , the reactor was made critical by the uniform addition of thermal poison. The flux was normalized by the condition that the total power be 250 Mw. This is equivalent to the statement that during each 24-hr period the flux retains its shape, but increases slowly in over-all magnitude. The core was divided radially into three regions and the uranium burnup and the iodine and xenon production were computed using the PROD-II code in conjunction with the IBM-650.

The results (Table IX) show a slight amount of excess reactivity at  $t = 120$  hr. This is attributed to the original calculation wherein the ratio  $Xe(120)/U(120)$  was assumed to be  $1.5 \times 10^{-5}$ , which, as Table IX shows, is a little high. Figure 36 attests the validity of the assumption of relative constancy of flux shape during any 24-hr period.

### C. Control

#### 1. Burnable Poisons

Several factors lend strong support to the use of burnable poisons to compensate for the excess reactivity. The void coefficient ( $\sim -0.5 \times 10^{-6}$  k/cm<sup>3</sup> of void) is such that large amounts of control by the introduction of voids is not possible without encountering serious heat transfer problems. The large flux depressions reflected by massive control rods would put some experimental facilities at a disadvantage. Moreover, rod movement would incur serious shifts in the flux distribution, which is undesirable in many types of experiments using neutron beams. Finally, too much control in the form of movable rods is unsafe by comparison with the same amount of control in the form of fixed poisons. The question of what constitutes "too much" control will not be discussed further other than to say that 3% in rods is generally acceptable, but 6% is not.

Ward's criterion for the onset of xenon instability<sup>10</sup> shows that if xenon-induced oscillations are not to occur in Mighty Mouse, the burnable poison in the core at startup must total 681 cm<sup>2</sup>. His criterion is that

$$k = 1 + B_1^2 M^2 \quad ,$$

where  $M^2$  is the migration area, and  $B_1^2$  is the buckling of the first mode above the critical mode. In Mighty Mouse this is a mode with zero along a diameter; at startup  $M^2 \geq 240$  cm<sup>2</sup>, and  $B_1^2 = 0.003$  cm<sup>-2</sup>. Thus,  $k_\infty \leq 1.73$  for stability.

---

<sup>10</sup>A. G. Ward, "The Problem of Flux Instability in Large Power Reactors," CRRP-657 (July 26, 1956).

Table IX

SUMMARY OF BURNUP CALCULATIONS

Time, hr	$\frac{U(t)}{U(t-24)}$	$\frac{Xe(t)}{U(t)} \times 10^5$	$\bar{\phi} \times 10^{-18},$ $n/(cm^2)(sec)$	$\Sigma_p,$ $cm^{-1}$	$\Sigma_f,$ $cm^{-1}$	$\frac{(Xe)(\sigma_a^{Xe})}{(U)(\sigma_f^U)}$	$\frac{U(t)}{U(0)}$
REGION II							
0	1.00000	--	--	0.00400	0.00798	--	1.00000
24	0.88910	1.252	8.18048	0.00300	0.00710	0.06165	0.88910
48	0.87667	1.247	9.18276	0.00240	0.00622	0.06059	0.77944
72	0.86334	1.264	10.25151	0.00175	0.00537	0.06045	0.67293
96	0.84171	1.272	12.02067	0.00125	0.00452	0.05934	0.56641
120	0.81416	1.287	14.34305	0.00064	0.00368	0.05807	0.46115
REGION III							
0	1.00000	--	--	0.00400	0.00798	--	1.00000
24	0.90852	1.240	6.69294	0.00300	0.00725	0.06241	0.90852
48	0.89655	1.235	7.61843	0.00240	0.00650	0.06134	0.81453
72	0.88308	1.250	8.67489	0.00175	0.00574	0.06115	0.71930
96	0.86585	1.259	10.04920	0.00125	0.00497	0.06039	0.62280
120	0.84105	1.270	12.07718	0.00064	0.00418	0.05917	0.52381
REGION IV							
0	1.00000	--	--	0.00400	0.00798	--	1.00000
24	0.90225	1.244	7.17030	0.00300	0.00720	0.06217	0.90225
48	0.89306	1.242	7.89077	0.00240	0.00643	0.06144	0.80576
72	0.88025	1.253	8.89813	0.00175	0.00566	0.06110	0.70927
96	0.86572	1.262	10.05339	0.00125	0.00490	0.06052	0.61403
120	0.84490	1.271	11.75837	0.00064	0.00414	0.05948	0.51879

Nomenclature

- $\frac{U(t)}{U(t-24)}$

= Concentration of  $U^{235}$  at time t/  
concentration 24 hr earlier.
- $\frac{Xe(t)}{U(t)}$

= Relative concentration of Xe and U at time t.
- $\bar{\phi}$

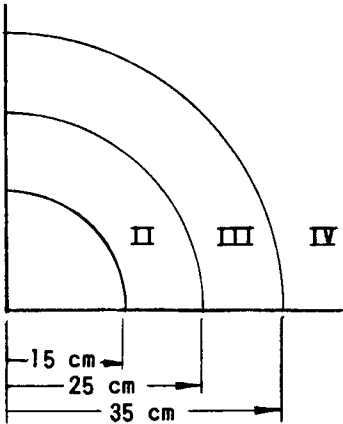
= Avg. neutron flux during 24-hr period  
ending at time t.
- $\Sigma_p$

= Macroscopic cross section of uniformly  
distributed thermal poison necessary to  
maintain criticality; represents all  
reactivity effects, rods, burnable poisons, and experiments.
- $\Sigma_f$

= Macroscopic fission cross section.
- $\frac{(Xe)(\sigma_a^{Xe})}{(U)(\sigma_f^U)}$

= Xenon absorption cross section/macroscopic fission cross section;  
nearly proportional to the reactivity held in the xenon.
- $\frac{U(t)}{U(0)}$

= Relative uranium concentration at time t and time t = 0.



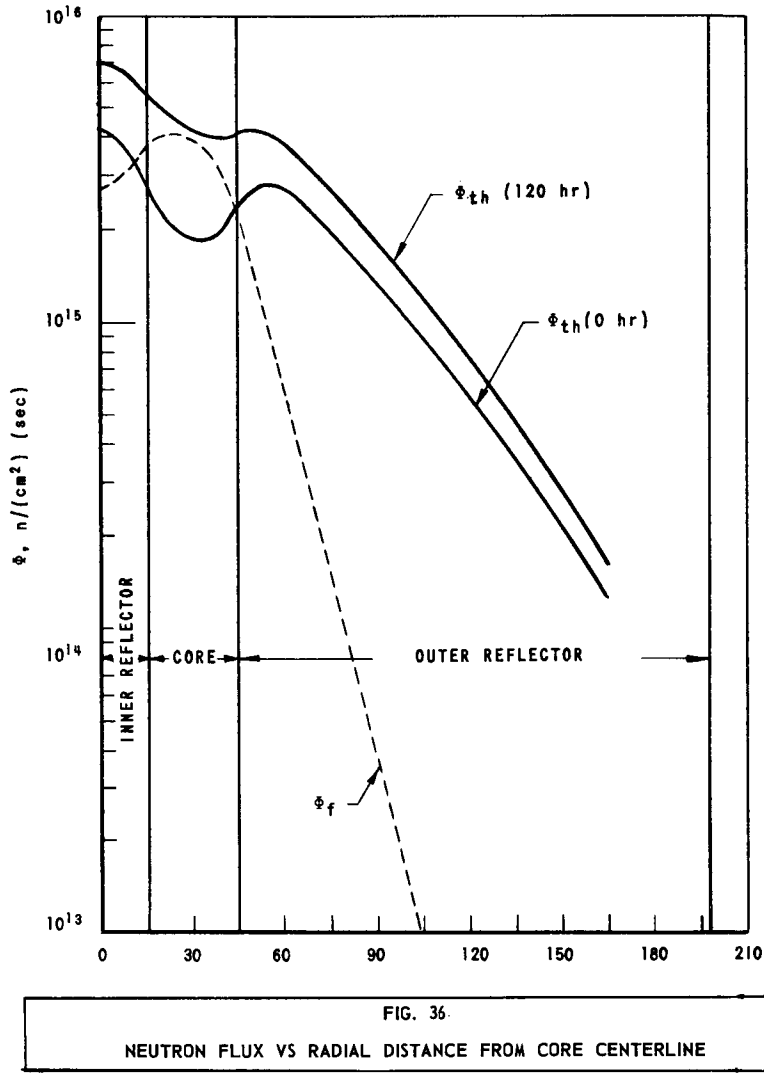


Table IX gives the amount of thermal poison necessary to maintain criticality as a function of time. Similar calculations can be made to determine the reactivity worth of such poison and, hence, the excess reactivity in the core. The effect of experimental apparatus must be subtracted from the latter value. A calculation based on the average of beam hole worths per unit area and importance in CP-5, MTR, and DIDO shows that approximately 4% must be allowed for experiments in Mighty Mouse. (This value is subject to experimental verification and/or correction.)

A calculation of the rate of xenon buildup following instantaneous loss of 50% power shows that subsequent startup will require the addition of reactivity at about  $3\phi/\text{sec}$  (initially), and a total of about 2.5% in 2 min, and 6% in 5 min. The initial rate of addition ( $3\phi/\text{sec}$ ) corresponds approximately to the maximum permissible rate of rod withdrawal, since prompt critical occurs within 30 sec after delayed critical.



Table X lists the burnable poison requirements to balance  $k_{ex}$  over the fuel cycle; 4%  $k_{ex}$  is compensated by experiments, and 3% (or 6%) by rods.

Table X

BURNABLE POISONS REQUIRED TO BALANCE $k_{ex}$ OVER THE FUEL CYCLE					
Time, day	$k_{ex},^*$ %	Poison, $cm^2$			
		Xe <sup>†</sup>	1%k	3% in rods	6% in rods
0	24.4	270	83	1174	925
1	24	0	66	1122	924
2	24	0	46	782	644
3	24	0	37	629	518
4	19.3	0	33	406	307
5	10.4	0	32	109	12.8

\*4%  $k_{ex}$  is used up by experimental facilities.

†Xenon is compensated by dispersed cadmium.

The column entitled "Xenon" assumes no xenon is present initially, but after 24 hr practically all of the xenon has appeared. The average rate at which xenon appears is proportional to the total fission yield of xenon and iodine. The latter is modified slightly to account for its decay in the first 24 hr, minus the capture rate and decay rate based on the average amount of xenon present. Since finely dispersed cadmium burns out in about the same time, it is appropriate that cadmium be introduced to compensate for the xenon that has not yet appeared.

In Mighty Mouse, the average amount of xenon present in the first 24 hr is about 60% of the maximum xenon. Accordingly, matching the average burnup rate of cadmium to the average rate of appearance of xenon yields an initial requirement of 1660  $cm^2$  of cadmium. However, such a loading would provide essentially no poison for control purposes after the first day of operation. Consequently, the value of 270  $cm^2$  listed in Table X stems from the decision to match the total absorption area of xenon instead. After 24 hr, the xenon is in quasistatic equilibrium with the uranium and no further compensation will be required.

Boron-10 has a half-life of  $\sim 1$  day in Mighty Mouse, while lithium-6 has a half-life of  $\sim 4$  days. A good fit of the logarithm of the burnable poison area can be achieved with a form quadratic in time. A

least-squares fit to the decay curve of  $B^{10}$  and  $Li^6$  yields initial quantities for control. The latter fit, in turn, must be modified to be consistent with the additional requirement that the maximum deviation between actual and required amounts of burnable poison be within the range of the control blades.

The best fit is obtained by placing the  $Li^6$  in the high-flux region (Region II), the  $B^{10}$  in the low-flux region (Region III), with the control blades occupying the outer 10 cm of the core to give a little flux flattening. The results of such a fit are listed in Table XI.

Table XI

ADJUSTED LEAST-SQUARES FIT TO  $\ln(\Sigma_p/\Sigma_{p0}) = At^2 + Bt$   
(A = -0.09539; B = -0.0119)

(1) Time, day	(2) $Li^6$ , cm <sup>2</sup>	(3) $\phi(II) \times 10^{-21}$ , n/(cm <sup>2</sup> )(day)	(4) $B^{10}$ , cm <sup>2</sup>	(5) $\phi(III) \times 10^{-21}$ , n/(cm <sup>2</sup> )(day)	(6) $\Sigma_p$ , cm <sup>2</sup>	(7) $\Delta k_{ex}$ , % (6% in rods)	(8) $\Delta k_{ex}$ , % (3% in rods)
0	551	0.174	949	0.142	1500	-6.9	-3.9
1	467	0.196	536	0.161	1003	-1.2	+1.8
2	389	0.220	280	0.183	669	-0.5	+2.5
3	317	0.246	134	0.208	451	+1.8	+4.8
4	248	0.289	57	0.241	305	0	+3.1
5	186	0.344	20	0.290	206	-6	-3.0

Note: Columns (2) and (3) list the absorption area of  $Li^6$  and the flux to which  $Li^6$  is subject as a function of time.

Columns (4) and (5) list the corresponding values for  $B^{10}$ .

Column (6) lists the total absorption area.

Columns (7) and (8) list the reactivity that must be controlled by the rods over and above the amount arbitrarily assigned to them.

The difficulty in obtaining a good fit is occasioned by the facts that (1) the amount of poison required as a function of time has a negative second derivative, while the abundance of an isotope that is finely divided will have a positive second derivative; and (2) the amount of poison required at  $t = 5$  days is sufficiently low that slower burning  $Li^6$  can be present initially only in small amounts. The difficulty is further enhanced by the rapid burnup of  $B^{10}$  which results in an undesirable disparity between respective poison concentrations during the third and fourth days, or else at  $t = 0$  and at  $t = 5$  days. Studies on the use of other isotopes, i.e.,  $Hg^{199}$ , resulted in no substantial improvement.

An alternate solution is to use black rods that present a constant area of absorber to the flux for a prescribed period, then become transparent and burn up in a short time. The flux depression in the vicinity of the black rods can be isolated by placement of the rods in the forward part of the control blade slots; mechanical design limits the rod diameter to about  $\frac{3}{8}$  in. From the work of Davison and Kuskneriuk,<sup>11</sup> the linear extrapolation length of such a rod is determined to be  $1.15 \lambda_{tr}$ . The asymptotic flux is reduced approximately by a factor of 2 at the surface of the rod, and the neutron current into the rod is about one-sixth the average flux in the core.

Table XII  
RELATIVE LIFETIMES OF  
GADOLINIUM RODS IN  
MIGHTY MOUSE

Rod diameter = 0.375 in.

<u>Nσr</u>	<u>Lifetime,</u> <u>days</u>
2.74	1+
5.41	2
8.39	3
11.682	4
15.552	5

atoms per cm<sup>3</sup>, σ their absorption cross section, and r the rod radius.

2. Solid Absorbers

As evidenced by Table VIII, a small amount of solid absorber is required; therefore, each of the eight control blades will contain approximately 1 kg of stainless steel to provide adequate control of the reactor.

Calculations of the control rod disadvantage factors were made by using spherical harmonic expansions of the flux for two core compositions and three thicknesses of stainless steel control blades. In the expansions the second (P<sub>1</sub>) and fourth (P<sub>3</sub>) moments of the flux were set equal to zero. The accuracy of the P<sub>3</sub> approximation was checked by a P<sub>5</sub> calculation for one composition and control blade thickness.

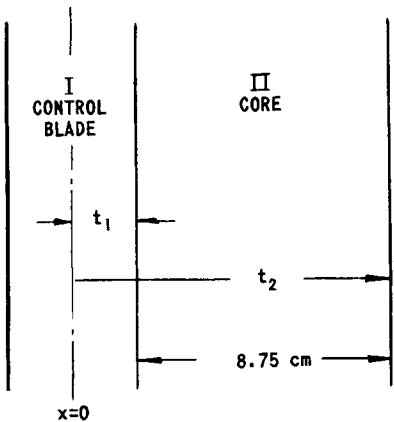
---

<sup>11</sup>B. Davison and S. Kuskneriuk, "Linear Extrapolation Length for a Black Sphere and a Black Cylinder," MT-214 (March 30, 1946).  
<sup>12</sup>G. M. Muller, "Burnout of Neutron Absorbers During Prolonged Irradiation," HW-15068 (November 10, 1949; Decl. May 10, 1957).  
<sup>13</sup>G. M. Muller, "Time-Dependent Absorption of Neutrons by Plane Slabs," HW-17331 (March 30, 1950).

It was assumed that the core and control rods were infinite slabs with infinite plane interfaces, as illustrated. Accordingly, the control blade disadvantage factors are given by:

$$d_1 = \frac{\bar{\phi}_I}{\bar{\phi}} = \frac{(1/t_1) \int_0^{t_1} \phi_I \, dx}{(1/t_2) \left( \int_0^{t_1} \phi_I \, dx + \int_{t_1}^{t_2} \phi_{II} \, dx \right)} \tag{3}$$

$$d_2 = \frac{\bar{\phi}_{II}}{\bar{\phi}} = \frac{[1/(t_2-t_1)] \int_{t_1}^{t_2} \phi_{II} \, dx}{(1/t_2) \left( \int_0^{t_1} \phi_I \, dx + \int_{t_1}^{t_2} \phi_{II} \, dx \right)} \tag{4}$$



The spherical harmonics method of Mark<sup>14</sup> was used to evaluate  $\phi_I$  and  $\phi_{II}$ . The thermal flux and disadvantage factors (see Table XIII) were calculated using the boundary conditions of symmetry of the moments of  $\phi$  about  $x = 0$  and  $x = t_2$ , and of the continuity of the moments at  $t_1$ .

Table XIII  
COMPARISON OF CALCULATED CONTROL ROD  
DISADVANTAGE FACTORS

$t_1$ , cm	$L^2_{core}$ , cm <sup>2</sup>	$P_1$		$P_3$		$P_5$	
		$d_1$	$d_2$	$d_1$	$d_2$	$d_1$	$d_2$
0.2	194.9	0.85524	1.00293	0.84185	1.01042		
	70.6	0.87631	1.00283	0.84783	1.00984		
0.4	194.9	0.76779	1.01062	0.73716	1.03465		
	70.6	0.77452	1.01031	0.74355	1.03302		
0.6	194.9	0.68238	1.02178	0.65747	1.06774		
	70.6	0.69012	1.02125	0.66593	1.06479	0.66217	1.06554

Figure 37 is a plot of the flux distributions calculated by the  $P_1$  and the  $P_5$  approximations for  $t_1 = 0.6$  cm and  $L^2_{core} = 70.6$  cm<sup>2</sup>. Although the  $P_1$  approximation overestimates the effectiveness of the control rods in depressing the core flux, the inaccuracies are within tolerable

<sup>14</sup>C. Mark, "The Spherical Harmonic Method. II: Application to Problems with Plane and Spherical Symmetry," MT-97 (February, 1957).

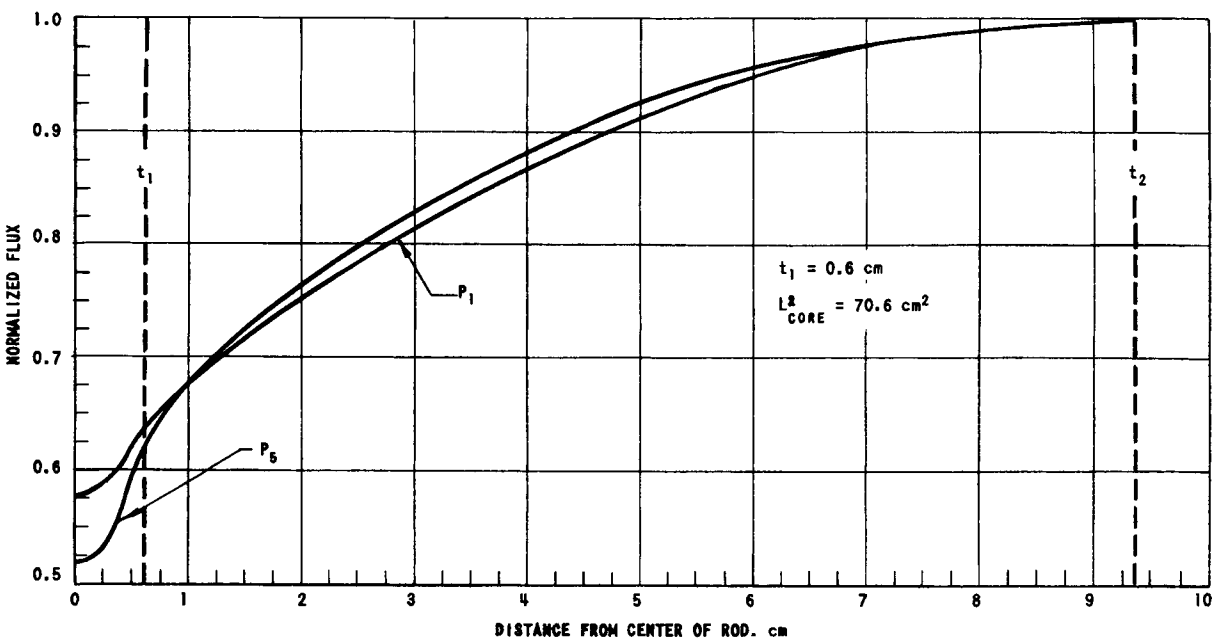


FIG. 37  
COMPARISON OF FLUX DISTRIBUTIONS FOR STAINLESS STEEL CONTROL ROD  
CALCULATED BY  $P_1$  AND  $P_5$  APPROXIMATIONS

bounds. The maximum discrepancy between the  $P_1$  and  $P_5$  calculations, which occurs at the center of the blade, is only about 10%. If somewhat greater accuracy is desired, the  $P_3$  calculation is sufficient in view of small differences in values obtained by the latter method and the more complicated  $P_5$  calculation.

The control blade does not give rise to a hot spot, since the average core flux is never higher than 6.7% above the desired flux level in a homogeneous system.

D. Future Supporting Studies

During the course of final design and construction of the reactor, many detailed problems involving flux distributions in the various structural elements will arise and can be resolved only by reference to a critical assembly.

The evaluation of reactivity effects of the various components represents an appreciable avenue of effort. For example, it is assumed that beryllium end pieces on the beam holes will forestall a major flux depletion in these regions; however, this contention is subject to experimental verification. The reactivity effect of the beam holes in the Mighty Mouse is based on the averaged worths of beam holes in existing research reactors. A less crude approach is essential; more specifically, experimental results on a critical assembly are required.

Future work on xenon-135 effects should be planned in connection with a reactor simulator. The difference in response of the reactor to a power increase as compared with a power decrease will require a carefully balanced control system. Moreover, the rate of xenon production is proportional to the power level but the rate of destruction is flux- and neutron-temperature sensitive. Thus, a slow rise in water temperature could give rise to long-term xenon effects that could shorten the fuel cycle. The various effects are interrelated to the extent that the problems can best be resolved with the aid of a reactor simulator. The control problem will require extensive machine computations to determine the optimum response to any major perturbation. In this connection the reactor simulator could be used to determine those problems that are suitable for resolution by an automatic control system.

## V. CORE HEAT TRANSFER AND FLUID FLOW

The heat transfer and fluid flow characteristics of the core are listed in Table I, page 13. The supporting calculations and analyses are described in Appendix D.

### A. Steady-state Conditions

#### 1. Selection of Fuel Elements

The basic function of the reactor dictated the core size and the metal-to-water ratio of 1:4. Studies of various fuel element configurations that conformed to the physics requirements revealed no significant difference in heat flux or temperature characteristics. The tubular fuel element (0.375 in. OD) was selected on the basis of structural rigidity consistent with the desire to minimize the volume of supporting structures in the core region. The inactive ends of the tubes are flared and formed to facilitate assembly into a square-pitched bundle. The pitch was selected so that equivalent diameter of the outside flow path was equal to the inside diameter of the tubes (0.315 in.).

#### 2. Selection of Heat Transfer Values

Temperature limitations are of prime importance in the core for two reasons: (1) there must be no boiling at low pressure; and (2) the corrosion resistance of the magnesium cladding in water at the design temperature is rather poor. Therefore, relatively high velocities were considered for the production of a high convection coefficient to lower the maximum surface temperature. The established D<sub>2</sub>O inlet temperature of 100° F approaches the lower limit consistent with the use of cooling towers or other methods that employ ambient air temperature for the secondary cooling system. On the basis of preliminary corrosion tests on magnesium, a maximum surface temperature of 248° F (120° C) was set as an upper limit (without hot channel factors). Using a maximum heat flux of 750,000 Btu/(hr)(ft<sup>2</sup>) and a water film temperature difference of 100° F, the required convection coefficient is about 7500 Btu/(hr)(ft<sup>2</sup>)(° F) on the inside of the tubes. The internal coolant velocity is therefore approximately 25 fps. As shown in Appendix D, the internal heat flux is greater than the external flux; therefore a lower coolant velocity is required around the outside of the tubes. Thermal analysis of the core based on an internal coolant velocity of 25 fps showed that the outer velocity should be 18.6 fps.

#### 3. Distribution of Energy Input and Temperatures

The heat flow to the inside of the fuel tube is 51.6% of the total heat output in a tube. In view of the poor corrosion properties of magnesium, it is advantageous to maintain equal metal surface temperatures

along any horizontal plane in the tube. This also yields a condition of minimum thermal stress. The problem, therefore is to properly proportion the coolant mass flows to ensure an equal temperature rise on both sides of the tube wall. This condition is satisfied by using the crowned square end configuration on the fuel tubes. The calculated temperature profiles are plotted in Fig. 38. The point of maximum fuel internal temperature was found to deviate an insignificant amount from the point of maximum surface temperature. The maximum temperatures occur at the inner surface of the annulus 8.3 cm downstream of the horizontal centerplane. The hot channel factors used are listed in Table XIV.

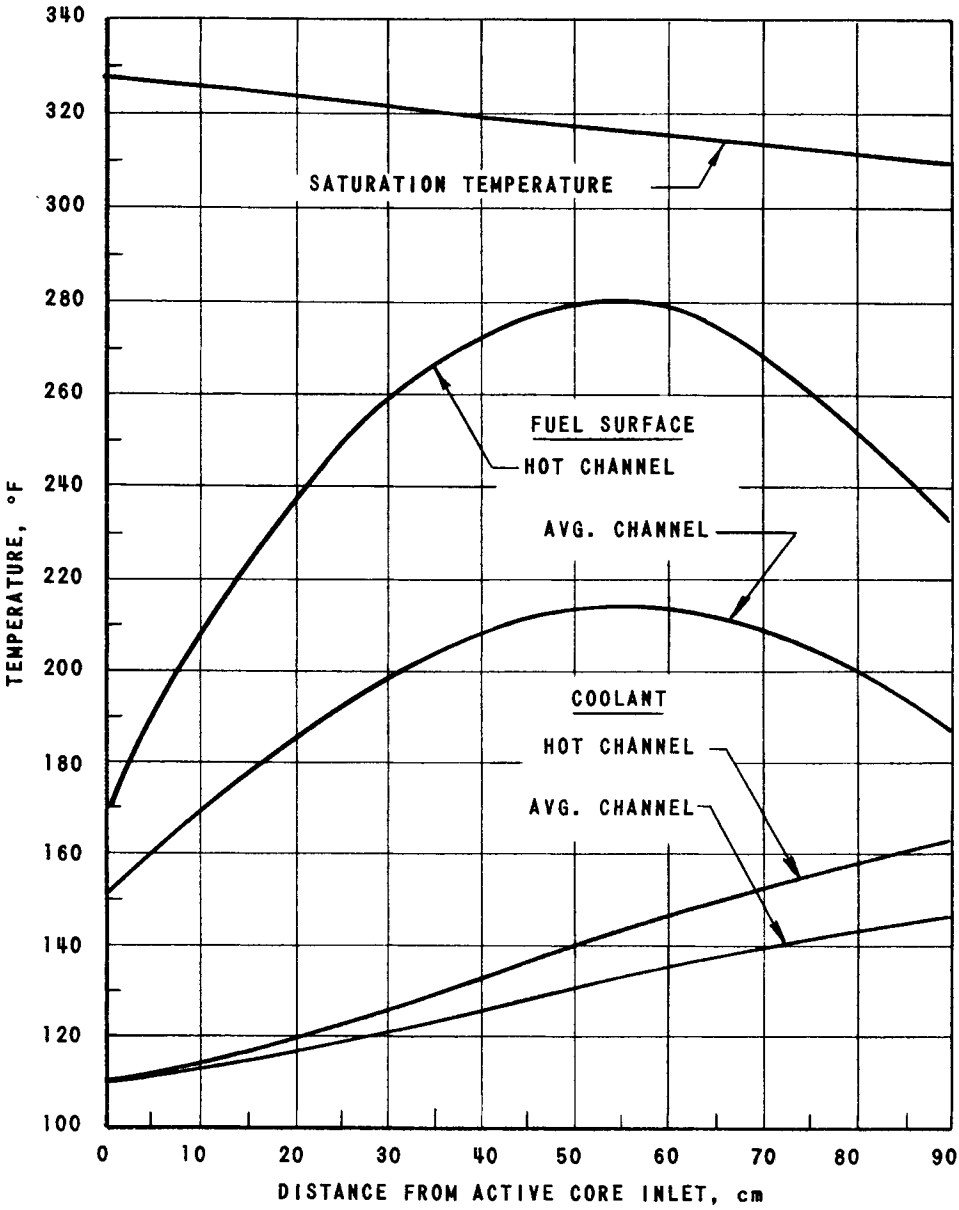


FIG. 38  
AXIAL TEMPERATURE PROFILES IN ACTIVE CORE REGION



Table XIV

HOT CHANNEL FACTORS

	Bulk Coolant Temp Rise	Film Temp Rise
Plenum chamber effects	1.02	1.02
Chamber tolerance	1.05	--
Convection coefficient	--	1.20
Fuel thickness	1.06	1.08
Fuel density	1.03	1.04
Precision of assumed cosine heat distribution	1.02	1.02
	1.19	1.40

4. Burnout

Since there is no local or net boiling in the core, burnout can occur only as a result of an increase in power or decrease in flow velocity. For example, assuming that the velocity remains constant, a power excursion 5.5 times normal power would be required to promote burnout. The reactor instrumentation is designed to prevent the advent of such an excursion.

B. Unsteady-state Conditions

A number of safeguards and automatic scram devices are incorporated in the coolant system to forestall core damage during unsteady-state conditions occasioned by: (1) reactor shutdown; (2) loss of power or pump failure in either the primary or secondary system; or (3) rupture of the primary coolant system.

1. Reactor Shutdown

Following normal shutdown, the primary coolant will be circulated by a low-capacity pump, or one of the four primary pumps, to remove the core decay heat (Fig. 39). The low-velocity flow will be maintained during fuel-unloading operations.

2. Loss of Primary or Secondary Coolant Flow

The primary system is designed to take advantage of the inertia of the coolant flow to provide sufficient cooling for about one minute following loss of power or pump failure. This is a reasonable time for an automatic diesel generator to start and power a low-capacity pump.

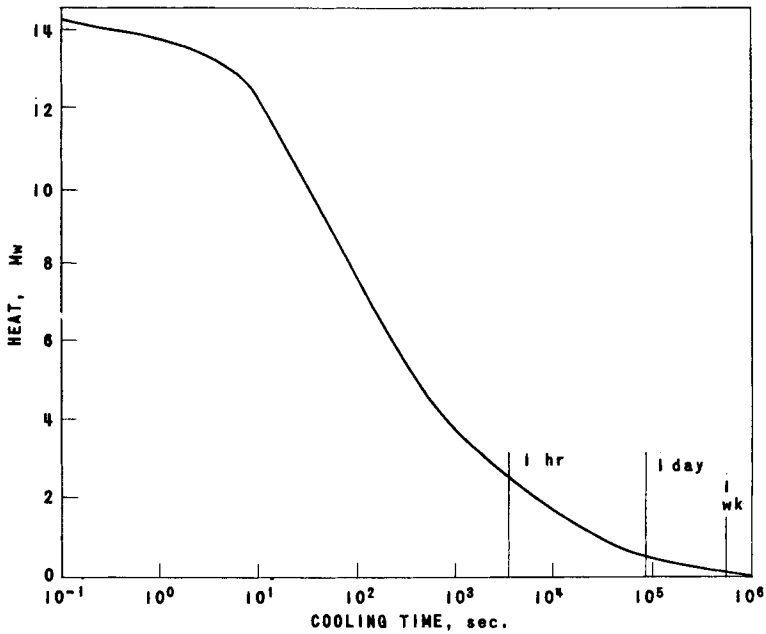


FIG. 39  
HEAT GENERATED IN CORE BY FISSION PRODUCT  
DECAY AFTER OPERATION AT 250 Mw FOR 5 DAYS

Figure 40 shows the available flow rate and the required flow rate for emergency cooling. The available flow is the "coastdown" of the flow rate derived from a consideration of the change in momentum of the fluid with time. Additional "coastdown" volume can be provided by installing fly wheels on the primary pumps. The required flow is based on maintaining the maximum hot spot temperature on the fuel elements below 300° F.

3. Rupture in Primary Coolant System

In the event of a major rupture in the primary coolant system external to the biological shield, the flow to the core will cease, and the consequent loss of system pressure will initiate automatic reactor shutdown. The primary piping within the biological shield is arranged to prevent loss of coolant from the reactor vessel.

The water in the core will boil, and the resultant lower density will promote natural circulation in the piping loop that extends from the side of the reactor vessel to the core inlet pipe (see Fig. 20). A check valve in this loop is designed to open upon loss of normal pump head.

Natural circulation can continue until the water evaporates to the level of the top of the core. This provides for the first 5 hr of decay heat removal without auxiliary cooling. In order to extend this period,

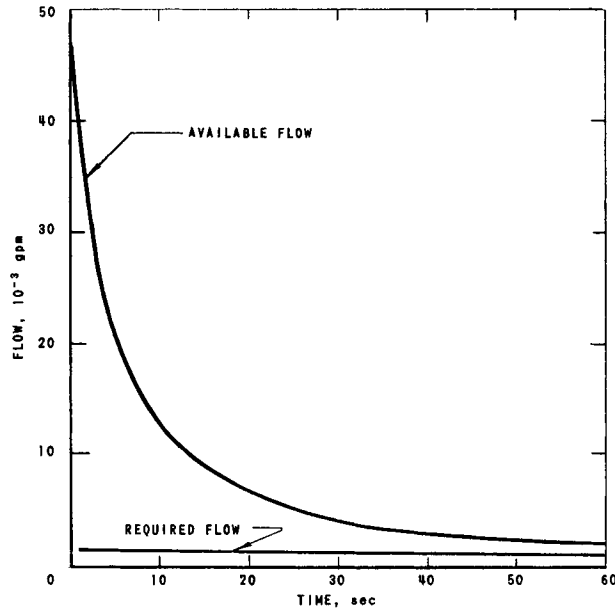


FIG. 40  
PRIMARY SYSTEM FLOW VS TIME AFTER LOSS OF PUMP POWER

an emergency condenser is provided in the upper region of the biological shield. A portion of the steam generated in the vessel will be condensed in the emergency condenser and the condensate will merge with the natural circulation flow into the vessel. This latter feature provides cooling for at least one day. Within this period measures can be taken to rectify the emergency, even to the extent of flooding a portion of the building.

### C. Associated Heat Removal Problems

#### 1. Thermal Shield

The rate of heat generation in the  $\frac{1}{4}$ -in. steel plate is about 0.29 Mw. The heat released in the heavy steel gamma shield is estimated as 0.04 Mw. The major portion of the heat is produced by neutron absorption in the borated solution ( $\sim 1.42$  Mw). Calculations indicate a flow rate of about 200 gpm of the borated solution will be required to remove the total heat generated in the thermal shield.

#### 2. Pressure Vessel

The zirconium pressure vessel will have internal heat generated within its wall by nuclear radiation. The outside surface of the

vessel is surrounded by a helium atmosphere. Therefore a study was made to evaluate the potential of natural convection cooling in the vessel to prevent boiling on the inner surface. The results indicate that natural convection cooling will be adequate. The upper part of the vessel is the most critical region due to the low unit surface conductance of heat downward to the heat-removing fluid. If the upward surge of the main coolant stream is ignored, calculations show that the inside surface temperature will not exceed 151° F.

### 3. Spent Fuel Heat Generation

Following normal reactor shutdown, the core decay heat will be removed by forced circulation of the primary coolant. Sometime within the 48-hr shutdown period, the fuel subassemblies will be removed from the core to the fuel-transfer tube for further transfer to the fuel-storage area beneath the reactor vessel. Within the fuel-transfer tube, the subassembly will be cooled by natural convection or, in unusual circumstances, by forced convection.

Studies show that after eight hours of forced cooling the fuel subassemblies can be removed from the core and stored indefinitely in D<sub>2</sub>O or H<sub>2</sub>O at ambient temperatures up to 148° F without exceeding a 200° F surface temperature at the hottest spot in the hottest channel.

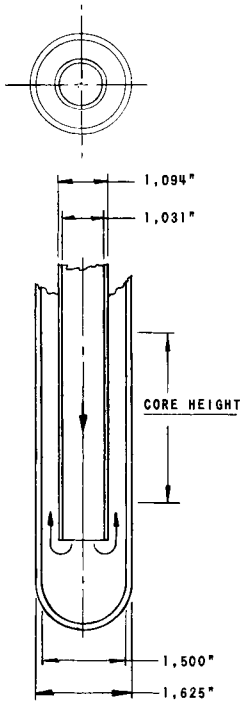


FIG. 41  
SCHEMATIC OF CENTRAL THIMBLE

### 4. Curium-245 Samples in the Center Thimble

It is proposed to insert one gram of curium-245 into the center thimble for the purpose of producing transuranic elements. The unperturbed flux in the thimble is  $5 \times 10^{15}$  n/(cm<sup>2</sup>)(sec) and, since curium-245 is fissionable, approximately 632 kw (heat) will be released in the sample.

The center thimble, shown schematically in Fig. 41, is a re-entry type of tube that permits flow either down through the center and up the outer annulus, or vice versa. The size of the center tube and the annulus is based on an engineering choice of 20 fps for the coolant flow in the annulus and 30 fps in the center tube.

The shape of the thimble suggests a tubular geometry for the sample. Accordingly, studies were made to select the sample size and geometry consistent with the following criteria:

- (1) maximum permissible length of 36 in.;
- (2) maximum surface temperature of 315° F;
- (3) cosine power distribution - axial peak to average of 1.25;
- (4) curium annulus (0.020 in.), clad with aluminum (0.020 in.); and
- (5) inlet temperature of D<sub>2</sub>O of 100° F.

As shown in Fig. 42, a tubular sample (No. 1) inserted in the center tube is impractical, since the required length of the sample would exceed the prescribed length of 36 in. A single tube sample (No. 2) within the annulus approaches the maximum permissible length when the velocity is 26 fps. A concentric tube sample (No. 3) arranged within the annulus on the basis of equivalent diameter could satisfy the design criteria provided the sample length was 12 in. and the problem of self-shielding is not critical.

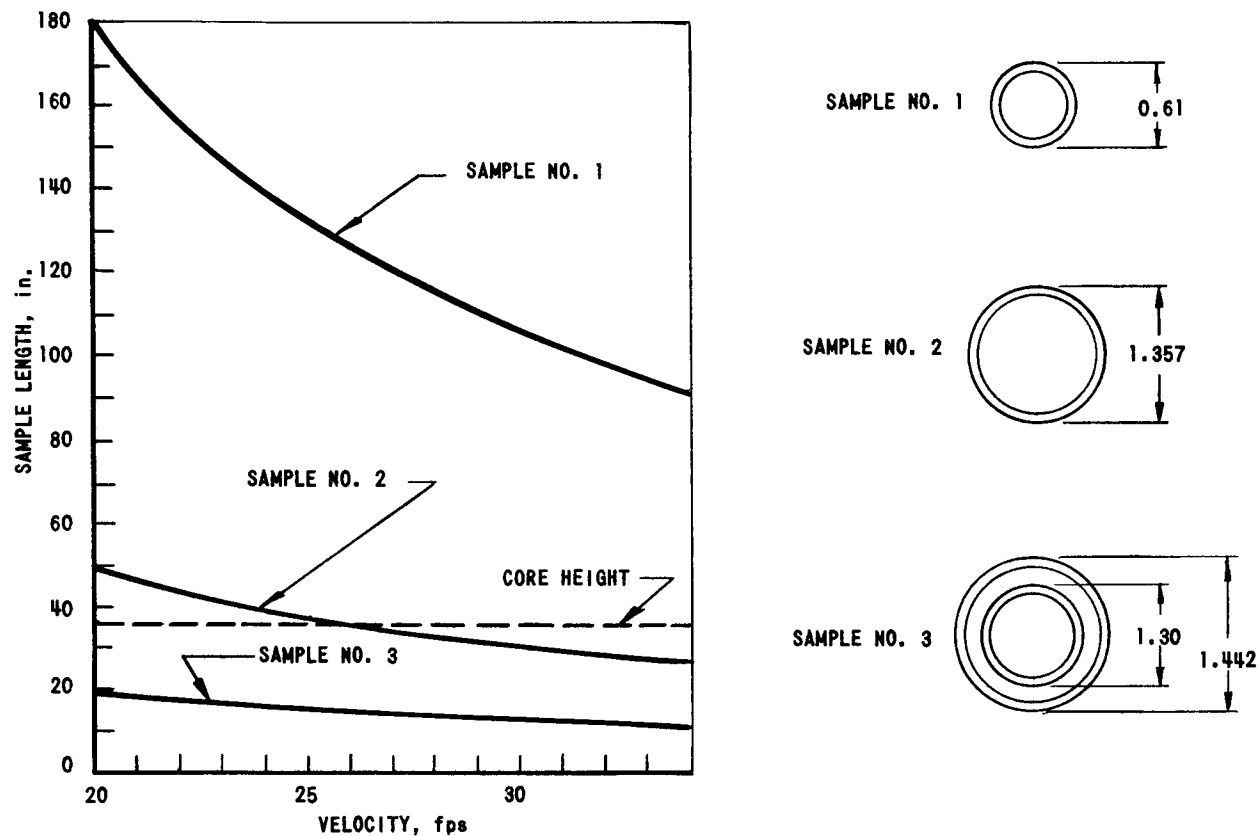


FIG. 42  
LENGTH AND FLOW REQUIREMENTS FOR THREE CURIUM SAMPLE GEOMETRIES FOR CENTER THIMBLE

## VI. RESEARCH AND DEVELOPMENT

### A. Fuel

The use of magnesium-clad, tubular fuel elements is a radical departure from the well-developed flat, MTR-type fuel plate. Coincident with this departure is the assemblance of the large number of tubes (455) that comprise a fuel subassembly. Both concepts, while vital to the design of the reactor core, will require an extensive research and development program to prove their acceptability.

#### 1. Cladding

Beryllium and magnesium were considered as potential cladding materials because of their low absorption cross sections. Beryllium was eliminated because of the higher cost and the limited technology with respect to its fabrication. However, available data on the corrosion behavior of magnesium indicated that water at 150°C (the maximum fuel cladding metal temperature) would be appreciably corrosive. The operating conditions of the reactor prescribed a maximum corrosion penetration of 1 mil/day at a temperature of 150°C (302°F). Consequently, specimens of 15 commercial alloys and 32 special alloys were corrosion tested in static, neutral water at 135°C, 140°C, and 150°C.

The results are summarized in Table XV. Most of the commercial alloys exceeded the prescribed corrosion rate in water temperature at 135°C and 140°C. The best results achieved with the commercial alloys at 140°C were exhibited by the unsuitable thorium alloy HZ32 (1.50 mils/day), and the high-aluminum alloy AZ91 (1.60 mils/day). The special Argonne alloys No. 1 and No. 2 showed much improved corrosion characteristics at 150°C. The best results were exhibited by the as-cast specimens: 2 mils/day for the No. 1 alloy, and 1.3 mils/day for the No. 2 alloy.

Further experimentation revealed that cold working improved the corrosion characteristics of the special alloys. Attempts to extrude both alloys into tubes (0.375 in. OD, 0.030 in. wall thickness) were partially successful; however, enough tubing was extruded for test purposes. The corrosion rates were 1.00 and 1.40 mils/day at 150°C, a marked improvement over the as-cast condition.

Earlier tests revealed the fluoride ion to be an effective corrosion inhibitor. Therefore, selected commercial and ANL special alloys were returned to test in 150°C water containing  $\text{PbF}_2$ ,  $\text{LiF}$ , and  $\text{NaF}$ , in proportions of 50 to 120 ppm. In every case the additive effected a decrease in the corrosion rate. For example, ANL special alloy No. 2 rolled



Table XV (cont'd.)

Alloy	Source and Treatment	Composition, % - Balance Mg																			Temp, °C	Time, hr	Inhibitor (ppm)	Loss, mil/day		
		Ag	Al	Be	Ca	Cd	Ce	Cu	Fe	Mn	Ni	Pb	Si	Sn	Th	Zn	Zr	Rare Earth	Other							
Z5Z	Howard Foundry No. 3 Alloy															4.50	0.70				140	120		Oxidized		
ZRE1	Howard Foundry No. 7 Alloy															2.50	0.60	3.00			140	139		11.80		
Magnox "C"	English Alloy		1.00	.05																	140	120		Oxidized		
Domal	Canadian Alloy	.0005	.006		.003	.0001		.0003	.0013	.0021	.0001	.0006	.003	.001		.002			.0025		130 120 120	120 70 70	Na F(50)	Oxidized Oxidized Oxidized		
RED No. 1	ANL Alloy-Cast by Brooks and Perkins			.005												7.00 3.50 1.00					150 140 140 140 140 140 140 140 150 140 140 140 150 140 140 140 150 150 150	120 120 120 120 120 120 120 120 120 120 120 120 120 120 120 120 120 120 120 120		Oxidized Oxidized Oxidized Oxidized Oxidized Oxidized Oxidized Oxidized Oxidized Oxidized Oxidized Oxidized Oxidized Oxidized Oxidized Oxidized Oxidized Oxidized Oxidized Oxidized		
RED No. 4																										
RED No. 5																										
RED No. 6																										
RED No. 7																										
RED No. 8																										
RED No. 9																										
RED No. 10																										
RED No. 13																										
RED No. 14																										
RED No. 15																										
RED No. 16																										
RED No. 17																										
RED No. 18																										
RED No. 19																										
PE	Special Alloy by ANL Met. Div.	3.20														0.10						135	120		0.88	
M1	Same. Rolled; 600°C quench; 260°C anneal																1.00					150	20		Oxidized	
M2	Special Alloy by ANL Met. Div. Chill cast; rolled and annealed at 160°C		5.00							0.50						0.10	<0.50					150	65		Oxidized	
M3			5.00														0.10	0.50				150	22		2.00	
M3X			5.00															0.50				150	22		2.20	
M4			15.00																			150	22		3.00	
M5			5.00																			150	22		13.70	
M6			5.00																			150	22		7.20	
M7			5.00																			150	22		1.90	
M8			5.00																			150	67		2.10	
M9			5.00																			150	22		8.40	
M10			5.00																			150	84		1.50	
M11	Same. Tested as cast; annealed at 260°C		10.00													0.50					150	20		12.00		
M12			10.00																		150	20		1.30		
M12			10.00																		150	65		1.60		
M13			10.00																		150	65		1.80		
M14	Same. Chill cast; rolled and annealed at 260°C		5.00													0.50					150	65		1.90		
ANL Special No. 1	Howard Foundry As cast		5.00													1.00					140 150 150 150	120 120 120 120		1.75 2.00 1.00 0.43		
	Same. Cast; extruded into tubes																				140 140 140 140	120 120 120 120		2.70		
ANL Special No. 2	Same. Cast; rolled																				150 140 150 150	120 120 120 120		1.30 0.70 1.59 0.27		
	Dow. As cast		3.00						0.60					1.00							150 140 150 150 150 150 150 170	120 120 120 120 120 120 120 120 66 66 45	NaF(120)	1.40 0.83 1.79 0.10 3.66		
ANL Special No. 2	Dow. Cast; rolled into plates																				150 140 150 150 150 150 150 170	120 120 120 120 120 120 120 120 66 66 45	NaF(120)	1.40 0.83 1.79 0.10 3.66		
	Dow. Cast; extruded into tubes.																				150 140 150 150 150 150 150 170	120 120 120 120 120 120 120 120 66 66 45	NaF(120) NaF(120)	1.40 0.83 1.79 0.10 3.66		



plate showed a rate of 0.27 mil/day in water containing 120 ppm NaF. Extruded tube specimens exposed to similar conditions showed a rate of 0.10 mil/day. Consequently, the ANL special alloy No. 2 has been selected as the cladding material.

## 2. Fabrication

The selection of a tubular unit fuel tube presents the problem of including the fissile material and its matrix in a bonded, magnesium-clad tube. The process considered involves an outer tube and an inner tube of very thin-walled magnesium alloy. The interspace between the tubes contains the meat in the form of thin-walled bushings produced essentially in the same manner as sintered bushings. The bushings are placed over the inner tube for the required 36-in. active length, the unit inserted in the oversized outer tube, and the ends are sealed. The completed tube is drawn through a mandrel and die. During the drawing operation, the outer tube is compressed, and the inner tube is enlarged to effect the bond between matrix and clad.

The proposed 5-day fuel cycle will necessitate a simple straight-line production technique to fulfill the weekly requirements of 3750 tubes (3% spares). Preliminary efforts in this connection indicate that all phases of magnesium tube production must be investigated in order to establish quality control, starting with the basic ingot. For example, the ingot must be cast under closely controlled conditions to ensure a sound ingot free of impurities, blow holes, and inclusions.

The design of extrusion dies, and the extrusion process, poses considerable research and development effort. The initial dies were not satisfactory. The first attempt to extrude special ANL alloy No. 2 involved a four-cavity, port hole die to process an ingot 5 in. OD and 20 in. long. Due to improper preheat and extrusion temperature, only a small quantity of tubing was extruded before the feed metal froze in the die. In some instances the extrusion failed to reweld due to improper die temperature, while in others the extrusion tended to "corkscrew" as it left the die apertures. Equipment to stretch-straighten the extrusions in the hot state was not available. Attempts to cold stretch the material were unsuccessful.

The second extrusion attempt was made with ANL special alloy No. 2, using a single cavity port hole die and ingots 3 in. OD by 6 in. long. This attempt also failed due to the metal freezing in the die cavity.

In view of the foregoing, it is evident that much remains to be done before magnesium can be used on a production basis. Although the reference design specifies ANL special alloy No. 2, it is possible that continued exploration of other alloying elements may eliminate the need for

fluoride additives. Future corrosion studies should include both static and dynamic environments. The basic concept of tubular fuel elements is contingent upon successful resolution of the problems related to the design of extrusion dies, preheating, and extruding temperatures.

### 3. Assembly

The original concept of the crowned square configuration was to spot weld the corners of adjacent fuel tubes at two places per juncture. However, attempts by ANL and a commercial welding company indicated corner spot welding of thin-walled magnesium is not feasible. Owing to the small inside diameter, it is impossible to cool the inside weld tip.

Brazing presents problems of corrosion. Torch brazing by ANL and by two commercial firms, using conventional brazing alloy and flux AZ 125 (12% Al, 5% Zn), resulted in increased corrosion of the brazed assembly. However, this may have been caused by failure to remove residual weld flux from the brazed area. Tentatively, it is presumed the reference design will specify either an oven or dip brazed joint, and that proper cleaning will eliminate the corrosion problem. If all attempts to braze the crowned square tube ends are unsuccessful, two alternate designs are proposed. Both designs feature plain tube ends and tube sheets as shown in an experimental 16-tube section (Fig. 43).

### 4. Heat Transfer and Flow Sheet

The heat transfer and flow characteristics of the proposed cladding material were evaluated at conditions simulating reactor full-power operation. The majority of the tube specimens (0.375 in. OD, 0.035 in. wall, 36 in. long) were prepared from AZ31B magnesium, principally because it was the most readily available alloy. Fortunately, it was also one of the more successful alloys exposed in the static corrosion tests. A limited number of tests were made with tubes (0.375 in. OD, 0.030-in. wall) specially cast and extruded from ANL special alloy No. 1.

The test encompassed the following range of variables:

Heat flux	385,000 - 553,000 Btu/(hr)(ft <sup>2</sup> )
Water velocity	25 fps
Surface temperature	120 - 150°C
System pressure	100 psig
Method of heating tube wall	Electrical resistance or Steam

It was obvious at the outset that scale formation due to rapid corrosion of the magnesium was the major problem. Subsequent experimental efforts were directed toward the measurement of the magnitude of the heat barrier created by the scale, and the reduction of the corrosion rate by addition of inhibitors to the coolant.

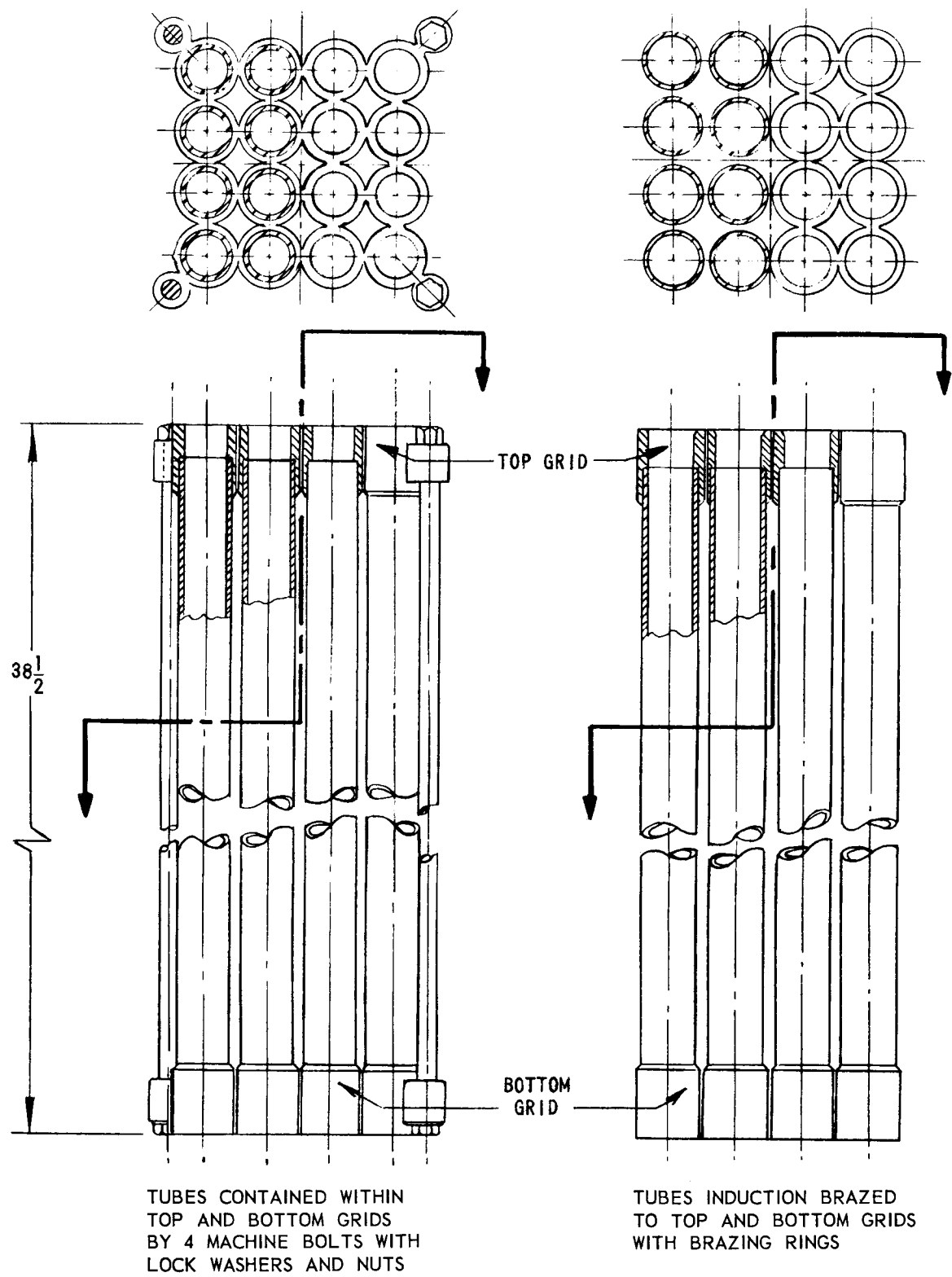


FIG. 43  
ALTERNATE METHODS OF FUEL TUBE AND SHEET ASSEMBLY  
(Ref. Dwgs. RE-1-22696-D; RE-1-22693-D)

Efforts to increase the corrosion resistance included attempts to pretreat the tube surface. This treatment consisted of passing a very small flow of 150°C water through the tube while maintaining the pH of the water below 7.0 with HF, and maintaining a fluoride concentration of 10 ppm with sodium fluoride. The treatment was supposed to strip ~2 mil from the surface in 2-3 days, preparatory to testing. However, upon removal from the pretreatment environment, the tube was found severely corroded and could not be used. It is believed the extruded tubing used in these tests was not equal in quality to the rolled or ingot samples exposed in the static corrosion tests, since the latter had exhibited a much lower corrosion rate.

Considerable effort was expended toward the development of test techniques and the production of high heat fluxes through the metal wall. The techniques employed, the difficulties encountered, along with the data analyses, are described in Appendix D.

Most of the tubes failed well in advance of the projected core life expectancy of 120 hr. The test results are summarized in Table XVI.

Table XVI

SUMMARY OF SCALE COEFFICIENT TESTS ON ANL SPECIAL  
NO. 1 AND AZ31 MAGNESIUM TUBING

Test No.	Heating; <sup>a</sup> Additive	Heat Flux, Btu/(hr)(ft <sup>2</sup> )	Temp., <sup>b</sup> °C	Time to Fail, hr	Min. Scale Coeff., Btu/(hr)(ft <sup>2</sup> )(° F)
Alloy Az31: 3% Al, 1% Zn					
1	E	470,000	120	24	~3,000
2	E	470,000	120	48	~3,000
3	S	300,000	120-130	138.5 <sup>c</sup>	2,300
4	S;F	150,000	125	59	4,200
5	E	418,000	125	40.5	1,300
6	E	406,000	125	60.5	1,900
7	E	402,000	120	66	1,600
8	E;F	395,000	120	100	2,300
9	E	436,000	130	74	1,700
10	E;F	418,000	135	30.5	1,500
11	E	494,000	143	17	1,500
12	E;F	515,000	130	49	1,500
13	E;F	380,000	135	69.5	1,000
14	E;F	428,000	150	31.5	1,200
15	E;F	553,000	135	7 <sup>d</sup>	-
16	E;F	270,000	102	156 <sup>c</sup>	Not detected
18	E;F	300,000	110	130	Not detected
20	E;F	500,000	130	102.5	2,900
ANL Special No. 1: 5% Al, 1% Zn, 0.5% Cu					
17	E;F	450,000	141	16	~2,000
22	E;F	500,000	120	112	Small Scale
23	E;F	500,000	Early failure		

<sup>a</sup> E = electric resistance; F = fluoride inhibitor added; S = steam  
<sup>b</sup> Initial surface at point of significance (usually hottest point on tube).  
<sup>c</sup> Did not fail  
<sup>d</sup> Tube machined to thin wall at center 4 in.; early failure

## 5. Full-scale Flow and Vibration Test

While the tubular fuel elements afford greater rigidity and strength than the plate-type elements, it is recognized that flow-induced vibration may preclude the use of a 36-in. tube with no intermediate vertical support in the final subassembly.

The required flow of proper internal and external velocities in the tube bundle has been calculated (see Appendix D). Full-scale flow tests should be conducted to confirm the flow distribution. Since the thermal neutron flux is highest at the inside edge of the core and, consequently, a tube in this vicinity is subjected to the highest heating rates, the tests should be designed to determine flow abnormalities in these regions. In addition, these tests would serve to check the structural integrity of the unit.

Thermal stress investigations should be made of the fuel subassembly under operating flow conditions. The fuel subassembly could be heated to produce thermal expansions within the bundle. The structural integrity of the unit under thermal stress conditions could then be ascertained.

The full-flow and thermal stress investigations may reveal the need for adjustments in the thermal hot spot analysis because of variations in the flow and spacing of the tubes.

While a margin of safety exists such that burnout is not a limiting factor in the reference fuel subassembly, the full flow and thermal stress investigations may indicate the need for an upward revision. In this event burnout of the fuel subassemblies should be investigated.

### B. Zircaloy-2 Pressure Vessel

The technology of Zircaloy-2 pressure vessels is limited to the short-term operation of the moderately-sized HRT vessel at Oak Ridge. Since the life expectancy of the Mighty Mouse vessel will be at least 10 years (and possibly 20 years), positive action must be taken to ensure a sound vessel. Studies are under way to include Zircaloy-2 in the ASME Code for Unfired Pressure Vessels. Code approval is contingent upon accumulation of reliable physical, mechanical, and nuclear test data, including welding specifications.

### C. Control and Instrumentation

The mechanical control system presents no development problems. However, the  $\text{BF}_3$  control system will require considerable research and tests to evaluate performance. The effect of radiation damage on

dissociation, the possible deposition of metallic boron on the container wall, and changes in density represent specific avenues of study that initially could be conducted in the CP-5 reactor and subsequently extended to systems with higher flux environments.

The high neutron flux in the Mighty Mouse may require improved instrumentation capable of withstanding these radiation levels. The high degree of automation in fuel handling will require exceptionally accurate indicating devices.

#### D. Experimental Facilities

The cryogenic facilities represent a highly specialized investigation that can best be performed by firms with considerable experience with low-temperature apparatus.

The water-cooled shield gates will require studies to evolve the best combination of borated water and lead.

The retractable center thimble will necessitate performance evaluation tests for the proper functioning of the withdrawal mechanism.

#### E. Fuel-handling System

The fuel-handling system poses a problem of considerable magnitude. The 120-hr operating cycle allows a total elapsed time of 48 hr/week from shutdown to startup. Since the entire system is operated by remote control, the multiplicity of compound mechanical motions dictate extreme precision of manufacture, and positioning mechanisms with pinpoint accuracy.

The foregoing imply an extensive performance test program to ensure the integrity of all phases of the fueling process.

VII. ESTIMATED COSTS

A. Capital Costs

The estimated cost of the Mighty Mouse reactor, including escalation and contingencies, is \$70,467,000.

The building costs in Table XVII are based on prices prevailing in the Chicago area. Although the basic functional requirements dictate the floor plans of the various buildings and wings, the architecture of the Mighty Mouse complex will be similar to existing buildings at Argonne.

Table XVII

<u>MIGHTY MOUSE RESEARCH REACTOR COST ESTIMATE</u>		<u>Thousands of \$</u>
<u>BUILDINGS</u>		
Construction		
Land Improvement	275	
Buildings		
Reactor (includes stack and utilities)	10,380	
Laboratory Wing	2,022	
Administration Wing	961	
Mock-up and Ventilation Annex	1,052	
Shield Storage	40	
Other Structures (mainly cooling tower)	1,282	
Outside Utilities	914	
Equipment (other than reactor and its associated equipment)	<u>1,094</u>	
Total Construction Costs		18,020
Architect - Engineering (7½%)		1,352
ANL Liaison (2½%)		451
Indirect Costs		
Payment and Performance Bond (1%)		<u>180</u>
		20,003
Contingencies (15%)		3,000
Probable Utility Addition		
Boiler		1,250
Water System from Sag Canal		<u>840</u>
<u>TOTAL BUILDINGS COSTS</u>		25,093
<u>REACTOR</u>		
Components and Systems		
Pressure Vessel	2,998	
Control Systems	491	
Shields and Shield Cooling	1,957	
Instrumentation	2,832	
Fuel and Control Rod Handling System	530	
Experimental Facilities and Handling Equipment	6,949	
Primary Cooling System	3,603	
Emergency and Waste Disposal Systems	600	
Acceptance Tests and Replacements	500	
Miscellaneous	<u>150</u>	
Total Components and Systems		20,610
Architect - Engineering (10%)		2,061
ANL Liaison (2½%)		<u>515</u>
		23,186
Contingency (25%)		<u>5,797</u>
<u>TOTAL REACTOR COSTS</u>		28,983
<u>TOTAL BUILDINGS AND REACTOR COSTS</u>		54,076
Escalation (5%/yr for 3 years)		8,111
D <sub>2</sub> O for Reactor and Critical Mock-up (230 ton @ \$18/lb)		<u>8,280</u>
<u>GRAND TOTAL</u>		70,467

Wherever possible, the costs are based on actual quotations for the building elements and for the reactor components. For example, the machine shop in the Reactor Building is essentially a duplicate of the present machining facilities in the Reactor Engineering Division Building (D-208), but its cost is increased by a 10% escalation. The critical installation is also a duplicate of one installed on the Argonne site; the costs are identical. The costs for the pressure vessel, main circulating pumps, cooling towers, heat exchangers, and cranes were established by quotations from respective vendors.

The initial fuel-loading costs are not included since the reference fuel, i.e., magnesium-clad tubes represent a substantial developmental program. Early in the development of the project, calculations demonstrated that the lower absorption of magnesium, relative to aluminum and zirconium, would effect appreciable savings in power expended (25 to 100 Mw) to achieve the desired neutron flux of  $5 \times 10^{15} \text{ n}/(\text{cm}^2) (\text{sec})$ .

While magnesium is a suitable structural material, its corrosion-resistant properties are not good, and the techniques for fabricating this metal are not well established for an application peculiar to the Mighty Mouse.

Consequently, many of the fuel design features and costs are contingent upon the successful culmination of the magnesium-clad fuel program explored partially during the course of the Project. If re-activated, such a program could parallel the initial construction phases and, on this basis, the reactor buildup time from site preparation to initial criticality could be accomplished in 36 months.

Designing for aluminum- or zirconium-clad fuel represents an alternate path to hasten the theoretical completion date; however, the potential savings in power warrant an exhaustive survey of the magnesium field.

#### B. Annual Operating Costs

The annual operating costs of the Mighty Mouse, summarized in Table XVIII, are estimated at \$2,900,000. No attempt is made to include the operating costs of experiments.

The magnitude of wages and overhead is motivated by several factors. Discussions with AEC personnel resulted in opinions that such a unique and costly facility, while operated by Argonne, must be considered a national research reactor. Consequently, services and quarters must be provided for transient experimenters. This provision is equally applicable to Argonne experimenters since, in both instances, the proximity of reactor experiment to office-laboratories is especially conducive to the orderly,



efficient, and expeditious conduct of the various research activities. The high performance and integrity required of a sytem to produce the neutron flux level of Mighty Mouse justifies added investment in administrative and operating personnel and auxiliary facilities to ensure that reactor operations are consistent with the intent and scope of these research efforts.

Table XVIII

ANNUAL OPERATING COSTS

	<u>Thousands of \$</u>
Wages and Overhead	1,800
Water @ \$0.10/1000 gal	130
Power @ \$0.008/kw-hr	400
D <sub>2</sub> O Loss (20,000 lb @ \$15/lb)	300
Miscellaneous Supplies	250
TOTAL	2,900

The basic operating force comprises 150 personnel in the following capacities:

Director	1
Assistant Directors	2
Shift Supervisors	5
Reactor Operators	15
Water Plant Operators	13
Instrument Maintenance	10
General Maintenance and Repair	33
Health Physics	6
Special Materials	3
Reactor Service Group	15
Engineering and Review Group	20
Shops	6
Secretarial and Clerical	6
Janitorial	15

With the exception of the reactor service group, and the Engineering and Review Group, the titles are explanatory of the duties performed. The Reactor Service Group, subject to shift work, are a liaison between the experimenters and the reactor operators. The Engineering and Review Group provide engineering and design services, perform calculations, mock-up tests and critical experiments for all apparatus and irradiations prior to installation in the reactor.

Other major annual operating costs listed in Table XVIII are the cooling water and power supply. Based on a 300-day year, the H<sub>2</sub>O coolant consumption rate is calculated at 300 gpm, and the power at 7,000 kw. The annual loss of D<sub>2</sub>O is estimated at 20,000 lb.

The fuel cycle costs are not included. However, the annual quantities of fuel required listed in Table XIX are based on the assumptions that (1) the fuel contains  $U^{235}$  enriched to 90%, and (2) the uranium recovered from the spent fuel is not recycled; thus the initial enrichment is a constant.

Table XIX

<u>ANNUAL QUANTITIES OF FUEL</u>		
Core loadings	50	
Uranium per core loading (90% $U^{235}$ )	3.5	kg
Uranium (new fuel)	175	kg
$U^{235}$ burnup at 1.25 gm/Mwd	78	kg
Spent uranium recovered	109	kg
Quality of spent uranium	$\left\{ \begin{array}{l} \sim 75\% \text{ } U^{235} \\ \sim 11\% \text{ } U^{236} \end{array} \right.$	

ACKNOWLEDGEMENT

The research, design, and development activities pertinent to the Mighty Mouse Project encompassed several Argonne Divisions. The following Division members, in particular, contributed substantially during the course of the Project:

REACTOR ENGINEERING DIVISION

<u>Corrosion and Irradiation Group</u>	<u>Reactor Control Section</u>
C. R. Breden	R. V. Batch
A. P. Gavin	P. E. Brown
N. R. Grant	J. M. Harrer
S. B. Skladzien	W. J. Kann
	R. L. Ramp
<u>Theoretical Physics Section</u>	<u>Heat Engineering Section</u>
A. D. Rossin	J. A. Chase
	P. A. Lottes
<u>Computing Group</u>	J. F. Marchaterre
Joan M. Ramuta	J. J. Santori

METALLURGY DIVISION

C. H. Bean	R. A. Noland
J. E. Draley	W. E. Ruther
F. G. Foote	J. F. Schumar
S. Greenberg	C. C. Stone
R. E. Macherey	D. E. Walker

REMOTE CONTROL ENGINEERING DIVISION

R. C. Goertz	A. H. Marchertas	J. P. Simon
--------------	------------------	-------------

CENTRAL SHOPS

C. T. Szymko		L. F. Franck
A. A. Denst	L. E. Wright	H. V. Ross

PLANT ENGINEERING DIVISION

A. W. Hothan		A. W. R. Oswald
E. W. Landow		B. F. Oswald
R. E. Loewe	A. K. Stein	U. K. Sick

The proposed research programs for an advanced high-flux reactor, prepared by R. M. Adams of the Laboratory Director's Office, was initially published as a limited-distribution document. For convenience, it is reproduced as Appendix A.

## APPENDIX A

### PROPOSED RESEARCH PROGRAMS FOR AN ADVANCED HIGH-FLUX REACTOR

#### I. INTRODUCTION

The Argonne National Laboratory research programs in the fields of chemistry, physics, and metallurgy have been carried out in the CP-5 reactor at a current flux level of about  $3 \times 10^{13}$  n/(cm<sup>2</sup>)(sec). Although some irradiations for nuclear chemistry and metallurgical studies have been made in the MTR at a flux level above  $10^{14}$  n/(cm<sup>2</sup>)(sec), this reactor is used predominantly as an engineering test reactor. The power level of CP-5 is being raised to 4 Mw, and will be raised to 10 Mw in the fall of 1959. This will provide a flux of approximately  $10^{14}$  n/(cm<sup>2</sup>)(sec). However, the advanced research programs in the fields mentioned above are expected to have exhausted in a few years the potentialities of this modest increase in flux. Indeed, many of the advanced research programs indicate a present need for thermal fluxes in the range of  $10^{15}$ - $10^{16}$  n/(cm<sup>2</sup>)(sec), which would be provided in the proposed high-flux research reactor. This need is defined in terms of the actual research programs as detailed in the following sections.

#### II. CHEMISTRY

##### A. Isotope Production

One of the most important uses of the proposed high-flux reactor is the production of isotopes of the heavy elements, in particular of the transuranium elements, in sufficient quantity to permit study of their basic nuclear and chemical properties. Some of the most important areas of investigation of the heavy elements are discussed in the following sections.

##### 1. Determination of Long-term Reactivity of Recycled Fuels

The future trend in power reactors indicates higher fluxes, both fast and thermal, higher burnup of fuel, and recycling of fuels, including Pu<sup>239</sup> and U<sup>233</sup>. Proper design of such reactors requires a more complete knowledge of the changes in nuclear properties of the fuel, blanket material, fission products, and structural materials under prolonged irradiation. A knowledge of the capture and fission cross sections, the number of neutrons per fission ( $\nu$ ) in the case of fissionable isotopes and the delayed neutron properties is necessary to calculate reactivity changes which affect control. A high-flux reactor is needed to produce sufficient quantities of the isotopes formed by multiple-order neutron capture so that these nuclear properties can be measured.

## 2. Production of Spontaneous Fission Neutron Sources

Some of the transuranium nuclides (such as  $\text{Cf}^{252}$  and  $\text{Cm}^{244}$ ) decay by spontaneous fission with simultaneous emission of neutrons. These spontaneous fission properties suggest a multitude of uses:

a. The equivalent of small portable reactors (which are noncritical) can be made. Such sources can be used for activation work, trace analysis, neutron experiments, etc. These sources will not have the usual high beta and gamma activities associated with a reactor.

b. Neutron standards made as point sources or in other shapes can be readily prepared.

c. The energy distribution of neutrons from  $\text{Cf}^{252}$  is very similar to that from neutron-induced fission of  $\text{U}^{235}$ . This fact makes possible the use of point sources of  $\text{Cf}^{252}$  for accurate measurements of reactor constants, such as neutron age, moderating power, etc.

d. These intense sources of fast neutrons can be used for fast cross-section measurements without using fast critical assemblies.

e. Californium makes an excellent source for a study of the fission process, since such a source simulates a reactor in constant operation but does not have the interfering radiation common to a reactor. For example, a californium sample allows the study of the primary fission fragments which are in equilibrium with the spontaneous fissions.

f. Biological studies of radiation damage in general should be carried out with sources involving only one type of radiation.  $\text{Cf}^{252}$  would provide a relatively pure source of fast neutrons suitable for such studies. Alpha emitters plus beryllium are not suitable, and accelerators are unable to provide a source of neutrons constant over long periods of time.

g. Many practical industrial uses are possible, e.g., oil well logging, atomic batteries, fission-induced chemical reactions, etc.  $\text{Cf}^{252}$  or  $\text{Cm}^{244}$  can possibly be used as power sources in earth satellites.

h.  $\text{Cf}^{252}$  can be used to investigate the mechanism of radiation damage in some solid-state studies.

## 3. Production of Various Elements and Their Isotopes

The greater availability of low-specific-activity isotopes of plutonium ( $\text{Pu}^{242}$ ), americium ( $\text{Am}^{243}$ ) and curium ( $\text{Cm}^{244}$  and - in the more remote future - heavier curium isotopes) will facilitate investigations of the chemical properties of these elements by reduction of radioactivity hazards and of interfering radiation effects. Further, the production of milligram quantities of the higher Z elements (berkelium, californium and perhaps eventually even higher) will permit more effective chemical studies of these

interesting elements than are now possible on a tracer basis. Detailed knowledge of the chemical properties of these heavy elements will be necessary in designing future processing methods particularly for high-burnup plutonium fuels.

#### 4. Determination of the Systematics of Neutron Interactions with Fissionable Materials

The primary problem in these studies is production of sufficient quantities of nuclides to allow measurement of such properties as: neutron fission cross sections as a function of neutron energy; decay properties of the compound nucleus formed by neutron capture; inelastic scattering cross sections; and thermal neutron fission cross sections of short-lived nuclides.

Such measurements have not yet been made on many of the most interesting and important nuclides simply because they cannot be produced in large enough quantities at presently available fluxes.

#### 5. Production of Target Material for Charged Particle Bombardments to Prepare Additional Heavy Element Nuclides for Basic Research

The most promising possibility at present for preparation of new elements of  $Z$  greater than 102 lies in the bombardment of curium and heavier elements with heavy ions such as carbon, nitrogen and oxygen. In addition, there are many nuclides of the heavy elements which cannot be produced in a reactor, but which can be formed by heavy ion bombardment of the appropriate nuclide. For example, at the present time the only available isotope of berkelium with a half-life greater than a few days is  $\text{Bk}^{249}$ . This isotope ( $\beta^-$ ,  $t_{1/2} = 1$  yr) has been produced in only microgram quantities over a period of six years in the plutonium irradiation program. However, it would be much more desirable to produce the longer-lived  $\text{Bk}^{247}$  ( $\alpha$ ,  $t_{1/2} = 10,000$  yr) for chemical studies.  $\text{Bk}^{247}$  cannot be made in reactors, but could be readily made by irradiating curium in a cyclotron. In fact, cyclotron bombardments could yield appreciable quantities of  $\text{Bk}^{247}$  in a matter of months, if sufficient  $\text{Cm}^{244}$  were made available for the target material.

#### 6. Production of Sufficient Quantities of Various Elements to Feed into Electromagnetic Separators

Electromagnetic separation would produce useful enrichments of nuclides which are normally produced only as minor isotopic constituents by neutron irradiation in reactors. Examples of such nuclides are  $\text{Pu}^{244}$ ,  $\text{Cm}^{245}$ ,  $\text{Cm}^{246}$ ,  $\text{Cm}^{247}$ ,  $\text{Cf}^{250}$  and  $\text{Cf}^{251}$ .

## 7. Determination of Nuclear Properties and Isotopic Distribution of Fission Products in High-flux, High-burnup Reactors

In future high-flux reactors there may be significant changes in the fission product composition as a result of multiple-order neutron capture by the initial fission products. These changes may require modifications of present methods of processing and waste disposal. Changes in shielding requirements may also be necessary because of a different distribution of radioactivity in the fission products.

## 8. Production of Other Nuclides

There are many interesting nuclides other than the trans-uranics involving multiple order captures which have not yet been found but which could be formed at higher fluxes. Examples of such isotopes are  $\text{Hg}^{206}$ ,  $\text{Zr}^{98}$ ,  $\text{Nd}^{152}$ , etc.

In most of the cases discussed thus far the nuclides of interest result from multiple-order neutron capture. For example, one of the most interesting and potentially useful isotopes,  $\text{Cf}^{252}$ , is formed by thirteen successive neutron captures starting with  $\text{Pu}^{239}$ . Owing to some intermediate short-lived isotopes, the production rate of  $\text{Cf}^{252}$  is proportional to the 9th or 10th (rather than the 13th) power of the neutron flux. Up to the present, only a few micrograms of this isotope have been produced from  $\text{Pu}^{239}$  after six years irradiation in the highest available flux ( $\sim 5 \times 10^{14} \text{ n}/(\text{cm}^2)(\text{sec})$ ) using all available space in the MTR. Within two years there will be available 100-gram quantities of  $\text{Cm}^{244}$ . If 100 gm of  $\text{Cm}^{244}$  were irradiated at MTR flux levels for one year, only 50  $\mu\text{g}$  of  $\text{Cf}^{252}$  would be formed; after 15 yr (at saturation) there would still be produced only 85 mg of  $\text{Cf}^{252}$ . On the other hand, in the proposed high-flux reactor the same amount of  $\text{Cm}^{244}$  would produce about 100 mg of  $\text{Cf}^{252}$  in one year. The time scale and feasibility of producing other nuclides which are formed by multiple neutron capture will likewise be highly dependent on the flux level.

## B. Fission Studies

The increased resolution of crystal spectrometer measurements resulting from an increased flux would make possible the study of the fission process as a function of neutron energy to determine whether symmetric or asymmetric fission predominates. The results would give a better insight into the Bohr-Mottelson theory of fission. In a flux of  $2 \times 10^{13} \text{ n}/(\text{cm}^2)(\text{sec})$  the neutron crystal spectrometer will produce a flux of neutrons in a specific energy interval (e.g., 5 ev) of about  $500 \text{ n}/(\text{cm}^2)(\text{sec})$ . With this flux it is necessary to use a 100-gm sample of  $\text{U}^{235}$  to produce about 1000 d/min at saturation of a nuclide with 1% fission yield. This

sets the practical lower limit for study at about 0.1% fission yield. However, in normal thermal fission symmetric fission yields are of the order of 0.01%. Thus, to establish an asymmetric level with even lower symmetric fission yields, a much higher thermal flux is needed. A thermal flux above  $10^{15}$  n/(cm<sup>2</sup>)(sec) would give significant results.

The study of thermal fission cross sections of isotopes with low cross sections, e.g., Np<sup>237</sup>, cannot be carried out in existing neutron flux environments. To ensure that observed fissions are not due to fast neutrons, the neutrons must be well thermalized. This requires a high initial thermal flux. In addition to permitting the determination of low fission cross sections, it would also be possible to obtain some information about fission barriers by studying fission as a function of energy well below the threshold using a neutron spectrometer.

There is much information to be obtained on fission kinetics of heavy elements. Present fluxes are not high enough to prepare these elements in sufficiently large quantity for such studies. With thermal neutron fluxes above  $10^{15}$  n/(cm<sup>2</sup>)(sec) there can be prepared the quantities of isotopes such as Fm<sup>254</sup> needed to study the fission kinetics of spontaneous fission processes. It might also be possible to separate the excited from the spontaneous fission cross section for those nuclides (i.e., some isotopes of curium) having low total fission cross sections.

A flux of the order of  $10^{15}$  n/(cm<sup>2</sup>)(sec) will facilitate beam experiments, such as measuring  $\nu$  for isotopes of Cm<sup>245,247</sup> and Cf isotopes. Owing to the low neutron flux available, the present samples required are so large that alpha pile-up and spontaneous fission cause too high a background.

### C. Radiation Damage and Radiation Chemistry

The accident at Windscale in 1957 has shown how important an adequate foreknowledge of radiation damage may be to the operation of a reactor. For graphite reactors in particular, it will become increasingly important to know how much stored energy is accumulated after very heavy exposures at rather high temperatures. It is known that at relatively low temperatures (300°C) sufficient stored energy accumulates to cause a possibly catastrophic self-heating of the graphite. Future power reactors will probably operate at much higher temperatures. Self-heating of the graphite due to stored energy release may occur after heavy exposures even at temperatures above 500°C. The answer to questions of this kind sufficiently in advance of design of such power reactors will require experiments with neutron fluxes far in excess of those now available.

It seems probable that power reactors and particularly thermonuclear reactors will be built in which the neutron fluxes will be much greater than in present irradiation facilities. Since radiation damage is



expected to be nonlinear at very high integrated flux, it will be necessary to have a research reactor in which samples can be irradiated to a high integrated flux in a reasonable period of time. There is also reason to believe that additional radiation damage effects may result from an increased rate of irradiation. Such effects can be studied only in a reactor providing a much higher fast neutron flux than is now available.

Since some radiation damage effects anneal even at very low temperatures, a complete study of these effects often requires experiments at liquid nitrogen or even liquid helium temperatures. The Mighty Mouse Reactor features two cryogenic facilities for such studies.

Another possible use may be made of a cryogenic facility. A system in part of which thermal neutrons are at temperatures close to absolute zero would, in principle, represent a means of obtaining increased reaction rates. It is usually the reaction rate that is important and this is given by the product of the flux and the reaction cross section. Reaction cross sections are mostly proportional to  $1/v$  and thus increase with decreasing neutron temperature. In a cold region the reaction rate will be increased by a factor  $(T/T_n)^{1/2}$ , where  $T$  is some normal reference temperature, say  $300^\circ\text{K}$ , and  $T_n$  is the neutron temperature. If  $T_n = 3^\circ\text{K}$ , then the reaction rate increases by a factor of 10. The higher reaction rates for this type of system will hold only for  $1/v$ -absorption events and not for scattering events; however, most of the interest in high thermal flux reactions is in connection with absorption rather than scattering. With the rate of reaction enhanced by an increased neutron flux and the cross section increased by the low temperatures, it would be possible to study the energy stored in a solid by chemical decomposition resulting from nuclear transformations.

Among the irradiation facilities planned for the proposed high-flux reactor are two vertical thimbles in the water exit lines; these will serve as gamma-irradiation facilities, using the  $\text{N}^{16}$  gammas as a source. These, along with the intense gamma-irradiation facility provided by the storage of spent fuel, will provide valuable new gamma-ray sources for radiation chemistry studies. For instance, the radiation chemistry of gamma-ray-irradiated gases could be studied in detail. Such studies have not yet been attempted since the available gamma-ray sources have been too weak. Studies of radical-radical interactions in aqueous solutions and organic liquids could be carried out. At high intensities the local concentration of radicals may be large enough to permit radical-radical interactions. This would lead to an intensity-dependence of the yield of a given product. Further, the steady-state concentration of water decomposition products is known to increase as the square root of electron irradiation intensity. In the proposed high gamma intensities, investigations could be carried out to determine whether the same square root relationship holds for gamma irradiation.

#### D. Miscellaneous

There are other general areas in the field of chemistry in which higher neutron flux is necessary for continued progress. Thus, the higher the flux the smaller the sample or amount of impurity which can be detected by activation analysis. For example, with a flux of above  $10^{15}$  n/(cm<sup>2</sup>)(sec) it becomes feasible to analyze for uranium or thorium in concentrations below  $10^{-12}$  gm.

Of particular importance are the larger quantities of short-lived isotopes which can be produced at higher fluxes, thus permitting studies to be made of many interesting nuclides which are now available only in quantities too small to be useful.

Beta spectrometer measurements are directly dependent upon the specific activities of the samples used. With samples of highly increased specific activities resulting from irradiations in higher fluxes these measurements can be greatly improved with consequent improvement in understanding of the theory of beta decay.

An increased flux would permit measurement of the beta spectra of neutrons with better resolution. The present results were obtained using the Chalk River reactor with about 5% resolution. The error in the beta end point is several kev, due to the low neutron flux. The end-point error could be reduced to below 1 kev at a flux of about  $10^{15}$  n/(cm<sup>2</sup>)(sec). The increased accuracy would be of great importance in the theory of beta decay and in establishing the neutron-proton mass difference.

It would also be possible to improve significantly the measurements of small capture cross sections of elements which are of great importance in reactor design, e.g., C<sup>14</sup>, H<sup>2</sup>, O<sup>16</sup>, etc.

### III. PHYSICS

#### A. Measurements of Neutron Cross Sections

In this section the measurement of neutron cross sections, using the time-of-flight method with a mechanical chopper, is considered. Qualitatively, the discussion is also applicable to measurements with a crystal spectrometer.

##### 1. Total Cross Sections

The total neutron cross section is usually determined by a measurement of the neutron transmission of a sample of the material being studied. For measurements of this kind an increase in the flux to above

$10^{15} \text{ n}/(\text{cm}^2)(\text{sec})$  would permit a great improvement in the resolution of the time-of-flight system and a reduction in the minimum weight of the sample being studied. These two effects may be considered in more detail.

The narrowest resolution width now in use in neutron transmission measurements is that of the Argonne Fast Chopper at CP-5, for which the resolution width is  $12 \text{ }\mu\text{sec}/\text{meter}$ . With existing detectors and electronic equipment the resolution width could be reduced to  $6 \text{ }\mu\text{sec}/\text{meter}$ , with the same counting rate per channel, if the neutron source strength were increased by a factor of about 12. If the flux were increased to above  $10^{15} \text{ n}/(\text{cm}^2)(\text{sec})$ , a resolution of  $1.5 \text{ }\mu\text{sec}/\text{meter}$  could be obtained by major modifications of the chopper and its associated equipment (but using well-established techniques). The relative resolution as a function of energy of a system having this resolution is given in Table XX.

Table XX

RELATIVE RESOLUTION VS ENERGY FOR  
A TIME-OF-FLIGHT SPECTROMETER  
HAVING A RESOLUTION OF  
 $1.5 \text{ }\mu\text{sec}/\text{meter}$

E, ev	$\Delta E/E$	$\Delta E$ , ev
20	0.0002	0.004
$10^2$	0.00042	0.042
$10^3$	0.0013	1.3
$10^4$	0.0042	42
$10^5$	0.013	1,300
$10^6$	0.042	42,000
$10^7$	0.13	1,300,000

An examination of Table XX indicated several ways in which an extremely high-resolution spectrometer could extend the range of measurements of slow neutron spectroscopy:

a. The chopper would be competitive with all other techniques of measuring total cross sections up to an energy of 50 kev, and would be far superior to the Van de Graaff generator below 10 kev.

b. Useful measurements of average cross sec-

tions could be made up to an energy of 10 Mev. At the present time very few cross sections of this kind have been measured in the energy range from about 3 to 10 Mev.

c. All resonances of 90% of the stable nuclides would be well resolved up to an energy of about 100 ev.

d. Almost all resonances of 90% of all nuclides would be detected up to an energy of 500 ev.

An alternative use of a great increase in neutron source strength would be to study extremely small samples. At the present time it is necessary to have a sample with a cross-sectional area of at least  $2 \text{ mm}^2$  to obtain a resolution of about  $0.1 \text{ }\mu\text{sec}/\text{meter}$ , the poorest resolution which should be used if resonance structure is to be studied. For

heavy nuclides, such an area corresponds to a weight of about 10 mg of material, if only resonant structure is to be studied. A weight of about 200 mg is needed if the off-resonant cross sections are also to be measured. With a neutron flux of over  $10^{15}$  n/(cm<sup>2</sup>)(sec) it seems feasible, with minor modifications of existing equipment, to obtain a useable counting rate and a resolution of 0.1  $\mu$ sec/meter for a sample having a cross section of only 0.1 mm<sup>2</sup>; major modifications in the design of the chopper might make it feasible to use an even smaller sample. An area of 0.1 mm<sup>2</sup> corresponds to masses of 0.5 and 10 mg of a heavy nuclide for studies of the resonance and the off-resonance cross sections, respectively. These masses are small enough that it should be possible to obtain satisfactory samples for the study of all of the stable nuclides, many of the rare nuclides which are alpha unstable, and many of the lighter nuclides which are beta unstable. The latter category of nuclides especially constitutes an almost untouched field for neutron cross-section measurements. In addition to making it feasible to procure a wider range of samples, the use of a small sample makes it much easier to handle very radioactive materials.

## 2. Radiative Capture Cross Sections

The measurement of radiative capture cross sections is of the highest priority to meet the needs of the U. S. reactor program.<sup>15</sup> At the present time the only known technique for measuring this cross section by the time-of-flight method, i.e., in the range of energy from 10 to 10,000 ev, is to observe the prompt gamma rays from capture with a detector that is so large that it is almost certain to detect some of the binding energy released in the form of gamma rays. It has not been possible to use this technique in the region of energy accessible to the chopper because of the high background rate (from natural causes, such as cosmic rays, etc.) in the large detectors required for the measurement. However, an increase in the neutron source strength to give a flux of about  $10^{15}$  n/(cm<sup>2</sup>)(sec) would cause the rate from capture to be large enough to be measurable for most nuclides over the full range from thermal energy to about 10 kev.

Perhaps the most important (for reactor applications) and difficult measurement would be that of an average capture cross section in a range of energy where individual resonances could not be resolved. As an example of results which might be obtained in such measurements, there are compared in Table XXI estimates of the minimum detectable cross section with the actual cross section for the typical material U<sup>238</sup>. In the calculation it is assumed that a rate of capture of 10 n/sec could be detected. Also, the sample is assumed to be thin enough that the effect of self-shielding of the resonances would be unimportant.

---

<sup>15</sup>Nuclear Cross Sections Advisory Group, "Compilation of Request for Nuclear Cross-Section Measurements," BNL-463, T-103, (September, 1957).

Table XXI

ESTIMATES OF THE MINIMUM DETECTABLE  
CAPTURE CROSS SECTION ( $\bar{\sigma}_\gamma$ ) FOR  $U^{238}$

E	$\frac{\Delta E}{E}$	$\bar{\sigma}_\gamma$ , barns		
		Minimum Detectable	Actual Value	$\frac{\bar{\sigma}_\gamma(\text{actual})}{\bar{\sigma}_\gamma(\text{min})}$
$10^2$	0.10	0.180	25	140
$10^3$	0.10	0.030	4.3	140
$10^4$	0.23	0.0018	0.56	310

It is seen that over a wide range of energy the actual cross section is several orders of magnitude greater than the minimum cross section detectable with a flux of above  $10^{15}$  n/(cm<sup>2</sup>)(sec). However, it is also clear that useful measurements cannot be made with the present source of neutrons. Thus the availability of

a much higher neutron source strength opens up an entirely new area for cross-section investigations.

3. Scattering Cross Sections

The measurement of the scattering cross section for slow neutrons is important for nuclear theory because it is the most straightforward and only proven way of determining the total angular momenta of the neutron resonances. With the present source strength only the most favorable resonances can be studied. However, with a flux density of above  $10^{15}$  n/(cm<sup>2</sup>)(sec) the scattering cross section could be measured with accuracy for essentially all of the resonances which can be resolved with a resolution of about 0.1  $\mu$ sec/meter, including the levels in the fissionable nuclides. The determination of the total angular momenta of the resonances in the fissionable nuclides is of particular interest because of the bearing of these results on the theory of fission.

4. Fission Cross Sections

A substantial increase in flux would have much the same effect on the measurement of fission cross sections, as has already been discussed for the total cross section, i.e., it would allow measurements to be made with higher resolution and smaller quantities of material than is now possible. For a material such as  $U^{235}$ , which can be used in large quantities, the resolution of a fission cross-section measurement can come within a factor of two of that obtainable in a transmission measurement; thus Table XX may be used as an indication of the resolution which could be achieved with a reactor having a flux of above  $10^{15}$  n/(cm<sup>2</sup>)(sec). Alternatively, if the higher flux were used to study the fission cross section of small quantities of rare fissionable materials, measurements with a resolution of about 0.1  $\mu$ sec/meter, which now requires 20 mg to achieve refined results, could be done with 100  $\mu$ g; and measurements of lower resolution, which might cover the energy range below 10 ev, could be done

with as little as  $1\ \mu\text{g}$  of material. The ability to work with such a small quantity of material would, in time, increase by a large factor the number of fissionable nuclides for which the resonance structure could be studied.

## B. Energy Dependence of Nuclear Properties

In this section the influence of a large increase in the available flux is considered for experiments which use the fast chopper to study nuclear properties other than the total, capture, scattering, and fission cross sections.

### 1. Gamma-ray Spectra from Neutron Capture in Resonances

An important branch of neutron spectroscopy is the study of the gamma-ray spectra resulting from capture of neutrons in resonances. Experiments of this kind may be expected to contribute to a determination of the spins of the initial state of the compound nucleus; to a determination of the spins and parities of the low-energy states of the compound nucleus; to the properties of high-energy gamma-ray transitions; and to the isotopic assignment of resonances in the target nucleus. At the present time many of these experiments are just barely possible and only qualitative information can be obtained. However, an increase in the source strength to that proposed would permit the gamma-ray spectra to be studied with great refinement by the use of two or three NaI scintillation spectrometers in coincidence. The value of studying gamma rays from resonant capture may be illustrated by one of the experiments mentioned above, i.e., the study of properties of high-energy gamma-ray transitions. Until now, these characteristics could be determined for heavy nuclides only for those cases where the thermal capture cross section of the sample (whether normal or isotopically enriched) is dominated by a single isotope. By the observation of the gamma-ray spectra from capture in resonances, however, essentially all of the stable nuclides having a mass greater than 50 could be studied. Thus one might search for a systematic dependence of the transition probabilities on the multipolarity of the transitions, the shell structure of the nucleus, the character of the lower state, etc.

### 2. Fission Fragments (also see Sec II B., Fission Studies)

At the present time there is a considerable interest in the dependence of the modes of fission on the energy of the incident neutron. One aspect of the problem concerns variations from resonance to resonance in the characteristics of fission. The use of the fast chopper in such studies is at present entirely impossible because of low counting rates. It is not certain that an increase in the flux to a level of above  $10^{15}\ \text{n}/(\text{cm}^2)(\text{sec})$  would make it possible to see the small variations which are expected, but at least the experiments would then be within the realm of possibility.

### C. Internally Converted Capture Gamma Rays

While the study of gamma-ray spectra resulting from capture of thermal neutrons has been pursued vigorously, almost no work has been done in the closely related area of studying the beta rays resulting from the internal conversion of these gamma rays. This neglect of an apparently fruitful field is a direct result of an inadequate source of neutrons. If a source strength greater than  $10^{15}$  n/(cm<sup>2</sup>)(sec) were made available, the study of internal conversion could become at least as important as the study of capture gamma rays because of the usefulness of internal conversion coefficients in assigning spins and parities to the states involved in transitions.

To be really powerful as a tool for studying the low-energy state of a compound nucleus through observation of internally converted beta rays, it is highly desirable to eliminate some of the complexity that is present when all of the beta rays are detected. One technique (which has not yet been tried) of obtaining this greater simplicity is to detect only those beta rays which are in coincidence with a high-energy gamma ray. In this way, only transitions between low-lying states are permitted to be observed. In CP-5 this technique would be limited to materials having a thermal capture cross section greater than about 200 barns, so that very few nuclides could be studied. With a neutron source strength above  $10^{15}$  n/(cm<sup>2</sup>)(sec), however, a large fraction of the stable nuclides could be studied. Thus a new and powerful tool would become available for determining the energies, spins and parities of the low-lying states in most of the stable nuclides.

### D. Neutron Diffraction

One of the most fruitful techniques in the field of neutron physics has been, and will continue to be, the use of thermal neutron diffraction to investigate the structure and properties of solids, liquids and gases. However, at all stages in the development of neutron diffraction techniques, the experimenter has frequently been confronted with the necessity to accept incomplete or uncertain results owing to insufficient intensity. This compromise of resolution often seriously limits the potential utility of the method or requires the experimenter to adopt awkward procedures that tie up equipment and use human effort extravagantly.

Progress in neutron diffraction techniques is dependent upon (1) the resolution with which diffraction data can be obtained; (2) the intensity of the neutron beam; and (3) the size of the sample available. For the past 45 years the use of X-ray diffraction techniques to determine atomic structure has established the limits of resolution with which the diffraction data need to be obtained. The use of neutron diffraction techniques for similar studies would require comparable resolution. To obtain such a resolution the necessary thermal flux of a neutron source may be calculated as follows:

Assume that:<sup>16</sup>

Sample height	= 1 mm
Sample diameter	= 0.3 mm
Horizontal collimation (fractional spread in wave length, or resolution)	= 10 min or 0.003 radian
Vertical collimation	= 0.01 radian
Efficiency of monochromator	= 0.2
Reflectivity of sample	= 0.02

For a resolution of 10 min, which is readily attainable in X-ray diffraction work, a source flux of  $10^{14}$  n/(cm<sup>2</sup>)(sec) would give a reflected beam of 10 n/sec intensity; and for statistical accuracy of 1% it would take 15 min of recording for each point on a curve. For a satisfactory neutron diffraction pattern, the present scanning speed is 0.1° per counting period. To scan the desired span of  $2\theta$  angle, 100 to 135°, it would take from 250 to 337.5 hr for a single neutron diffraction pattern. If the source flux were increased to  $10^{15}$  n/(cm<sup>2</sup>)(sec), assuming the rest of the factors remain constant, it would still take 25 to 34 hr to obtain a single neutron diffraction pattern. This is by no means a short time for a single pattern, but it does make possible neutron diffraction data of comparable resolution to that obtainable by X rays. It is apparent, therefore, that until a high neutron flux source is available, diffraction data cannot be obtained with adequate resolution.

The list of neutron diffraction experiments for which a high-flux research reactor is necessary is long. A few of the areas are reviewed below and examples cited in terms of problems established as feasible at a flux level of  $10^{15}$  n/(cm<sup>2</sup>)(sec).

1. Coherent scattering amplitudes and cross sections for a number of nuclei have been determined experimentally, but there remain many more isotopes for which neither the intensity of the neutron beam nor the size of the sample is sufficient to give neutron diffraction patterns with adequate resolution.

2. The location of light atoms among heavy ones in crystals continues to be a fruitful study (supplementing X-ray diffraction studies) and is an area accessible almost exclusively to neutron diffraction. In particular, the role played by hydrogen atoms in crystals is the subject of work that is likely to be productive for a long time to come.

---

<sup>16</sup>Values for illustration from G. R. Ringo, "Neutron Diffraction and Interference," Handbuch der Physik, (Berlin: Springer Verlag, 1957), Vol. 32, pp 594-595.



3. Second in general interest only to the structure of a solid is probably the vibrational spectrum or variation of sound velocity with wavelength in the solid. From this spectrum the nature of the potential between the atoms in the solid and most thermal and mechanical properties of the solid can be determined. A measurement of the spectrum of monochromatic neutrons scattered by the solid is a uniquely powerful way of observing these properties, but it is only of marginal use with existing reactors. Such studies would be much more useful owing to greater resolution and speed with the proposed reactor.

4. The fact that neutrons have magnetic moments makes neutron diffraction an indispensable technique in the study of the theories of magnetism and magnetic materials. The so-called magnetic structure of crystals can be determined directly, and the crystals classified accordingly as ferromagnetic, antiferromagnetic or ferrimagnetic. It is possible to determine the magnitude and direction of atomic magnetic moments in crystals, and to observe effects due to changes in these atomic moments under different conditions. In this connection, neutrons which have been polarized with the aid of a magnetic field can be used in the study of magnetic properties of materials but here the need for increased neutron intensity is especially great. Thus far, this area of investigation has only begun and its future appears very promising.

5. Early work in the field of neutron diffraction by liquids shows promise of surpassing the utility of X-ray diffraction in many cases. Atomic distribution curves for elements in the liquid state can be computed from this work to give results that would provide information leading to a more complete understanding of the liquid state. With mixtures of liquids and with compounds, similar problems can be solved through the application of neutron diffraction techniques. However, neutron beam intensities now available impose limitations that restrict both the quantity and quality of the results obtainable.

6. In a study of neutron energy changes upon scattering by liquids, a new method has been found whereby self-diffusion coefficients can be obtained from the analysis of the experimentally observable energy distribution of the scattered neutrons. This promising new procedure resolves finer detail in the structure of matter, but can only be done with the prospect of significant results if higher neutron intensities are available.

## E. Studies of Fundamental Particles

### 1. Neutron

The neutron is among the most interesting of elementary particles and studies of its properties furnish critical tests of fundamental theory on several points. There is every prospect that there will be continuing interest in improved measurements of such properties as neutron lifetime, electron-neutron interaction, neutron-proton interaction

(at low energies), and angular correlations of neutron decay products. All of these will be advanced considerably by the availability of fluxes above  $10^{15}$  n/(cm<sup>2</sup>)(sec). In addition, there is a possibility, admittedly not large, of studying the neutron-neutron interaction through observation of dineutrons. The possibility of observing such an entity would rise as the square of the available flux; hence high flux would be crucial in such an observation.

## 2. Positron

The positron is another particle of great interest, in part because it is an antiparticle to the electron. A number of studies of this particle, notably of its behavior under gravity, depend on the availability of very intense sources of such particles. A high-flux reactor would be necessary to produce such sources.

## F. Studies of Nuclei

### 1. Microscopic Properties

Certain properties of nuclei can be measured only with microscopic ( $\leq 1$   $\mu$ g) amounts of material. Among these properties are optical spectra (which in turn give nuclear sizes and shapes) and nuclear magnetic resonances (which give very accurate values of the nuclear magnetic moments). The study of short-lived or otherwise hard-to-produce isotopes by these methods requires a high-flux reactor. The higher the flux the more isotopes that can be studied. With a flux of about  $10^{15}$  n/(cm<sup>2</sup>)(sec) available, such studies might be extended to include at least 50 more isotopes.

### 2. General Properties of Nuclei

At present, reactors are used in measurements of energy levels, lifetimes, decay schemes, spins, parities and magnetic moments of unstable nuclei. Without going into details for each of these measurements, it is a safe assertion that the conclusions to be drawn from such measurements can all be improved enormously if more isotopes can be studied with the greater accuracy that would result from a higher flux. While this may seem routine in a sense, it is the kind of routine which has on occasion produced major developments. Knowing a given property for a large number of nuclei or nuclear levels may allow correlations with other properties, or systematic changes with atomic number may show up in a way suggesting a significant pattern.

## G. Miscellaneous

### 1. Delayed-neutron Emitters

Delayed-neutron emitters have been determined by a technique of briefly irradiating U<sup>235</sup> solutions and extracting halogen fission

products by fast-flow methods. In this manner separations have been made in 1 sec and delayed-neutron precursors identified with lifetimes of 1.5 sec and longer. This type of study is reaching its limits for CP-5 and requires higher flux in order to measure precursors with shorter lifetimes. In addition, this technique will, with high flux available, have wider applicability and permit a variety of studies on short-lifetime nuclides formed by  $(n,\gamma)$  and  $(n,f)$  reactions.

## 2. Nuclear Interaction Forces

Recent physics work has had among its aims the study of both weak and strong nuclear interaction forces. The weak nuclear interactions, in particular beta decay, have been studied for many years by means of reactor-produced beta activities and neutron beta decay. The study of the symmetry properties of the beta decay of polarized neutrons has produced much definitive knowledge concerning the beta-decay interaction. These measurements are limited in accuracy due to available neutron flux. As more accurate experiments of this type are needed to further define the correct theory of beta decay, higher-flux reactors are needed to provide neutron beams of sufficient intensity.

An extension of these experiments lies in the production of polarized nuclei by the absorption of polarized neutrons. This new technique requires high-flux neutron beams and offers the possibility of many new studies utilizing polarized nuclei.

The study of reactions of antineutrinos, which has been very difficult with present reactors, will be made easier with a high-flux reactor.

The problem of understanding the strong nuclear interactions is being attacked by means of high-energy particle accelerators. It is, however, quite possible that experiments involving reactor neutrons may contribute equally well to this understanding. The absence of Coulomb effects in neutron absorption and the availability of high fluxes which make more sensitive measurements possible are strong advantages.

## 3. Quantum Electrodynamics

High-flux gamma beams will facilitate photon-photon scattering measurements. This is a fundamental experiment of quantum electrodynamics.

# IV. METALLURGY

Studies of the separate phenomena which collectively result in radiation damage, already discussed in the Chemistry program, are of prime importance also to the metallurgists. Although the fuel element

and reactor materials irradiation programs do not require the highest possible flux, nevertheless somewhat higher fluxes than are now available will be beneficial in two ways: (1) permit the study of the rate at which damage occurs, and (2) shorten the length of test periods. These irradiation programs are worthy of description, since they will constitute a rather large use of the proposed high-flux reactor. This is true for a number of reasons. First, in general these programs are not incompatible with the other proposed research uses of the reactor. Second, the design of the reactor is such that appreciable volumes of experimental facilities in the form of vertical thimbles will be available in regions of flux varying from  $10^{13}$  to  $5 \times 10^{14}$  n/(cm<sup>2</sup>)(sec). Third, the reactor is expected to operate continuously from the beginning to the end of the fuel cycle, a point of considerable importance in kinetic studies of radiation effects.

The emphasis on the development of high-temperature, high-burnup fuels for power reactors has greatly increased the desirability of radiation experiments conducted at controlled, elevated temperatures. A number of important in-pile experiments on coupons of typical fuels and on samples of control and structural materials could be performed in the proposed reactor. For example, it would be possible to measure continuously during irradiation volume changes resulting from swelling, dimensional changes resulting from anisotropy, changes in thermal conductivity, the release of fission gases (in the case of fuel elements), etc. At present these changes must be determined on the basis of measurements made before and after irradiation in the MTR. This leads only to a knowledge of what happened. For an understanding of how it happened it is necessary to know the effect of rate and the mechanism of the radiation damage.

Shortening the length of test periods is a matter of some importance. The feasibility of many of the investigations implied above would depend upon the ability to carry them out over a period of weeks or months rather than years as would now be necessary. Further, with power reactors now having flux levels over  $10^{14}$  n/(cm<sup>2</sup>)(sec) some structural materials will receive an nvt of  $10^{23}$  n/cm<sup>2</sup> over a reactor "lifetime" of some 20 to 30 years. It is important that information concerning the effects of such high total accumulated radiation be available for the design of future reactors. Such exposures could be accumulated in a reasonably short time in the proposed reactor.

## V. CONCLUSION

The basic research program envisioned in the foregoing presentation is exceedingly important for many reasons. It is one way of providing a more fundamental understanding of nature which may in the future, as in the past, lead to major advances. It is also a way of assuring the uninterrupted flow of basic information which must be available to solve problems which will surely arise in the practical programs.

The distinction between basic and applied research lies primarily in the motivation behind the research and the criteria used to determine the direction of the research. In actual practice, basic research often turns out to be applied research with a time delay. The advanced basic research program of today forms the basis of the applied development program of tomorrow.

In the final analysis the value of an advanced high-flux reactor in a basic research program cannot be spelled out in great detail because the most important results cannot be predicted in advance. On the basis of past experience it is frequently the unexpected, unforeseen result which proves to be the most important.

On the other hand, it is not difficult to recognize when basic research is hampered by lack of sufficiently advanced tools. This would appear to be the situation today in the fields of basic research utilizing reactor radiations. It seems certain that the next major advances in these fields will be dependent on the availability of neutron fluxes in excess of  $10^{15} \text{ n}/(\text{cm}^2)(\text{sec})$ .

# APPENDIX B

## SURVEY OF D<sub>2</sub>O-MODERATED ANNULAR CORES WITH H<sub>2</sub>O INNER REFLECTORS

### I. CORE DESCRIPTION

The annular core is comprised of an inner H<sub>2</sub>O reflector, a D<sub>2</sub>O-cooled fuel annulus (60 cm high), and an outer D<sub>2</sub>O reflector (~150 cm thick). No structural material is contained in the inner or the outer reflectors. The fuel region contains equal parts of Al and D<sub>2</sub>O at 300°K, with sufficient U<sup>235</sup> to achieve criticality. No allowances are made for beam holes, samples, burnup, fission product poisons, etc.

### II. CROSS SECTIONS

The cross sections were computed by the method of Deutsch and reduced to a two-group description. The two-group age in the D<sub>2</sub>O reflector was assumed to be  $\tau = 200 \text{ cm}^2$ . The axial reflector savings at the top and bottom of the core were assumed to be 7.5 cm, based on previous experience in LITR, MTR, BORAX, and ARGONAUT.

### III. COMPUTATIONAL METHOD AND RESULTS

The UNIVAC Code, RE-6, was used to calculate the cold clean critical mass and the flux distribution at critical. The results are summarized in Table XXII.

Table XXII

OPERATING CHARACTERISTICS OF H<sub>2</sub>O-D<sub>2</sub>O-REFLECTED  
D<sub>2</sub>O-COOLED AND MODERATED ANNULAR CORES

Core Type	Inner Reflector Radius, cm	Fuel Annulus Thickness, cm	Core Volume, liter	Critical Mass, kg U <sup>235</sup>	Peak Flux/Mw $\times 10^{-14} \text{ n}/(\text{cm}^2)(\text{sec})$	Maximum Permissible Flux, $\text{n}/(\text{cm}^2)(\text{sec})$	Total Power, Mw
1	4	4	9.048	2.368	1.04	$5.65 \times 10^{14}$	5.43
2	4	6	15.833	1.694	0.924	$8.78 \times 10^{14}$	9.5
3	6	4	12.064	2.545	1.02	$7.38 \times 10^{14}$	7.24
4	6	6	20.358	2.028	0.878	$1.07 \times 10^{15}$	12.2
5	8	4	15.08	3.136	0.798	$7.22 \times 10^{14}$	9.05
6	8	6	24.88	2.525	0.67	$1.00 \times 10^{15}$	14.9
7	4	10	33.93	1.584	0.689	$1.40 \times 10^{15}$	20.4

The maximum permissible thermal flux corresponds to a power density of 0.6 Mw/liter, which is the highest power extraction level consistent with the established design criteria for Mighty Mouse.

## APPENDIX C

SHIELDING AND IRRADIATION HEATING CALCULATIONSI. CRITERIA

The shielding design criteria for the experimental area outside the concrete were set as follows:

- (1) The total gamma energy flux should not exceed 10 Mev/(cm<sup>2</sup>)(sec).
- (2) The neutron flux, regardless of energy, should not exceed 1 n/(cm<sup>2</sup>)(sec).
- (3) The temperature differential across the concrete must not exceed 50° F.

Accordingly, the maximum allowable gamma flux at the inside surface of the concrete biological shield was approximated by assuming that all the gammas were at the 8-Mev energy level. By considering slab geometry and linear buildup, the gamma flux at the inside surface of ordinary and magnetite concrete was determined by the expression

$$\phi_{\gamma}(0) = \phi_{\gamma} e^{\mu t}, \quad (1)$$

where

$\phi_{\gamma}$  = maximum allowable gamma flux at outer surface of concrete

$\mu$  = absorption cross section of concrete.

= 0.058 cm<sup>-1</sup> for ordinary concrete ( $\rho = 2.39$  gm/cc).

= 0.102 cm<sup>-1</sup> for magnetite concrete ( $\rho = 3.62$  gm/cc).

$t$  = concrete thickness.

= 274 cm.

Example:

For ordinary concrete

$$\begin{aligned} \phi_{\gamma}(0) &= \phi_{\gamma} e^{\mu t} \\ &= (10) \exp [(0.058)(274)] \\ &= 7.96 \times 10^7 \text{ Mev}/(\text{cm}^2)(\text{sec}). \end{aligned}$$

The temperature differential across the concrete was calculated by assuming that (1) only the inside surface was cooled, and (2) the heat generation rate decreased exponentially with distance through the concrete slab:

$$\Delta T = q_0 / \Sigma^2 k$$

(2)

where

- $\Delta T$  = temperature difference = 50° F.
- $q_0$  = volumetric heating rate, Btu/(hr)(ft<sup>3</sup>)
- $\Sigma$  = slope of heating curve, ft<sup>-1</sup>
- $k$  = thermal conductivity = 0.5 Btu/(hr)(ft)(° F)

Example:

For ordinary concrete

$q_0 = (50)(1.768)^2(0.5)$

$= 78.15 \text{ Btu}/(\text{hr})(\text{ft}^3)$

$= 9.9 \times 10^{10} \text{ Mev}/(\text{cm}^2)(\text{sec}).$

Based on the foregoing calculations, Table XXIII shows the maximum gamma-ray flux that may impinge upon the inside surface of a 9 ft thick concrete shield without exceeding the specified design criteria.

Table XXIII

PERMISSIBLE GAMMA-RAY ENERGY FLUX

AT INSIDE OF CONCRETE BIOLOGICAL SHIELD

TO SATISFY DESIGN CRITERIA

Concrete	Mev/(cm <sup>2</sup> )(sec)	
	Dose	Temp. Diff.
Ordinary	7.96 x 10 <sup>7</sup>	9.9 x 10 <sup>10</sup>
Magnetite	1.37 x 10 <sup>13</sup>	2 x 10 <sup>11</sup>

Magnetite concrete appears more than adequate; however, the margin available will be less because of the experimental holes and streaming.



II. FAST NEUTRON FLUX

The fast flux was approximated by removal theory. The core was considered to be a solid sphere with a diameter equal to the diameter of the annular core (90 cm). The value of the fast flux,

$$\phi_f = 5.4 \times 10^{14} \text{ n}/(\text{cm}^2)(\text{sec}),$$

at the radial centerline of the core surface was taken from Fig. 44.

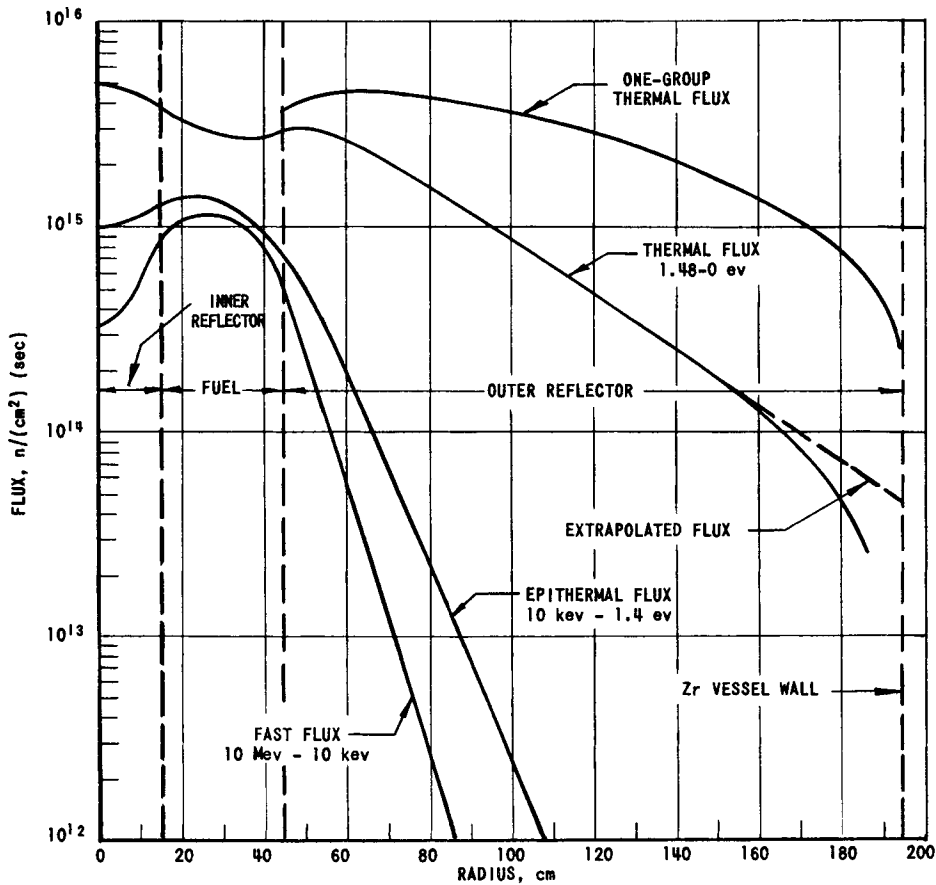


FIG. 44  
NEUTRON FLUXES USED IN SHIELDING CALCULATIONS

The equation used to express the fast flux as a function of distance is

$$\phi_f \left( \sum_{i=1}^i t_i \right) = \phi_f (0) (r/r_0) E_1 \left( \sum_{i=1}^i \Sigma_{r_i} t_i \right) , \tag{3}$$

where

$\phi_f$  = fast neutron flux,  $n/(cm^2)(sec)$

$t_i$  = thickness of  $i$ ' th region, cm

$r$  = radius of sphere, cm

$$r_0 = r + \sum_{i=1}^i t_i$$

$\Sigma_{r_i}$  = effective fast neutron removal cross section of the  $i$ ' th region,  $cm^{-1}$

$E_1$  = function as defined in TID-7004.<sup>17</sup>

The effective fast neutron removal cross sections used are given in Table XXIV.

Table XXIV

EFFECTIVE FAST NEUTRON REMOVAL CROSS SECTIONS

<u>Region</u>	<u><math>\Sigma_r, cm^{-1}</math></u>
D <sub>2</sub> O	0.0993
Steel	0.168
Zirconium	0.1288
Ordinary concrete	0.086
Magnetite concrete	0.103

Example:

At the D<sub>2</sub>O and pressure vessel interface,

$r = 45$  cm,

$r_0 = 198$  cm,

$t = 153$  cm;

---

<sup>17</sup>Theodore Rockwell III (ed.) "Reactor Shielding Design Manual," TID-7004 (March 1956), Chapt. 9.

thus,

$$\begin{aligned}\phi_f(153) &= 5.4 \times 10^{14} (45/198) E_1 (0.0993 \times 153) \\ &= 1.9 \times 10^6 \text{ n}/(\text{cm}^2)(\text{sec}).\end{aligned}$$

III. CORE GAMMAS

The core gammas were calculated on the following assumptions:

- (1) The gammas were grouped into 1-, 2.5-, and 6-Mev energy groups.
- (2) Prompt fission gammas,  $\gamma_p$ :  
3.2 photon/fission at 1 Mev/photon  
1.4 photon/fission at 2.5 Mev/photon  
0.2 photon/fission at 6 Mev/photon
- (3) Decay gammas from fission products,  $\gamma_D$ :  
6.2 photon/fission at 1 Mev/photon  
1.0 photon/fission at 2.5 Mev/photon
- (4) Secondary gammas from neutron capture in core,  $N_\gamma$ :  
0.12 photon/capture at 1 Mev/photon  
0.60 photon/capture at 2.5 Mev/photon  
1.46 photon/capture at 6 Mev/photon
- (5) The source is uniformly distributed in the core.
- (6) The metal to water ratio is 1:4.
- (7) The thermal flux in the core structural members is  $10^{15} \text{ n}/(\text{cm}^2)(\text{sec})$ .

Table XXV lists the gamma absorption cross sections used to determine the gamma flux at various locations in the core.

Table XXV

GAMMA-RAY CONSTANTS

Linear Absorption Cross Section ( $\Sigma$ ), $\text{cm}^{-1}$						
E, Mev	D <sub>2</sub> O	Mg	Zr	Core	Ordinary Concrete	Magnetite Concrete
1.0	0.077	0.11	0.374	0.084	0.156	0.226
2.5	0.047	0.069	0.244	0.052	0.088	0.142
6.0	0.030	0.048	0.219	0.034	0.061	0.104

The core volumetric source strength,  $Q_3$ , in Mev/(cc)(sec), of each energy group was estimated for a power level of 250 Mw (500 watt/cc) and increased by a factor of 1.5 to account for the spatial variation of the power.

$$Q_3 = 1.5 \left\{ [3.1 \times 10^{10} \text{ fission}/(\text{watt})(\text{sec})] [(500 \text{ watt/cc}) (\gamma_p + \gamma_D)] + \phi_{th} \Sigma_a N_\gamma \right\} E \quad (4)$$

$$Q_3 = 1.5 [1.55 \times 10^{13} (\gamma_p + \gamma_D) + (2.5 \times 10^{12}) N_\gamma] E. \quad (4a)$$

#### A. Gamma Flux in Core

The gamma flux in the core was estimated by treating the core as a solid cylinder, applying the upper limit equation (for point  $P_3$ ) of TID-7004,<sup>18</sup> and including the buildup factors for water described therein.<sup>19</sup> The results are plotted in Fig. 45.

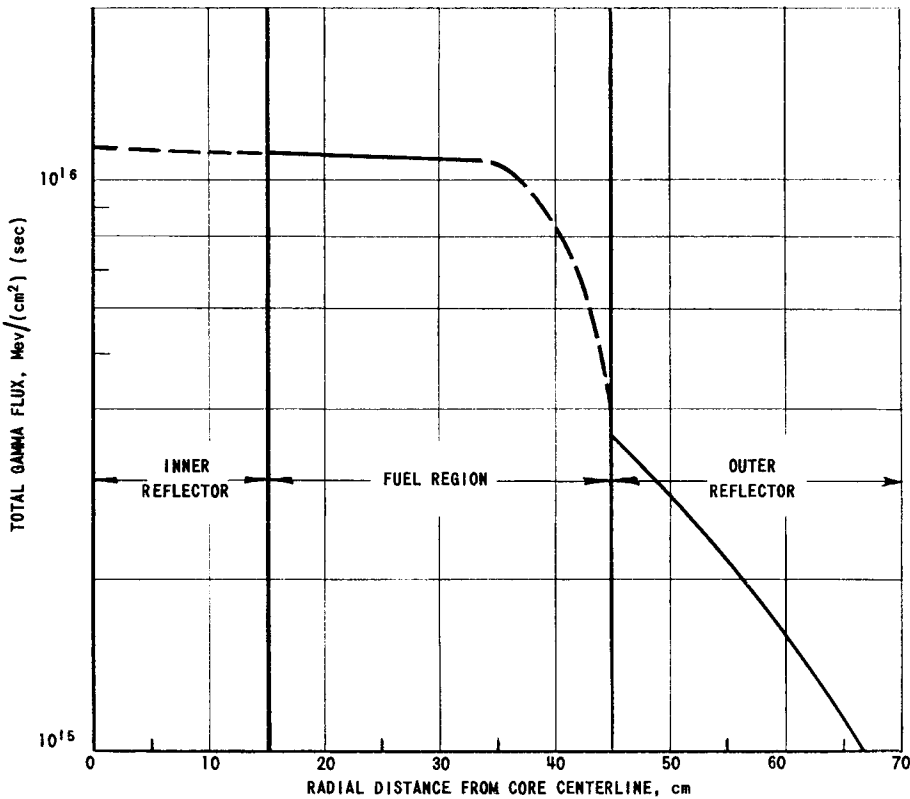


FIG. 45  
ESTIMATED TOTAL CORE GAMMA FLUX

<sup>18</sup> Theodore Rockwell III, *ibid*, p. 365.

<sup>19</sup> *Ibid*, Part IV, Section IV-2, p. 413.

### B. Gamma Flux outside Core

The core gamma flux in the shield region exterior to the core was calculated by the following relation that includes linear buildup:

$$\phi_{\gamma} \left( \sum_{i=1}^i t_i \right) = \frac{Q_3}{2\mu_s} \frac{r}{r_0} \exp \left( - \sum_{i=1}^i \mu_i t_i \right) , \quad (5)$$

where the terms  $\mu_s$  and  $\mu_i$  are the gamma linear absorption coefficients for the core and the i'th shield, respectively.

#### Example:

Determine the 6-Mev core gamma flux at the D<sub>2</sub>O and zirconium vessel interface.

$$\gamma_D = 0$$

$$\gamma_p = 0.2 \text{ photon/fission}$$

$$N_{\gamma} = 1.46 \text{ photons/capture}$$

$$E = 6 \text{ Mev/photon}$$

$$\phi_{th} = 10^{15} \text{ n}/(\text{cm}^2)(\text{sec})$$

$$\Sigma_a = 2.54 \times 10^{-3} \text{ cm}^{-1}$$

$$Q_3 = [(1.55)(10^{13})(0.2) + (2.54)(10^{12})(1.46)]$$

$$Q_3 = 6.13 \times 10^{13} \text{ Mev}/(\text{cm}^3)(\text{sec}).$$

Substituting the appropriate constants in Eq. (5),

$$\begin{aligned} \phi_{\gamma}(153) &= \left[ \frac{6.13 \times 10^{13}}{2(0.034)} \right] \left( \frac{45}{198} \right) e^{-0.03(153)} \\ &= 2.08 \times 10^{12} \text{ Mev}/(\text{cm}^2)(\text{sec}). \end{aligned}$$

The results of the calculations are listed in Table XXVI. The total gamma flux is plotted in Figs. 46 and 47.

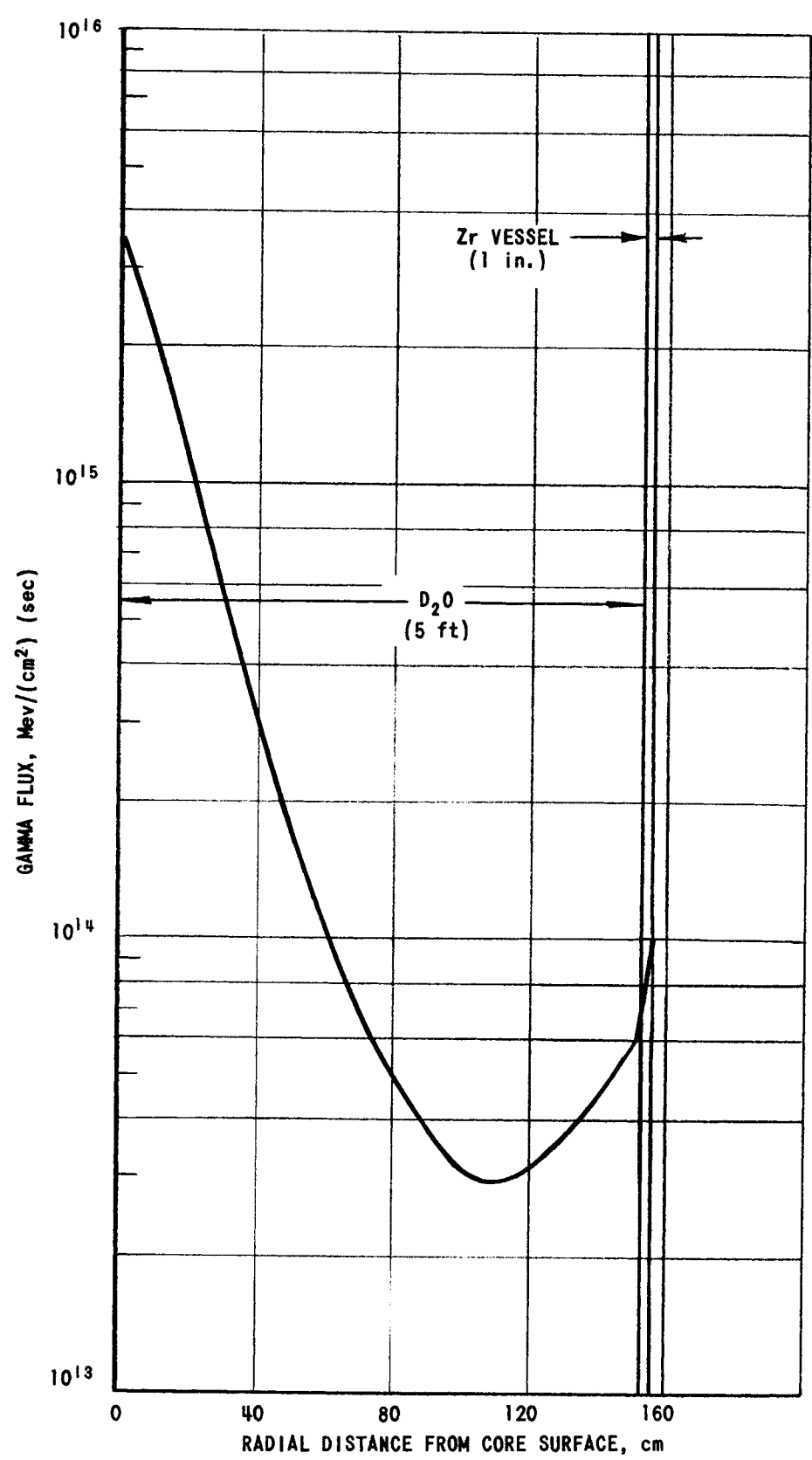
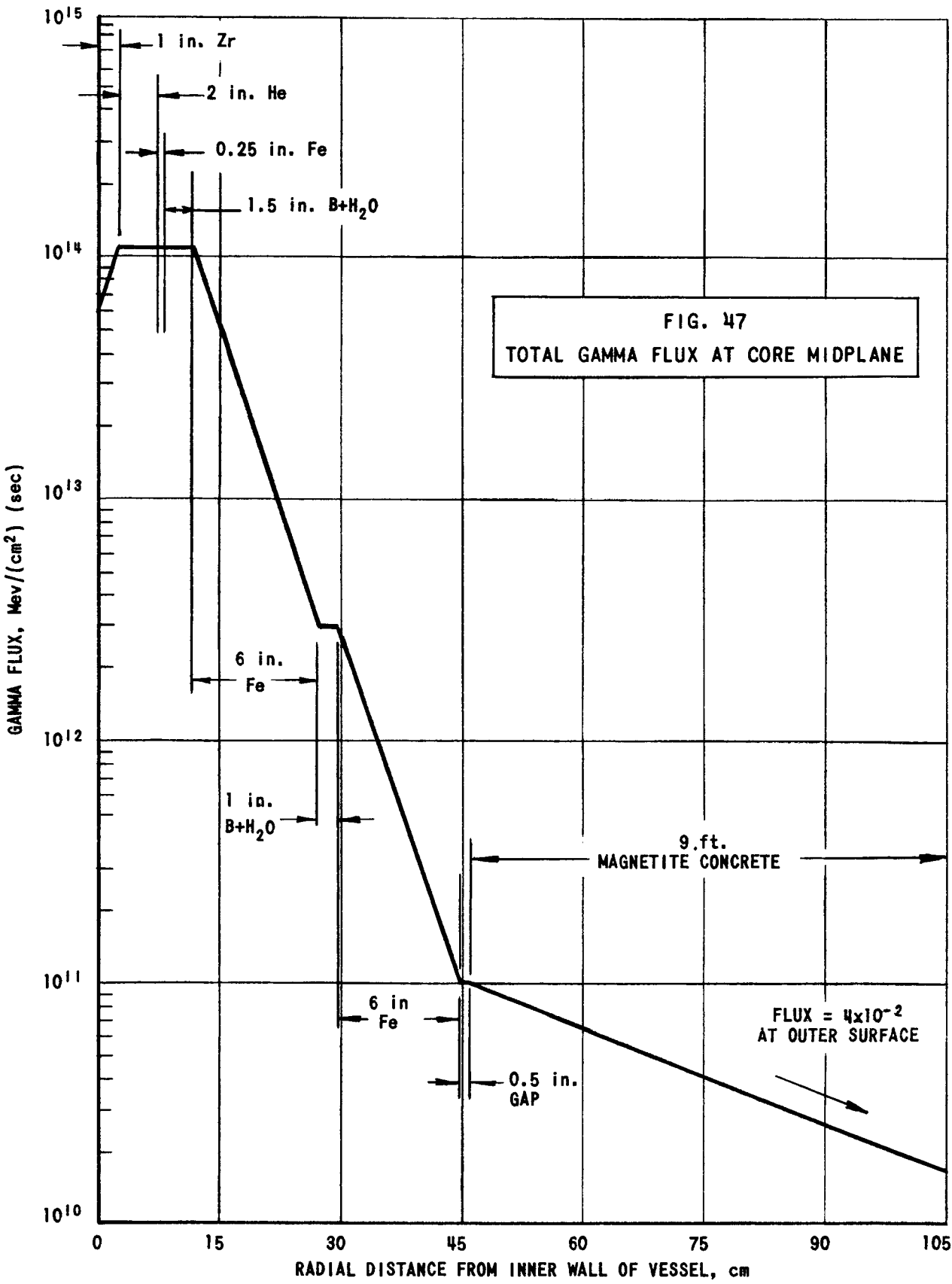


FIG. 46  
TOTAL GAMMA FLUX AT CORE MIDPLANE FROM CORE  
SURFACE TO OUTER SURFACE OF PRESSURE VESSEL



#### IV. THERMAL NEUTRON FLUX AND CAPTURE GAMMA RAYS

The thermal neutron flux in the region exterior to the core was calculated by the expression

$$\begin{aligned}\phi_{th}(x) = & A_i \exp(\kappa_i x) + B_i \exp(-\kappa_i x) \\ & + C_i \exp(-\Sigma_i x) \quad ,\end{aligned}\tag{6}$$

where

$A_i, B_i$  = coefficients determined by the boundary conditions for the  $i$ 'th region

$$C_i = \Sigma_i \phi_{f_i}(0) \exp(-\Sigma_i x) / D_i (\kappa_i^2 - \Sigma_i^2)$$

$$\Sigma_i = \text{Slope of fast flux in the } i\text{'th region, cm}^{-1}.$$

$$\kappa_i^2 = \Sigma_{a_i} / D_i, \text{ cm}^{-2}$$

$$\Sigma_{a_i} = \text{thermal absorption cross section, cm}^{-1}$$

$$x = \text{running thickness variable for region } i, \text{ cm}$$

$$\phi_{f_i} = \text{value of fast flux at beginning of region } i, \text{ n}/(\text{cm}^2)(\text{sec})$$

The boundary conditions for Eq. (6) are:

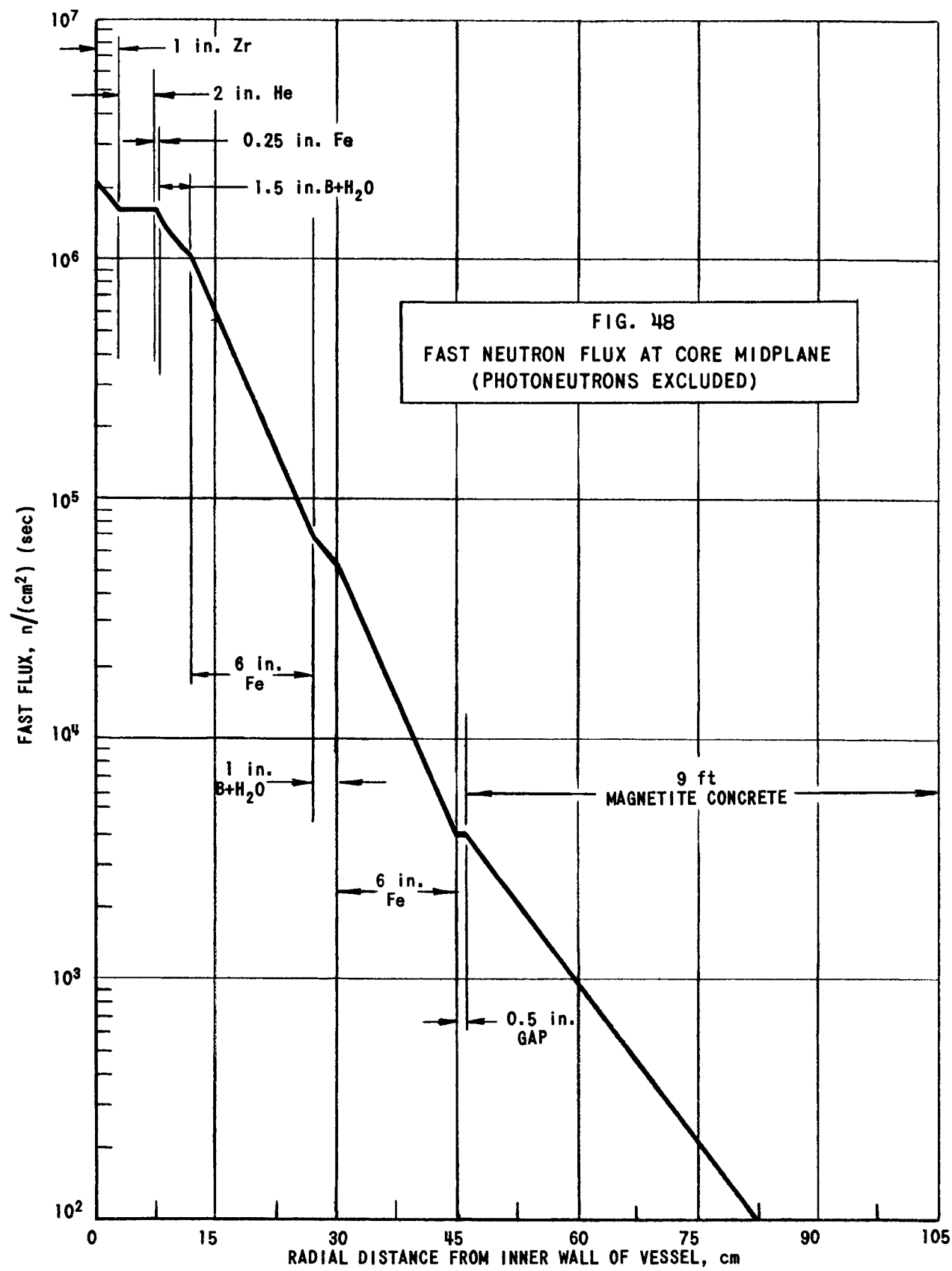
- (1) Two adjacent regions are considered at a time; the thickness of the second region is assumed to be infinite.
- (2) The thermal neutron fluxes and currents are equal and continuous across region interfaces.
- (3)  $\phi_{th}(0)$  and  $\phi_f(0)$  for the  $D_2O$  region are  $3.6 \times 10^{15}$  and  $5.4 \times 10^{14} \text{ n}/(\text{cm}^2)(\text{sec})$ .
- (4)  $\phi_{th}(153)$  is  $1 \times 10^{14} \text{ n}/(\text{cm}^2)(\text{sec})$
- (5)  $\phi_f(0)$  for the other regions was taken from Fig. 48.

Where the thermal neutron flux could best be represented by an exponential, the appropriate equations from ANL-6000<sup>20</sup> were used to calculate the capture gamma flux at either surface of the region. Where the

---

<sup>20</sup> M. Grotenhuis, "Lecture Notes on Reactor Shielding," ANL-6000 (March 1959), p. 73.





thermal flux could be safely approximated by a constant value across a region, the capture gamma flux was calculated by

$$\phi_{\gamma}(x) = (BQ_3/2\mu_s) \left\{ 2 - E_2(\mu_s x) - E_2 \left[ \mu_s (h-x) \right] \right\} \quad , \quad (7)$$

where

B = buildup factor

$Q_3$  = volumetric source strength, Mev/(cm<sup>3</sup>)(sec)

$\mu_s$  = gamma linear absorption coefficient of source, cm<sup>-1</sup>

x = running thickness variable, cm

h = region thickness, cm

$E_2$  = function as defined in TID-7004.<sup>17</sup>

#### Example:

Estimate the capture gamma flux in the pressure vessel.

For 4-Mev gammas:

$$\mu = 0.218 \text{ cm}^{-1}$$

$$t = 2.54 \text{ cm}$$

$$B = 1.5$$

$$\phi_{th} = 10^{14} \text{ n}/(\text{cm}^2)(\text{sec})$$

$$N_{\gamma} = 1.13 \text{ photon/neutron capture}$$

$$E = 4 \text{ Mev/photon}$$

$$\Sigma_a = 0.00765 \text{ cm}^{-1}$$

$$D = 0$$

$$h = 2.54 \text{ cm}$$

$$\begin{aligned} Q_3 &= \phi_{th} \Sigma_a N_{\gamma} E \\ &= (10^{14})(0.00765)(1.13)(4) \\ &= 3.46 \times 10^{12} \text{ Mev}/(\text{cm}^3)(\text{sec}). \end{aligned}$$

By Eq. (7):

$$\begin{aligned} \phi_{\gamma} &= \frac{1.5 (3.46 \times 10^{12})}{2(0.218)} \left\{ 2 - E_2(0) - E_2 \left[ (0.218)(2.54) \right] \right\} \\ &= 8.4 \times 10^{12} \text{ Mev}/(\text{cm}^2)(\text{sec}). \end{aligned}$$

The thermal neutron and capture gamma-ray constants are listed in Table XXVI.

Table XXVI  
CONSTANTS FOR THERMAL FLUX AND CAPTURE GAMMA CALCULATIONS

Region	$\Sigma_i, \text{ cm}^{-1}$	$\kappa, \text{ cm}^{-1}$	$D_s, \text{ cm}$	$\Sigma_a, \text{ cm}^{-1}$	Gamma Linear Absorption Coefficient, $\text{ cm}^{-1}$				Photon/Neutron Capture			
					2 Mev	4 Mev	6 Mev	8 Mev	2 Mev	4 Mev	6 Mev	8 Mev
Zirconium	0.1414	0.088	0.9871	0.00765	0.257	0.218	0.218	0.218	--	1.13	0.35	0.04
Steel	0.189	0.775	0.364	0.219	0.31	0.248	0.228	0.222	0.1	0.24	0.22	0.5
Borated Solution	--	5.94	0.0841	--	--	--	--	--	--	--	--	--
Ordinary Concrete, 2.39 gm/cc	0.0948	0.126	0.564	0.00892	0.097	0.076	0.064	0.058	0.69	0.51	0.45	0.077
Magnetite Concrete, 3.62 gm/cc	0.112	0.436	0.331	0.073	0.202	0.133	0.112	0.102	0.38	0.25	0.37	0.35

V. NEUTRON CURRENT

The neutron current entering the borated solution was estimated at  $5 \times 10^{13} \text{ n}/(\text{cm}^2)(\text{sec})$ , based on the extrapolated neutron flux at a point two mean free paths from the zirconium in the  $\text{D}_2\text{O}$ , (see Fig. 44). The flux was assumed to go to zero at a distance  $0.712_{\text{tr}}$  beyond the vessel boundary. The slope, or  $d\phi/dx$ , could then be calculated. The neutron current is given by

$$J = -D \frac{d\phi}{dx} \quad .$$

Example:

Mean free path  $\quad \quad \quad = \lambda_{\text{tr}} = 2.25 \text{ cm}$   
Diffusion coefficient  $= D \quad = 0.752 \text{ cm}$   
Neutron flux  $\quad \quad \quad = \phi_{\text{th}} = 5 \times 10^{13} \text{ n}/(\text{cm}^2)(\text{sec})$   
$$\frac{\Delta\phi}{\Delta x} = - \frac{\Delta\phi}{2\lambda_{\text{tr}} + 0.71\lambda_{\text{tr}}} = \frac{\Delta\phi}{6.098}$$
$$J = (0.752) (5 \times 10^{13})/(6.098)$$
$$= 6.17 \times 10^{12} \text{ n}/(\text{cm}^2)(\text{sec}).$$

VI. HEAT GENERATION

A. Fast Flux

The fast neutron heating was estimated by assuming that each neutron "removed" liberated 1 Mev in the form of heat:

$$q = \phi_f \Sigma_r \frac{1 \text{ Mev}}{\text{removal}} \left[ 1.6 \times 10^{13} \frac{(\text{watt})(\text{sec})}{\text{Mev}} \right] \quad . \tag{8}$$

Example:

The fast flux at the edge of the core is  $5.4 \times 10^{14} \text{ n}/(\text{cm}^2)(\text{sec})$ .  
The heat generation in the zirconium at this point is

$$\begin{aligned} q &= (5.4 \times 10^{14})(0.1288)(1)(1.6 \times 10^{13} \text{ watt}/\text{cm}^3) \\ &= 11.1 \text{ watt}/\text{cm}^3 \end{aligned}$$

or

$$q = 1.73 \text{ watt}/\text{gm Zr}.$$

B. Gamma Flux

The gamma heat generation is given by

$$q = \phi \mu_e (1.6 \times 10^{-13} \text{ watt}/\text{cm}^3) \quad . \tag{9}$$

The constants used are listed in Table XXVII.

Table XXVII

ENERGY ABSORPTION COEFFICIENTS ( $\mu_e$ )

Material	Energy, Mev						$\bar{\mu}_e, \text{ cm}^{-1}$
	1	2	2.5	4	6	8	
D <sub>2</sub> O	0.034	0.029	0.027	0.024	0.021	0.019	0.024
Zirconium	0.17	0.14	0.14	0.16	0.17	0.19	0.167
Steel	0.20	0.18	0.18	0.17	0.18	0.19	0.181
Concrete							
Ordinary	0.066	0.057	0.056	0.052	0.052	0.047	0.051
Magnetite	0.096	0.089	0.087	0.081	0.074	0.074	0.078

Example:

The gamma flux in the vessel from all sources is given in Fig. 46 and Table XXVIII. Using the weighted average energy absorption coefficient for zirconium (Table XXVII),

$$\bar{\mu}_e = 0.167 \text{ cm}^{-1}$$

and the total gamma flux (Table XXVIII),

$$\phi = 6.6 \times 10^{13} \text{ Mev}/(\text{cm}^2)(\text{sec}),$$

the volumetric heat generation rate for the inside surface of the pressure vessel by Eq. (9) is

$$\begin{aligned} q''' &= (6.6 \times 10^{13})(0.176)(1.6 \times 10^{-13}) \\ &= 1.76 \text{ watt}/\text{cm}^3, \text{ or } 0.274 \text{ watt}/\text{gm}. \end{aligned}$$

Table XXVIII  
SUMMARY OF GAMMA-FLUX CALCULATIONS

Distance From Core Face, cm	Core Gamma Flux, Mev/(cm <sup>2</sup> )(sec)				Capture Gamma Flux from Pressure Vessel, Mev/(cm <sup>2</sup> )(sec)				Capture Gamma Flux from Thermal Shield, Mev/(cm <sup>2</sup> )(sec)				Total, Mev/(cm <sup>2</sup> )(sec)
	1 Mev	2.5 Mev	6 Mev	Sub-Total	4 Mev	6 Mev	8 Mev	Sub-Total	2 Mev	4 Mev	6 Mev	8 Mev	
0	1.31x10 <sup>15</sup>	1.41x10 <sup>15</sup>	8.90x10 <sup>14</sup>	3.61x10 <sup>15</sup>	--	--	--	--	--	--	--	--	3.61x10 <sup>15</sup>
50	1.32x10 <sup>13</sup>	6.42x10 <sup>13</sup>	9.40x10 <sup>13</sup>	1.71x10 <sup>14</sup>	1.99x10 <sup>11</sup>	1.75x10 <sup>11</sup>	3.95x10 <sup>10</sup>	4.14x10 <sup>11</sup>	1.82x10 <sup>9</sup>	1.40x10 <sup>11</sup>	4.42x10 <sup>11</sup>	2.05x10 <sup>9</sup>	5.68x10 <sup>11</sup>
100	1.84x10 <sup>11</sup>	3.98x10 <sup>12</sup>	1.38x10 <sup>13</sup>	1.70x10 <sup>13</sup>	1.30x10 <sup>12</sup>	8.23x10 <sup>11</sup>	1.48x10 <sup>11</sup>	2.27x10 <sup>12</sup>	6.78x10 <sup>10</sup>	3.94x10 <sup>11</sup>	2.06x10 <sup>12</sup>	7.71x10 <sup>12</sup>	1.02x10 <sup>13</sup>
125	2.34x10 <sup>10</sup>	1.04x10 <sup>12</sup>	5.56x10 <sup>12</sup>	6.62x10 <sup>12</sup>	3.28x10 <sup>12</sup>	1.77x10 <sup>12</sup>	2.87x10 <sup>11</sup>	5.34x10 <sup>12</sup>	2.27x10 <sup>11</sup>	2.31x10 <sup>12</sup>	4.40x10 <sup>12</sup>	1.49x10 <sup>13</sup>	2.18x10 <sup>13</sup>
153.1	2.31x10 <sup>9</sup>	2.43x10 <sup>11</sup>	2.08x10 <sup>12</sup>	2.26x10 <sup>12</sup>	9.4 x10 <sup>12</sup>	4.2 x10 <sup>12</sup>	6.00x10 <sup>11</sup>	1.42x10 <sup>13</sup>	1.25x10 <sup>12</sup>	6.60x10 <sup>12</sup>	1.05x10 <sup>13</sup>	3.12x10 <sup>13</sup>	4.96x10 <sup>13</sup>
155.64	8.69x10 <sup>8</sup>	1.27x10 <sup>11</sup>	1.14x10 <sup>12</sup>	1.27x10 <sup>12</sup>	9.2 x10 <sup>12</sup>	4.0 x10 <sup>12</sup>	6.00x10 <sup>11</sup>	1.38x10 <sup>13</sup>	2.40x10 <sup>12</sup>	1.26x10 <sup>13</sup>	1.82x10 <sup>13</sup>	5.40x10 <sup>13</sup>	8.72x10 <sup>13</sup>
160.72	8.47x10 <sup>8</sup>	1.20x10 <sup>11</sup>	1.11x10 <sup>12</sup>	1.23x10 <sup>12</sup>	9.2 x10 <sup>12</sup>	4.0 x10 <sup>12</sup>	6.00x10 <sup>11</sup>	1.38x10 <sup>13</sup>	2.40x10 <sup>12</sup>	1.26x10 <sup>13</sup>	1.82x10 <sup>13</sup>	5.40x10 <sup>13</sup>	8.72x10 <sup>13</sup>
161.36	8.45x10 <sup>8</sup>	1.19x10 <sup>11</sup>	1.10x10 <sup>12</sup>	1.22x10 <sup>12</sup>	9.2 x10 <sup>12</sup>	4.0 x10 <sup>12</sup>	6.00x10 <sup>11</sup>	1.38x10 <sup>13</sup>	2.40x10 <sup>12</sup>	1.26x10 <sup>13</sup>	1.82x10 <sup>13</sup>	5.40x10 <sup>13</sup>	8.72x10 <sup>13</sup>
165.16	8.31x10 <sup>8</sup>	1.17x10 <sup>11</sup>	1.09x10 <sup>12</sup>	1.21x10 <sup>12</sup>	9.2 x10 <sup>12</sup>	4.0 x10 <sup>12</sup>	6.00x10 <sup>11</sup>	1.38x10 <sup>13</sup>	2.40x10 <sup>12</sup>	1.26x10 <sup>13</sup>	1.82x10 <sup>13</sup>	5.40x10 <sup>13</sup>	8.72x10 <sup>13</sup>
180.41	5.87x10 <sup>5</sup>	1.09x10 <sup>9</sup>	3.23x10 <sup>10</sup>	3.34x10 <sup>10</sup>	2.12x10 <sup>11</sup>	1.25x10 <sup>11</sup>	2.04x10 <sup>10</sup>	3.57x10 <sup>11</sup>	2.16x10 <sup>10</sup>	2.91x10 <sup>11</sup>	5.97x10 <sup>11</sup>	1.84x10 <sup>12</sup>	3.14x10 <sup>12</sup>
182.95	5.80x10 <sup>5</sup>	1.08x10 <sup>9</sup>	3.20x10 <sup>10</sup>	3.31x10 <sup>10</sup>	2.12x10 <sup>11</sup>	1.25x10 <sup>11</sup>	2.04x10 <sup>10</sup>	3.57x10 <sup>11</sup>	2.16x10 <sup>10</sup>	2.91x10 <sup>11</sup>	5.97x10 <sup>11</sup>	1.84x10 <sup>12</sup>	3.14x10 <sup>12</sup>
198.18	4.21x10 <sup>2</sup>	1.60x10 <sup>7</sup>	9.68x10 <sup>8</sup>	9.84x10 <sup>8</sup>	4.81x10 <sup>9</sup>	4.00x10 <sup>9</sup>	6.98x10 <sup>8</sup>	9.51x10 <sup>9</sup>	1.45x10 <sup>8</sup>	6.70x10 <sup>9</sup>	1.96x10 <sup>10</sup>	6.35x10 <sup>10</sup>	1.00x10 <sup>11</sup>
199.45	4.18x10 <sup>2</sup>	1.59x10 <sup>7</sup>	9.62x10 <sup>8</sup>	9.78x10 <sup>8</sup>	4.81x10 <sup>9</sup>	4.00x10 <sup>9</sup>	6.98x10 <sup>8</sup>	9.51x10 <sup>9</sup>	1.95x10 <sup>8</sup>	6.70x10 <sup>9</sup>	1.96x10 <sup>10</sup>	6.35x10 <sup>10</sup>	1.00x10 <sup>11</sup>
300	--	7.36x10 <sup>0</sup>	2.02x10 <sup>4</sup>	2.02x10 <sup>4</sup>	7.19x10 <sup>3</sup>	5.03x10 <sup>2</sup>	2.56x10 <sup>4</sup>	3.33x10 <sup>4</sup>	3.03x10 <sup>-1</sup>	1.09x10 <sup>4</sup>	2.57x10 <sup>5</sup>	2.01x10 <sup>6</sup>	2.33x10 <sup>6</sup>
400	--	--	6.19x10 <sup>-1</sup>	6.19x10 <sup>-1</sup>	1.39x10 <sup>-2</sup>	9.59x10 <sup>-1</sup>	8.90x10 <sup>-1</sup>	1.86x10 <sup>0</sup>	--	1.91x10 <sup>-2</sup>	3.59x10 <sup>0</sup>	8.58x10 <sup>1</sup>	9.19x10 <sup>1</sup>
473.45	--	--	--	--	--	--	--	--	--	--	3.62x10 <sup>-5</sup>	4.29x10 <sup>-2</sup>	4.29x10 <sup>-2</sup>

### C. Spent Fuel

The spent fuel elements will be a source of radiation and heat. The activity of the elements was estimated by the method of Clark,<sup>21</sup> which has the fission product decay gammas comprised into seven energy groups. It was assumed that the fuel elements were allowed to cool in the core for 8 hr after shutdown following operation for 120 hr at 250 Mw. Table XXIX lists the energy release of the fuel elements after 8 hr and 48 hr of cooling in the core.

Table XXIX

<u>DECAY GAMMA ENERGY DISTRIBUTION OF SPENT FUEL ELEMENTS</u>		
[in Mev/(watt)(sec) of operating power level]		
Energy, Mev	Hours After Shutdown	
	8	48
0.1 - 0.4	0.71	0.37
0.4 - 0.9	4.2	1.50
0.9 - 1.35	0.43	0.02
1.35 - 1.8	0.60	0.054
1.8 - 2.2	0.35	0.025
2.2 - 2.6	0.07	0.040
2.8	0.004	0.0
TOTAL	<u>6.364 x 10<sup>9</sup></u>	<u>2.495 x 10<sup>9</sup></u>

The gamma flux from a subassembly was calculated by treating each subassembly as a cylinder, 12 in. in diameter and 90 cm long. The cylinder was converted to an equivalent line source and the surface flux (including buildup) was calculated.

#### Example:

The source strength,  $Q_3$ , of a fuel subassembly after 120-hr operation at 250 Mw and a cooling period of 8 hr is calculated by:

$$\begin{aligned}
 Q_3 &= \left[ \frac{\text{Mev}}{(\text{watt})(\text{sec})} \right] \left[ \frac{\text{watt}}{\text{core volume}} \right] & (10) \\
 &= (6.364 \times 10^9) (2.5 \times 10^8) / 5.08 \times 10^5 \\
 &= 3.13 \times 10^{12} \text{ Mev}/(\text{cm}^3)(\text{sec}).
 \end{aligned}$$

The source strength was increased by a factor of 1.5 to account for the spatial variation in power distribution. Thus,

$$Q_3 = 4.77 \times 10^{12} \text{ Mev}/(\text{cm}^3)(\text{sec}).$$

---

<sup>21</sup>F. H. Clark, "Decay of Fission Product Gamma," NDA-27-39 (December 30, 1954).

The surface gamma flux ( $\phi_\gamma$ ) was estimated by using a probability escape factor,  $P_e$ , of 0.5 and a buildup factor,  $B$ , of 2.5:

$$\begin{aligned}\phi_\gamma &= P_e Q_3 B \left( \frac{\text{Cylinder Volume}}{\text{Surface Area}} \right) \\ &= (0.5)(4.77 \times 10^{12})(2.5)(7.6) \\ &= 4.53 \times 10^{13} \text{ Mev}/(\text{cm}^2)(\text{sec}).\end{aligned}\tag{11}$$

#### D. Gamma Heating in Central Thimble

The heat generation rate for any material in the  $D_2O$  region can be estimated by using Fig. 46. However, this will yield only the gamma heating from the core, vessel, and thermal shield. In close to the core where the fast flux is high, the heating rate will be higher due to the removal of fast neutrons. Thermal neutron capture also poses a problem, particularly in metals. Consequently, the heating was estimated by calculating the heat generated by the fast and the thermal neutron fluxes in  $\frac{1}{4}$ -in.-thick sheet of zirconium. At the core edge this amounts to 1.73 watt/gm due to fast flux removal and to 1.17 watt/gm due to thermal neutron capture.

The final heating equation that was obtained and kept in a single exponential form for further conservatism is shown in Fig. 49. The fast flux heating is negligible after about 60 cm of  $D_2O$ , and the core gamma heating is very small after about 120 cm  $D_2O$ . The heating beyond this point is due primarily to the capture gammas in the vessel and the adjacent  $\frac{1}{4}$ -in. steel annulus.

Figure 49 is applicable only to thin-walled zirconium tubes that are located in the  $D_2O$  reflector, and primarily for establishing the cooling requirements for the thimbles and beam holes. In the event the calculated heating rates reflect any design limitations, a detailed analysis must be made of the particular thimble or beam hole in question.

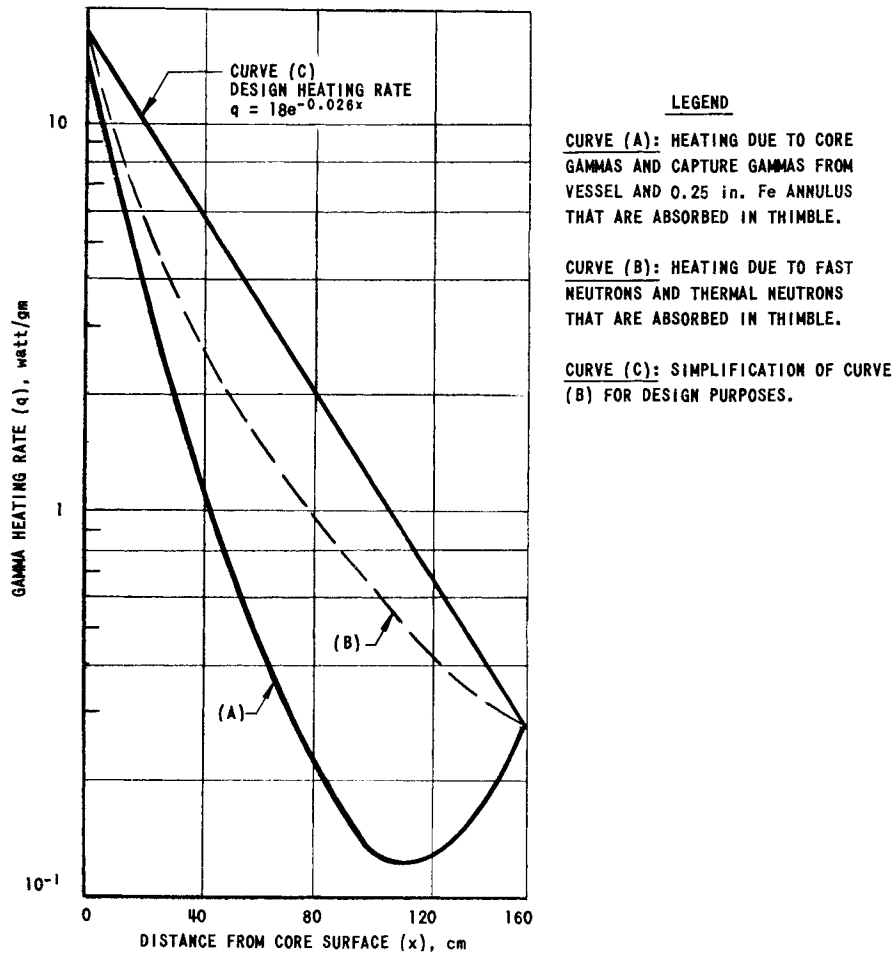
The heating in the central thimble was calculated by assuming that the gamma-ray flux was constant across the thimble at any given distance,  $x$ , from the edge of the core. From Fig. 49, the gamma-ray flux is seen to be attenuated with an exponential slope of  $0.026 \text{ cm}^{-1}$ . For heating in zirconium, the heat source can be expressed by

$$q'''(\text{Zr}) = 116e^{-0.026x} \text{ watt/cc Zr}.\tag{12}$$

The density and mass energy absorption coefficients will be less for  $D_2O$  than for Zr:

$$q'''(D_2O) = 2.81 e^{-0.026x} \text{ watt/cc } D_2O.\tag{13}$$

Thus, the total heat release,  $q$ , can be obtained by multiplying the heating rate in each material by its cross-sectional area, and integrating between any two distances,  $x_1$  and  $x_2$ , from the edge of the core.



Example:

$$q(D_2O) = \int_0^{35.6} (11.4)2.81 e^{-0.026x} dx + \int_{35.6}^{244} (45.6)2.81 e^{-0.026x} dx.$$

Table XXX summarizes the heating in the central thimble. The total heat released is 119,327 watts, or about 120 kw. This value does not include the heat generated by a sample within the thimble. For the case of 1 gm of curium-245, the heat release would be about 632 kw. It is evident that the cooling requirements are governed, in this case, by the curium-245 (see page 117).



Table XXX

CENTRAL THIMBLE HEATING INSIDE AND OUTSIDE CORE

Material:	<u>D<sub>2</sub>O</u>	<u>Zr</u>
Volume, cc	1,026	236
<u>Heating inside core</u>		
Heat generation rate, watt/cc	8.78	362
Total heat, watt	9,008	85,432
<u>Heating outside core</u>		
Region x <sub>1</sub> = 0 to x <sub>2</sub> = 35.6 cm		
Cross-sectional area, cm <sup>2</sup>	11.4	2.62
Heating, watt	743	7052
Region x <sub>2</sub> = 35.6 to x <sub>3</sub> = 244 cm		
Cross-sectional area, cm <sup>2</sup>	45.6	8.55
Heating, watt	1,954	15,138
Total heat at surface, watt	2,697	22,190

E. Thermal Shield

The thermal shield is designed to absorb the high thermal neutron current. The consequent heat will be released in the borated solution. The heat released in the solution should present no unusual design difficulties; however, the velocity of the borated coolant must be sufficient to prevent boiling.

The neutron current entering the borated solution was estimated at

$$J = 6.17 \times 10^{12} \text{ n}/(\text{cm}^2)(\text{sec}).$$

Essentially all of the neutrons will be absorbed, thereby producing an energy of 2.69 Mev/neutron capture.<sup>22</sup> The total area of the thermal shield exposed to the neutron current can be approximated by the surface area of a sphere with a radius of 203 cm. The total heating in the solution is given by:

$$\begin{aligned} q &= (6.17 \times 10^{12})(2.79)(1.6 \times 10^{-19}) (4\pi)(203)^2 \\ &= 1.42 \text{ Mw.} \end{aligned}$$

The heat produced in borated solution will be removed by circulating the solution at a rate of about 200 gpm.

F. Pressure Vessel

The volumetric heat generation in the pressure vessel was estimated by the expression

---

<sup>22</sup>B. T. Price, C. C. Horton, and K. T. Spinney, "Radiation Shielding," Pergamon Press, New York (1957).

$$q''' = (1.8 \times 10^5) e^{6.096x}, \quad (14)$$

where

$q'''$  = volumetric heat generation rate, Btu/(hr)(ft<sup>3</sup>)

$x$  = distance into pressure vessel wall, ft.

Calculations were made to determine whether natural convection cooling was sufficient to remove the heat generated in the wall. The film coefficient was approximated by the correlation of Montsinger and Ackerman:<sup>23</sup>

$$h = 0.165 (T_w + 30) \theta^{1/2}.$$

#### Example:

The bulk water temperature,  $T_w$ , is 125°F. The heat flux at the inside surface of the vessel, that is assumed to be insulated on the outside, is

$$q'' = 1954 \text{ Btu}/(\text{hr})(\text{ft}^2).$$

Therefore,

$$\theta = q''/h = q''/(0.165) (T_w + 30) \theta^{1/2}$$

$$\theta^{3/2} = q''/25.58 = 1954/25.58$$

$$\theta = (76.39)^{2/3}$$

$$= 18^\circ\text{F}.$$

The temperature of the vessel wall,  $T_s$ , is

$$T_s = T_w + \theta = 125 + 18 = 143^\circ\text{F}.$$

A rough rule<sup>23</sup> for the heat transfer coefficient for a liquid and surface is that a horizontal surface passing heat upward will have a 30% higher film coefficient than a vertical surface, while a horizontal surface passing heat downward will have a 30% lower heat transfer coefficient. Even under these approximations, the removal of heat produced in the vessel wall does not represent a design problem.

#### G. Core Shroud Transfer Coffin

It is suspected that the soundness of the core shroud will be threatened by prolonged irradiation. Therefore, the shroud has been designed to facilitate its eventual removal and replacement through the top closure of the pressure vessel. Accordingly, calculations were made to ensure that the radiation levels are within biological tolerance at any time during shroud exchange operations.

---

<sup>23</sup>W. J. King, "The Basic Laws and Data of Heat Transmission," Mech. Eng., 54, 347-353 (1932).

1. Sources of Radiation

The two sources of radiation that are of major concern are the core shroud and the vessel neck. The activation is assumed to result from the decay of radioactive isotopes formed by thermal neutron bombardment of the respective component materials. Further, that the thermal neutron fluxes [ $5 \times 10^{15}$  n/(cm<sup>2</sup>)(sec) for the shroud, and  $2 \times 10^{14}$  n/(cm<sup>2</sup>)(sec) for the vessel neck] are constant throughout each component for 10 yr (equivalent to 14-yr operation at the proposed fuel cycle).

The composition of the shroud (reactor-grade zirconium) and of the pressure vessel (Zircaloy-2) represents a total of 21 elements, including impurities that are present to the extent of 0.12% and 2.4%, respectively. This percentage difference is primarily due to the difference in concentrations of Sn, Ni, and Fe in the two grades of zirconium:<sup>24</sup>

Element	wt. %	
	Zirconium	Zircaloy-2
Sn	0.002	1.6
Ni	0.001	0.32
Fe	0.05	0.2

The effects of neutron irradiation of pure zirconium were investigated by writing differential equations for eight zirconium isotopes and two decay products for analogue computation. Following are three of these equations for Zr<sup>96</sup> (N<sub>1</sub>), Zr<sup>97</sup> (N<sub>2</sub>), and Nb<sup>97</sup> (N<sub>3</sub>):

$$\frac{dN_1}{dt} = -\phi_{th} N_1 \sigma_1 \tag{15}$$

$$\frac{dN_2}{dt} = \phi_{th} N_1 \sigma_1 - N_2 \lambda_2 \tag{16}$$

$$\frac{dN_3}{dt} = N_2 \lambda_2 - N_3 \lambda_3 \quad , \tag{17}$$

where

- N = isotopic concentration, atom/cm<sup>3</sup>
- σ = microscopic absorption cross section, cm<sup>2</sup>/atom
- φ<sub>th</sub> = thermal neutron flux, n/(cm<sup>2</sup>)(sec)
- t = time, sec
- λ = decay constant, sec<sup>-1</sup>.

The results for the zirconium series are reproduced as Fig. 50. Portions of the iron and tin series are reproduced in Fig. 51 and Fig. 52. The graphical results were used to calculate the activities of the major radioactive isotopes formed in the shroud after 10-yr exposure (Table XXXI).

---

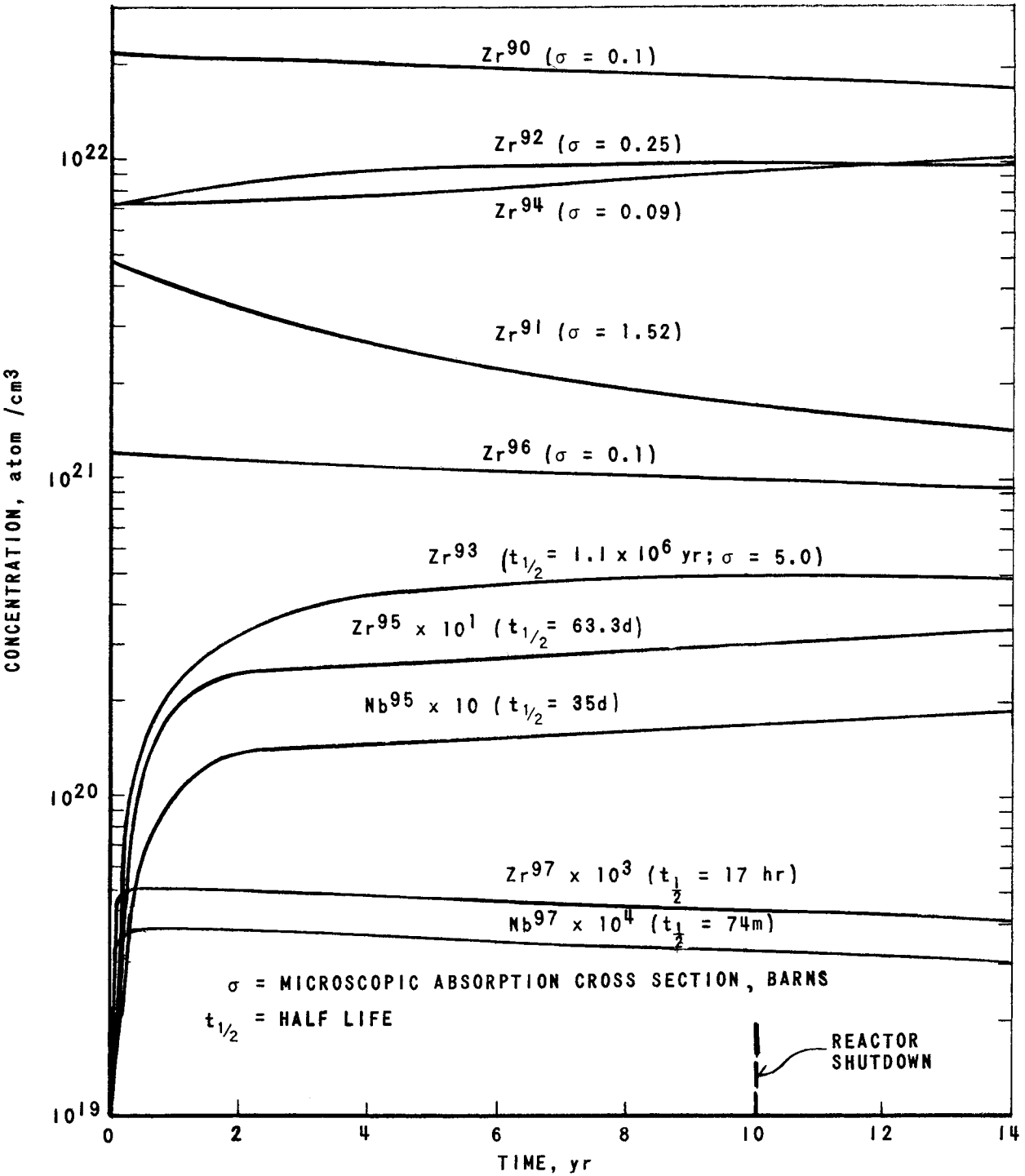


FIG. 50

ISOTOPIC CONCENTRATION OF THE ZIRCONIUM SERIES IN A  
THERMAL NEUTRON FLUX OF  $5 \times 10^{15}$  n/(cm<sup>2</sup>) (sec)  
(SAMPLE IS 100% ZIRCONIUM)

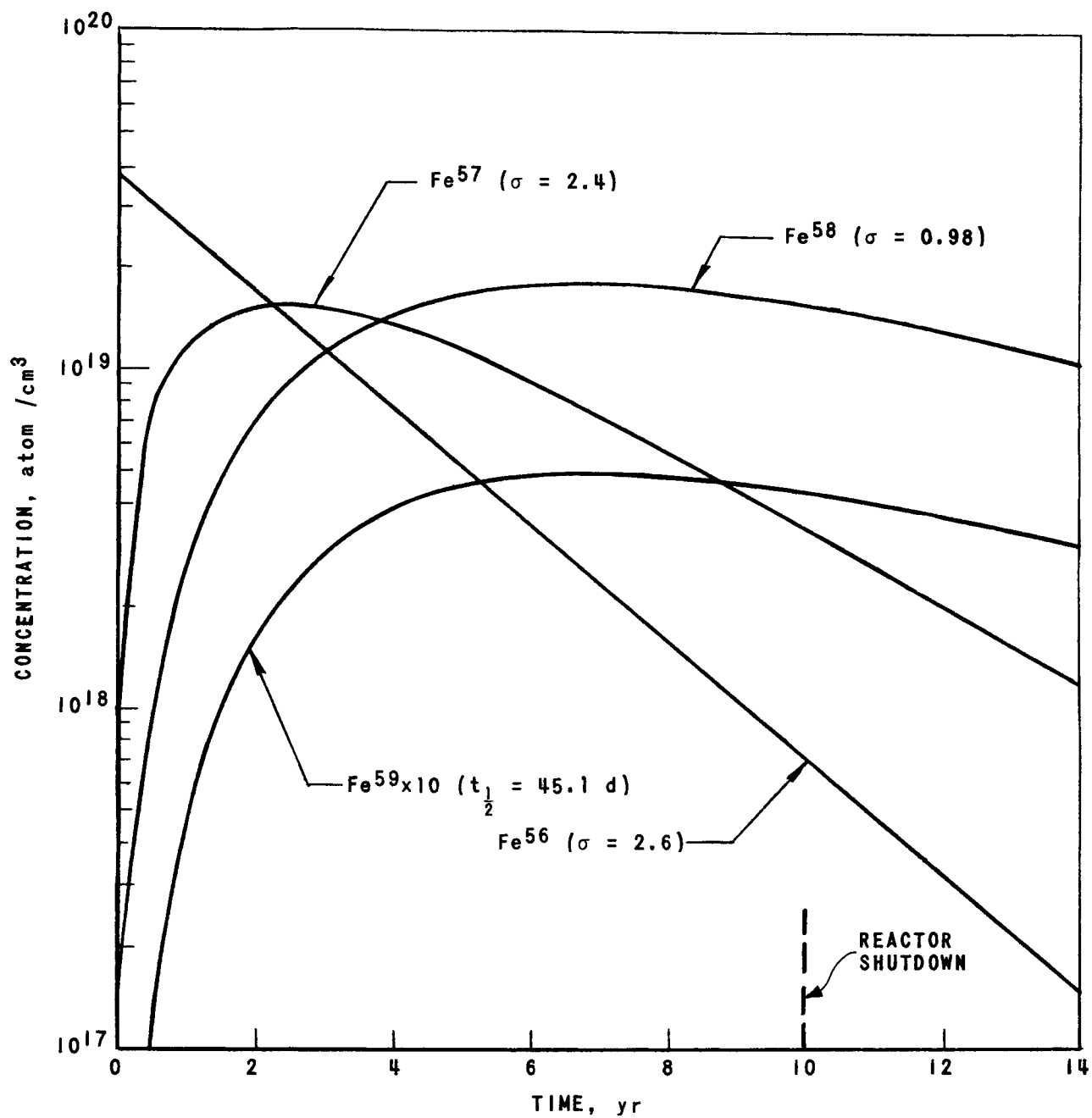


FIG. 51

ISOTOPIC CONCENTRATION FOR THE IRON SERIES IN A  
THERMAL FLUX OF  $5 \times 10^{15}$  n/(cm<sup>2</sup>) (sec).  
(Zr SAMPLE CONTAINS 0.05% IRON INITIALLY)

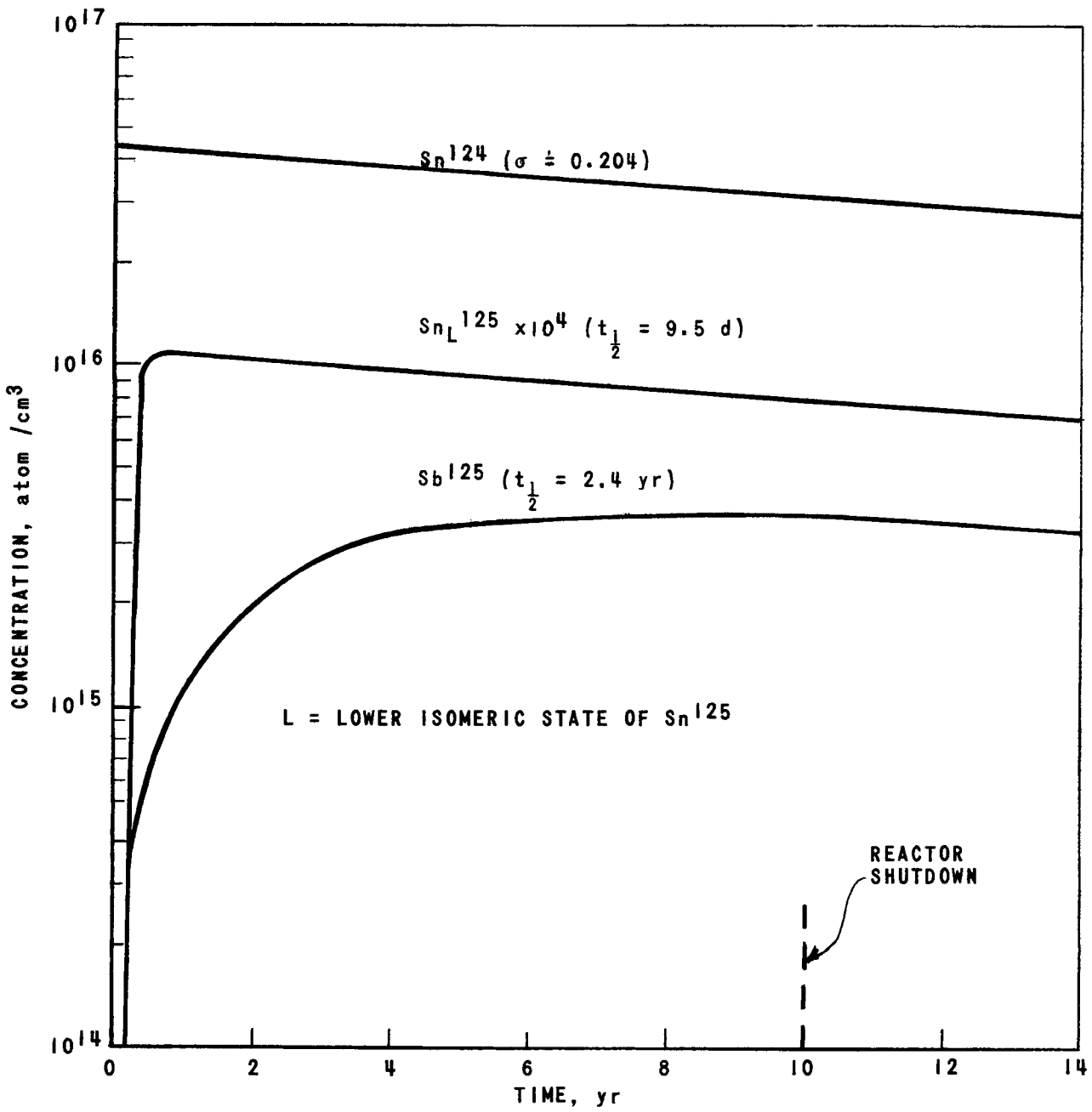


FIG. 52

ISOTOPIC CONCENTRATION FOR THE TIN SERIES IN A  
THERMAL NEUTRON FLUX OF  $5 \times 10^{15} \text{ n}/(\text{cm}^2) (\text{sec})$ .  
(Zr SAMPLE CONTAINS 0.002% TIN INITIALLY)

Table XXXI

ACTIVITY IN CORE SHROUD

Radioactive Isotope	N, atom/cm <sup>3</sup>	λ, sec <sup>-1</sup>	Activity, d/(cm <sup>3</sup> )(sec)	Energy, Mev/photon	Photon per disintegration
Zr <sup>95</sup>	3.17 x 10 <sup>19</sup>	1.267 x 10 <sup>-7</sup>	4.02 x 10 <sup>12</sup>	0.74	0.97
Nb <sup>95</sup>	1.77 x 10 <sup>19</sup>	2.292 x 10 <sup>-7</sup>	4.06 x 10 <sup>12</sup>	0.77	0.99
Zr <sup>97</sup>	4.4 x 10 <sup>16</sup>	1.132 x 10 <sup>-5</sup>	4.98 x 10 <sup>11</sup>	{ 1.15, 0.57 1.72	0.80 0.20
Nb <sup>97</sup>	3.28 x 10 <sup>15</sup>	1.561 x 10 <sup>-4</sup>	5.12 x 10 <sup>11</sup>	0.67	1.00
Fe <sup>59</sup>	4.5 x 10 <sup>17</sup>	1.778 x 10 <sup>-7</sup>	8.00 x 10 <sup>10</sup>	{ 1.29 1.10	0.43 0.57
Sb <sup>125</sup>	3.7 x 10 <sup>15</sup>	9.156 x 10 <sup>-9</sup>	3.39 x 10 <sup>7</sup>	{ 0.64 0.47	0.11 0.30

An analogous procedure was used to determine the activation of the vessel neck. Figure 53 shows the isotopic concentration versus thermal flux for the first portion of the zirconium series. The data were

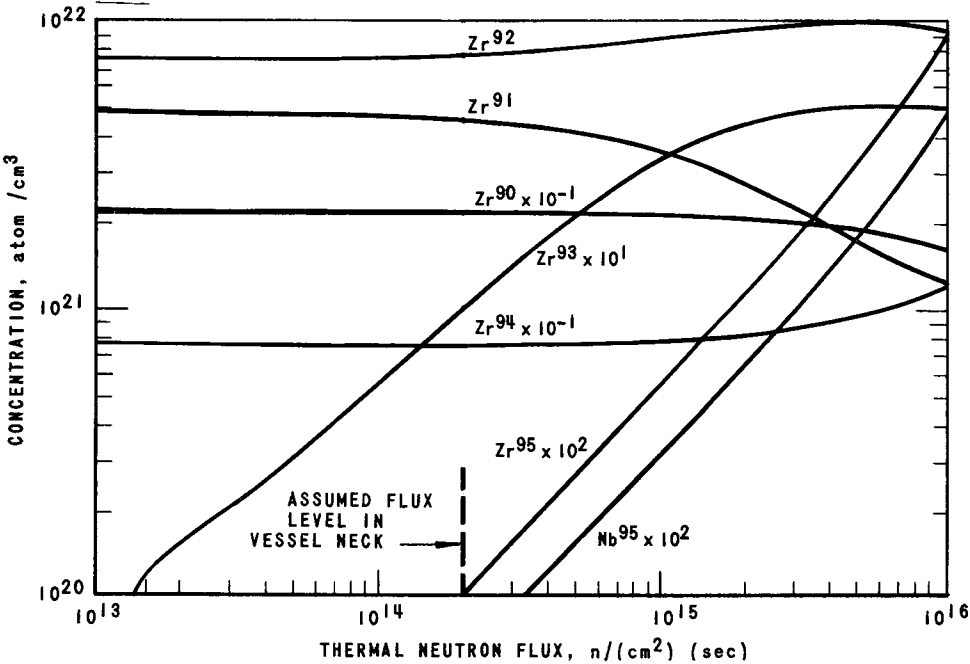


FIG. 53  
CONCENTRATION VS FLUX FOR A PORTION OF THE Zr SERIES AT  
AN IRRADIATION TIME OF 10 YEARS. (SAMPLE IS 100% Zr)

replotted from machine plots of concentration versus time for a specified flux level. The latter curves indicate that the Zr<sup>94</sup> (N<sub>1</sub>), Zr<sup>95</sup> (N<sub>2</sub>) and Nb<sup>95</sup> (N<sub>3</sub>) isotopes will have reached equilibrium after 4-yr operation at flux levels up to 10<sup>16</sup> n/(cm<sup>2</sup>)(sec). Accordingly, the activities of Zr<sup>95</sup> (N<sub>2</sub>)

and of  $\text{Nb}^{95}$  ( $N_3$ ) were determined by

$$N_2 \lambda_2 \sim N_3 \lambda_3 \sim \phi_{th} N_1 \sigma_1 \quad , \quad (18)$$

where  $N_1$  is taken from Fig. 53. The concentrations of  $\text{Fe}^{59}$  and  $\text{Sb}^{125}$  at shutdown were solved by the appropriate differential equations. The most significant radioactive isotopes formed are listed in Table XXXII.

Table XXXII

ACTIVITY OF VESSEL NECK

<u>Radioactive Isotope</u>	<u>Activity, d/(cm<sup>3</sup>)(sec)</u>
Zr <sup>95</sup>	1.33 x 10 <sup>11</sup>
Nb <sup>95</sup>	1.33 x 10 <sup>11</sup>
Fe <sup>59</sup>	4.60 x 10 <sup>8</sup>
Sb <sup>125</sup>	1.43 x 10 <sup>9</sup>

The activity from  $\text{Fe}^{59}$  and  $\text{Sb}^{125}$  can be neglected, since it is less than 1% of the total activity emitted by the decay of  $\text{Zr}^{95}$  and  $\text{Nb}^{95}$ . The activity from  $\text{Zr}^{97}$ ,  $\text{Nb}^{97}$ , and other short-lived isotopes is relatively unimportant after a shutdown period of 7 days. Therefore, the activity of the core shroud and the vessel neck is considered to be  $8.2 \times 10^{12}$  photons/(cm<sup>3</sup>)(sec) and  $2.66 \times 10^{11}$  photons/(cm<sup>3</sup>)(sec), respectively, which is based only upon the concentrations of  $\text{Zr}^{95}$  and  $\text{Nb}^{95}$  at shutdown.

An analysis of the concentration equations discloses that an increase in the initial abundance of a specific element can be applied directly to the activity of any radioactive isotope formed from this element. Thus, if a Zircaloy-2 shroud were used, the  $\text{Sb}^{125}$  activity would be  $2.7 \times 10^{10}$  d/(cm<sup>3</sup>)(sec), since the tin content is a factor of 800 greater in Zircaloy-2 than it is in reactor-grade zirconium. Similarly, the activity of  $\text{Fe}^{59}$  would be  $3.2 \times 10^{11}$  d/(cm<sup>3</sup>)(sec). Excluding differences in the number of photons per disintegration, these values represent an increase in the activity of only 4.2% over the above value of  $8.2 \times 10^{12}$  photons/(cm<sup>3</sup>)(sec). Consequently, if, for reasons of cost, corrosion, strength, etc., it is advantageous to employ Zircaloy-2 as the shroud material, it will not be necessary to alter the shielding design of the shroud coffin.

Although it is desirable because of the short-lived isotopes to delay shroud exchange operations for one week, the half-lives of  $\text{Zr}^{95}$  (63.3 days) and  $\text{Nb}^{95}$  (35 days) make it impractical, in terms of the saving in shield thickness, to delay for a longer period.



## 2. Water Shield

The section of the shroud that extends from 8 in. above to 12 in. below the active core region was assumed to be a homogenous cylinder of water and zirconium, having a radius of 46.11 cm and a height of 141.6 cm. The cylinder contains 61,000 cm<sup>3</sup> of zirconium that has a 0.75-Mev gamma activation of  $8.2 \times 10^{12}$  photons/(cm<sup>3</sup>)(sec). Owing to the zirconium dispersion, the activity of the cylinder is only  $5.3 \times 10^{11}$  photons/(cm<sup>3</sup>)(sec).

The gamma flux above and from the core shroud was calculated by using the upper limit, exterior on end (height  $\geq 3/\mu_s$ ) formula:<sup>25</sup>

$$\phi_\gamma = \frac{BS_V}{2\mu_s} \left[ E_2(b_1) - \frac{E_2(b_1 \sec \theta_1)}{\sec \theta_1} \right] \quad (19)$$

The dose rate from the core shroud for a point lying on the axial centerline of the pressure vessel and located at the surface of the water shield, is  $5.5 \times 10^{-7}$  mr/hr. This value is determined for a water shield that engulfs the shroud and extends 15 ft above it to the top of the biological shield.

At the same point the flux from the vessel neck flange [ $8.1 \times 10^2$  photons/(cm<sup>2</sup>)(sec)] was assumed to be the difference between the fluxes from two solid cylinders having diameters equivalent to the inner and outer diameters of the flange and calculated according to the upper limit, exterior on end (height  $< 3/\mu_s$ ) formula:

$$\phi_\gamma = \frac{BS_V}{2\mu_s} \left[ E_2(b_1) - E_2(b_3) + \frac{E_2(b_3 \sec \theta_1)}{\sec \theta_1} \right] \quad (20)$$

The zirconium flange is a cylindrical annulus having an inner diameter of 114.3 cm, a thickness of 15.24 cm, a height of 6.35 cm and a 0.75-Mev gamma activation of  $2.66 \times 10^{11}$  photons/(cm<sup>3</sup>)(sec).

The flux from the vessel neck ( $6.26 \times 10^3$ ), which has the same activation and inner diameter as the flange, a thickness of 2.54 cm, and a height of 83.82 cm, was calculated by the equation for the flux from the inside surface of a cylindrical annulus:<sup>26</sup>

$$\phi_\gamma = \frac{BQ_2}{2} [\text{seci}(\mu R, \alpha_2) - \text{seci}(\mu R, \alpha_1)] \quad (21)$$

<sup>25</sup> Theodore Rockwell III (ed.), "Reactor Shielding Design Manual," TID-7004 (March 1956), Chapt. 9, p. 364.

<sup>26</sup> M. Grotenhuis, "Lecture Notes on Reactor Shielding," ANL-6000 (March 1959), p. 83.

where

$B$  = buildup factor for a point isotropic source  
 $Q_2/2$  = inside surface source, photon/(cm<sup>2</sup>)(sec)  
 $\mu$  = linear absorption coefficient for the water shield, cm<sup>-1</sup>  
 $R$  = inside radius of annulus, cm  
 $\alpha_1 = \arctan Z/R$ ,  $\alpha_2 = \arctan (Z + H)/R$   
 $Z$  = distance between the point at the surface of the water shield and the top of the annulus, cm  
 $H$  = height of the annulus, cm  
 $\text{seci}$  = secant integral.

The dose rate resulting from gamma emission from the vessel neck and flange is 10.4 mr/hr on the surface of the water shield.

### 3. Coffin Shielding

The proposed core shroud transfer coffin is a lead annulus (6-in. wall thickness) clad internally and externally with 1-in. thick steel (41 in. ID, 57 in. OD, 10 ft high).

The flux at the outer surface of the coffin was calculated by the expression.

$$\phi_\gamma = \sum_{i=0}^n (B_i) \frac{Q_2}{2} E_1 \left[ \sum_{i=0}^n (\mu_i t_i) \right] \quad , \quad (22)$$

where

$B_i$  = buildup factor of the i'th region (point isotropic source)  
 $Q_2/2$  = infinite plane source strength, photon/(cm<sup>2</sup>)(sec)  
 $\mu_i$  = gamma-ray linear absorption coefficient of i'th region, cm<sup>-1</sup>  
 $t_i$  = thickness of i'th shield, cm.

For purposes of calculation, the core shroud was converted to a cylindrical annulus of the same height, outer diameter, and containing the same amount of zirconium. The wall thickness of such an annulus is 1.51 cm. The  $Q_2/2$  term of Eq. (22) was assumed to be equal to the outside surface source of the annulus ( $Q_2/2 = 6.1 \times 10^{12}$ ):

$$Q_2/2 = Q_3 V/A \quad , \quad (23)$$

where

$Q_3$  = volumetric source strength of the activated zirconium, photon/(cm<sup>3</sup>)(sec)  
 $V$  = volume of zirconium, cm<sup>3</sup>  
 $A$  = inside and outside annular surface area, cm<sup>2</sup>.

Equation (23) assumes no self-shielding, nor does it allow for the nearly counterbalancing effect of inside surface radiation that penetrates the outside surface of the annulus. Therefore, the expression is pessimistic in nature and fairly accurate because the wall of the annulus is thin as compared to its radius. Accordingly, the gamma flux calculated through the coffin wall results in a dose of 12.9 mr/hr on the outside surface (see Fig. 54). Further calculations showed that the top and bottom closures of the coffin would require an additional  $\frac{1}{4}$  in. of lead.

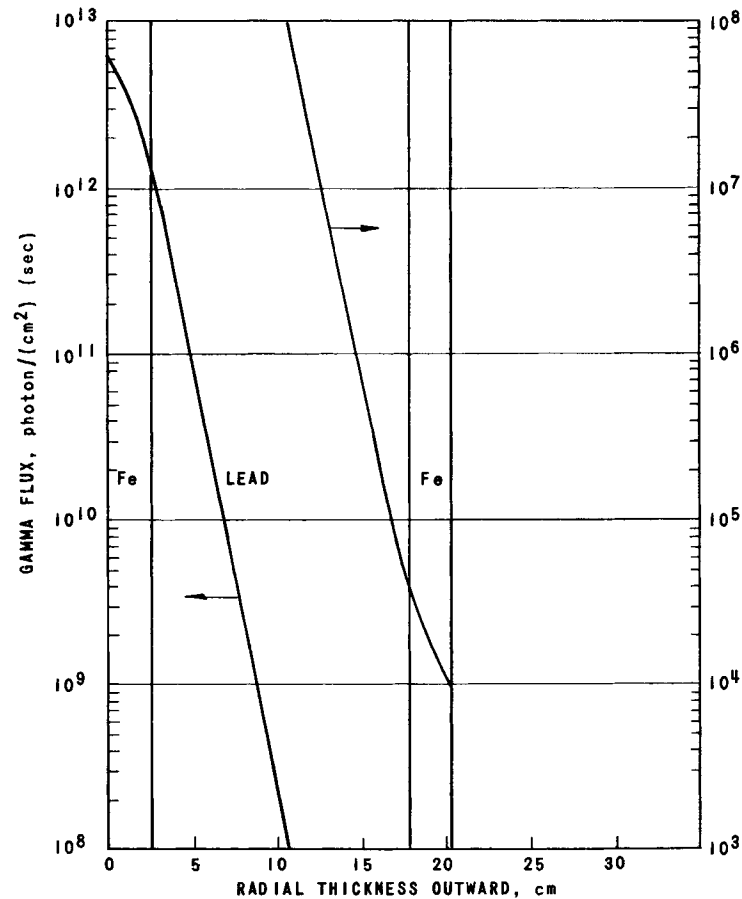


FIG. 54  
GAMMA FLUX FROM RADIOACTIVE CORE SHROUD VS  
THICKNESS OF SHROUD COFFIN, ( $E_\gamma = 0.75$  Mev)

The foregoing calculations were based on the assumption that the shroud coffin is air cooled. If the air were replaced by water, the dose level would decrease by a factor of 10, which would effect a savings of 0.6 in. of lead.

APPENDIX D

HEAT TRANSFER AND FLUID FLOW STUDIES

I. HEAT TRANSFER AND SCALE COEFFICIENT TESTS

The scale observed on magnesium alloys in the static corrosion tests (see Section VI) prompted an investigation of the effect of the scale on the heat transfer characteristics and the life expectancy of magnesium tubes in a facility designed to simulate anticipated reactor operating conditions.

A. Apparatus

The apparatus used to facilitate measurement of the scale coefficient is shown schematically in Fig. 55. The system was designed to circulate water at 25 fps and 100 psig through a magnesium tube heated to flux levels ranging from 385,000 to 553,000 Btu/(hr)(ft<sup>2</sup>). The surface temperature of the tube ranged from 120 to 150°C. The specimen tubes (0.305 in. ID x 0.375 in. OD x 36 in. long) were fabricated from magnesium alloys AZ 31 B and AZ 51 + 0.5% Cu.

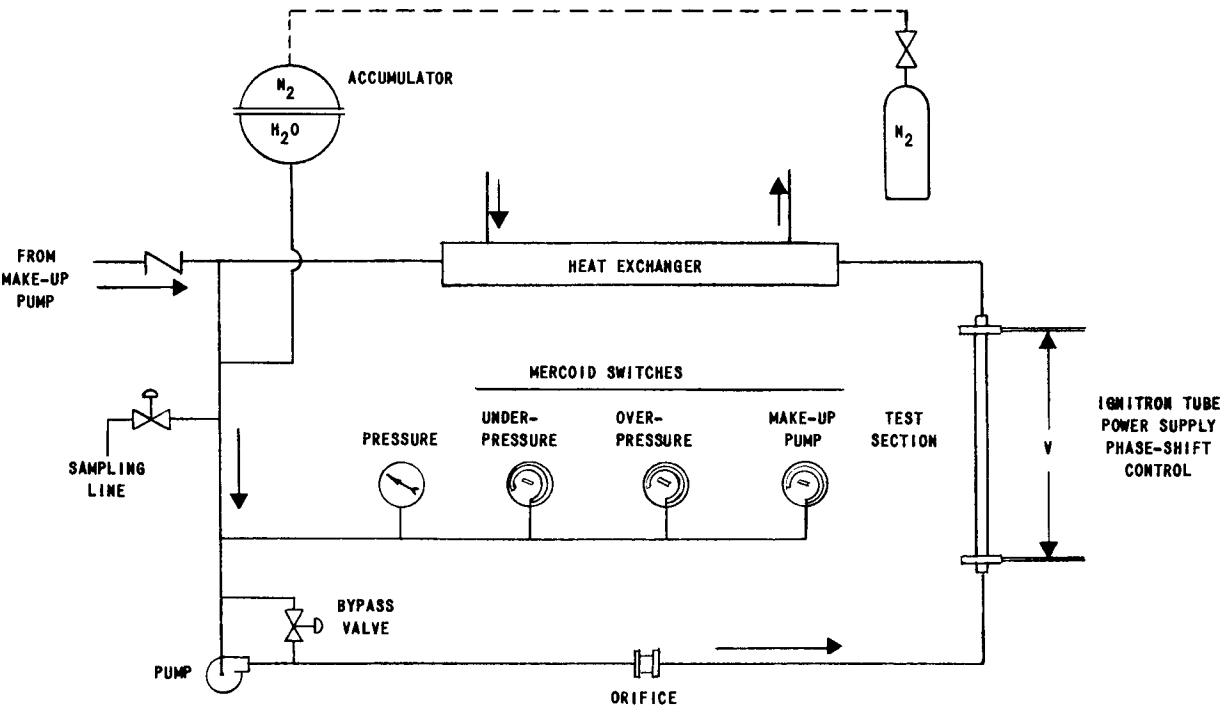


FIG. 55  
SCHEMATIC OF MAGNESIUM SCALE COEFFICIENT TEST LOOP

Both electric and steam heating were employed to simulate internal heat generation in the tube wall. However, the latter method was discontinued on the basis of initial tests that produced erratic data and revealed that steam heating was an ineffective simulation.

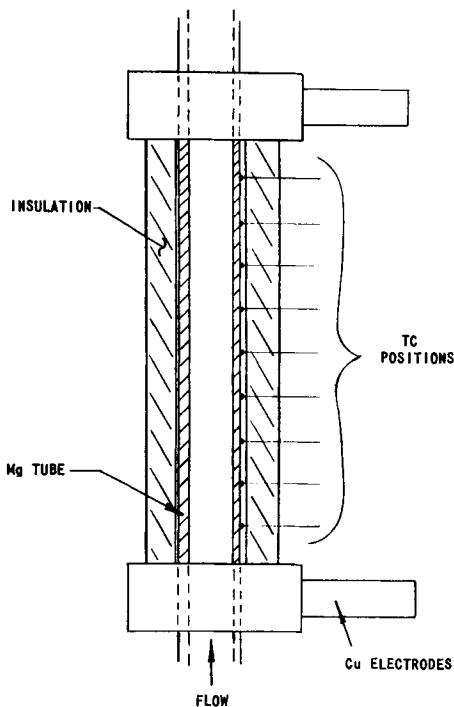


FIG. 56  
ELECTRIC-HEATED TUBE TEST SECTION

The electrically heated tube test section is shown in Fig. 56. Prior to assembly, the specimen tube was carefully cleaned with a weak nitric acid solution. Nine iron-constantan thermocouples were attached to the outer surface equidistant along the heated section between the clamp-on copper electrodes. The clamped surface of the tube was polished and coated with vaseline for the best possible electrical contact. The outer insulation was applied and the completed assembly installed between companion flanges in the test loop. The test section was surrounded by a blast shield at all times during each test.

Additional thermocouples were installed to measure the bulk water temperatures upstream and downstream of the test section, and the secondary cooling water temperatures in the heat exchanger. All temperatures were recorded continuously on a 16-point Brown instrument. The bulk water temperatures were measured separately by a thermopile in order to check the heat input against the power input as read from a

wattmeter, volt meter, and ammeter.

The flow was measured by an orifice calibrated in place.

The system pressure was maintained between 92 and 100 psig by three mercoid pressure switches interlocked with the coolant make-up pump.

### B. Theory

The scale coefficient is a measure of the heat barrier created by the formation of adherent scale on the heat transfer surface. The coefficient is inversely proportional to the temperature difference across the scale and follows the relation:

$$h_s = q''/\theta_s \quad (1)$$

where

$$h_s = \text{scale coefficient, Btu}/(\text{hr})(\text{ft}^2)(^\circ\text{F})$$

$$q'' = \text{constant heat flux, Btu}/(\text{hr})(\text{ft}^2),$$

and  $\theta_s$  is the difference in temperature at the hottest point (point of significance) of the heat transfer surface measured before and after the surface has become covered with scale.

In general, the point of significance occurred very near the upper end of the heated section. Hence, this point was set at the desired surface temperature at the beginning of each test.

The inner surface temperature was computed by the relation:

$$\Delta t_w = q'' (\Delta x)/2k \quad , \quad (2)$$

where

$$\Delta t_w = \text{temperature difference through the wall, } ^\circ\text{F}$$

$$q'' = \text{measured heat flux at the outer surface, Btu}/(\text{hr})(\text{ft}^2)$$

$$\Delta x = \text{wall thickness, ft}$$

$$k = \text{thermal conductivity of wall, Btu}/(\text{hr})(\text{ft})(^\circ\text{F}).$$

The convection coefficient at the start of each test was calculated by the relation:

$$h_c = q''/\theta_c \quad , \quad (3)$$

where

$$h_c = \text{convection coefficient, Btu}/(\text{hr})(\text{ft}^2)(^\circ\text{F})$$

$$\theta_c = \text{difference between inner surface and bulk water temperatures at the point of measurement.}$$

Although the value may have increased slightly due to surface changes and a slight increase in coolant velocity (noted in most of the tests), the convection coefficient was assumed to remain constant throughout the test.

### C. Results

The foregoing method results in a plot of scale coefficient as a function of test time and operating conditions. Typical results are plotted in Fig. 57. The scale coefficient decreases from an assumed value for a clean tube until rupture occurs. In some cases of scale erosion or

break-off, the tube either ruptures a short time after the break-off cycle, or another scale buildup is noted until final rupture. The pertinent test data are summarized in Table XVI, page 125.

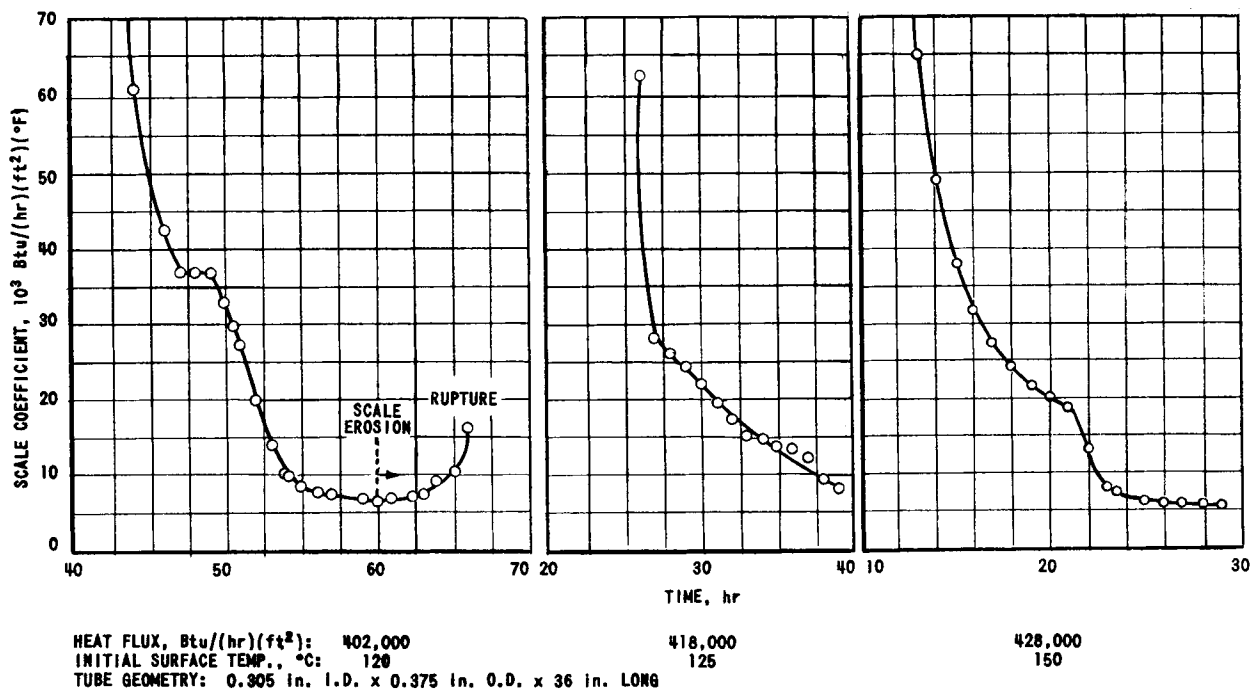


FIG. 57  
TYPICAL PLOTS OF SCALE COEFFICIENT AS A FUNCTION OF TEST  
CONDITIONS FOR ELECTRICALLY HEATED MAGNESIUM ALLOY AZ31B TUBES

D. Evaluation

Electric vs Steam Heating

The electrically heated tests are a slightly more severe simulation of internal heat generation in the fuel element because of the possibility of increased local heating rates due to changes in cross section. The heat flux remains constant throughout the test and, when scale forms, the interface temperature is increased. However, the point of significance did not always occur at the highest point of measurement as expected. Occasionally one of the lower points evidenced an increase in temperature, in which case that particular point was used to compute the scale coefficient. In other instances one or two of the points immediately below the point of significance indicated a lower rate of scale buildup with respect to the buildup at the hottest point. This is to be expected since, if the tubes last long enough, corrosion of the cooler surface is not as rapid, hence the lower rate of scale buildup.

In the steam-heated tests, the tubes were heated by steam circulated through a jacket that encircled the test specimen. Initial tests showed that the time to failure was somewhat longer than for the electric-heated specimens (see Table XVI); however, the data were erratic and the scale buildup and ruptures were not appreciably different. The extended time of failure was attributed to the fact that the condensing steam maintains a constant surface temperature and the heat flux decreases during the test. Therefore the temperature at the interface of the scale and tube wall is not driven up as would occur in a fuel element. Consequently, the test is not a simulation of internal heat generation in a fuel element.

### Mechanism of Rupture

Three types of tube ruptures were observed. In the simplest cases, a small hole was formed by accelerated local corrosion attack, and the loss of pressure signaled the end of the test. The second type of rupture was characterized by a longitudinal split in the tube wall. It is postulated that the rupture was precipitated by scale break-off and the consequent very high thermal stress induced in the short temperature-transition length between the exposed wall and the adhering scale. The initial temperature difference through the scale was usually about 300°F. The third type of rupture was prefaced by a considerable scale buildup. Evidently the corrosion attack was more uniform and the decrease in wall thickness resulted in an increase in the localized heating rate.

The majority of the ruptures were of the third type, and may have involved a combination of all three mechanisms.

### Corrosion

While the method of heating and the mechanism of rupture are of interest, the most important factor is the self-accelerating process that precedes and promotes rupture, namely, the formation of scale. A small amount of scale raises the interface temperature. The higher temperature increases the rate of corrosion attack and, hence, the rate of scale buildup. The process continues until rupture or scale break-off. In the latter case the cycle is repeated on the newly exposed surface until ultimate rupture occurs.

Scale break-off cycles were noted only in some of the non-fluoride tests. This suggests that while fluoride may be an effective corrosion inhibitor, it creates a more adhesive scale. Sodium fluoride (10 to 100 ppm) was particularly effective at surface temperatures of 120-130°C; however, at the higher temperatures (140-150°C), the tubes did not last long enough to note any benefits that might be expected from fluoride additives.



One test (No. 17-EF) of the AZ51 + 0.5% Cu alloy at 140°C initial surface temperature showed evidence of some scale formation at all nine points of measurement along the tube wall. The time of test was comparable to a 140°C test (No. 11-E) of the AZ31 B alloy. This indicates that while the absolute corrosion rate of the copper alloy is slightly less than that reported for the AZ31 B alloy, the corrosion rate-temperature curve obtained from the static tests should not be as steep.

Two tests of the AZ51 + 0.5% Cu alloy at 120°C showed no appreciable scale buildup and the tubes lasted longer than 100 hr. These results indicate that (1) the corrosion rate is not as rapid at the lower temperature since only a small amount of scale is formed, hence there is no large temperature gradient present to promote tube rupture before the wall is corroded through; or (2) there is a possibility that the corrosion rate-temperature curve for the copper alloy is not as steep as the curve for the AZ31 B alloy.

The effect of system pressure on corrosion was also investigated. It was felt that since the scale was porous, a small amount of stagnant water could accumulate between the scale and tube wall, and flash to steam when the saturation temperature was achieved. The formation of steam could accelerate the rate of corrosion and thus shorten the time to tube failure.

Accordingly, the saturation temperature was increased from 173°C to 200°C, and both alloys were tested at 130°C surface temperature. These tests lasted no longer than previous comparable tests, indicating that if steam is formed it does not influence the time of failure. In most of the tests, rupture occurred when the temperature drop across the scale reached 300°F. When tested at initial surface temperatures below 120°C (No. 16-EF at 102°C; No. 18-EF at 110°C), both alloys lasted longer than 120 hr at corresponding heat fluxes of 270,000 and 300,000 Btu/(hr)(ft<sup>2</sup>), indicating that magnesium may be feasible at temperatures below 120°C; however, this leaves only a small safety margin.

The present hot spot temperature in the reference core is about 283°F without scale formation. If it is proposed to limit the scale-metal interface temperature to 328°F (saturation temperature at 100 psia), then 45°F is the maximum allowable temperature difference that the scale can sustain without steam formation. Calculation shows that at the hot spot [ $q'' = 750,000 \text{ Btu}/(\text{hr})(\text{ft}^2)(^\circ\text{F})$ ], the minimum allowable scale coefficient is 16,670 Btu/(hr)(ft<sup>2</sup>)(°F). If the temperature limit is raised, based on a percentage of the rupture point temperature difference, a reasonable limit might be 10,000 Btu/(hr)(ft<sup>2</sup>)(°F). All of the tests (except the two below 120°C) descended to 10,000 in a relatively short time.

II. HEAT FLOW IN A TUBULAR FUEL ELEMENT

Figure 58 shows the mathematical model and the constants used to derive an expression for the percentage of heat flow through the inner and the outer surfaces of the reference fuel element.

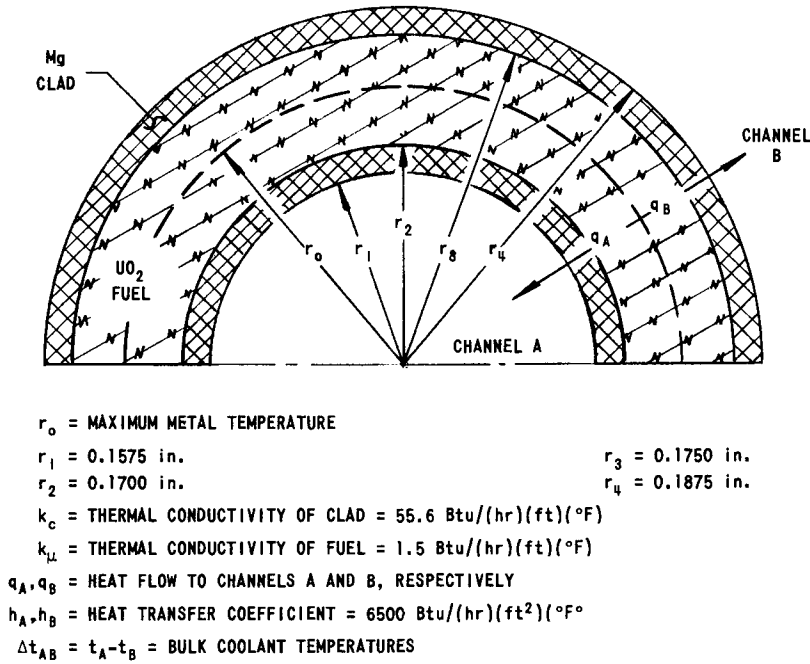


FIG. 58  
MATHEMATICAL MODEL AND CONSTANTS

The differential equation for temperature distribution through an infinitely long, hollow cylinder with internal heat generation (fuel zone) at steady-state conditions is

$$\frac{d^2 t}{dr^2} + \frac{1}{r} \frac{dt}{dr} = - \frac{q'''}{k} \quad , \tag{4}$$

where  $q'''$  is the rate of heat flow per unit volume.

The differential equation for same geometry without internal heat generation (clad) is

$$\frac{d^2 t}{dr^2} + \frac{1}{r} \frac{dt}{dr} = 0 \quad . \tag{5}$$

The general solutions of Eqs. (4) and (5) are, respectively,

$$t = -\frac{q''' r^2}{4k} + B \ln r + C \quad (6)$$

and

$$t = M \ln r + N \quad (7)$$

Proper application of the boundary conditions and nomenclature of Fig. 58 yields an expression for the radius,  $r_0$ , at which the maximum temperature occurs:

$$r_0^2 = \frac{\alpha + (r_3^2/h_B r_4) + (r_2^2/h_A r_1) - [2(\Delta t)_{AB}/q''']}{\beta + (1/h_B r_4) + (1/h_A r_1)} \quad (8)$$

$$\alpha = r_3^2 \left[ \frac{1}{k_C} \ln \left( \frac{r_4}{r_3} \right) + \frac{1}{2k_u} \right] + r_2^2 \left[ \frac{1}{k_C} \ln \left( \frac{r_2}{r_1} \right) - \frac{1}{2k_u} \right] \quad (9)$$

$$\beta = \frac{1}{k_C} \ln \left( \frac{r_4 r_2}{r_3 r_1} \right) + \frac{1}{k_u} \ln \left( \frac{r_3}{r_2} \right) \quad (10)$$

The percentage of heat flowing into Channel A is given by

$$\gamma = q_A/q = (r_0^2 - r_2^2)/(r_3^2 - r_2^2) \quad (11)$$

Evaluation of the foregoing equation gives

$$r_0 = 0.1726 \text{ in.}$$

and

$$\gamma = q_A/q = 51.62\%.$$

The proportion of heat transferred to the inner and outer channels depends, in part, upon the respective film coefficients. The film coefficients, in turn, are dependent upon the coolant velocity in the respective channels. The coolant velocities required to maintain equal surface temperatures in both channels were derived in the following manner.

The heat flow across the water films are

$$q_A = h_A A_A \theta_A \quad (12)$$

and

$$q_B = h_B A_B \theta_B \quad (13)$$

where

$h$  = convection coefficient,  $\text{Btu}/(\text{hr})(\text{ft}^2)(^\circ\text{F})$

$A$  = heat transfer area,  $\text{ft}^2$

$\theta$  = film temperature difference,  $^\circ\text{F}$ .

Since the bulk coolant temperatures and the metal surface temperatures are equal,

$$\theta_A = \theta_B$$

Therefore,

$$\frac{h_A}{h_B} = \frac{q_{AB}}{q_{BA}} = \frac{(0.5162)(250)(0.375)}{(0.4838)(250)(0.315)} = 1.270 \quad (14)$$

The film coefficient,  $h_A$ , is determined from the equation

$$h = 0.023 \left( \frac{k}{D} \right) \left( \frac{VD\rho}{\mu} \right)^{0.8} \left( \frac{C_p\mu}{k} \right)^{0.4}, \quad (15)$$

where

$V$  = bulk coolant velocity,  $\text{ft}/\text{hr}$

$D$  = equivalent diameter of channel,  $\text{ft}$

$k$  = conductivity of fluid at average film temperature,  $\text{Btu}/(\text{hr})(\text{ft})(^\circ\text{F})$

$\rho$  = density of fluid at average film temperature,  $\text{lb}/\text{ft}^3$

$\mu$  = viscosity of fluid at average film temperature,  $\text{lb}/(\text{ft})(\text{hr})$

$C_p$  = specific heat of fluid at average film temperature,  $\text{Btu}/(\text{lb})(^\circ\text{F})$ .

For channel A,  $V = 25$  fps. Hence, by Eq. (12),

$$h_A = 7300 \text{ Btu}/(\text{hr})(\text{ft}^2)(^\circ\text{F})$$

Therefore, the film coefficient required in channel B is

$$h_B = 7300/1.270 = 5740 \text{ Btu}/(\text{hr})(\text{ft}^2)(^\circ\text{F})$$

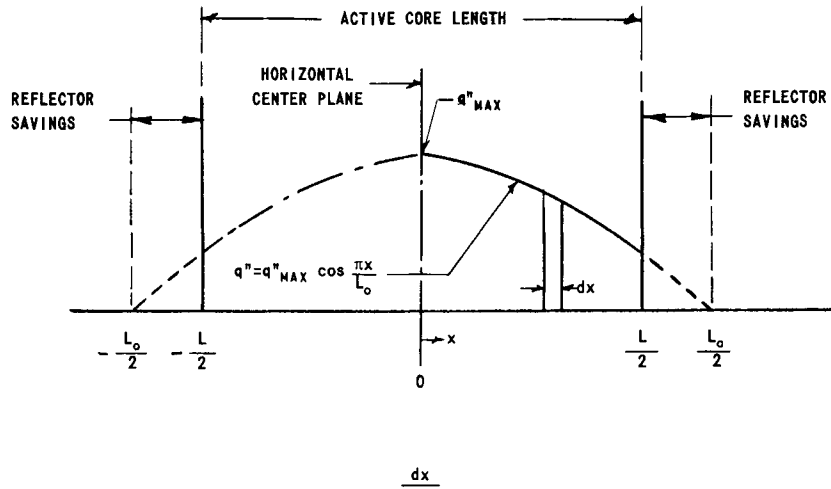
The equivalent diameters of both channels are equal; therefore, the coolant velocity in Channel B is given by

$$\begin{aligned} V_B &= \left( h_B/h_A \right)^{1.25} (V_A) \\ &= \left( 1/1.270 \right)^{1.25} (25) \\ &= 18.6 \text{ fps} \end{aligned} \quad (16)$$

Substitution of the values  $h_A = 7300$  and  $h_B = 5740$  into Eq. (15) produces essentially the same value for  $r_0$ . This indicates that a considerable variation of the convection coefficient is permissible without affecting the proportion of heat flow to the respective channels. Similarly, the conductivity of the fuel may be varied appreciably. Therefore, the determining factors are the placement of fuel and the thickness of the clad.

### III. DERIVATION OF TEMPERATURE PROFILES

The derivation of temperature profiles is based on an assumed cosine thermal flux distribution along any axial centerline of the active core as illustrated.



Accordingly, the temperature distribution for bulk channel flow is given by

$$W C_p \Delta t = W C_p (t_x - t_i) = \int q' dx \quad , \quad (17)$$

where

$$\begin{aligned} W &= \text{Mass flow rate} \\ C_p &= \text{specific heat of coolant} \\ t_x &= \text{temperature of bulk coolant at point } x \\ x &= \text{distance from horizontal centerline of core} \\ t_i &= \text{temperature of bulk coolant at core inlet} \\ q' &= \text{heat input per unit length of channel} \\ q' &= q'_{max} \cos (\pi x / L_0) \end{aligned} \quad (18)$$

and where  $L_0$  is the length of the active core plus reflector savings. Accordingly,

$$t_x - t_i = \frac{q'_{max}}{W C_p} \int_{-L/2}^x \cos \frac{\pi x}{L_0} dx \quad , \quad (19)$$

where  $L$  is the axial length of the active core, or

$$t_x = t_i + \frac{q'_{\max} L_0}{WC_p \pi} \left( \sin \frac{\pi x}{L_0} + \sin \frac{\pi L}{2L_0} \right) \quad (20)$$

The surface temperature distribution at point  $x$  is given by

$$t_s - t_x = (q''_{\max}/h) \cos (\pi x/L_0) \quad , \quad (21)$$

where  $q''$  is the heat flux and  $h$  is the film convection coefficient. Substituting Eq. (17) into Eq. (21) and differentiating,

$$t_s = t_i + \frac{q'_{\max} L_0}{WC_p \pi} \left[ \sin \frac{\pi x}{L_0} + \sin \frac{\pi L}{2L_0} \right] + \frac{q''_{\max}}{h} \cos \frac{\pi x}{L_0} \quad (22)$$

and

$$\frac{dt_s}{dx} = \frac{q'_{\max}}{WC_p} \cos \frac{\pi x}{L_0} - \frac{\pi q''_{\max}}{L_0 h} \sin \frac{\pi x}{L_0} \quad (23)$$

Setting  $dt_s/dx = 0$ ,

$$\frac{q'_{\max}}{WC_p} \cos \frac{\pi x}{L_0} = \frac{\pi q''_{\max}}{L_0 h} \sin \frac{\pi x}{L_0} \quad (24)$$

$$q_{\max} = q''_{\max} A/L \quad ,$$

where  $A$  = heat transfer area. Now

$$L_0 h A / \pi W C_p L = \tan (\pi x / L_0) \quad , \quad (25)$$

and the point of maximum surface temperature is

$$x = \frac{L_0}{\pi} \tan^{-1} \frac{L_0 h A}{\pi W C_p L} \quad (26)$$

The derivation of the maximum internal fuel temperature is based on the assumption that the fuel is concentrated in the geometrical center of the tube wall. This was done in anticipation of a very thin layer of fuel, since there is approximately one gram of  $U^{235}$  per fuel tube. Thus,

$$t_0 - t_s = a q'' / k \quad , \quad (27)$$

where

$$\begin{aligned} a &= \text{thickness of clad} \\ k &= \text{thermal conductivity of clad} \\ q'' &= q''_{\max} \cos (\pi x / L_0) \quad . \end{aligned} \quad (28)$$

Hence,

$$t_0 = t_s + (aq_{\max}''/k) \cos (\pi x/L_0) \quad . \quad (29)$$

Equation (29) was differentiated and set equal to zero to find the point of maximum fuel temperature. The point determined was found to deviate only slightly from the point of maximum surface temperature; therefore, the two points were assumed to occur in the same horizontal plane. Accordingly, the maximum internal fuel temperature at the inner edge of the clad is 295°F, and the maximum surface temperature is 280°F.

#### IV. HOT CHANNEL FACTORS

The hot channel factors used in the thermal and hydraulic design of the core are a combination of those listed in the Reactor Handbook<sup>27</sup> and some of the factors derived by LeTourneau and Grimble.<sup>28</sup> Since the actual tolerances, density variations, roughness, and irradiation effects cannot be determined until the fuel elements are fabricated, most of the factors are educated guesses.

Plenum chamber effects account for variations in the entering velocity profile. Based on a maximum commercial diametral variation of 8 mils, the factor for channel tolerances was determined as

$$F = (0.315/0.307)^{5/3} = 1.05 \quad .$$

The normal data spread for convection coefficient correlations is  $\pm 20\%$ ; hence the factor 1.20 was used.

Variation in fuel thickness and density promotes local heat flux peaking at the clad surface. Using the same 8-mil fabrication tolerance, and assuming the average tolerance would not exceed 6%, the factors for the bulk coolant temperature rise and the film rise are, respectively,  $F_t = 1.06$  and  $F_\theta = 1.08$ . The corresponding factors for variations in fuel density were assumed to be  $F_t = 1.03$  and  $F_\theta = 1.04$ .

The cosine heat distribution is suspect; therefore, in anticipation of a sharper maximum peak, 1.02 was applied to the total factors. The resultant multiplication gave

$$f_t \text{ (bulk rise)} = 1.19$$

---

<sup>27</sup>"The Reactor Handbook," AECD-3646, Vol. II (1955).

<sup>28</sup>B. W. LeTourneau and R. E. Grimble, "Engineering Hot Channel Factors for Nuclear Reactor Design," Nucl. Sci. Eng., Vol. I, No. 5, October, 1956.

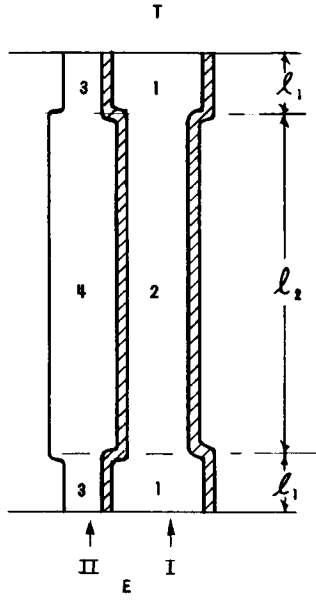
and

$$F_{\theta} \text{ (film rise)} = 1.40 \quad .$$

## V. ORIFICING ANALYSIS

The following analysis was performed to establish the configuration of the inactive ends of the fuel tubes consistent with maintaining: (1) a 0.450-inch square pitch core lattice; (2) an internal coolant velocity of 25 fps; and (3) an external coolant velocity of 18.6 fps.

With reference to the illustration:



E = inlet header

I = inner flow channel

II = outer flow channel

$l$  = length of region indicated

T = exit area (pressure vessel)

Since  $\Delta P_I = \Delta P_{II}$ , expressions for each pressure drop can be found and equated. Thus:

$$\begin{aligned} \Delta P_I = & K_{E-1} \frac{V_1^2}{2g} + 2 \frac{f l_1}{D_1} \frac{V_1^2}{2g} + K_{1-2} \frac{V_1^2}{2g} + \frac{f l_2}{D_2} \frac{V_2^2}{2g} + K_{2-1} \frac{V_2^2}{2g} \\ & + K_{1-T} \frac{V_1^2}{2g} \quad . \end{aligned} \quad (30)$$

Similarly,

$$\begin{aligned} \Delta P_{II} = & K_{E-3} \frac{V_3^2}{2g} + 2 \frac{f l_1}{D_3} \frac{V_3^2}{2g} + K_{3-4} \frac{V_3^2}{2g} + \frac{f l_2}{D_4} \frac{V_4^2}{2g} + K_{4-3} \frac{V_3^2}{2g} \\ & + K_{3-T} \frac{V_3^2}{2g} \quad , \end{aligned} \quad (31)$$



where

V = velocity of coolant  
 f = friction factor  
 D = equivalent diameter  
 K = contraction or expansion loss factor

in the regions denoted by the subscripts.

The expressions for the expansion and contraction losses are<sup>29</sup>

$$K_{E-1} = K_{E-3} = 0.4 \left[ 1 - \left( \frac{A_1 + A_3}{A_E} \right)^2 \right] \quad (32)$$

$$K_{1-2} = 0.4 \left[ 1 - \left( \frac{A_1}{A_2} \right)^2 \right] \quad (33)$$

$$K_{2-1} = \left( 1 - \frac{A_2}{A_1} \right)^2 \quad (34)$$

$$K_{3-4} = \left( 1 - \frac{A_3}{A_4} \right)^2 \quad (35)$$

$$K_{4-3} = 0.4 \left[ 1 - \left( \frac{A_3}{A_4} \right)^2 \right] \quad (36)$$

$$K_{1-T} = \left[ 1 - \left( \frac{A_1}{A_T} \right)^2 \right] = 1 \quad (37)$$

$$A_1/A_T \approx 0$$

$$K_{3-T} = 1 \quad , \quad (38)$$

where A is the flow area denoted by the subscripts.

Since the friction losses at the short end channels are small, it is assumed that the friction loss coefficients (C) are proportional to the channel lengths only. Therefore, let

$$C_1 = f\ell_2/D_2 = f\ell_2/D_4 \quad (39)$$

and

$$C_2 = f\ell_1/D_1 = f\ell_1/D_3 \quad . \quad (40)$$

---

<sup>29</sup>W. H. Jens and P. A. Lottes, "Hydrodynamics," Reactor Handbook, AECD-3646, Vol. II (1955).

Consequently,

$$C_2 = (\ell_1/\ell_2) C_1 \quad . \quad (41)$$

Substituting the above equations and rearranging,

$$\begin{aligned} \Delta P_I = & \frac{V_2^2}{2g} \left[ C_1 + \left( 1 - \frac{A_2}{A_1} \right)^2 \right] + \frac{V_1^2}{2g} \left\{ 0.4 \left[ 1 - \left( \frac{A_1 + A_3}{A_E} \right)^2 \right] \right. \\ & \left. + 2 \frac{\ell_1}{\ell_2} C_1 + 0.4 \left[ 1 - \left( \frac{A_1}{A_2} \right)^2 \right] + 1 \right\} \quad ; \end{aligned} \quad (42)$$

$$\begin{aligned} \Delta P_{II} = & C_1 \frac{V_4^2}{2g} + \frac{V_3^2}{2g} \left\{ 0.4 \left[ 1 - \left( \frac{A_1 + A_3}{A_E} \right)^2 \right] + 2 \frac{\ell_1}{\ell_2} C_1 \right. \\ & \left. + \left( 1 - \frac{A_3}{A_4} \right)^2 + 0.4 \left[ 1 - \left( \frac{A_3}{A_4} \right)^2 \right] + 1 \right\} \quad . \end{aligned} \quad (43)$$

The continuity equation gives the relationships:

$$V_1 = V_2 (A_2/A_1) \quad ; \quad V_3 = V_4 (A_4/A_3) \quad . \quad (44)$$

The following area relationship applies:

$$A_1 + A_3 = A_2 + A_4 \quad . \quad (45)$$

Let  $A_m$  be the cross-sectional area of the tube ends. Then

$$A_1 + A_3 = A_E - A_m \quad . \quad (46)$$

The values of  $V_2$  and  $V_4$  are known, so that for the core,

$$V_2/V_4 = 1.343 \quad .$$

By substitution and algebraic manipulation, the following expression is derived:

$$\begin{aligned} 2.629 \left[ 1.685 (A_2/A_1)^2 - (A_4/A_3)^2 \right] - 2 \left[ 1.685 (A_2/A_1) - (A_4/A_3) \right] \\ + 1.820 = 0 \quad . \end{aligned} \quad (47)$$

Letting  $x = A_2/A_1$  and  $y = A_4/A_3$ , it is found that

$$(2.104 x - 0.801)^2 = 2.629 y^2 - 2y - 1.179 \quad .$$

Furthermore,

$$\begin{aligned} A_2 &= 1.970 \text{ ft}^2 \\ A_4 &= 2.495 \text{ ft}^2 \\ A_3 &= 4.465 - A_1 \\ y &= A_4 / (4.465 - A_1) \end{aligned} .$$

Substitution gives

$$A_1^4 - 15.320 A_1^3 + 65.206 A_1^2 - 157.040 A_1 + 188.198 = 0 .$$

Graphical solution gives

$$A_1 = 2.550 \text{ ft}^2$$

and

$$A_3 = 1.915 \text{ ft}^2 .$$

The above areas are total core values. The required internal area per tube end is  $0.10088 \text{ in.}^2$ . This area is too small to fit a circular end and too large for a square end, if the 0.450-in. pitch is maintained by the flared end. The result is the crowned square configuration.

## VI. BURNOUT HEAT FLUX

There are a number of empirical burnout correlations that may be used to compute the burnout heat flux. The relation selected as most applicable to conditions prevailing in the Mighty Mouse core is given by Gunther:<sup>30</sup>

$$q_{\text{B.O.}}'' = 7000 (V)^{1/2} \Delta T_{\text{sub}} , \quad (48)$$

where

$$q_{\text{B.O.}}'' = \text{burnout heat flux, Btu/(hr)(ft}^2\text{)}$$

$$V = \text{coolant velocity, fps}$$

$$\Delta T_{\text{sub}} = \text{subcooling} = T_{\text{saturation}} - T_{\text{liquid}}, \text{ } ^\circ\text{F}$$

$$T_{\text{liquid}} = \text{mixed outlet temperature.}$$

For the inside of a fuel tube  $V = 25 \text{ fps}$  and  $\Delta T_{\text{sub}} = 173$ . Hence, by Eq. (48),

---

<sup>30</sup>F. C. Gunther, "Photographic Study of Surface Boiling Heat Transfer to Water with Forced Convection," Trans. ASME, 73 115 (1951).

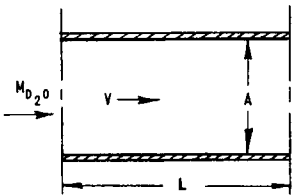
$$\begin{aligned} q''_{B.O.} &= (7000)(25)^{1/2} (173) \\ &= 6.06 \times 10^6 \text{ Btu}/(\text{hr})(\text{ft}^2) \end{aligned}$$

The burnout ratio used for design purposes is based on 67% of the calculated burnout heat flux and the maximum internal heat flux of 734,000 Btu/(hr)(ft<sup>2</sup>). The value of 67% is conservative and is based on the data scatter of ±33% from Gunther's experiment. The resultant value of 5.5 is considered adequate. The ultimate safe limit can be determined only by reactor experiments with fast excursions, since increased temperature as well as the production of steam in a fast power transient reduces reactivity and shuts down the reactor.

### VII. INTERIM EMERGENCY SHUTDOWN COOLING BY INERTIAL FLOW OF PRIMARY COOLANT

The physical characteristics of the primary coolant system are designed to facilitate emergency shutdown cooling by inertial flow of the coolant during the interim between loss of normal power supply to the primary pumps, and restoration of power by the auxiliary diesel generator. The following analysis is based upon the decrease in momentum of the primary coolant.

For any particular uniform section,



$$F = M dV/dt \tag{49}$$

$$F = A \Delta P \tag{50}$$

$$W = AV\rho \tag{51}$$

$$dV = dW/A\rho \tag{52}$$

$$M = AL\rho/g$$

where

- F = force
- M = mass
- V = velocity
- A = flow area of section
- $\Delta P$  = pressure drop through section
- W = flow rate
- $\rho$  = density of coolant
- g = gravitational constant

Substitution of Eqs. (50), (51) and (52) into Eq. (49) gives

$$\Delta P = - \frac{L}{Ag} \frac{dW}{dt}$$

The probable over-all pressure drop is equal to the sum of the individual pressure drops in the sections through which the coolant is circulated:

$$\Delta P_T = - \frac{1}{g} \left( \frac{L_1}{A_1} + \frac{L_2}{A_2} + \frac{L_3}{A_3} + \dots \right) \frac{dW}{dt} \quad (53)$$

Multiplying and dividing Eq. (53) by  $W^2$  gives

$$K = \frac{\Delta P_T}{W^2} \quad , \quad (54)$$

where  $K$  is the sytem flow constant, which may be obtained from Fig. 59. Letting  $K_1$  equal the bracketed terms in Eq. (53),

$$KW^2 = \frac{K_1}{g} \left( - \frac{dW}{dt} \right) \quad (55)$$

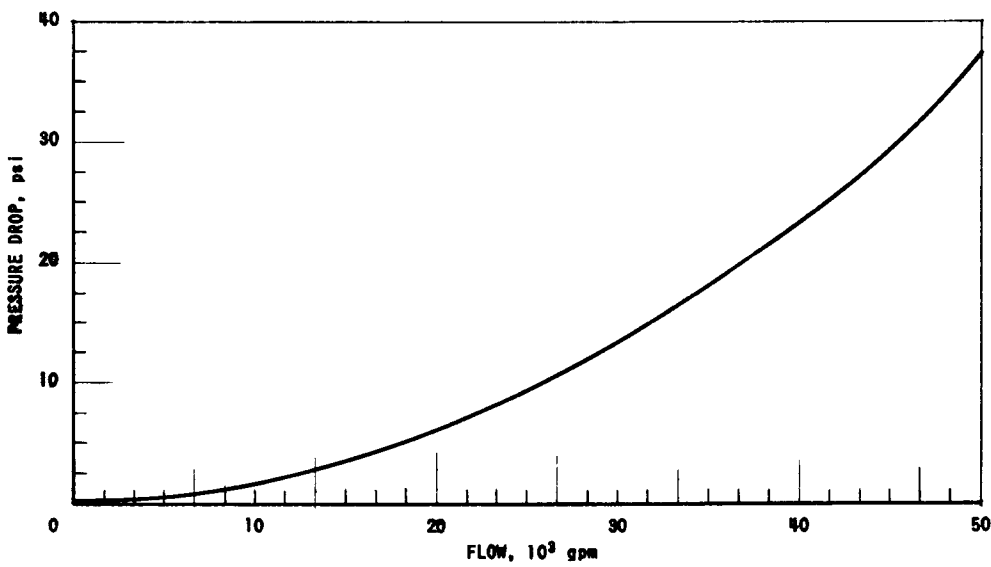


FIG. 59  
PRESSURE DROP VS. FLOW OF PRIMARY COOLANT

Integrating,

$$\int_0^t K dt = \frac{K_1}{g} \int_{W_0}^W - \frac{dW}{W^2} \quad (56)$$

or

$$t = \frac{K_1}{Kg} \left( \frac{1}{W} - \frac{1}{W_0} \right) \quad , \quad (57)$$

where  $t$  is the time after loss of pump power. Then

$$K = 36.93 / (50,000)^2 = 1.44 \times 10^{-8} \text{ psi}/(\text{gpm})^2 \quad .$$

The sections considered for pressure drop and the corresponding values are summarized in Table XXXIII.

Table XXXIII  
SUMMARY OF SYSTEM FLOW  
CHARACTERISTICS

Section	$\Delta P,$ psi	$L/A,$ $\text{in.}^{-1}$
Core	23.0	0.0429
Header	1.0	0.0907
Inlet-Outlet Lines	2.72	1.944
24-in. Lines	3.64	4.59
Degassing Tank	0.85	$\sim 0$
Heat Exchangers	5.72	0.1033
Total	36.93	6.771

Accordingly,

$$K_1 = 6.771 \text{ in.}^{-1}$$

and

$$\frac{1}{W} = 5.40 \times 10^{-6} t + \frac{1}{W_0} \quad ,$$

where

- $W$  = flow rate, gpm
- $t$  = time after loss of power, sec
- $W_0$  = flow rate at time of power failure = 50,000 gpm.

Curve (A) in Fig. 60 shows the resultant decrease in total coolant flow rate as a function of time after loss of pump power. Curve (B) is corrected for the increase in friction factor as the flow decreases.

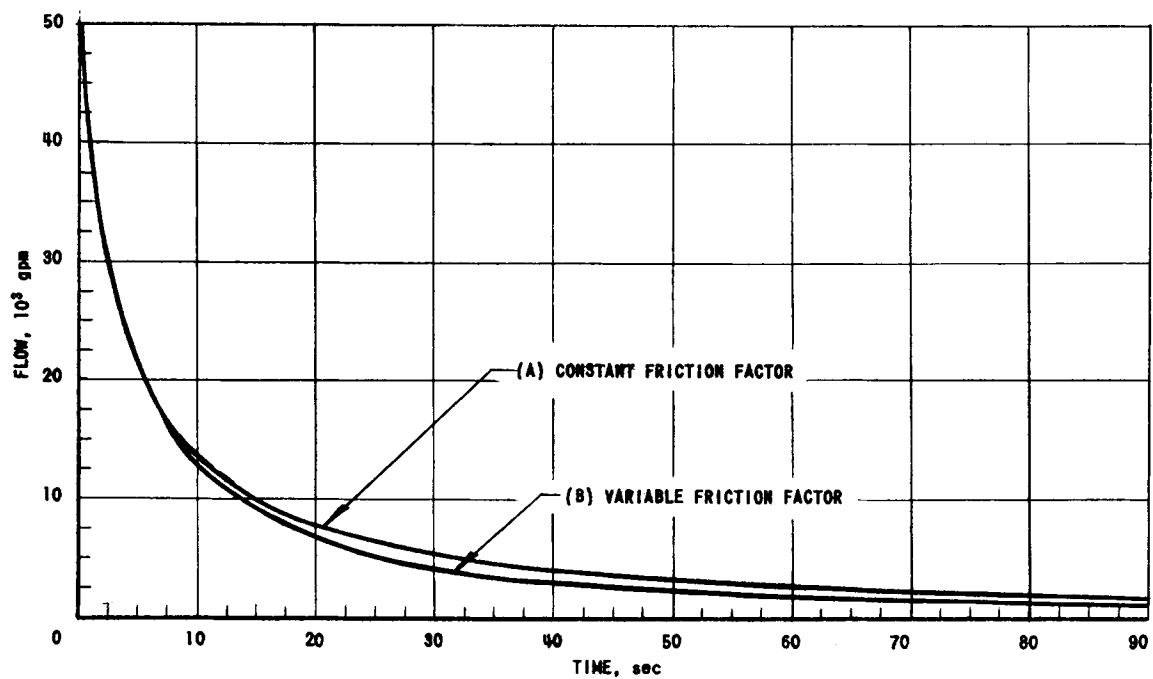


FIG. 80  
TOTAL PRIMARY COOLANT FLOW FOLLOWING LOSS OF PRIMARY PUMP POWER

VIII. CONTROL BLADE COOLING

The following analysis was performed to determine the coolant mass flow and flow area required to provide adequate convection cooling of each stainless steel control blade (12 in. x 0.25 in. x 5 in.). It was assumed that the blade was fully inserted within the active core, the position of maximum restriction to coolant flow.

The total heat generation in the blade is given by

$$q = q''' \rho V_B \quad , \tag{58}$$

where

$$\begin{aligned} q''' &= \text{volumetric heat generation, watt/gm} \\ \rho &= \text{density of stainless steel, lb/ft}^3 \\ V_B &= \text{volume of blade, ft}^3 \end{aligned}$$

Assuming a conservative gamma heating rate of 75 watt/gm,

$$\begin{aligned} q &= (75)(501)(0.00868)(454)(3.413) \\ &= 5.05 \times 10^5 \text{ Btu/hr} \end{aligned}$$

The required, volumetric coolant flow is therefore

$$A_f V = q / \Delta t C_p \rho_w \quad , \quad (59)$$

where

$A_f V$  = product of flow area and velocity at any point in the flow channel

$\Delta t$  = temperature difference through channel, °F

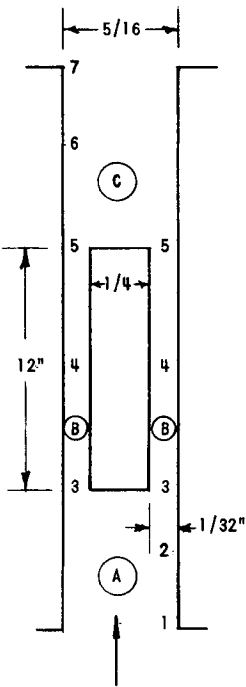
$C_p$  = specific heat of heavy water, Btu/(lb)(°F)

$\rho_w$  = density of heavy water, lb/ft<sup>3</sup>.

Assuming that the temperature rise matches the core flow temperature rise,

$$\begin{aligned} A_f V &= 5.05 \times 10^5 / (40)(1)(68.2) \\ &= 1.85 \times 10^2 \text{ ft}^3/\text{hr}. \end{aligned}$$

The pressure drop through the core is 23 psi. Therefore, dividing the control blade channel into three regions (see illustration):



$$\Delta P \text{ (total)} = \Delta P_A + \Delta P_B + \Delta P_C = 23 \text{ psi} \quad (60)$$

$$\Delta P_A = (K_1 + K_2) V_A^2 / 2g \quad (61)$$

$$\Delta P_B = (K_3 + K_4 + K_5) V_B^2 / 2g \quad (62)$$

$$\Delta P_C = (K_6 + K_7) V_C^2 / 2g \quad , \quad (63)$$

where

$V$  = velocity in region denoted by subscript, fps

$K_1, K_3, K_5, K_7$  = entrance and exit head losses due to changes in cross section

$K_2, K_4, K_6$  = head loss due to wall friction.



The geometry of regions A and C are known; therefore  $V_A$ ,  $V_C$ ,  $K_1$ ,  $K_7$ ,  $K_2$ , and  $K_6$  can be readily calculated. The values for  $K_3$  and  $K_5$  can be approximated by assuming that the  $\frac{1}{32}$ -in. flow path is fairly close to the required width. Thus

$$K_4 = f \ell_B / D_e \quad , \quad (64)$$

where

$$\begin{aligned} f &= \text{friction factor} \\ \ell_B &= \text{length of channel B, in.} \\ D_e &= \text{equivalent diameter, in.} \\ &= 4A_f / S \\ S &= \text{wetted perimeter of the channel} \\ A_f &= \text{flow area of channel B.} \end{aligned}$$

Substitution gives:

$$K_4 = (0.02)(12)(0.4 A_f + 20) / 4 A_f = 0.024 + (1.2 / A_f) \quad .$$

Calculation and combination of the above set of equations yields

$$\begin{aligned} \Delta P_A &= 0.478 \\ \Delta P_C &= 0.805 \\ \Delta P_B &= \left( 0.864 + \frac{1.2}{A_f} \right) \frac{V_B^2}{2g} \end{aligned}$$

Therefore,

$$1.283 + \left( 0.864 + \frac{1.2}{A_f} \right) \frac{V_B^2}{2g} = 23 \text{ psi} = 48.5 \text{ ft of } D_2O \quad . \quad (65)$$

As previously determined,

$$\begin{aligned} A_f V_B &= 1.85 \times 10^2 \text{ ft}^3/\text{hr.} \\ V_B &= (1.85)(10^2)(144) / 3600 A_f = 7.40 / A_f \text{ fps} \quad . \end{aligned} \quad (66)$$

Substituting Eq. (66) into Eq. (65) gives

$$48.5 = 1.283 + \left( 0.864 + \frac{1.2}{A_f} \right) \left[ \frac{(7.40)^2}{A_f^2 2g} \right]$$

Rearranging terms,

$$A_f^3 - 0.0155 A_f - 0.0215 = 0 \quad . \quad (67)$$

Graphical solution of Eq. (67) yields the required flow area between control blade and channel wall:

$$A_f = 0.297 \text{ in.}^2$$

The assumed flow gap of  $\frac{1}{32}$  in. yields an area of  $0.3125 \text{ in.}^2$ , which is slightly greater than required. The velocity in the gas is

$$V_B = 7.40/0.3125 = 23.7 \text{ fps} \quad ,$$

which will produce a sufficiently large convection coefficient for adequate cooling of the control blade.

#### IX. COOLING OF SPENT FUEL SUBASSEMBLIES

Following normal shutdown and prior to removal from the core, the spent fuel subassemblies will be cooled for about 8 hr by forced circulation of the primary coolant. Figure 39 shows the decay heat generated in the core as a function of time after shutdown. Subsequent cooling of the subassemblies in the  $D_2O$  or  $H_2O$  storage area will be accomplished by natural convection.

The adequacy of natural convection cooling was determined in the following manner. The fuel subassembly was assumed to be vertical at all times. The coolant velocity required to maintain the surface temperature of the hottest tube below  $200^\circ\text{F}$  was calculated by assuming: (1) the heat released corresponded to the maximum to average radial flux distribution (1.5) that existed during reactor operation; and (2) hot spot factors of 1.2 for flow and film temperature drop, respectively.

The available flow rate was determined by equating the driving head available to the hydraulic characteristics of the subassembly, based on the lowest possible heat release of the tubes. The available driving head is given by

$$\Delta P = L (\rho_0 - \rho_{\text{avg}}) \quad , \quad (68)$$

where

$$\begin{aligned} \Delta P &= \text{driving head, lb/ft}^2 \\ L &= \text{core length, ft} \\ \rho_0 &= \text{ambient density of water, lb/ft}^3 \\ \rho_{\text{avg}} &= \text{average density of water inside tube with lowest heat output,} \\ &\quad \text{lb/ft}^3. \end{aligned}$$

The total temperature rise for such a channel is

$$\Delta T = 3.18q/V \quad , \quad (69)$$

where

$q$  = heat output, Mw  
 $V$  = velocity inside tube, fps

The average temperature is

$$T_{avg} = T_{in} + (1.59q/V) \quad , \quad (70)$$

where

$T_{in}$  = inlet temperature, °F.

The hydraulic characteristics are described by the relation

$$\Delta P = (1.28 + 117.5f) (V^2/2g) \rho_{avg} \quad , \quad (71)$$

where

$\Delta P$  = pressure drop, lb/ft<sup>2</sup>  
 $f$  = friction factor  
 $g = 32.2 \text{ ft/sec}^2$ .

The surface temperature of the hottest tube is

$$T_s = T_{in} + (2.689q/V) (3548q/h) \quad (72)$$

where

$h$  = film coefficient, Btu/(hr)(ft<sup>2</sup>)(°F)

The film coefficient for the case of streamline flow is:

$$\frac{hD}{k} = 1.86 \left( \frac{VD\rho}{\mu} \right)^{1/3} \left( \frac{\mu C_p}{k} \right)^{1/3} \left( \frac{D}{L} \right)^{1/3} \left( \frac{\mu}{\mu_s} \right)^{0.14} \quad (73)$$

Example:

At the end of 8 hr of cooling, the decay heat (from Fig. 39) is  $P = 1.125 \text{ Mw}$ . Assuming  $V = 0.178 \text{ fps}$ :

$$T_{avg} = 100 + \frac{1.59 (1.125)}{0.178} = 110^\circ\text{F} \quad ;$$

therefore,

$$\rho_{avg} = 68.533 \text{ lb/ft}^3$$

and

$$\mu_{avg} = 1.78 \text{ lb/(ft)(hr)} \quad .$$

The driving head available is:

$$\Delta P = 3 (68.686 - 68.533) = 0.459 \text{ lb/ft}^2 \quad .$$

The velocity, based on the flow characteristics for streamline flow, is determined by equating the driving head to the hydraulic head:

$$\left(1.28 + 117.5 \frac{64\mu}{VD\rho}\right)\left(\frac{V^2}{2g}\right)\rho_{avg} = 0.459$$

$$1.28 V^2 + \frac{(117.5)(64)(1.78 V)}{(0.315/12)(68.533)(3600)} = \frac{(0.459)(62.4)}{68.533}$$

$$1.28 V^2 + 2.067 V - 0.418 = 0$$

$$V = 0.178 \text{ fps} \quad .$$

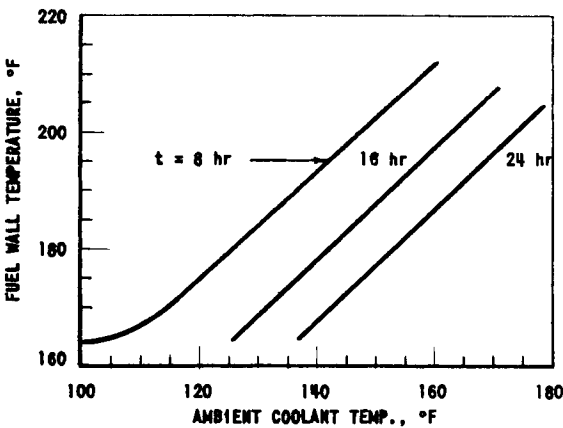


FIG. 61  
NATURAL CONVECTION COOLING OF SPENT FUEL  
SUBASSEMBLIES AT TIME  $t$  AFTER SHUTDOWN

The surface temperature is:

$$\begin{aligned} T_s &= 100 + \frac{(2.689)(1.125)}{V} + \frac{(3548)(1.125)}{(150)(V)^{1/3}} \\ &= 100 + \frac{(2.689)(1.125)}{0.178} + \frac{(23.65)(1.125)}{(0.178)^{1/3}} \\ &= 164.3^\circ\text{F} \end{aligned}$$

Figure 61 shows the variation of fuel element wall temperature with ambient coolant temperature as based on the foregoing analysis. After an initial forced circulation cooling period of 8 hr, natural convection cooling with ambient coolant

temperature as high as 148°F can be tolerated without exceeding a surface temperature of 200°F.

## APPENDIX E

STRESS ANALYSES OF PRESSURE VESSEL AND  
EXPERIMENTAL THIMBLES

I. PRESSURE VESSEL

The design of the pressure vessel conforms with the ASME Code for Unfired Pressure Vessels.<sup>31</sup> Accordingly, the tentative working stress of 12,500 psi is based on 25% of the lowest tensile strength (50,000 psi) exhibited by Zircaloy-2 samples at room temperature.<sup>32</sup>

The major contributions to the tensile stress at the inside surface of the vessel are the pressure stress and the radiation heating in the vessel wall. The pressure stress,  $\sigma_S$ , in the vessel wall is given by

$$\sigma_S = \frac{PR}{E_f t} + \frac{0.6P}{E_f} \quad , \quad (1)$$

where

P = design pressure  
R = inside radius of vessel  
E<sub>f</sub> = efficiency of the welded joint  
t = wall thickness

The thermal stress was determined by estimating the variation of the heat generation rate in the vessel wall. The vessel is subjected to a high gamma flux from the core, and an even higher capture gamma flux from within. In addition, the  $\frac{1}{4}$ -in. steel plate (thermal shield) located outside the vessel represents a source of gammas that will exceed the capture gamma flux in the vessel wall.

The respective sources of gamma heating in the vessel are plotted in Fig. 62. The resultant volumetric heat generation rate is

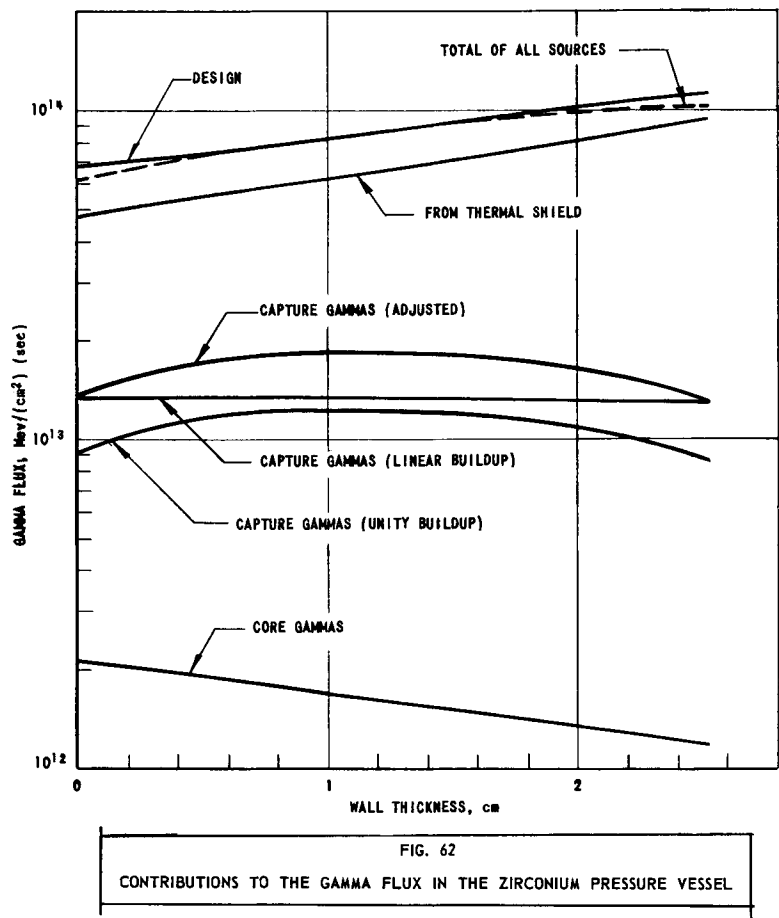
$$q''' = 1.8 \times 10^5 \exp(6.096x) \quad \text{Btu}/(\text{hr})(\text{ft}^3) \quad ,$$

where x is the vessel wall thickness (ft).

---

<sup>31</sup>"Basis for Establishing Stress Values for Nonferrous Materials," ASME Boiler and Pressure Vessel Code, Section VIII, Appendix Q, p. 173 (1956).

<sup>32</sup>R. M. Lieberman, "The Zircaloy-2 In-Pile Tube for the NRX Central Thimble," WAPD-TM-51 (April 1, 1957).



by<sup>33</sup> The thermal stress,  $\sigma_t$ , for an externally insulated vessel is given

$$\sigma_t = \frac{E \alpha \Delta T'}{1 - \nu} \quad ; \quad (2)$$

$$\Delta T' = \frac{q_0}{K \Sigma} \left[ \frac{1 - e^{\Sigma l}}{\Sigma} + \frac{1}{\Sigma} + \frac{l e^{\Sigma l}}{2} \right] \quad , \quad (3)$$

where

- $\sigma_t$  = thermal stress, lb/in.<sup>2</sup>
- $E$  = modulus of elasticity, lb/in.<sup>2</sup>
- $\alpha$  = coefficient of linear expansion, in./(in.)(° F)
- $\nu$  = Poisson's ratio
- $\Delta T'$  = average temperature drop across vessel wall, ° F
- $q_0$  = initial heat generation rate, Btu/(hr)(ft<sup>3</sup>)
- $\Sigma$  = slope of heating curve, ft<sup>-1</sup>
- $l$  = wall thickness, ft
- $K$  = thermal conductivity of vessel wall, Btu/(hr)(ft)(° F) .

<sup>33</sup>F. P. Durham, "Optimum Heat Transfer for Minimum Thermal Stress in Nuclear Reactor Shells," ASME Paper No. 54-A-126 (1954).

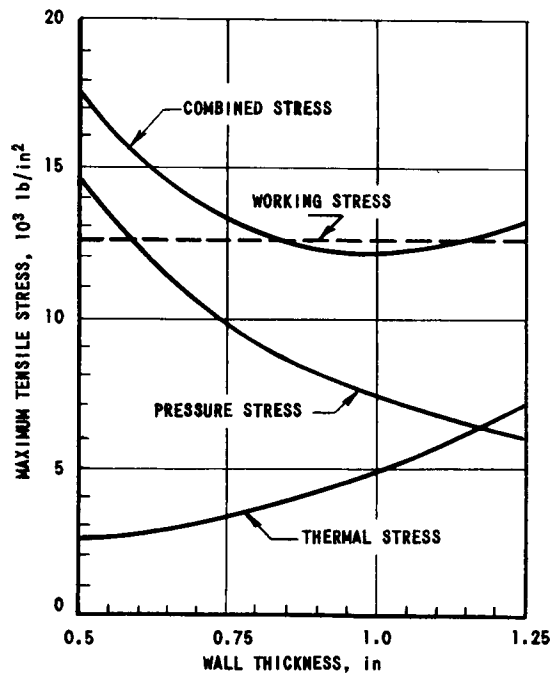


FIG. 63  
TENSILE STRESS VS WALL THICKNESS FOR THE  
ZIRCONIUM PRESSURE VESSEL

wall thickness of 1 in. Since the geometry of the vessel approaches a sphere, the thermal stress and the pressure stress in the ellipsoidal heads approximates the stresses in the vessel wall. Consequently, the heads should also be 1 in. thick.

II. THIMBLES

A. Central Thimble

The design of the central thimble is governed by several factors. The volume of nonfissionable metal in the core region adversely affects the core loading; therefore, the thimble wall must be as thin as possible. The minimum wall thickness, in turn, is influenced by the rigidity of the tube to sustain internal and external pressures, and the load imposed by the fuel hold-down mechanism.

The wall thickness for tubes under external pressure was obtained from Fig. UG-31 of the ASME Boiler and Pressure Vessel Code:

$$t = 0.020 D_0 = (0.020)(1.5632) = 0.03125 \text{ in.}$$

The minimum thickness of 0.0098 in. for the thimble under internal pressure was calculated using Eq. (1), Par. UG-27, ASME Code:

The constants used were

$$\begin{aligned} P &= 85 \text{ lb/in.}^2 \\ R &= 78 \text{ in.} \\ t &= 1 \text{ in.} \\ E_f &= 0.9 \\ K &= 9.5 \text{ Btu}/(\text{hr})(\text{ft})(^\circ \text{F}) \\ \ell &= 0.0833 \text{ ft} \\ E &= 12 \times 10^6 \text{ lb/in.}^2 \\ \alpha &= 4.3 \times 10^{-6} \text{ in.}/(\text{in.})(^\circ \text{F}) \\ \nu &= 0.35 \\ \Sigma &= 6.096 \text{ ft}^{-1} \end{aligned}$$

Substitution in Eqs. (1), (2), and (3) gives

$$\begin{aligned} \sigma_S &= 7,423 \text{ lb/in.}^2 ; \\ \Delta T' &= 60.6 ^\circ \text{F} ; \\ \sigma_t &= 4,811 \text{ lb/in.}^2 . \end{aligned}$$

The combined stress is then:

$$\sigma_S + \sigma_t = 12,234 \text{ lb/in.}^2 .$$

Figure 63 shows that the combined stress reaches a minimum value ( $12,234 \text{ lb/in.}^2$ ) for a

$$t = PR / (SE_f - 0.6P) \quad , \quad (4)$$

where

- $t$  = minimum required wall thickness, exclusive of corrosion allowance, in.
- $P$  = design pressure, lb/in.<sup>2</sup>
- $R$  = inner radius of thimble, in.
- $S$  = maximum allowable stress, lb/in.<sup>2</sup>
- $E_f$  = efficiency of longitudinal joints.

The results showed that the external pressure is more critical than the internal pressure; therefore the wall thickness was established as 0.03125 in. The foregoing analysis is typical of the method used to determine the wall thickness of all thimbles and beam hole liners.

The inside diameter of the central thimble increases to 3 in. at a point 4 ft 3 in. from the lower end. From Fig. UG-31 of the ASME Code, the wall thickness of this section is

$$t = 0.020 D_0 = (0.020)(3.125) = 0.0625 \text{ in.}$$

No allowance was made for loss due to corrosion since the thimble is accessible for removal and replacement, if necessary.

The ultimate load limit ( $p$ ) for buckling of the thimble due to compressive force ( $F$ ) developed by the fuel hold-down mechanism on a column of cross-sectional area ( $a$ ) is given by

$$F = p a \quad . \quad (5)$$

From Rankine's formula for a column with fixed ends

$$p = \frac{S}{1 + [\ell^2 / (5000 r^2)]} \quad (6)$$

$$= 45,300 \text{ lb/in.}^2 \quad ,$$

where

- $S$  = ultimate compressive strength = 60,000 lb/in.<sup>2</sup>
- $I$  = least moment of inertia = 0.71 in.<sup>4</sup>
- $\ell/r$  = slenderness ratio = 56
- $r$  = least radius of gyration = 1.08 in.
- $\ell$  = length of unsupported tube = 60 in.
- $d_i$  = inside diameter of thimble = 3.00 in.
- $d_o$  = outside diameter of thimble = 3.125 in.



Therefore,

$$F = (45,300)(0.605) = 24,400 \text{ lb.}$$

The axial load on the column due to the hold-down function was estimated at approximately 5,000 lb; hence the column strength is satisfactory.

For the 1-in. I.D. thimbles, the most pessimistic condition is an external pressure on the inner tube equal to 150 psi. From Fig. UG-31 of the ASME Code, the minimum wall thickness is

$$t = (0.020)(D_0) = (0.020)(1.0625) = 0.02125 \text{ in.}$$

The thickness is taken as a nominal  $\frac{1}{32}$  in., since this is a commercially available tubing. The outer shroud tube is also fabricated of  $\frac{1}{32}$  -in. wall tubing for reason of rigidity.

# APPENDIX F

## ALTERNATE FUEL ELEMENT DESIGNS

### I. SPIRAL-WOUND TUBE

The fuel tube shown in Fig. 64 uses a plate of the picture-frame type with the ends cut at a 45° angle. The plate is wound spirally on a mandrel, and the edges seam welded as the winding progresses. The ends of the finished tube are then flared to conform to the reference fuel tube geometry.

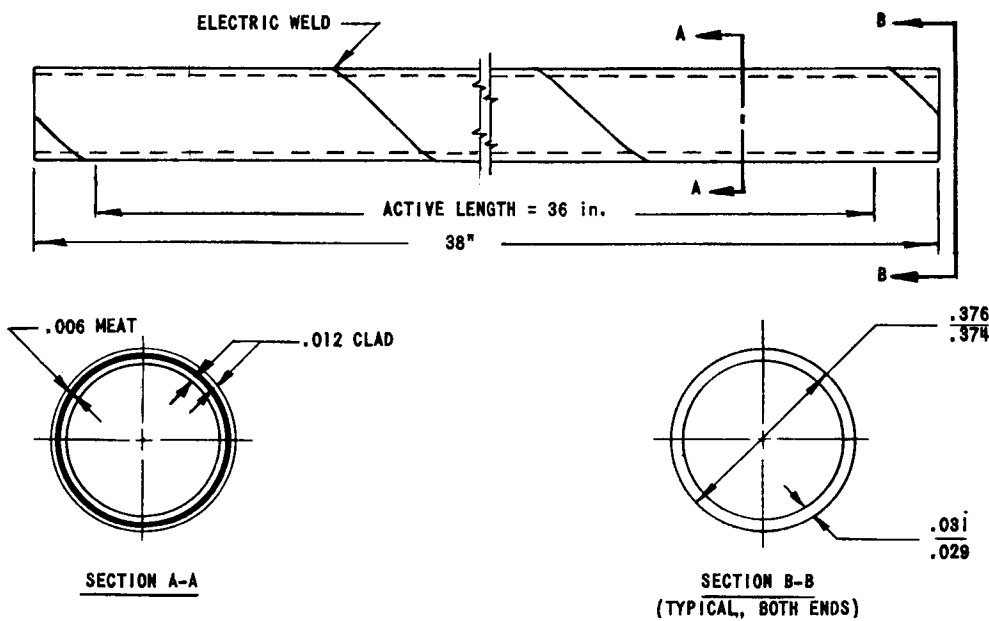


FIG. 64  
SPIRAL-WOUND-SEAM WELDED FUEL TUBE

### II. SECTIONAL FUEL SUBASSEMBLY (SPLIT CORE)

The concept of dividing the core into two horizontal sections with a void zone of 4 to 6 in. between sections offers advantages with respect to the experiments, fuel-tube production, and the elimination of tube vibration.

The tentative design features a hold-down bridge with provision for attachment at four corners to the assembly studs rather than to the tube extension collars. Assuming a 4-in. void between upper and lower sections, and an over-all length of 40 in. between the outer faces of the tube sheets, each tube would measure 17.5 in. long with a 0.75-in. inactive zone at each end. The active length of 16 in. would contain 0.5 gm of highly enriched  $U^{235}$ . The total number of tubes for one core would be 7,280. The fuel assembly would be completely interchangeable with the reference design assembly.

### III. TRIANGULAR PITCH FUEL TUBE SUBASSEMBLY (SOLID CORE)

Two earlier core concepts were based on triangular lattices with pitch dimensions of 0.415 in. and 0.485 in. However, the triangular arrays were eliminated because of the difficulty in achieving a three-point welded juncture between the triangular flared tube ends.

### IV. SQUARE PITCH-UNCROWNED FUEL TUBE SUBASSEMBLY

The initial concept of fuel tubes with square ends was eliminated as a result of flow calculations that indicated the necessity of improved orificing. Consequently the crowned square configuration was selected.

## APPENDIX G

### ALTERNATE ROTATABLE VESSEL CLOSURE AND FUEL-HANDLING SYSTEM

The system shown in Fig. '65 consists of a rotatable vessel closure and integral compound fuel-handling system.

#### I. ROTATABLE CLOSURE

The rotatable closure provides a static seal during reactor operation and a rotating seal during indexing operations with the fuel-exchange mechanism. To perform these two functions, the periphery of lower face of the closure contains a series of machined grooves that seat on metallic sealing rings contained in mating grooves machined in the upper face of the pressure vessel flange.

The upper face of the closure is machined to mate with grooves in a ring-shaped pressure pad that also seats on metallic seal rings interposed between the mating grooves.

The rotatable closure is clamped between the pressure vessel flange and the pressure rings by an expandable torus bellows to provide a gastight barrier. During reactor operation, the torus bellows is pressurized to a value above the pressure in the vessel to ensure against out-leakage. During the fueling cycle the respective pressures are equalized to allow the closure to "float" within the confines of the machined grooves.

#### II. FUEL-HANDLING SYSTEM

The fuel-handling system consists of (1) an index mechanism that is assembled into the rotatable closure; (2) a closure hold-down mechanism; (3) a riser mechanism that contains the fuel and the control rod grappling device; (4) a traverse mechanism that transfers the components from the riser mechanism to the elevator station; and (5) the conveyor system that effects ultimate transfer to the storage area.

#### III. SEQUENCE OF OPERATION

The unloading sequence is as follows:

(1) The hold-down mechanism is elevated to release and lift the fuel subassembly hold-down bars from the fuel zone to the upper region of the pressure vessel and to clear the area for subsequent operations.

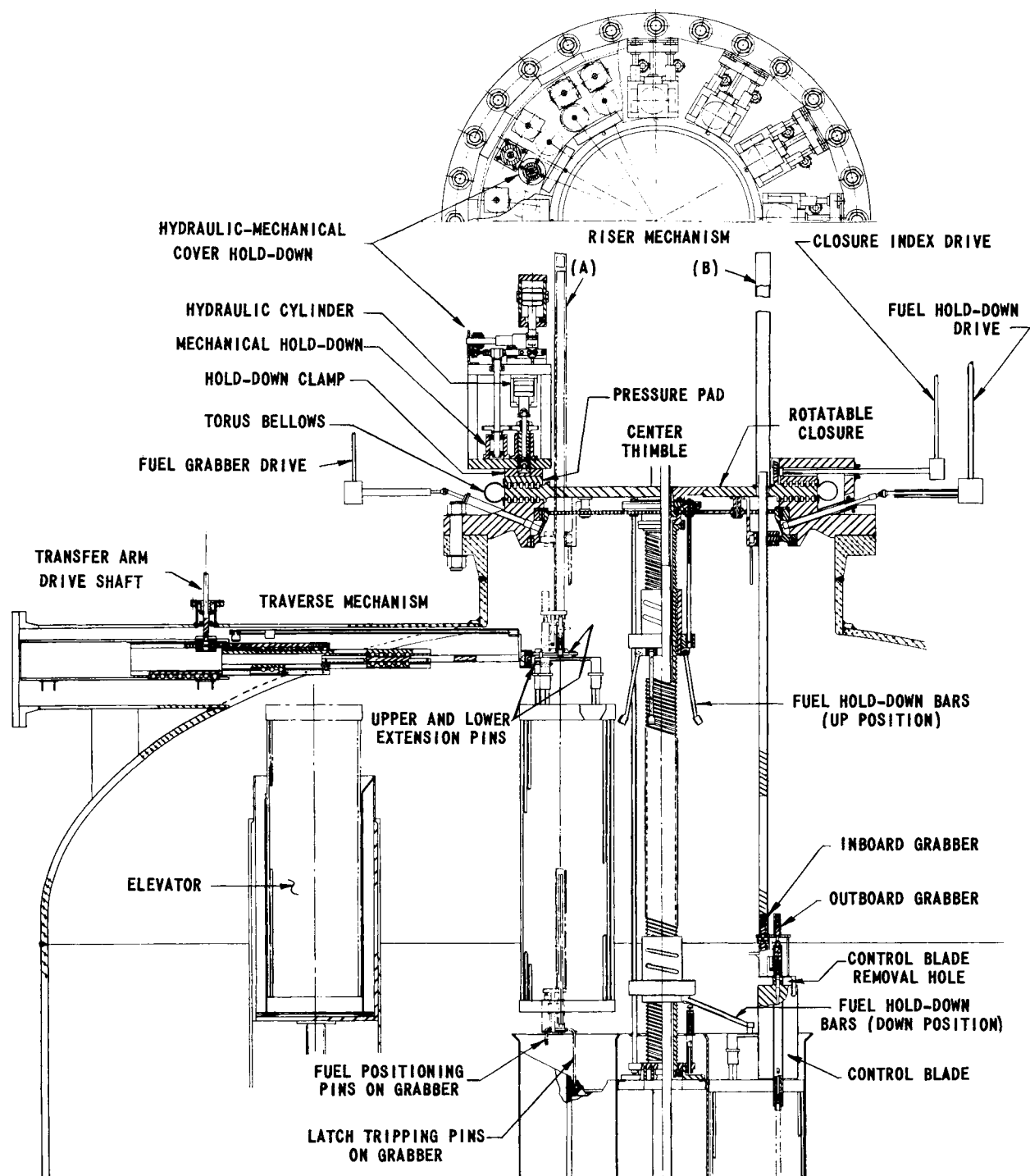


FIG. 65  
INTEGRAL ROTATABLE CLOSURE AND FUEL-CONTROL BLADE HANDLING MECHANISM  
(REF. DWG. RE-1-21875-E)

(2) The pressure in the torus bellows is reduced to the pressure in the vessel and thus allows the closure to float in the annular grooves.

(3) The hold-down clamps over the closure are released to permit indexing operations.

(4) The closure-indexing drive mechanism is operated to position the riser mechanism above the fuel subassembly or the control rod to be removed.

(5) When positioned above a fuel subassembly (see Position A, Fig. 65), the riser mechanism is activated to engage the inboard grabber chuck to the pilot pin on the fuel subassembly. Simultaneously, positioning pins on the grabber assembly engage positioning holes in the fuel subassembly bridge. These pins are intended to eliminate lateral motion of the subassembly during lifting operations. Additional latch-tripping pins engage slots in the control blade area and trip open a latching device that locks the subassembly in the core position. The subassembly is then lifted clear of the core by the rack-and-pinion riser drive mechanism.

(6) The closure is rotated to position the riser mechanism (and suspended fuel assembly) in line with the traverse mechanism. The riser and indexing mechanisms are de-energized.

(7) The traverse mechanism is extended from its retracted position (in the tube above the pressure vessel) to the fuel subassembly. A ball detent in the extension pins locks the fuel subassembly bridge to the traverse arm. The riser mechanism grabber is delatched and the traverse mechanism and the subassembly are retracted to a position above the elevator.

(8) The elevator and holding fixture is raised to encase the subassembly. The traverse pins are retracted from the subassembly, and the elevator is lowered to the conveyor system beneath the pressure vessel. The subassembly is then transferred to the decay storage area or to the spent fuel irradiation facility, as described previously.

The removal and transfer of a control rod is accomplished in a similar manner, but with the outboard grabber of the riser mechanism (see Position B, Fig. 65). A detent arrangement at the lower end of the control blade is activated by the downward motion of the grabber to disengage the blade from the blade extension shaft. The outboard grabber also features extension prongs that maintain vertical alignment of the blade during transport to the traverse arm. The lower extension pin of the traverse arm engages a hole in the pin riveted to the control blade. The balance of the unloading operation is identical to that of the fuel-removal cycle.

The loading of the subassembly and the control blade is accomplished by reversing the respective sequence of operations.

Exploratory studies were also made on a fuel removal system that represents a radical departure from the design philosophy used in locating the control rod drive mechanisms. This concept places the control rod drive mechanisms in the upper shield plug, the scram action being downward. Recent investigations indicate that the EBWR-type drive mechanism can be realigned to fit in the available space. The small cross section of the magnetic-jack drive mechanism also merits consideration. In any event, the top-mounted drive mechanism makes it necessary to use a bottom-loading method for fuel-exchange operations.

The proposed method features the fuel cradle and locking devices mounted on an indexing turntable. The turntable is elevated from the fuel conveyor station to the core region by a triple collapsible lead screw drive, or a four-element slider elevating mechanism.

## LEGAL NOTICE

*This report was prepared as an account of Government sponsored work. Neither the United States, nor the Commission, nor any person acting on behalf of the Commission:*

- A. Makes any warranty or representation, expressed or implied, with respect to the accuracy, completeness, or usefulness of the information contained in this report, or that the use of any information, apparatus, method, or process disclosed in this report may not infringe privately owned rights; or*
- B. Assumes any liabilities with respect to the use of, or for damages resulting from the use of any information, apparatus, method, or process disclosed in this report.*

*As used in the above, "person acting on behalf of the Commission" includes any employee or contractor of the Commission, or employee of such contractor, to the extent that such employee or contractor of the Commission, or employee of such contractor prepares, disseminates, or provides access to, any information pursuant to his employment or contract with the Commission, or his employment with such contractor.*

*Price \$3.50 . Available from the Office of Technical Services,  
Department of Commerce, Washington 25, D.C.*